Energy Saving for Pneumatic Actuation using Dynamic Model Prediction

Submitted for the degree of PhD

by

M Y Mohd Yusop

School of Engineering,
Cardiff University
Wales, UK

2006

ProQuest LLC
789 East Eisenhower Parkway
P.O. Box 1346
Ann Arbor, MI 48106-1346

Declaration

This work has not previously been accepted in substance for any degree and is not concurrently submitted for any degree.

Signed.....(candidate) Date 6/11/2006

Statement 1

This thesis is being submitted in partial fulfilment of the requirements for the degree of PhD.

Signed.....(candidate) Date 6/11/2006

Statement 2

This thesis is the result of my own independent work/investigation, except where otherwise stated. Other sources are acknowledged by explicit references.

Signed.....(candidate) Date 6/11/2006

Statement 3

I hereby give consent for my thesis, if accepted, to be available for photocopying and for inter-library loan, and for the title and summary to be made available to outside organisations.

Signed.....(candidate) Date 6/11/2006

Statement 4

I hereby give consent for my thesis, if accepted, to be available for photocopying and for inter-library loan **after expiry of a bar on access** approved by the Graduate Development Committee

Signed.....(candidate) Date 6/11/2006

Abstract

This research investigates a novel method for energy saving in a point-to-point actuation of a pneumatic system. The method predicts the system's actuation using the Gas Law and the actuator model, and commits air supply cut-off at the time when the energy in the actuator is sufficient to complete the actuation task. Experimental implementation is compared with simulation. The effect of the method is compared with conventional no cut-off and end-stroke cut-off actuations.

Lumped and finite difference methods are used for transmission line and system actuation modelling. The transmission line, actuator and control valves are modelled and integrated for the system actuation simulation and comparisons between simulation and measured data are performed.

Pressure oscillation in the transmission line exists and is captured by stimulating the air dynamics using a new transmission line experimental method. The friction model of the pneumatic actuator is determined by experiment and applied to the energy saving control system as well as the computer modelling algorithm. The determination of pneumatic transmission line bulk modulus is performed through experiment due to the confidentiality of Young's modulus value needed for its calculation.

Significant effect has been achieved in implementation and it is found that cut-off at end-stroke and cut-off using model prediction can reduce the amount of air potential energy wasted in conventional actuation by up to 43.5% and 80.2% respectively. However the actuation time of predicted cut-off increases by up to 25%.

Table of Contents

Nomenclatures

A	Area	m^2
A_h	Sensor cross-sectional area	m^2
A_p	Piston cross-sectional area	m^2
A_t	Transmission line cross-sectional area	m^2
a	Air flow acceleration	m/s^2
a_p	Piston's acceleration	m/s^2
C_c	Contraction coefficient	-
C_d	Discharge coefficient	-
C_m	Mass flow coefficient	-
C_{vel}	Flow velocity coefficient	-
c	Sound wave velocity	m/s
c_{fr}	Friction constant	N
C_p	Specific heat capacity of air at constant pressure	J/kgK
C_v	Specific heat capacity of air at constant volume	J/kgK
d_i	Inner diameter of transmission line	m
d_o	Outer diameter of transmission line	m
d_{ori}	Orifice diameter	m
E_a	Air potential energy	J
E_{ac}	Potential energy of pneumatic cylinder under cut-off actuations	J
E_{an}	Potential energy of pneumatic cylinder under conventional actuation	J
E_c	Total air energy consumption	J
E_k	Kinetic energy	J
E_l	Energy losses	J
E_t	Total energy	J
e	Strain rate	1/s
e_{int}	Internal energy	J
F	Force	N
F_{fr}	Friction force against air flow	N
F_{frp}	Friction force against cylinder's piston	N
F_{net}	Net driving force	N
F_s	Static friction	N

f	Body force per unit mass	m/s^2
g	Gravitational acceleration	m/s^2
h	Enthalpy	J
i, j, k	Orthogonal curvilinear coordinates	-
K	Cut-off modifying factor	-
K_v	Viscous coefficient	Ns/m
k	Heat transfer coefficient	J/K
l_t	Transmission line length	m
l_h	Sensor length	m
l_j	Transmission line segment length	m
M	Mass attached at the end of the cylinder's rod	kg
M_{mach}	Mach number	-
M_o	Other masses	kg
M_p	Total mass of piston-rod	kg
m	Air mass	kg
$\dot{m}$	Mass flowrate	kg/s
N_s	Number of samples	-
n	Time level	s
P	Pressure	N/m^2
P_a/P_{Atm}	Atmospheric pressure	N/m^2
P_c	Pressure at cut-off implementation	N/m^2
Pl	Pressure in left chamber	N/m^2
Pl_{pre}	Predicted pressure in left chamber	N/m^2
Pr	Pressure in right chamber	N/m^2
Pr_{pre}	Predicted pressure in right chamber	N/m^2
Ps	System pressure	N/m^2
P_{st}	Static pressure	N/m^2
P_u	Upstream pressure	N/m^2
P_{vc}	Pressure at vena contracta	N/m^2
Q	Volumetric flowrate	m^3/s
q	Heat transfer by conduction	J
R	Gas constant	m^2/s^2K
Re	Reynolds number	-

R_h	Sensor electrical resistance	Ω
R_t	Transmission line radius	m
r, θ, z	Cylindrical coordinates	-
T	Sampling time	s
T_s	System temperature	K or ^{0}C
t	Time	s
U	Fluid velocity vector	m/s
u_m	Mean velocity of air	m/s
$u_{z\text{-}max}$	Maximum air flow velocity in z-direction	m/s
u_∞	Free stream velocity of air	m/s
u, v, w	Fluid velocity components in Cartesian coordinates	m/s
V	Volume	m^3
V_a	Air volume expanded to atmospheric pressure	m^3
V_c	Volume at cut-off implementation	m^3
V_{lm}	Lumped volume	m^3
V_{mv}	Electrical signal to main directional valve	V
V_o	Full volume of cylinder	m^3
V_t	Transmission line volume	m^3
V1-V5	Voltages to solenoid valves	V
v_p	Piston velocity	m/s
W_d	Work done by air	J
$X_{1\text{-}4}$	Directional valve designation	-
$\overline{X}$	Valve floor opening	-
x_p	Piston displacement	m
x_{pmax}	Maximum piston displacement	m
x_{pre}	Predicted piston displacement	m
x, y, z	Cartesian coordinates	-
Z	Air flow displacement	m
z^{-1}	Sampling time shift operator	-
$(4f)$	D'Arcy friction factor	-
β_a	Air bulk modulus	N/m^2
β_e	Effective bulk modulus	N/m^2
β_t	Transmission line bulk modulus	N/m^2

α	Poisson's ratio	-
σ	Thermal resistivity of sensor	Ωm/K
δ^0	Flow discharge angle (jet angle)	degree
ε	Young's modulus	N/m^2
γ	Air expansion index	-
κ	Bulk viscosity	kg/ms
η	Percentage energy saving ratio	%
ρ	Density	kg/m^3
τ	Viscous stress tensor	N/m^2
μ	Coefficient of bulk viscosity, dynamic viscosity	kg/ms
$\mu`$	Second coefficient of bulk viscosity, dynamic viscosity	kg/ms
ν	Kinematic viscosity	m^2/s
Π	Stress tensor	N/m^2
Φ	Energy dissipative function	kg/ms^3
Δ	Increment	-
∇	Gradient	-

Chapter 1

Introduction

Pneumatic systems use pressurised gases for power transmission. The use of compressed air as power source has grown rapidly recently and at present is used in all branches of industry[1]. They are mainly used in production lines, food preparation, robotics etc. The advantages of pneumatics can be summarised below:

a) Pneumatic components are relatively cheap and readily available off the shelf with wide choice of specifications.
b) Pneumatic components are reliable, adaptable and can be cheaply maintained.
c) There is no fire hazard when pneumatics is used. Therefore it can be operated under high risk conditions where risk of explosion would prohibit the use of electricity.
d) Compressed air is not inflammable and pneumatic system can be used in high temperature conditions (80^0C-90^0C).
e) Pneumatic systems are clean.

As with other type of power transmission, a pneumatic system also has its disadvantages such as:

a) Compressed air is expensive on a power basis as compared to electricity or hydraulics.
b) It is difficult to achieve extreme accuracy of feed since air is compressible and thus it cannot compete with hydraulics.
c) The transmission of air in pipe is slower than the transmission of hydraulic fluids. This effect is important especially in long transmission line.
d) In large force actuator applications, the pneumatic cylinder needs to be large in size compared to using a hydraulic cylinder.
e) Air leakage is hard to control.

Energy issues have long been neglected in the sector of pneumatic systems. In the past decade these topics have begun to attract increasing interest, partly as a result of changes on the international scene. Energy consumption is an increasing global concern in various industrial sectors, which are reported by the UK government energy efficiency best practice program.

Of particular in this context was the 1997 Tokyo conference[2], which called for a 7% reduction in CO_2 emissions from 1995 levels. This is in accordance of ISO 14000 series in relation to environmental management and international agreement held in Kyoto in the same year.

This cut impacts a number of general aspects of pneumatic systems, from the generation of compressed air to its distribution and end use. In practical industrial application of pneumatics, issues of energy saving are receiving attention due to the considerable amount of compressed air wasted in operation.

Kagawa[3] investigated pneumatic energy assessment considering energy consumption in the production of compressed air and in the application of the air energy, and reported that a compressed air system is actually expensive to operate.

As regards to the efficiency of end circuits, it should be noted that the efficiency of pneumatic circuits can be rated at only 20%, as against 80% for electrical systems and 40% for hydraulic systems.

Regarding the use of air cylinders in pneumatic systems, several energy-saving methods have been investigated previously. In general, most researches suggested that air economy should feature much more in future machine design considerations, particularly with large or frequently-operated actuators, and proposes variety of methods that can be considered for pneumatic energy saving in machine design, system operation and the re-use of wasted energy.

There are a variety of techniques developed for pneumatic applications, such as multiple air compressor installations, variable-speed compressors, pressure conservation, and computerized automatic control. For example automatic control

system has reduced compressed air generation costs by 18.5% at Land Rover, without disrupting production schedules. The overall costs for the systems produced a payback of 16 months, which could be replicated on most compressed air system using three or more compressors[2].

Pu[4] suggested a new flow path that can be created between the inlet and outlet chambers of the pneumatic cylinder. For example during the deceleration phase in a point-to-point actuator positioning applications, the inlet and outlet chambers can be connected thus allowing pressure in the cylinder chambers to be charged or discharged much more rapidly. The author also suggested the use of compressed air in the outlet chamber for increasing the pressure level of the current inlet chamber rather than exhausting the air to atmosphere to reduce energy waste.

Wang[5] presented an energy analysis method of servo pneumatic actuators systems. In this study, the author investigated the profile for servo pneumatic actuators that leads the system to use the least amount of compressed air. This was done by linearizing the non-linear system using input/output state feedback and by applying energy efficient optimal control theory to the linearized system.

Dakkan[6] meanwhile suggested an energy saving approach to the control of pneumatic servo systems in which the author proposed that a fluid powered system only needs to draw energy from high pressure fluid supply during the power stroke of the actuator and not when dissipating power.

1.1 Call for efficient energy consumption

The total annual compressed air wasted in UK is about £100 million[7]. The tragedy is it would cost considerably less than £100 million to fix. With energy taxes that came into effect in 2002, it is a legal requirement to use energy efficiently. Designers of air-driven machines are forced to make their creations more energy efficient. Many people think compressed air is free because it is available on tap, people think nothing of leaving it running. This is due to ignorance since few are aware that it costs up to ten times more than equivalent power in electricity.

Energy Audit Management Procedure (AUDIT) project was launched in March 1998 to look at energy auditing within the European Union. The objectives of the AUDIT are:

a) To develop common state-of-the-art energy audit models.
b) To harmonise the definitions on energy auditing.
c) To develop adaptable schemes and procedures for program administration.
d) To encourage authorities to start-up national program activities.

Therefore, with the existence of such a project, the industrial sectors can benefit from the evaluation of current energy consumption and the identification of energy saving possibilities that can be efficiently utilised.

Another effort by the government is the introduction of Energy Efficiency Best Practice Program (EEBPP) which is urging industry to be more frugal and efficient in its use of energy. Now the Carbon Trust and other UK government research councils are holding a series of seminars run jointly by the EEBPP and fluid power component manufacturers. The seminars aim to raise awareness of the importance of energy efficiency.

The aim of the Carbon Trust is to help organisations reduce their carbon emissions and develop commercial low carbon technologies through improved energy efficiency and the broader strategic issues of carbon management. They also provide financial incentive schemes to help organisations invest in the necessary technology. In addition to this Carbon Trust encourage changes in attitudes, behaviour and business processes by informing business, government and investors on how they can most effectively respond to climate change.

1.2 Energy saving possibilities in compressed air system

Steps that can be taken to improve the efficiency of air consumption in compressed air system can be divided into 3 main areas namely generation, distribution and machine design.

1.2.1 Generation

In many cases, heat generated is usually wasted in the generation of compressed air. Efforts should be made to utilise this wasted form of energy by the use of heat of compression and preferably also the mechanical and electrical losses in the compressor and drive motor.

It is ideal if the heat can be used for an application. For example if air is heated, it can be employed for space heating in winter. Furthermore since it is easy to pipe compressed air rather than to duct the warm air over long distances, compressors can be located singly where heat is needed. With current availability of modern silencing and remote monitoring, this of course can be made possible.

1.2.2 Distribution

In the distribution of compressed air, various measures can be taken to improve the accuracy of system control for example in different working pressure conditions, it is better to separate compressors for high and low pressure applications.

In the control of system pressure, it is more accurate if the pressure is sensed near mid-point rather than adjacent to the compressor. However in doing so, care must be taken to avoid control instability.

Using standard flow velocity to determine pipe size can be very inaccurate. Instead one should decide on the pressure drop which can be tolerated and then using available charts to decide appropriate pipe size.

Pneumatic systems used in industry apply a ring main loop where the off-takes are located in a ring. This is better than positioning multiple off-takes along the main supply line. However isolation of a section is rather awkward and flow measurement is difficult to implement. It is proposed that a single branching main with off-takes to groups of machines may probably be better off than using a ring main loop.

Air off-takes are of course fitted with an isolating valve, and where necessary a filter and lubricator. It is recommended that the use of pressure reducing valves to enable the supply to each machine should be kept at a minimum though keeping a satisfactory operation. It is also appropriate that the consumption is to be monitored by using a commercially available flowmeter. A good design is to include quick-release couplings to enable one to be fitted when needed.

In areas where reliable air pressure is essential for a particular application and large demands elsewhere can disrupt this, the outlet can be protected by a non-return valve or pressure-maintaining valve with a local reservoir where necessary. This will be cheaper than utilising special compressors to remedy this. The availability of air-to-air intensifiers to provide a higher local pressure can also be used.

1.2.3 Machine design and control

Regarding the aspect of machine design, air economy should be featured more prominently in design considerations particularly with large or frequently operated actuators. Directing initial discharges to intermediate pressure line for use in cushioning etc. and remainder of it goes to the exhaust is a great way of harnessing the best out of compressed air.

One of the steps in reducing air consumption when using pneumatic actuator is in the case of light advance followed by high force. Built-in intensifiers or other lever motion can be used. It is an advantage to avoid having to fill a long and fat actuator for each stroke.

For movement (without the need for a high final force), air should be cut-off when stroke reaches the end. It is also possible to cut-off earlier and allowing the air in the actuator to expand and complete the stroke. These are known as end-stroke cut-off and predicted cut-off respectively. These aspect of energy saving are elaborated further in segment 1.4 Energy Saving Possibilities in PTP actuation as well as some suggestions for better actuator design.

1.3 The conventional point-to-point (PTP) actuation

In the actuation process of a cylinder, pressurised air which contains potential energy is being delivered to the driving chamber, the other side being the exhausting chamber. In a conventional operation, the cylinder is actuated without the cut-off of the supply pressure at the main directional valve in the whole process. Note that as the piston reaches the stroke end, compressed air is still being delivered to the driving chamber. The pressure in the driving chamber increases until it reaches the supply pressure while the pressure in the exhausting chamber drops to atmospheric pressure. The potential energy stored in the driving chamber is often wasted by exhausting the air to atmosphere in the return stroke. This conventional actuation will be the basis on which all energy saving methods presented in this thesis shall be compared with.

Figure (1.1) outlines a typical PTP circuit set-up, where a double-rod-double acting pneumatic cylinder is used. Actuation of the cylinder is controlled by a directional valve. Piston displacement is determined by the use of an LVDT. Pressures in both chambers (Pl and Pr) are measured using pressure transducers and the supply pressure is controlled using a pressure regulator. A commercial data acquisition processor (DAP) can be incorporated into the system to capture measured data from sensors and to provide control signals (V1, V2, V3) to the valves and pressure regulator.

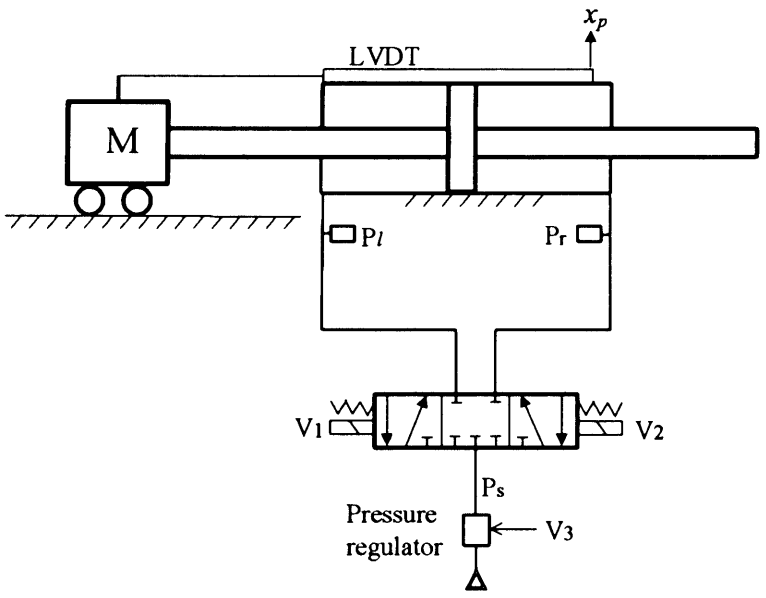

Figure 1.1: PTP Circuit

1.4 Energy saving methods in PTP actuation

Technically one of the favourable approaches to energy saving in pneumatic point-to-point actuation is to recycle all exhaust air back to the compressor and operating a whole installation between two pressure levels both well above atmospheric pressure. However it is too complicated and costly. Previous experience shows that in implementing such an idea one should consider a hydraulic system instead rather than dwell consistently with complexities in utilising highly compressible working fluid.

Based on work by Arinaga[8], possible ways of energy saving can be divided into 4 and they are:

a) The reduction in the air consumption of pneumatic equipments.
b) The effective use of exhaust air.
c) Measures to reduce the pressure loss and prevent air leakage from the air source to the equipments.
d) The pressure reduction of the air blow.

Furthermore in the case of pneumatic actuator usage, it is highly commendable to only use a required ram size and provide room for larger ram if there is a need for it. It is also worthwhile to minimise dead-space (air filled space) by incorporating features as listed below:

a) Piston should fit closely to ends of bores.
b) Inlet valves should be mounted onto rams with short pipe runs.
c) Short stroke actuator with mechanical adjustments if preferable instead of a long stroke actuator.

Reduction in the air consumption is the most effective way for energy saving since they are driven by the compressed air which is once saved in the air tank. It is necessary to improve the driving method and reduce the driving pressure.

It is in the above paragraph that two main ways in reducing air consumption in pneumatic system for pneumatic actuator especially in point-to-point (PTP) application were recognised and they can be classified as below:

a) Cutting off the air supply when piston reaches maximum stroke.
b) Cutting off the air supply **before** the piston reaches maximum stroke.

For case (a), in the case of PTP driving, the air supplied after the piston reaches the end stroke is wasted if the piston does not need to have a larger stiffness at the end stroke. Therefore in PTP applications, it is possible to reduce the air consumption by cutting off the supply pressure in both cases as stated above. Furthermore the latter energy saving method can be made possible by using prediction based on the Gas Law.

In this thesis, the investigation of both energy saving methods proposed above was carried out using computer simulations and practical experiment. Naturally both of the methods proposed were applied to the pneumatic actuator which is the most common element in pneumatic system.

1.4.1 Air supply cut-off at end stroke

Recent research undertaken by Arinaga[8] on cut-off methods in pneumatic actuation has presented energy saving though the optimum cut-off time still remains an undetermined issue. Attention was given to stick-slip phenomena at low speed actuation, and the mapping of stick-slip to driving speed and load mass. Research results reported show that there is potential for energy saving if an optimum cut-off time can be determined. This is also a critical point since there is risk of disrupting the actuation demand if the cut-off is committed at an inappropriate time. Figure (1.2) shows the experimental apparatus used.

The experimental set-up consists of a pneumatic cylinder[9,10]. The cart which moves on a linear bearing is connected to the rod. Piston displacement is measured by the use of a potentiometer. Pressures in both chambers (driving and exhausting sides)

are measured by pressure transducers. An analysing recorder was used to records these signal while the velocity of the piston is obtained by differentiating the signal of the piston displacement.

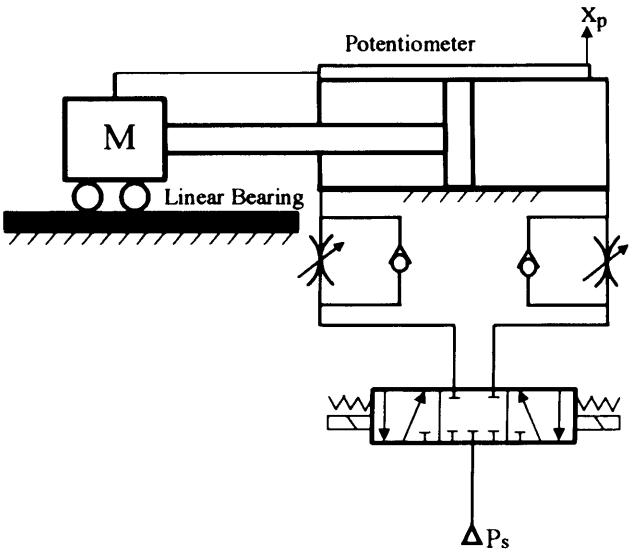

Figure 1.2: Meter-in PTP circuit as used by Arinaga[8]

It was found that in PTP driving with a meter-in circuit[10] where pressure in the rod-side cylinder chamber is equal to atmospheric pressure and that the supply-side restrictor reaches critical condition has the possibility of reducing air consumption because the air supply to the cylinder can be cut-off at the end stroke. It was proposed to take the method of energy saving by cutting off the supply air when the piston reaches the stroke-end if the piston does not need to have larger stiffness.

It turns out that the response after the piston reaches the stroke-end, using meter-in circuit is different from that of a conventional drive. The supply air pressure causes the pressure rise in the conventional drive method after the piston reaches the stroke-end. On the other hand, the heat transfer between the cylinder body and the air in the cylinder causes the pressure rise of adopting the method proposed. As a result, it was found that air consumption were able to be curtailed by approximately maximum of 70% in simulation and by 40% in experiment.

One of the problems of the method is stick-slip motion that often occurs at low speed however the tendency does not always apply to all driving conditions. Effects such as the mass of the load and thus the average driving speed of the piston play a major role in the stick-slip problem. It was found that stick-slip motion diminishes as the mass of load increases. As a conclusion, it is possible to apply the method proposed to the cylinder at low speeds (between 0.01m/s to 0.25m/s), depending on the driving conditions.

1.4.2 Air supply cut-off using model prediction

For the energy saving purpose, a cut-off may be applied prior to the piston reaching the full stroke. However there will be a doubt that the potential energy contained in the driving chamber would be enough for completing the actuation task satisfactorily. On the other side, the energy saving will not be significant if a late cut-off is applied. The problem now is to determine the time for the most effective energy saving and satisfactory completion of the actuation task.

A predicted cut-off method is proposed[11] to determine the cut-off time at which the potential energy contained in the driving chamber becomes enough to overcome the friction force and the loaded mass while completing the full stroke actuation.

If a cut-off is applied, the pressure will decrease as the stroke length increases. This can be confirmed with the Gas Law as follows.

$$PV^{\gamma} = P_c V_c^{\gamma} \quad \text{..... (1.1)}$$

P is the pressure in the enclosed chamber of varying volume V, and γ is the air expansion index. The pressure and the volume at the cut-off time are P_c and V_c respectively. The air expansion process in practice is neither isothermal nor adiabatic and γ needs to be identified using measured data.

The static friction force is F_s and the corresponding required pressure to overcome it is:

$$P_{st} = F_s / A_p \quad \text{..... (1.2)}$$

A_p is the cross-sectional area of the piston. With this knowledge, the predicted cut-off algorithm can be written as follows:

$$P > P_{st}\left(V_o / V\right)^{\gamma} \quad \text{..... (1.3)}$$

V_o is the volume of the driving chamber at the full stroke position. When the pressure P and volume V at the driving chamber matches the criterion in equation (1.3), cut-off to the supply pressure can be carried out and the stick-slip phenomena can be prevented provided that the static friction and the air expansion index are identified correctly. Once the cut-off is committed there is no pneumatic energy being delivered to the actuator from the main supply and the motion of the actuator is driven by the air potential energy in the driving chamber. The air state change on pressure and volume in the driving chamber follows the Gas Law as shown in equation (1.1) after the cut-off. Figure (1.3) shows the experimental set-up.

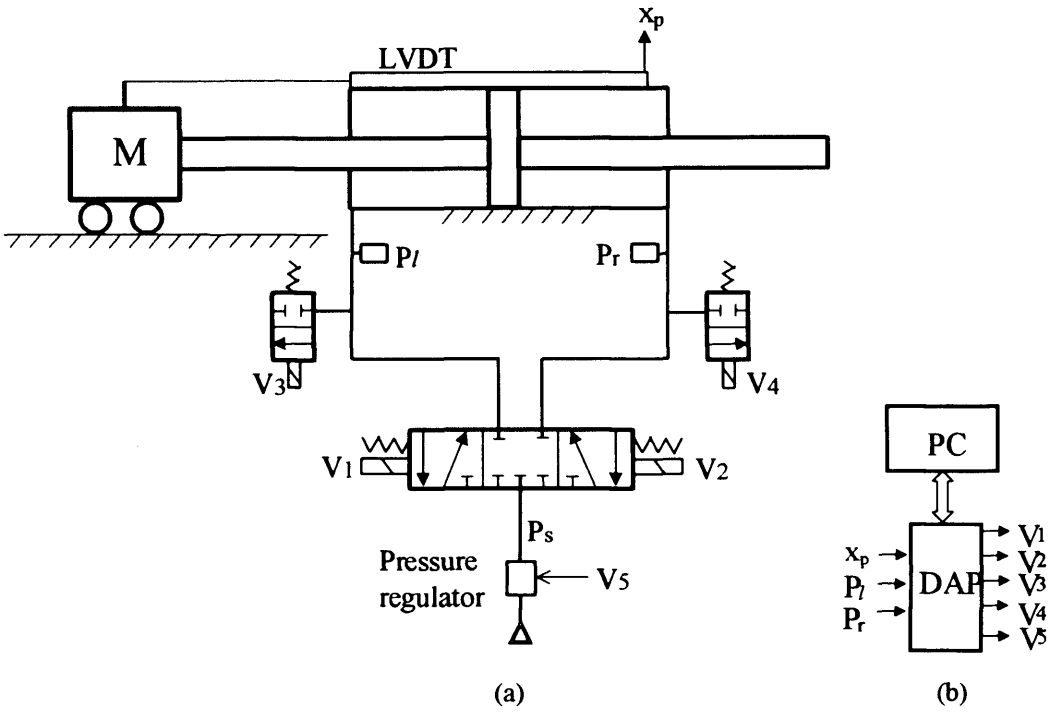

Figure 1.3: Experiment set-up (a) and DAP terminals (b)

1.4.3 Recycling exhaust air for return stroke

Another possibility for energy saving is to push the exhausted air from the outlet chamber into a reservoir and then use it to power the cylinder's return strokes. A partial amount of this air can also be channelled back to the driving chamber during the power stroke. Theoretically this approach will save air, speeds up the power stroke and permits smoother operation.

This approach increases both the efficiency and maximum actuation speed in a test system designed to work under typical industrial conditions. The technology is appropriate to any pneumatic systems but is currently optimised for automated production line applications. This technology has been developed at the University of Chemnitz in Germany.

This energy saving method can reduce the compressed air consumption and hence reducing the energy requirements and cost. Reducing the air consumption of pneumatic systems is important to make pneumatic systems more competitive

compared with direct electrically driven systems which although more efficient, generally cost considerably more to implement.

Based on a technical feature by Shelley[12] from September 1999 issue of Eureka Magazine, there are three possible ways of reducing energy wastage from pneumatic actuator systems. The first possibility is to have a high pressure on the power side of cylinders and use a lower pressure for the return stroke. Theoretically this energy saving approach is feasible. However this method can only give economic advantage if there are two air supply mains available to the system. Another possibility is to harness as much as possible the expansion work available in the compressed air supplied for the power stroke. The mechanism of this method is that after a certain pressure in the driving chamber of a pneumatic cylinder has been reached, the air supply is then cut-off and the remainder of the stroke is then powered by the expansion of the compressed air already in the cylinder. However this result in a decreasing force and reduced acceleration towards the end of the cylinder's stroke as shall be presented by studies presented in this thesis.

The third energy saving possibility which is the basis of the system developed at Chemnitz is the accumulation of air from the exhausting chamber and then using it to power the return stroke. The cushioning of the pneumatic cylinder at the end of the stroke is provided by the accumulated air in the air reservoir. This cushioning technique is called an air spring system and based on the performed experiments; this method improves the dynamic performance of the system while reducing impact damage and noise at the same time.

Based on the pneumatic circuit presented in Figure (1.4), the return stroke is powered almost entirely but not wholly by air compressed into the accumulator during the power stroke. Due to the fact that air that is being pushed out of the rod side of the cylinder is at lower pressure, the power stroke proceeds faster than previously since a smaller mass of air has to be pushed out of the exhausting chamber. The piston was then brought to a stop by the cushioning provided by the air in the accumulator.

Initially valve X_1 is actuated to allow the main supply pressure to push the piston during the power stroke. The air in the exhausting chamber then passes through valve X_3 and into the accumulator via a check valve. Valve X_3 is then shifted to allow the air in the accumulator to be used for powering the return stroke. During this process, the pressure regulator can also provide the necessary air pressure from the mains supply. The air in the exhausting chamber then passes through valve X_1 then valve X_2 and finally out to atmosphere.

The adjustable pressure regulator is used to maintain the needed pressure in the accumulator used for powering the return stroke and the cushioning of the cylinder during the power stroke. This also allows fresh supply of compressed air to be fed to the accumulator to compensate for any pressure loss.

Valve X_4 is used to ensure defined pre-actuation pressure in the accumulator. During the power and return strokes, this valve is shut. By defining the pre-actuation pressure in the accumulator, it is also possible to provide the required air cushioning of the cylinder during the initial power stroke when there is no air being accumulated in the accumulator.

From experiments results, it was found there is a large acceleration at the beginning of the stroke if the accumulator is set to have low pre-pressures. Because the counteracting pressure is then low, it is possible that the piston may run hard into the end stop and causes cylinder damage. With higher pre-pressures in the accumulator, the piston's accelerations and maximum speeds are relatively lower and the air spring provided by the accumulated air are then able to cushion the piston at the end of its stroke.

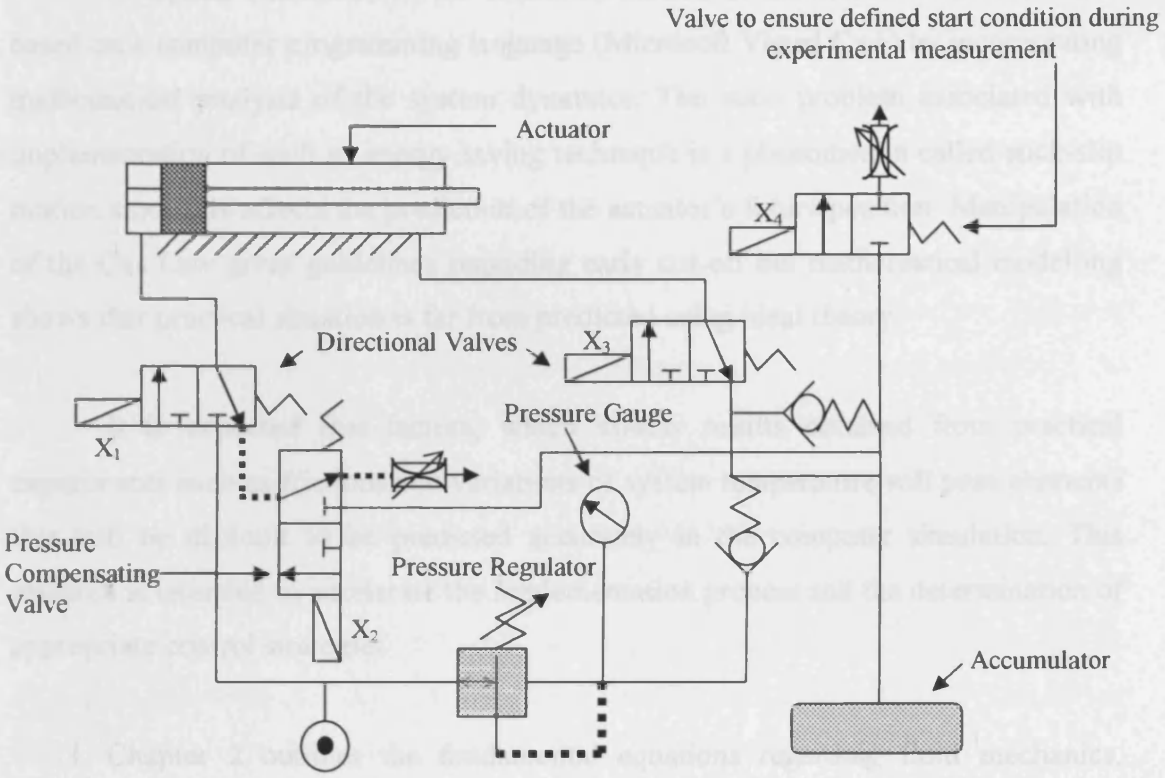

Figure 1.4: Experimental set-up of research in University of Chemnitz, Germany[12]

It was concluded that by reducing the accumulator volume in this energy saving approach results in increased pressure, greater piston deceleration at the end stroke while maintaining a smooth cylinder actuation. Short stroke times can be implemented by using an accumulator volume of 0.75 times the cylinder volume. It was also found that by using an accumulator volume of 0.25 times the cylinder volume, maximum compression work can be attained and the piston decelerates to 0.1m/s shortly before reaching the end stroke position.

1.5 Aims of this study and thesis organisation

This thesis studies the implementation of cut-off to the air-supply in a point-to-point (PTP) pneumatic actuator system and implications of this energy saving technique that will be incorporated in a conventional pneumatic system. The critical point is to determine the cut-off time to maximise energy saving while still performing the actuating task satisfactorily.

Computer simulation of the extension motion of the actuator was conducted based on a computer programming language (Microsoft Visual C++) by incorporating mathematical analysis of the system dynamics. The main problem associated with implementation of such an energy saving technique is a phenomenon called stick-slip motion since this affects the prediction of the actuator's future position. Manipulation of the Gas Law gives guidelines regarding early cut-off but mathematical modelling shows that practical situation is far from predicted using ideal theory.

It is expected that factors, which affects results obtained from practical experiments such as frictions and variations of system temperature will pose elements that will be difficult to be predicted accurately in the computer simulation. This research is intended to accelerate the implementation process and the determination of appropriate control strategies.

Chapter 2 outlines the fundamental equations regarding fluid mechanics. Continuity, momentum and energy equations are presented including the relevant equation of state. The derivation of Navier-Stokes equations based on the conservation laws is also included. These equations are then transformed into vector format in the form of Cartesian coordinates and finally converted to cylindrical coordinates.

Chapter 3 highlights the proposed energy saving test rig and its system components. Transducers, valves, pneumatic actuator, control package, electrical components and data acquisition peripherals are introduced. Working principles of components are also explained where necessary. Chapter 3 also introduces IFM high-speed flowmeter that uses hot-wire concept for fast response and the data acquisition processor (DAP) used to capture the measured data. Information regarding hot-wire and flowmeter working principles are outlined as well as the mathematical volumetric to mass flowrate conversion. Results of an investigation into temperature-pressure relationship using thermocouples installed in the test rig are also included. Brief description including a sample of the DAPView control program is provided at the end of the chapter.

Chapter 4 presents the study of mathematical modelling of a fluid transmission line. This includes the understanding of orifice equation, lumped volume, and types of finite difference modelling such as Lax, Lax-Wendroff, MacCormack and Upwind methods. Problems that are normally associated with finite difference schemes such as truncation error, discretization error including consistency and stability issues are also presented. The mechanism of applying finite difference approach to an air flow in a transmission line were outlined as well as steps to identify the primitive variables from vector form of the conservation laws. Calculation of mean air flow velocity as well as effective transmission line bulk modulus that can be included in future computer simulations are presented as well. The investigation into pressure and flowrate dynamics was done by utilising two IFM flowmeters. Using these fast response transducers allows pressure and flowrate dynamic behaviour in air transmission line to be observed. This provides data which are highly important in implementing computer simulations. The transmission line computer simulation results are presented for both lumped and finite difference approach.

Chapter 5 presents the energy saving realisation and results obtained from the test rig. Energy saving techniques are compared with conventional methods in terms of system response including air and energy consumption. Important parameters such as air expansion index and pneumatic cylinder friction characteristics are also outlined. Discussion regarding effects of cut-off to actuation process, time-delay of directional valve and effect of pneumatic cylinder cushioning are presented at the end of this chapter.

Chapter 6 presents the simulation of the proposed energy saving system. The air transmission line dynamics are incorporated into the energy saving system modelling. Simulations of the proposed energy saving system are performed and these include the conventional point-to-point (PTP) actuation, end stroke cut-off and predicted cut-off actuation. All computer simulations are done in the time-domain and results obtained are compared with the captured experimental data. Future research that can be done in order to improve the simulation and control of the proposed energy saving methods is outlined at the end of this chapter. This includes investigation on the bulk modulus effect that can be incorporated into the simulation

algorithm and online adaptive artificial neural networks implementation in the proposed energy saving control system.

Discussions are given throughout the chapters and conclusions are presented in chapter 7.

Chapter 2

Fundamental Equations

In this chapter, the governing equations of fluid mechanics are described. These are equations of great importance in modelling fluid dynamics.

The fundamental equations of fluid dynamics are based on the following universal laws of conservation[13,14,15,16]:

a) Conservation of Mass
b) Conservation of Momentum
c) Conservation of Energy

Conservation of mass to a fluid flow is called the continuity equation while the conservation of momentum is Newton's Second Law. When the latter law is applied to a fluid flow it yields a vector equation known as the momentum equation. The conservation of energy is the application of the First Law of Thermodynamics to a fluid passing through an infinitesimal, fixed control volume. Finally it is a must to close the system of equations. This is known as the equation of state which relates the variables of pressure P, density ρ and temperature T_s.

2.1 Continuity equation

This equation is the application of mass conservation law to a fluid passing through an infinitesimal fixed control volume and thus yields the following equation of continuity.

$$\frac{\partial \rho}{\partial t} + \nabla \cdot (\rho U) = 0 \quad \text{..... (2.1)}$$

Fluid density is designated as ρ and fluid velocity as U. The first term in this equation represents the rate of increase of density in the control volume and the

second term represents the rate of mass flux passing out of the control surface which surrounds the control volume per unit volume.

Equation (2.1) was derived using the Eularian approach. The Eularian approach concentrates on fluid properties at a point in space (x, y, z) within a time-domain t, thus it can be defined as a field approach. In this approach a fixed control volume is utilized and changes to the fluid are monitored as the fluid passes the control volume.

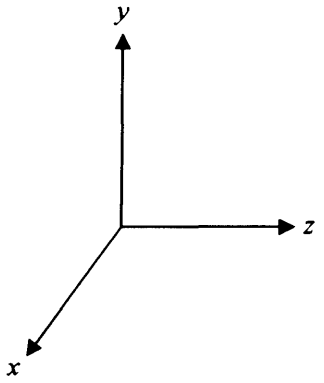

Figure 2.1: Cartesian coordinates

For Cartesian coordinate system where (u, v, w) represents the (x, y, z) components of the velocity vector, equation (2.1) yields as shown below.

$$\frac{\partial \rho}{\partial t}+\frac{\partial}{\partial x}(\rho u)+\frac{\partial}{\partial y}(\rho v)+\frac{\partial}{\partial z}(\rho w)=0 \quad \text{..... (2.2)}$$

Note that the above equation is in conservation-law (divergence) format. A flow in which the density of each fluid element remains constant is called incompressible and mathematically it can be presented as:

$$\frac{D\rho}{Dt}=0 \quad \text{..... (2.3)}$$

With the above assumption, the term ($\nabla \cdot U$) reduces to zero. Therefore we have:

$$\frac{\partial u}{\partial x}+\frac{\partial v}{\partial y}+\frac{\partial w}{\partial z}=0 \quad \text{..... (2.4)}$$

For steady air flows with velocity vector U of less than 100 m/s or Mach number M_{mach} of less than 0.3, the assumption of incompressibility can be accepted as a good approximation[13].

2.2 Momentum equation

When Newton's Second Law of motion is applied to a fluid passing through an infinitesimal fixed control volume, the following momentum equation is obtained[13,14,15]:

$$\frac{\partial}{\partial t}(\rho U)+\nabla\cdot\rho UU=\rho f+\nabla\cdot\Pi_{ij} \quad \text{..... (2.5)}$$

The first term in this equation represents the rate of increase of momentum per unit volume in the control volume.

The second term represents the rate of momentum lost by convection per unit volume through the control surface. ($\nabla\cdot\rho UU$) is called a tensor and this term is not of a simple divergence. This term can be expanded as:

$$\nabla\cdot\rho UU=\rho U\cdot\nabla U+U(\nabla\cdot\rho U) \quad \text{..... (2.6)}$$

When the above is substituted into equation (2.5) and by using the continuity equation, the momentum equation reduces to:

$$\rho\frac{DU}{Dt}=\rho f+\nabla\cdot\Pi_{ij} \quad \text{..... (2.7)}$$

The first term on the right-hand side is the body force per unit volume. Body forces act at a distance and apply to the entire mass of the fluid. The most common

body force is the gravitational force. In this case the force per unit mass f equals the acceleration of the gravity vector g:

$$\rho f = \rho g \qquad (2.8)$$

The second term on the right hand side represents the surface forces per unit volume. These forces are applied by the external stresses on the fluid element. The stresses consist of normal stresses and shearing stresses, and are represented by the components of the stress tensor Π_{ij}. When approximate expressions are inserted for the shear stress tensor, equation (2.5) loses its generality.

In orthogonal curvilinear coordinates (i, j, k), the momentum equation without considering the body forces can be expressed as shown below:

$$\rho \frac{DU}{Dt} = \nabla \cdot \Pi_{ij} \qquad (2.9)$$

For Newtonian fluid[13] it can be deduced that:

$$\Pi_{ij} = -P\delta_{ij} + \mu\left(\frac{\partial u_i}{\partial x_j} + \frac{\partial u_j}{\partial x_i}\right) + \delta_{ij}\mu' \frac{\partial u_k}{\partial x_k} \qquad i, j, k, = 1,2,3 \qquad (2.10)$$

The term δ_{ij} is called the Kronecker delta function ($\delta_{ij} = 1$ if $i = j$ and $\delta_{ij} = 0$ if $i \neq j$) while (u_1, u_2, u_3) represent the three components of the velocity vector U which are (x_1, x_2, x_3) that represents the three components of the position vector. μ is the coefficient of dynamic viscosity and μ' is the second coefficient of viscosity. The two coefficients of viscosity are related to the coefficient of bulk viscosity κ by the equation shown below:

$$\kappa = \tfrac{2}{3}\mu + \mu' \qquad (2.11)$$

In general, it is believed that κ is negligible except in the study of the structure of shock waves and in the absorption and attenuation of acoustic waves. For this

reason, the bulk viscosity is ignored. With ($\kappa = 0$), the second coefficient of viscosity becomes

$$\mu' = -\tfrac{2}{3}\mu \qquad (2.12)$$

The stress tensor can then be written as:

$$\Pi_{ij} = -P\delta_{ij} + \mu\left[\left(\frac{\partial u_i}{\partial x_j} + \frac{\partial u_j}{\partial x_i}\right) - \frac{2}{3}\delta_{ij}\frac{\partial u_k}{\partial x_k}\right] \qquad i,j,k = 1,2,3 \qquad (2.13)$$

The stress tensor Π is frequently separated in the following manner:

$$\Pi_{ij} = -P\delta_{ij} + \tau_{ij} \qquad (2.14)$$

where τ_{ij} represents the viscous stress tensor given by:

$$\tau_{ij} = \mu\left[\left(\frac{\partial u_i}{\partial x_j} + \frac{\partial u_j}{\partial x_i}\right) - \frac{2}{3}\delta_{ij}\frac{\partial u_k}{\partial x_k}\right] \qquad i,j,k = 1,2,3 \qquad (2.15)$$

Substituting equation (2.13) into equation (2.9) yield the Navier-Stokes equation which is shown below:

$$\rho\frac{DU}{Dt} = \rho f - \nabla P + \frac{\partial}{\partial x_j}\left[\mu\left(\frac{\partial u_i}{\partial x_j} + \frac{\partial u_j}{\partial x_i}\right) - \frac{2}{3}\delta_{ij}\mu\frac{\partial u_k}{\partial x_k}\right] \qquad (2.16)$$

The Navier-Stokes equations form the basis upon which the entire science of flow theory has been developed. For a three-dimensional Cartesian coordinate system, the Navier-Stokes equations can be represented as:

$$\rho\frac{Du}{Dt}=\rho f_x-\frac{\partial P}{\partial x}+\frac{\partial}{\partial x}\left[\frac{2}{3}\mu\left(2\frac{\partial u}{\partial x}-\frac{\partial v}{\partial y}-\frac{\partial w}{\partial z}\right)\right]+\frac{\partial}{\partial y}\left[\mu\left(\frac{\partial u}{\partial y}+\frac{\partial v}{\partial x}\right)\right]+\frac{\partial}{\partial z}\left[\mu\left(\frac{\partial w}{\partial x}+\frac{\partial u}{\partial z}\right)\right] \quad \text{..... (2.17)}$$

$$\rho\frac{Dv}{Dt}=\rho f_y-\frac{\partial P}{\partial y}+\frac{\partial}{\partial x}\left[\mu\left(\frac{\partial v}{\partial x}+\frac{\partial u}{\partial y}\right)\right]+\frac{\partial}{\partial y}\left[\frac{2}{3}\mu\left(2\frac{\partial v}{\partial y}-\frac{\partial u}{\partial x}-\frac{\partial w}{\partial z}\right)\right]+\frac{\partial}{\partial z}\left[\mu\left(\frac{\partial v}{\partial z}+\frac{\partial w}{\partial y}\right)\right] \quad \text{..... (2.18)}$$

$$\rho\frac{Dw}{Dt}=\rho f_z-\frac{\partial P}{\partial z}+\frac{\partial}{\partial x}\left[\mu\left(\frac{\partial w}{\partial x}+\frac{\partial u}{\partial z}\right)\right]+\frac{\partial}{\partial y}\left[\mu\left(\frac{\partial v}{\partial z}+\frac{\partial w}{\partial y}\right)\right]+\frac{\partial}{\partial z}\left[\frac{2}{3}\mu\left(2\frac{\partial w}{\partial z}-\frac{\partial u}{\partial x}-\frac{\partial v}{\partial y}\right)\right] \quad \text{..... (2.19)}$$

Utilizing momentum equation (2.5), these equations can be rewritten in conservation-law form as follows:

$$\frac{\partial\rho u}{\partial t}+\frac{\partial}{\partial x}\left(\rho u^2+P-\tau_{xx}\right)+\frac{\partial}{\partial y}\left(\rho uv-\tau_{xy}\right)+\frac{\partial}{\partial z}\left(\rho uw-\tau_{xz}\right)=\rho f_x \quad \text{..... (2.20)}$$

$$\frac{\partial\rho v}{\partial t}+\frac{\partial}{\partial x}\left(\rho uv-\tau_{xy}\right)+\frac{\partial}{\partial y}\left(\rho v^2+P-\tau_{yy}\right)+\frac{\partial}{\partial z}\left(\rho uw-\tau_{yz}\right)=\rho f_y \quad \text{..... (2.21)}$$

$$\frac{\partial\rho w}{\partial t}+\frac{\partial}{\partial x}\left(\rho uw-\tau_{xz}\right)+\frac{\partial}{\partial y}\left(\rho uw-\tau_{yz}\right)+\frac{\partial}{\partial z}\left(\rho w^2+P-\tau_{zz}\right)=\rho f_z \quad \text{..... (2.22)}$$

The components of the viscous stress tensor τ_{ij} are given by:

$$\tau_{xx}=\frac{2}{3}\mu\left(2\frac{\partial u}{\partial x}-\frac{\partial v}{\partial y}-\frac{\partial w}{\partial z}\right) \quad \text{..... (2.23)}$$

$$\tau_{yy}=\frac{2}{3}\mu\left(2\frac{\partial v}{\partial y}-\frac{\partial u}{\partial x}-\frac{\partial w}{\partial z}\right) \quad \text{..... (2.24)}$$

$$\tau_{zz} = \frac{2}{3}\mu\left(2\frac{\partial w}{\partial z} - \frac{\partial u}{\partial x} - \frac{\partial v}{\partial y}\right) \quad \text{(2.25)}$$

$$\tau_{xy} = \mu\left(\frac{\partial u}{\partial y} + \frac{\partial v}{\partial x}\right) = \tau_{yx} \quad \text{(2.26)}$$

$$\tau_{xz} = \mu\left(\frac{\partial w}{\partial x} + \frac{\partial u}{\partial z}\right) = \tau_{zx} \quad \text{(2.27)}$$

$$\tau_{yz} = \mu\left(\frac{\partial v}{\partial z} + \frac{\partial w}{\partial y}\right) = \tau_{zy} \quad \text{(2.28)}$$

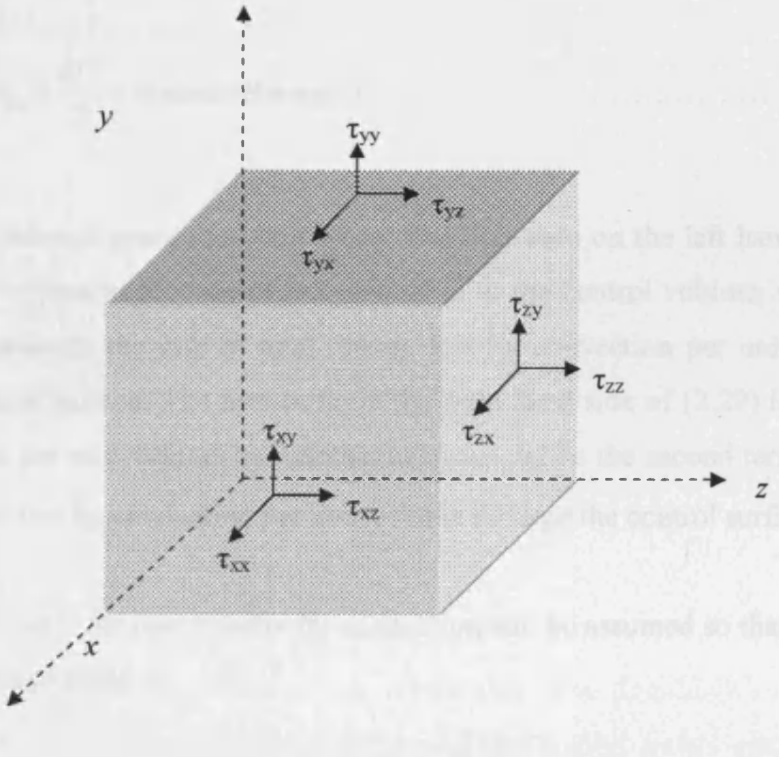

Figure 2.2: Viscous stress tensor diagram

Figure (2.2) shows the directions for the normal and shear stresses acting on three surfaces of the control volume. The outer subscript denotes the direction of the stress and the inner subscript denotes the plane in which the stress acts. These stresses create normal and tangential forces on the control surface.

2.3 Energy Equation

The first law of thermodynamics applied to a fluid passing through an infinitesimal, fixed control volume yields the following energy equation[13,14,15]

$$\frac{\partial E_t}{\partial t} + \nabla \cdot E_t U = \frac{\partial Q}{\partial t} - \nabla \cdot q + \rho f \cdot U + \nabla \cdot \left(\prod_{ij} \cdot U\right) \quad (2.29)$$

where E_t is the total energy per unit volume given by

$$E_t = \rho\left(e_{\text{int}} + \frac{U^2}{2} + PotentialEnergy + \ldots\right) \quad (2.30)$$

while e_{int} is the internal energy per unit mass. The first term on the left hand side of equation (2.29) represents the rate of increase of E_t in the control volume, while the second term represents the rate of total energy lost by convection per unit volume through the control surface. The first term on the right hand side of (2.29) is the rate of heat produced per unit volume by external agencies, while the second term $(\nabla \cdot q)$ is the rate of heat lost by conduction per unit volume through the control surface.

Fourier's law[15] for heat transfer by conduction will be assumed so that the heat transfer q can be expressed as

$$q = -k\nabla T_s \quad (2.31)$$

where k is the coefficient of thermal conductivity and T_s is the temperature. The third term on the right hand side of equation (2.29) represents the work done on the control

volume per unit volume by the body forces, while the fourth term represents the work done on the control volume per unit volume by the surface forces. The increase of energy in the system is equal to heat added to the system plus the work done on the system.

For Cartesian coordinate system, equation (2.29) can be rewritten in conservation law form as shown below.

$$\frac{\partial E_t}{\partial t} - \frac{\partial Q}{\partial t} - \rho\left(f_x u + f_y u + f_z w\right) + \frac{\partial}{\partial x}\left(E_t u + Pu - u\tau_{xx} - v\tau_{xy} - w\tau_{xz} + q_x\right)$$
$$+ \frac{\partial}{\partial y}\left(E_t v + Pv - u\tau_{xy} - v\tau_{yy} - w\tau_{yz} + q_y\right)$$
$$+ \frac{\partial}{\partial z}\left(E_t w + Pw - u\tau_{xz} - v\tau_{yz} - w\tau_{zz} + q_z\right) = 0 \quad \text{(2.32)}$$

Using continuity equation, the left hand side of equation (2.29) can be replaced as follows.

$$\rho \frac{D\left(E_t/\rho\right)}{Dt} = \frac{\partial E_t}{\partial t} + \nabla \cdot E_t U \quad \text{(2.33)}$$

The above is equivalent to

$$\rho \frac{D\left(E_t/\rho\right)}{Dt} = \rho \frac{De_{\text{int}}}{Dt} + \rho \frac{D\left(U^2/2\right)}{Dt} \quad \text{(2.34)}$$

if only internal energy and kinetic energy are considered to be significant in equation (2.30). By considering effects of internal energy e_{int} and kinetic energy and utilising momentum equation explained earlier in this chapter will yield the following equation.

$$\rho \frac{DU}{Dt} \cdot U = \rho f \cdot U - \nabla P \cdot U + \left(\nabla \cdot \tau_{ij}\right) \cdot U \quad \text{(2.35)}$$

Combination of equations (2.33, 2.34 and 2.35) yield:

$$\rho\frac{De_{\text{int}}}{Dt}+P(\nabla\cdot U)=\frac{\partial Q}{\partial t}-\nabla\cdot q+\nabla\cdot(\tau_{ij}\cdot U)-(\nabla\cdot\tau_{ij})\cdot U \quad \text{..... (2.36)}$$

The last two terms in equation (2.36) can be combined into a single term since:

$$\tau_{ij}\frac{\partial u_i}{\partial x_j}=\nabla\cdot(\tau_{ij}\cdot U)-(\nabla\cdot\tau_{ij})\cdot U \quad \text{..... (2.37)}$$

Equation (2.37) is called the dissipative function Φ and represents the rate at which mechanical energy is expended in the process of deformation of the fluid due to viscosity. Inserting the dissipation function into equation (2.36) yields:

$$\rho\frac{De_{\text{int}}}{Dt}+P(\nabla\cdot U)=\frac{\partial Q}{\partial t}-\nabla\cdot q+\Phi \quad \text{..... (2.38)}$$

Using the definition of enthalpy[13] of:

$$h=e_{\text{int}}+\frac{P}{\rho} \quad \text{..... (2.39)}$$

and the continuity equation, equation (2.38) can be written as:

$$\rho\frac{Dh}{Dt}=\frac{DP}{Dt}+\frac{\partial Q}{\partial t}-\nabla\cdot q+\Phi \quad \text{..... (2.40)}$$

For a Cartesian coordinate system, the dissipation function, which is always positive if $\mu'=-(2/3)\mu$ becomes:

$$\Phi = \mu\left[\begin{array}{l} 2\left(\frac{\partial u}{\partial x}\right)^2 + 2\left(\frac{\partial v}{\partial y}\right)^2 + 2\left(\frac{\partial w}{\partial z}\right)^2 + \left(\frac{\partial v}{\partial x} + \frac{\partial u}{\partial y}\right)^2 + \left(\frac{\partial w}{\partial y} + \frac{\partial v}{\partial z}\right)^2 \\ + \left(\frac{\partial u}{\partial z} + \frac{\partial w}{\partial x}\right)^2 - \frac{2}{3}\left(\frac{\partial u}{\partial x} + \frac{\partial v}{\partial y} + \frac{\partial w}{\partial z}\right)^2 \end{array}\right] \quad \ldots\ldots (2.41)$$

2.4 Equation of state

In order to close the system of fluid dynamic equation, it is necessary to establish the relationship between the thermodynamic variables (P, ρ, T_s, e_{int}, h) as well as to relate the transport properties which are dynamic viscosity variables (μ, k)[13,16].

In the case of compressible flow without external heat addition or body forces and by utilising equation (2.2) for the continuity equation, equations (2.17, 2.18, 2.19) for the momentum equations and energy equation (2.32), it can be deduced that there are 5 scalar equations containing 7 unknowns (ρ, P, e_{int}, T_s, u, v, w).

There is a need for 2 more equation to close the system. These equations can be obtained by determining the relationship that exists between the unknown variables. Relation of this type is known as equation of state. Based on the state principle of thermodynamics variables and assuming that the chemical composition of the fluid is not changing owing to diffusion or finite-rate chemical reactions, then equations of state in the form of perfect gas[15] as shown below can be used:

$$P = \rho R T_s \quad \ldots\ldots (2.42)$$

For most problems in gas dynamics, it is possible to assume a perfect gas. Perfect gas is defined as a gas whose intermolecular forces are negligible. R is defined as the gas constant. However it should be known that intermolecular forces become important under conditions of high pressure and relatively low temperature. For these conditions, the gas no longer obeys the perfect gas equation of state and alternative equation of state must be used.

The determination of the second state equation is based on a calorically perfect gas which is defined as a perfect gas with constant specific heats (C_p, C_v). Therefore the ratio of specific heats γ remains constant. For air at standard condition, $R = 287 m^2 s^{-2} K^{-1}$ and $\gamma = 1.4$. Below is the equation that relates the thermodynamic properties of a calorically perfect gas.

$$T_s = \frac{(\gamma - 1) e_{int}}{R} \quad \text{(2.43)}$$

2.5 Vector form of equations

It is convenient to combine the equations into a compact vector form. The compressible Navier-Stokes equations as shown earlier in equations (2.17, 2.18, 2.19) in three-dimensional Cartesian coordinates without body forces, mass diffusion, finite-rate chemical reactions, or external heat addition can be written in vector form as:

$$\frac{\partial D}{\partial t} + \frac{\partial E}{\partial x} + \frac{\partial F}{\partial y} + \frac{\partial G}{\partial z} = 0 \quad \text{(2.44)}$$

where D, E, F and G are vectors given by:

$$D = \begin{bmatrix} \rho \\ \rho u \\ \rho v \\ \rho w \\ E_t \end{bmatrix} \quad \text{(2.45)}$$

$$E = \begin{bmatrix} \rho u \\ \rho u^2 + P - \tau_{xx} \\ \rho uv - \tau_{xy} \\ \rho uw - \tau_{xz} \\ (E_t + P)u - u\tau_{xx} - v\tau_{xy} - w\tau_{xz} + q_x \end{bmatrix} \quad \text{(2.46)}$$

$$F = \begin{bmatrix} \rho v \\ \rho uv - \tau_{xy} \\ \rho v^2 + P - \tau_{yy} \\ \rho vw - \tau_{yz} \\ (E_t + P)v - u\tau_{xy} - v\tau_{yy} - w\tau_{yz} + q_y \end{bmatrix} \quad \text{(2.47)}$$

$$G = \begin{bmatrix} \rho w \\ \rho uw - \tau_{xz} \\ \rho vw - \tau_{yz} \\ \rho w^2 + P - \tau_{zz} \\ (E_t + P)w - u\tau_{xz} - v\tau_{yz} - w\tau_{zz} + q_z \end{bmatrix} \quad \text{(2.48)}$$

The first row of the vector corresponds to the continuity equation. The second, third and fourth rows are momentum equation and finally the fifth row is the energy equation. With the Navier-Stokes equations written in this form, it is often easier to code the desired numerical algorithm. These vector equations prove valuable later in finite difference schemes that will be discussed later in chapter 4.

The components of the shear-stress tensor and heat flux vector are given by:

$$\tau_{xx} = \frac{2}{3}\mu\left(2\frac{\partial u}{\partial x} - \frac{\partial v}{\partial y} - \frac{\partial w}{\partial z}\right) \quad \text{(2.49)}$$

$$\tau_{yy} = \frac{2}{3}\mu\left(2\frac{\partial v}{\partial y} - \frac{\partial u}{\partial x} - \frac{\partial w}{\partial z}\right) \quad \text{(2.50)}$$

$$\tau_{zz} = \frac{2}{3}\mu\left(2\frac{\partial w}{\partial z} - \frac{\partial u}{\partial x} - \frac{\partial v}{\partial y}\right) \quad \text{(2.51)}$$

$$\tau_{xy} = \mu\left(\frac{\partial u}{\partial y} + \frac{\partial v}{\partial x}\right) = \tau_{yx} \quad \text{(2.52)}$$

$$\tau_{xz} = \mu\left(\frac{\partial w}{\partial x} + \frac{\partial u}{\partial z}\right) = \tau_{zx} \quad \text{(2.53)}$$

$$\tau_{yz} = \mu\left(\frac{\partial v}{\partial z} + \frac{\partial w}{\partial y}\right) = \tau_{zy} \quad \text{(2.54)}$$

2.6 Conservation law in cylindrical coordinates

It is more convenient to convert the derived conservation laws in Cartesian coordinates (x, y, z) into cylindrical coordinates (r, θ, z) due to the fact that research was done on air flow in circular cross-section pneumatic transmission line. The dimension along the radius is r, dimension along the centre of the cylinder is z while the dimension along the circumference of the cylinder is θ.

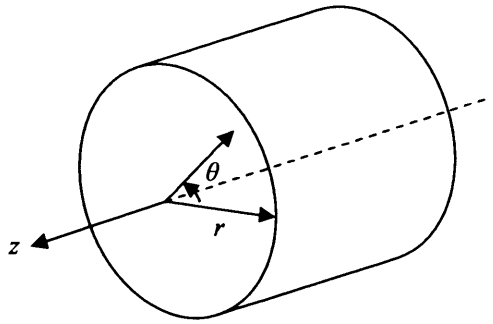

Figure 2.3: Cylindrical coordinates

The continuity equation as shown earlier in equation (2.2) can be written in cylindrical coordinate as below:

$$\frac{\partial \rho}{\partial t} + \frac{1}{r}\left[\frac{\partial}{\partial r}(r\rho u_r) + \frac{\partial}{\partial \theta}(\rho u_\theta) + \frac{\partial}{\partial z}(r\rho u_z)\right] = 0 \quad \text{(2.55)}$$

The momentum equation without body force is:

$$\frac{\partial}{\partial t}(\rho U) + \rho U \cdot \nabla U + U(\nabla \cdot \rho U) = \nabla \cdot \Pi_{ij} \quad \text{(2.56)}$$

Therefore in three-dimensional format it can be written as:

$$\frac{\partial}{\partial t}(\rho u_r)+\rho\left(u_r\frac{\partial u_r}{\partial r}+\frac{u_\theta}{r}\frac{\partial u_r}{\partial \theta}+u_z\frac{\partial u_r}{\partial z}\right)+\frac{u_r}{r}\left[\frac{\partial}{\partial r}(r\rho u_r)+\frac{\partial}{\partial \theta}(\rho u_\theta)+\frac{\partial}{\partial z}(r\rho u_z)\right]$$
$$=\frac{1}{r}\left[\frac{\partial}{\partial r}(r\Pi_{rr})+\frac{\partial}{\partial \theta}(\Pi_{r\theta})+\frac{\partial}{\partial z}(r\Pi_{rz})\right] \quad \text{..... (2.57)}$$

$$\frac{\partial}{\partial t}(\rho u_\theta)+\rho\left(u_r\frac{\partial u_\theta}{\partial r}+\frac{u_\theta}{r}\frac{\partial u_\theta}{\partial \theta}+u_z\frac{\partial u_\theta}{\partial z}\right)+\frac{u_\theta}{r}\left[\frac{\partial}{\partial r}(r\rho u_r)+\frac{\partial}{\partial \theta}(\rho u_\theta)+\frac{\partial}{\partial z}(r\rho u_z)\right]$$
$$=\frac{1}{r}\left[\frac{\partial}{\partial r}(r\Pi_{r\theta})+\frac{\partial}{\partial \theta}(\Pi_{\theta\theta})+\frac{\partial}{\partial z}(r\Pi_{\theta z})\right] \quad \text{..... (2.58)}$$

$$\frac{\partial}{\partial t}(\rho u_z)+\rho\left(u_r\frac{\partial u_z}{\partial r}+\frac{u_\theta}{r}\frac{\partial u_z}{\partial \theta}+u_z\frac{\partial u_z}{\partial z}\right)+\frac{u_z}{r}\left[\frac{\partial}{\partial r}(r\rho u_r)+\frac{\partial}{\partial \theta}(\rho u_\theta)+\frac{\partial}{\partial z}(r\rho u_z)\right]$$
$$=\frac{1}{r}\left[\frac{\partial}{\partial r}(r\Pi_{rz})+\frac{\partial}{\partial \theta}(\Pi_{\theta z})+\frac{\partial}{\partial z}(r\Pi_{zz})\right] \quad \text{..... (2.59)}$$

where the stress tensor (Π) is given by:

$$\Pi_{rr}=-P+\frac{2}{3}\mu(2e_{rr}-e_{\theta\theta}-e_{zz}) \quad \text{..... (2.60)}$$

$$\Pi_{\theta\theta}=-P+\frac{2}{3}\mu(2e_{\theta\theta}-e_{rr}-e_{zz}) \quad \text{..... (2.61)}$$

$$\Pi_{zz}=-P+\frac{2}{3}\mu(2e_{zz}-e_{rr}-e_{\theta\theta}) \quad \text{..... (2.62)}$$

$$\Pi_{\theta z}=\Pi_{z\theta}=\mu e_{\theta z} \quad \text{..... (2.63)}$$

$$\Pi_{rz}=\Pi_{zr}=\mu e_{rz} \quad \text{..... (2.64)}$$

$$\Pi_{r\theta} = \Pi_{\theta r} = \mu e_{r\theta} \quad \text{(2.65)}$$

and strain rates (e) are as follows:

$$e_{rr} = \frac{\partial u_r}{\partial r} \quad \text{(2.66)}$$

$$e_{\theta\theta} = \frac{1}{r}\frac{\partial u_\theta}{\partial \theta} \quad \text{(2.67)}$$

$$e_{zz} = \frac{\partial u_z}{\partial z} \quad \text{(2.68)}$$

$$e_{\theta z} = \frac{1}{r}\frac{\partial u_z}{\partial \theta} + r\frac{\partial}{\partial z}\left(\frac{u_\theta}{r}\right) \quad \text{(2.69)}$$

$$e_{rz} = \frac{\partial u_r}{\partial z} + \frac{\partial u_z}{\partial r} \quad \text{(2.70)}$$

$$e_{r\theta} = r\frac{\partial}{\partial r}\left(\frac{u_\theta}{r}\right) + \frac{1}{r}\frac{\partial u_r}{\partial \theta} \quad \text{(2.71)}$$

Regarding energy equation, the dissipation function Φ can be rewritten in cylindrical coordinates as shown below

$$\Phi = \mu\left[2\left(e_{rr}^2 + e_{\theta\theta}^2 + e_{zz}^2\right) + e_{\theta z}^2 + e_{rz}^2 + e_{r\theta}^2 - \frac{2}{3}\left(e_{rr} + e_{\theta\theta} + e_{zz}\right)^2\right] \quad \text{(2.72)}$$

where the functions for the strain rates e are as declared in equations (2.66 to 2.71).

It is now possible to construct a fluid dynamic simulation based on Navier-Stokes equation in three-dimensional format. However due to the number of equations involved, the complexity regarding the boundary conditions that needs to be specified in three-dimensional format and computing power needed to solve all these equations

numerous times to obtain a satisfied result, only one-dimensional model is considered in this thesis and several assumptions are made to reduce the complexity in completing the simulation.

These simplifications and assumptions were done since boundary conditions (which are vital in any computer simulation) in one-dimensional format can be specified confidently and makes debugging the mathematical algorithm in programming language more convenient. The implied assumptions will be as follows.

For continuity equation in cylindrical coordinate, if the swirl of the fluid in each cross-section is to be omitted, then this becomes:

$$\frac{\partial \rho}{\partial t}+\frac{1}{r}\left[\frac{\partial}{\partial r}(r\rho u_r)+\frac{\partial}{\partial z}(r\rho u_z)\right]=0 \quad \text{..... (2.73)}$$

For momentum equations in cylindrical coordinate, if the swirl of the fluid in each cross-section is to be omitted, then they become:

$$\frac{\partial}{\partial t}(\rho u_r)+\rho\left(u_r\frac{\partial u_r}{\partial r}+u_z\frac{\partial u_r}{\partial z}\right)+\frac{u_r}{r}\left[\frac{\partial}{\partial r}(r\rho u_r)+\frac{\partial}{\partial z}(r\rho u_z)\right] = \frac{1}{r}\left[\frac{\partial}{\partial r}(r\Pi_{rr})+\frac{\partial}{\partial z}(r\Pi_{rz})\right] \quad \text{..... (2.74)}$$

$$\frac{\partial}{\partial t}(\rho u_z)+\rho\left(u_r\frac{\partial u_z}{\partial r}+u_z\frac{\partial u_z}{\partial z}\right)+\frac{u_z}{r}\left[\frac{\partial}{\partial r}(r\rho u_r)+\frac{\partial}{\partial z}(r\rho u_z)\right] = \frac{1}{r}\left[\frac{\partial}{\partial r}(r\Pi_{rz})+\frac{\partial}{\partial z}(r\Pi_{zz})\right] \quad \text{..... (2.75)}$$

where the stress tensors are given by:

$$\Pi_{rr}=-P+\frac{2}{3}\mu(2e_{rr}-e_{zz}) \quad \text{..... (2.76)}$$

$$\Pi_{zz} = -P + \frac{2}{3}\mu(2e_{zz} - e_{rr}) \quad (2.77)$$

$$\Pi_{rz} = \Pi_{zr} = \mu e_{rz} \quad (2.78)$$

$$e_{rr} = \frac{\partial u_r}{\partial r} \quad (2.79)$$

$$e_{zz} = \frac{\partial u_z}{\partial z} \quad (2.80)$$

$$e_{rz} = \frac{\partial u_r}{\partial z} + \frac{\partial u_z}{\partial r} \quad (2.81)$$

Further assumption is that the fluid along the radius direction is to be omitted, then for continuity equation, this becomes:

$$\frac{\partial \rho}{\partial t} + \frac{\partial}{\partial z}(\rho u_z) = 0 \quad (2.82)$$

For momentum equations:

$$\frac{\partial}{\partial t}(\rho u_z) + \rho u_z \frac{\partial u_z}{\partial z} + u_z \frac{\partial}{\partial z}(\rho u_z) = \frac{\partial}{\partial z}(\Pi_{zz}) \quad (2.83)$$

where the stress tensor is given by:

$$\Pi_{zz} = -P + \frac{2}{3}\mu(2e_{zz}) \quad (2.84)$$

where e_{zz} is:

$$e_{zz} = \frac{\partial u_z}{\partial z} \quad (2.85)$$

Note that energy equations were not included in the simulation algorithm since it was found from conducted experiments as shown later in chapter 3 that the temperature variations T_s were relatively small compared to the pressure variations. Furthermore since the working fluid is air, the kinematic viscosity ν values are small ($15.13\times10^{-6}\,m^2s^{-1}$ at 293K and rises to $25.78\times10^{-6}\,m^2s^{-1}$ at 393K) and based on the tensor equations derived in the momentum equations (2.60 to 2.65), this poses little effect on the air flow with regards to the viscous effect.

Therefore as a conclusion on one-dimensional analysis of fluid flow, based on conservation laws described and assumptions implied, the equations that need to be incorporated into the computer simulation algorithm are as follows.

Continuity Equation

$$\frac{\partial \rho}{\partial t}+\frac{\partial}{\partial z}(\rho u_z)=0 \qquad (2.86)$$

Momentum Equation

$$\frac{\partial}{\partial t}(\rho u_z)+\rho u_z\frac{\partial u_z}{\partial z}+u_z\frac{\partial}{\partial z}(\rho u_z)=\frac{\partial}{\partial z}(\Pi_{zz}) \qquad (2.87)$$

where stress tensor is

$$\Pi_{zz}=-P+\frac{2}{3}\mu(2e_{zz}) \qquad (2.88)$$

and strain rate is

$$e_{zz}=\frac{\partial u_z}{\partial z} \qquad (2.89)$$

As a summary, the three-dimensional Navier-Stokes equations include the continuity, momentum and energy equations. However in this thesis, assumptions are used to reduce these equations into a one-dimensional format. Based on the thermal-dynamic experiment conducted in chapter 3, energy equation part of the Navier-Stokes equations was excluded. The derived equations are then utilised in the computer simulation using the finite difference approach as presented in chapter 4. It was concluded that from comparison between simulated and experimental results, the assumptions applied are acceptable and simulations of experimental results proves to be successful as presented in chapter 4 and chapter 6.

Chapter 3

Energy Saving Test Rig and System Components

In this chapter, the experimental setup is outlined including descriptions of crucial components of the test rig. These components in order are the pressure regulator, air operated valves, pneumatic cylinder, voltage relay unit and bench top power supplies, sensors and data acquisition processor (DAP). The later includes pressure transducers, IFM flowmeter, thermocouples and DAP control program (DAPView). Brief descriptions of working principle for components are also included where necessary.

There are a variety of fast response flowmeter available to sense the behaviour of flow due to pressure changes, however capturing the dynamic state of the flowrate is still a challenging task. The need for accurate and high speed measurement of flow is desirable for the determination of flow dynamic behaviour in the transmission line. Previously steady state flow has been determined using a range of instruments such as orifice meters, Venturi tube, flow nozzles, variable area flowmeter, pitot tubes, etc. In this chapter, a calorimetric type flowmeter is used since it has the advantage of a fast response while at the same time it poses minimized disruption to the measured fluid flow.

3.1 Energy saving test rig circuit

In the experimental setup as shown in Figure (3.1), a double-rod-double-acting pneumatic cylinder with a bore of 125mm and a stroke of 180mm was used. A mass of 10kg on a trolley is attached to the end rod of the cylinder. The pneumatic cylinder is controlled by three 3/5 air operated valves which are operated by four solenoid pilot valves. Two other 3/5 air operated valves were included for exhausting air when the main (V1 and V2) 3/5 valve is in the neutral position. Due to the fact that only one side of the valves (V3 and V4) is charged at any one time, the circuit diagram below display these two valves as 2/2 directional valves.

The piston displacement is then measured by the use of an LVDT and pressures in both chambers were measured using pressure transducers. The supply pressure is controlled by means of a pressure regulator. A data acquisition processor (DAP) is incorporated with a PC to capture transmitted data from transducers (x_p, Pl, Pr) and to provide control signals (V1, V2, V3, V4, V5) to the valves and pressure regulator.

The energy saving algorithm is implemented in a Microsoft Visual C++ program[17] and then downloaded to the DAP. Control signals from the DAP which are 5Volts DC are then amplified to 24Volts DC in an electric relay to actuate the valves. Circuit diagram and a picture of the experimental setup are shown in Figure (3.1) and Figure (3.2) respectively.

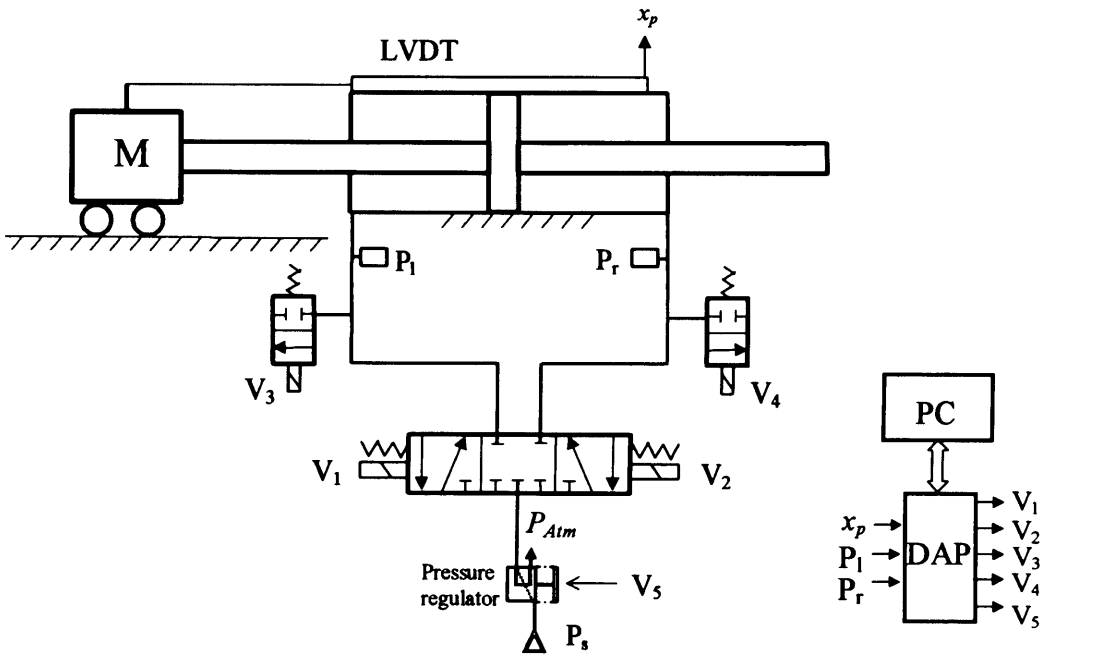

(a) Circuit (b) Signal termination board

Figure 3.1: Test rig circuit

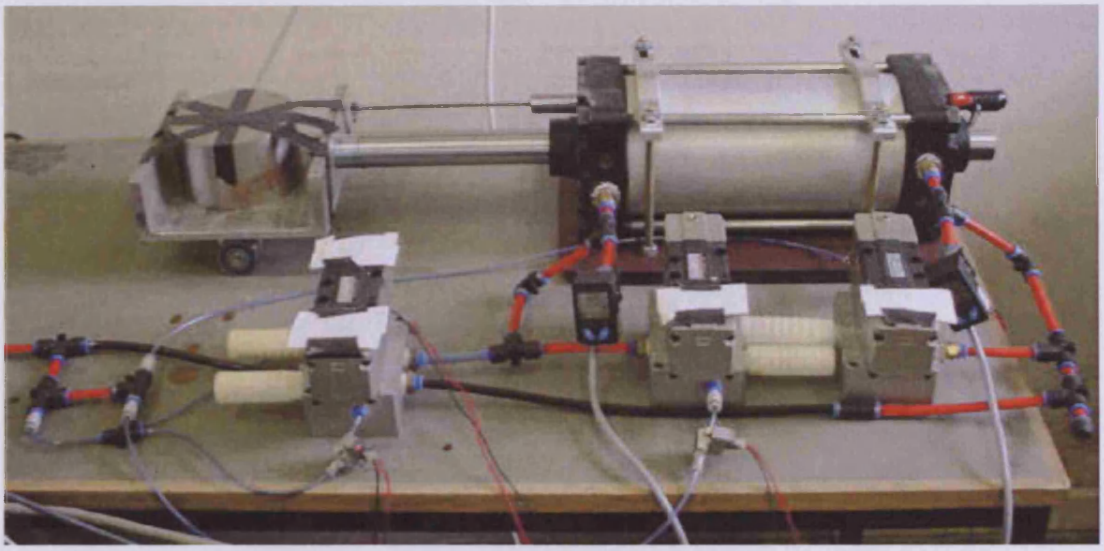

Figure 3.2: Picture of the test rig

3.2 SMC pressure regulator

SMC pressure regulator model ITV2030-31 is used for controlling the supply pressure from the main line. In this research two working pressures are used for energy saving experiments and they are 1.5bar and 2.5bar. This voltage type pressure regulator with analogue output has a maximum working pressure of 5bar and can handle up to 10bar maximum input pressure. These specifications make it suitable for laboratory use. Picture and working principle of the pressure regulator are as follows.

Figure 3.3: Pressure regulator ITV2030-31

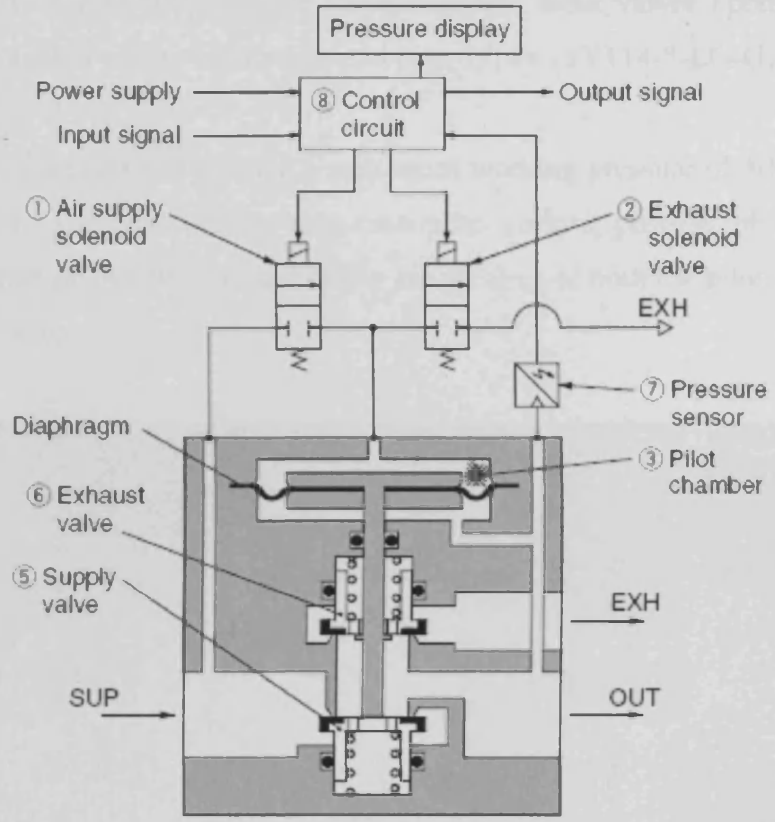

Figure 3.4: Pressure regulator working principle excerpted from ITV2030-31 product manual

As the input signal rises, the air supply solenoid valve 1 is switched ON while the exhaust solenoid valve 2 is switched OFF. The supply pressure then passes through the air supply solenoid valve 1 and is applied to the pilot chamber 3. The pressure in the pilot chamber 3 increases and operates on the upper surface of the diaphragm. As a result, the air supply valve 5 linked to the diaphragm opens, and a portion of the supply pressure becomes the output pressure. This output pressure feeds back to the control circuit 8 via the pressure sensor 7. Here, the correct operation continues until the output pressure is proportional to the input signal, making it possible to obtain an output pressure that is proportional to the input signal.

3.3 SMC air operated valves

Three air operated directional valves are used in the experiment. Based on Figure (3.1), signals (V1 and V2) are relayed to the first valve (VSA7-8-FHG-D-2), signal (V3) to the second valve (VSA7-8-FHG-D-2) and finally signal (V4) to the

third valve (VSA7-8-FJG-D-2). As the name suggests, these valves operate on air supply and are actuated using smaller solenoid pilot valves (SY114-5-LO-U).

These air operated valves have a maximum working pressure of 10bar while the solenoid pilot valves can operate to a maximum working pressure of 7bar. The pilot valves operate at 24Volts DC and below are pictures of both the pilot valve and the air operated valve.

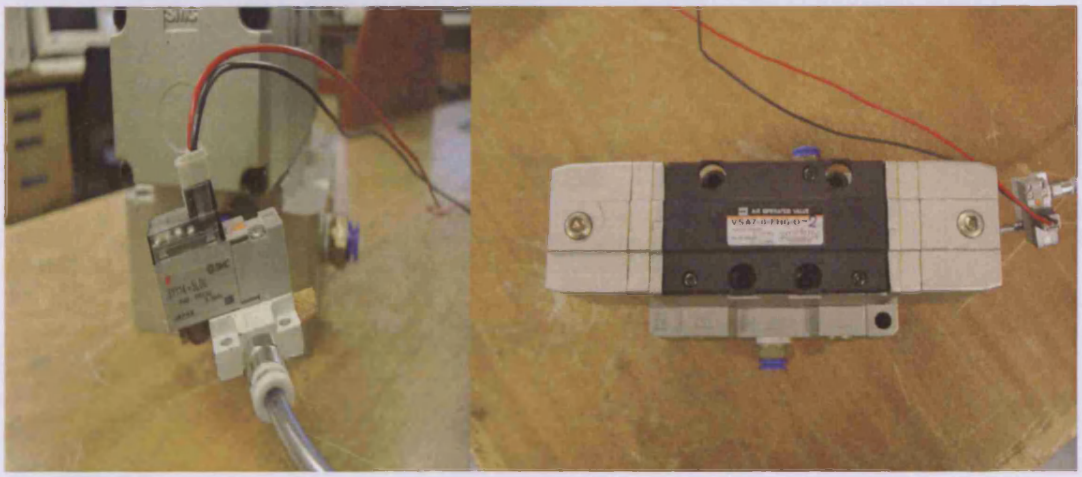

(a) Pilot valve (b) Close-up view of one of the air operated valve

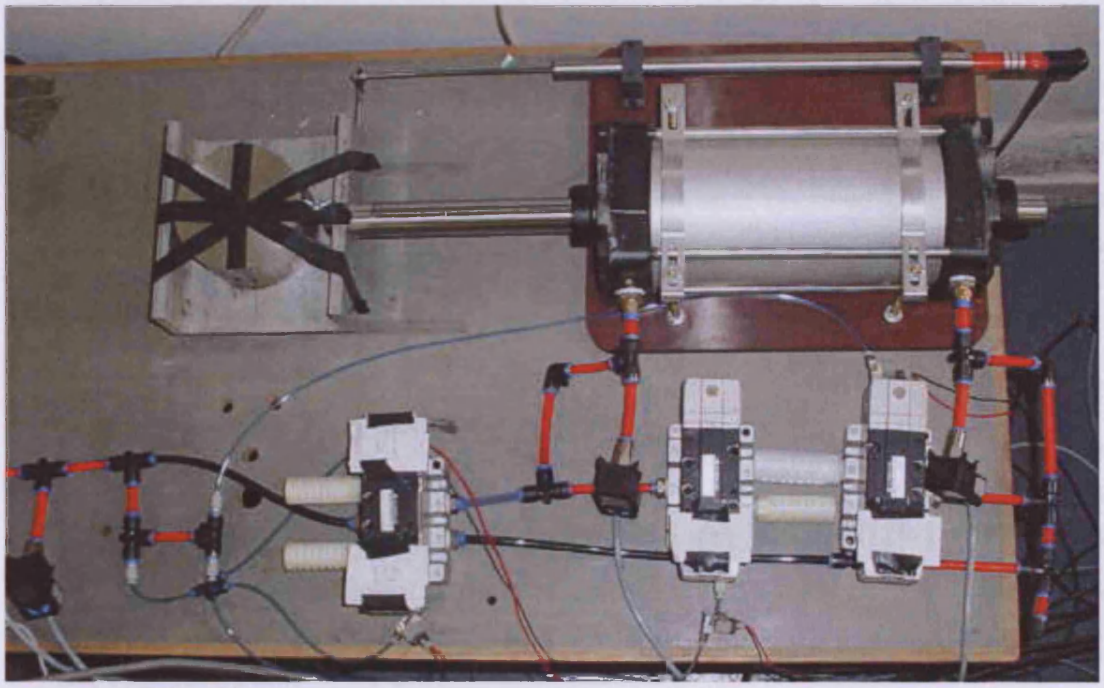

(c) Overview of the test rig

Figure 3.5

Due to the fact that air operated valves are used, time-delays for these valves are then pressure dependent. Tests were done to determine the time-delay of these valves by measuring the time difference between signal sent and the valve reaction time. This was done under 5 different system pressures in a range of 1.50bar to 2.50bar. Below are the averaged valve's reaction time based on experiments conducted under varying system pressures.

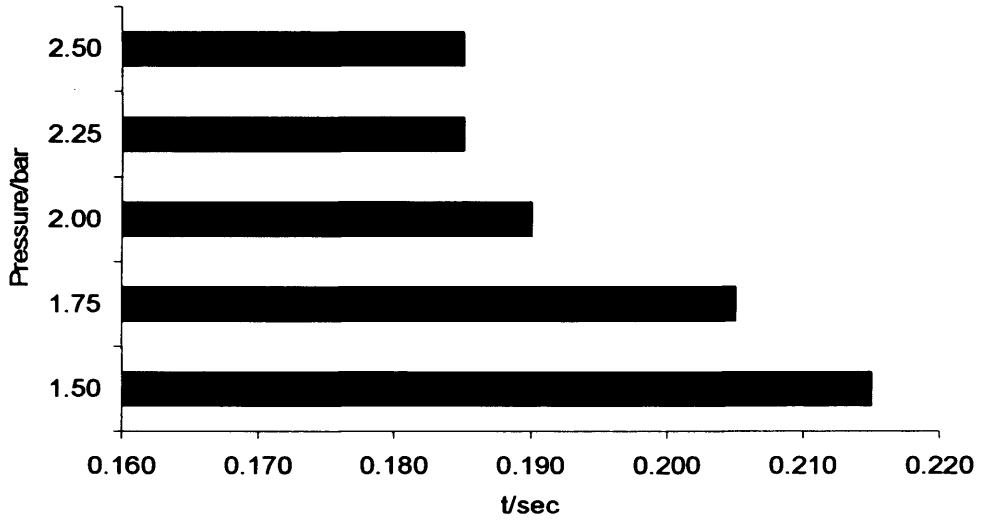

Figure 3.6: Air operated valve delay times

As expected, the delay time decreases with increasing supply pressure due to the fact that larger force is available at higher pressure to move the spool thus reducing the time taken to actuate the valves. From result obtained it can be deduced that the valve delay time at experimental working pressure of 1.5bar is 0.215s and reduces to 0.185s at 2.5bar.

4.4 SMC pneumatic cylinder

A double-rod-double-acting pneumatic cylinder (C92SB-125-180W) with a bore of 125mm and a stroke of 180mm is used to move a mass of 10kg on a trolley that is attached to the end rod of the cylinder. Below is the picture of the cylinder:

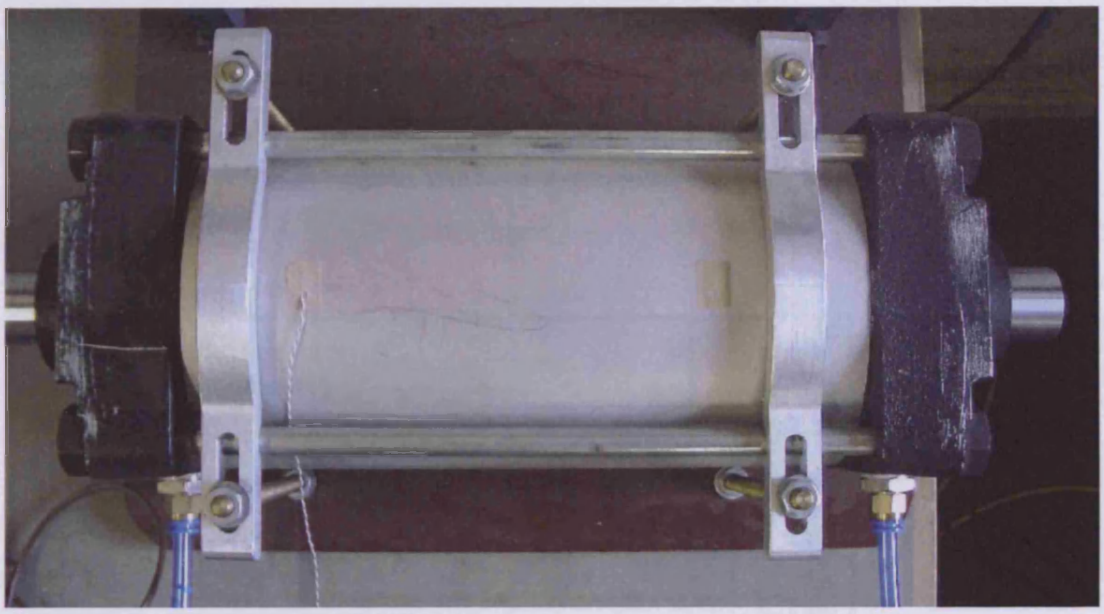

Figure 3.7: Pneumatic cylinder

The term double-rod[9,18,19] is used since the cylinder has two identical rods on either sides of the piston. Meanwhile the term double-acting means that the cylinder has powered motion in two directions, with pressure on both sides (driving and exhausting).

Another important aspect of pneumatic cylinder is cushioning[18,20]. The primary objective of cylinder cushioning is to decelerate the cylinder's piston rod at either ends of stroke. Piston deceleration is important to avoid hard metal-to-metal contact with the end caps. Hard metal-to-metal impact can cause damage or shortening to life span of the component.

There are two distinct cushion types. The first involves a mechanism external to the body of the cylinder known as external cushioning. External cushioning incorporates a shock absorber type mechanism that helps to decelerate the load. The drawback to external cushioning is that it increases the footprint of the cylinder, adds weight, and involves additional moving parts. The second mechanism is known as internal cushioning. This incorporates a design that is internal to the cylinder and thus operates within the cylinder footprint and tends to be simpler in function.

The pneumatic cylinder used in this experiment has internal adjustable air cushioning and the simplified mechanism for easy understanding is as shown below. Note that only cushion mechanism on one side of the cylinder is presented.

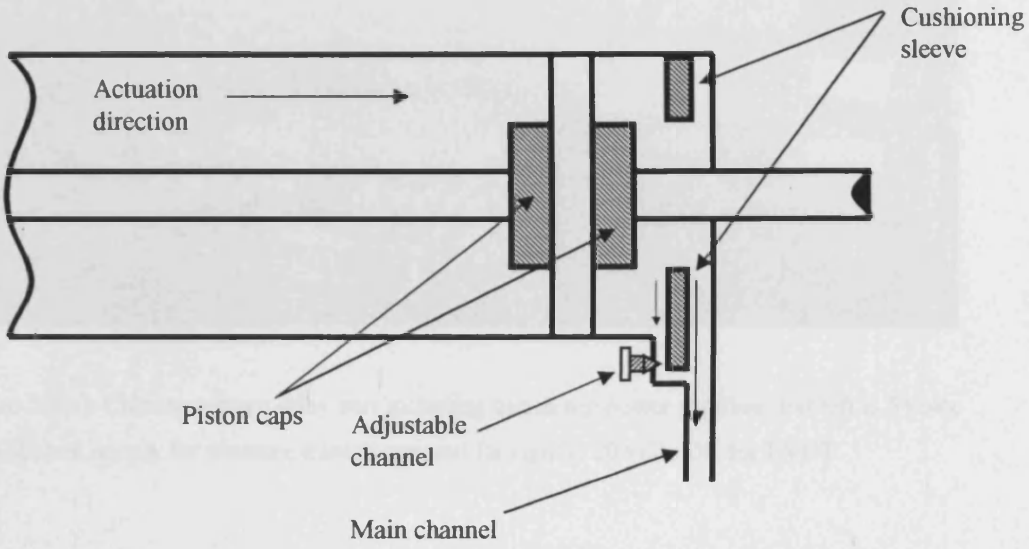

Figure 3.8: Air cushion mechanism

As the piston moves from left to right, the air in the exhausting chamber is being pushed out through two of the air channels. As the cap enters the cushion sleeve, the larger air channel is then blocked and air is only allowed to be exhausted through the smaller adjustable air channel. The air in the exhausting chamber quickly compresses thus providing sudden increase in pressure to decelerate the load.

3.5 Voltage relay unit and bench-top power supplies

The voltage relay unit was custom designed and built earlier in this research to enable 5Volts DC signals from DAP to be amplified to 24Volts DC. This amplification is needed to operate the valves incorporated in the test rig. The voltage relay unit has 12 input and 12 output channels. Bench top power supply units (5Volts DC and 20Volts DC) are used to provide power to pressure transducers and LVDT utilised in the test rig. The picture of the unit including the bench-top power supplies

are presented in Figure (3.9). Circuit diagram and PCB (printed circuit board) blueprint of the voltage relay unit is included in Appendix 6.

Figure 3.9(a): Custom voltage relay unit including bench top power supplies. Far left is 5Volts DC power supply for pressure transducers and far right is 20Volts DC for LVDT

Figure 3.9(b): Voltage relay unit

3.6 Sensors and Data Acquisition Processor (DAP)

In this subchapter, 5 important components are discussed namely the pressure transducer, LVDT, thermocouple, data acquisition processor (DAP) and DAPView control program.

3.6.1 Festo pressure transducers

4 units of Festo pressure transducer type (V)PENV-A-PS/O-K-LCD are used and have a measuring range of 0-12bar with operating voltage of 24Volts DC. As with the case of IFM flowmeter unit that will be discussed later in this chapter, high-speed response is favoured to capture the fluid dynamic data in the experimental test rig. This unit has a response time of 15ms according to manufacturer's technical specification which makes it suitable for high-speed data capture. The pressure transducer operates by means of calibrating strain experienced by the piezo-resistive elements in the transducer that is induced by the pressure in-situ. These transducers are located downstream of the main line, downstream of the pressure regulator and the other two units positioned at both the inlet and outlet ports of the pneumatic cylinder. Figure (3.10) shows the picture of one of the units.

Figure 3.10: Festo pressure transducer

3.6.2 RDP Electronics LVDT

The basic design of an LVDT comprises of a primary coil winding and two identical secondary windings on a common bobbin, and a moveable magnetic core or called armature. The primary winding on the LVDT is excited with a low voltage DC supply. The two secondary windings are connected so that their combined output represents the difference in the voltage induced into them. With the armature in the central position, the output is zero. Movement of the armature from this position produces an output which changes in phase and magnitude according to the armature displacement.

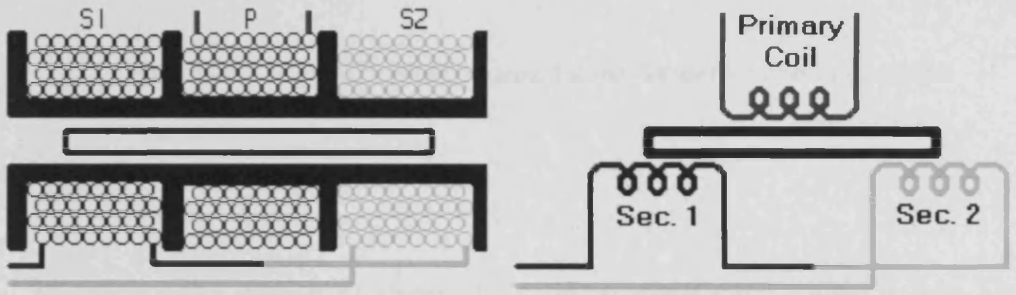

Figure 3.11: LVDT working principle

An RDP Electronics LVDT model ACT3000C is used in this experiment. The "C" in the model name refers to the LVDT being of captive armature type. This means that the armature is both restrained and guided by a low-friction bearing assembly. It has a maximum stroke of 200mm and operating voltage of 20Volts DC thus making it suitable for measuring the operating stroke of the pneumatic cylinder. Below is the picture of the LVDT mounted at the side of the cylinder.

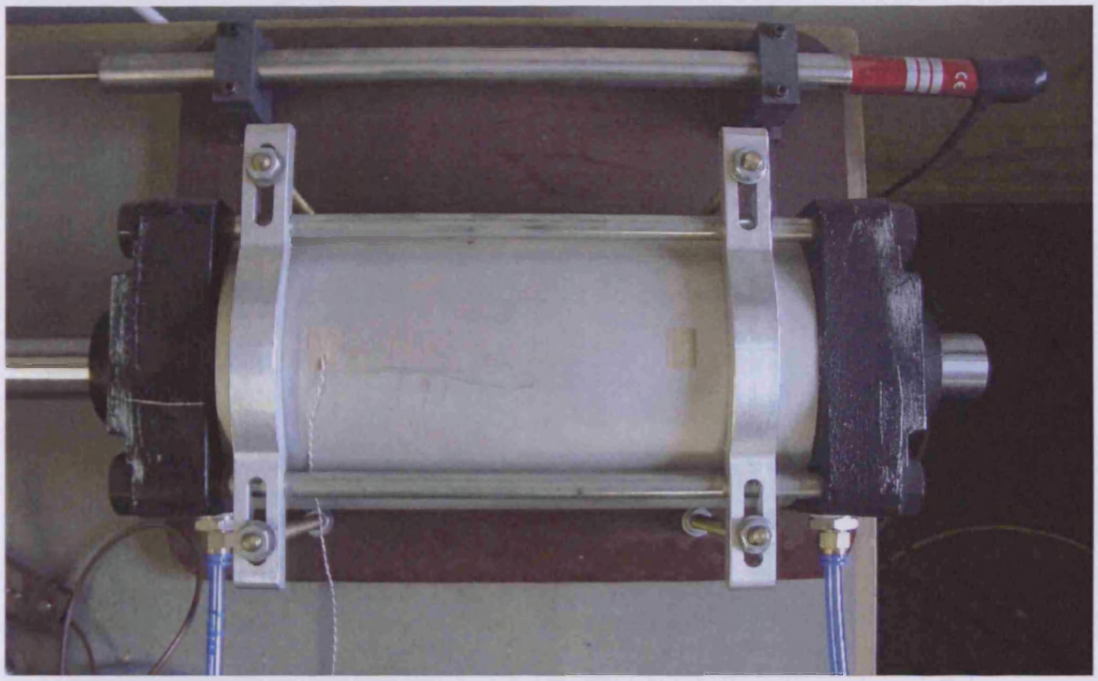

Figure 3.12: LVDT ACT 3000C mounted at the side of the pneumatic cylinder

3.6.3 Type-T thermocouples

Thermocouples consist of a pair of dissimilar metal wires joined at both ends in a circuit with their junctions at different temperatures. This configuration generates a net thermoelectric voltage which induces a continuous electric current between the pair according to the size of the temperature difference between the junctions. They are based on the Seebeck effect that occurs in electrical conductors that experience a temperature gradient along their length[21,22]. The Seebeck effect, or thermoelectric effect, is the direct conversion of heat differentials to electric voltage and vice versa. Since this voltage is measurable, it provides a means of indicating and measuring temperature difference. Thermocouples are simple, rugged, needs no power supply and can measure over very wide temperature ranges.

The test rig incorporates two type-T thermocouples. One positioned at the inlet port and another on the top surface of the pneumatic cylinder. The two dissimilar metals in contact for this type of thermocouple are copper and copper-nickel (constantan). This thermocouple is chosen due to the fact that it is cheap, has the smallest measurable temperature range compared to other types of commercially

available thermocouples and is widely employed in laboratory applications. Furthermore type-T thermocouple has excellent repeatability up to 200^0C[21,22].

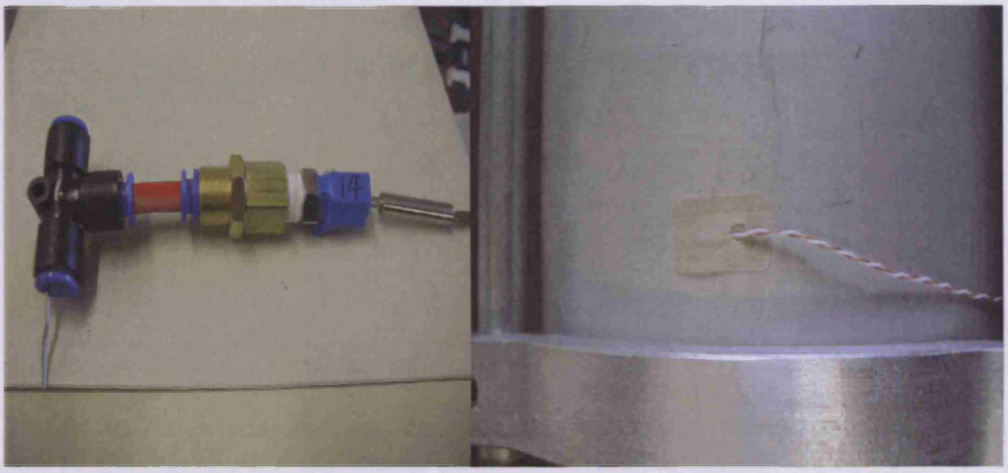

(a) (b)

Figure 3.13(a): Rod type-T thermocouple incorporated into a pneumatic tube

Figure 3.13(b): Sticker type-T thermocouple placed on the pneumatic cylinder surface

Experiments were conducted to investigate the relationship between temperature and pressure. The first experiment conducted was to confirm any major temperature changes during conventional PTP cylinder actuation. Below is the result of the experiment conducted.

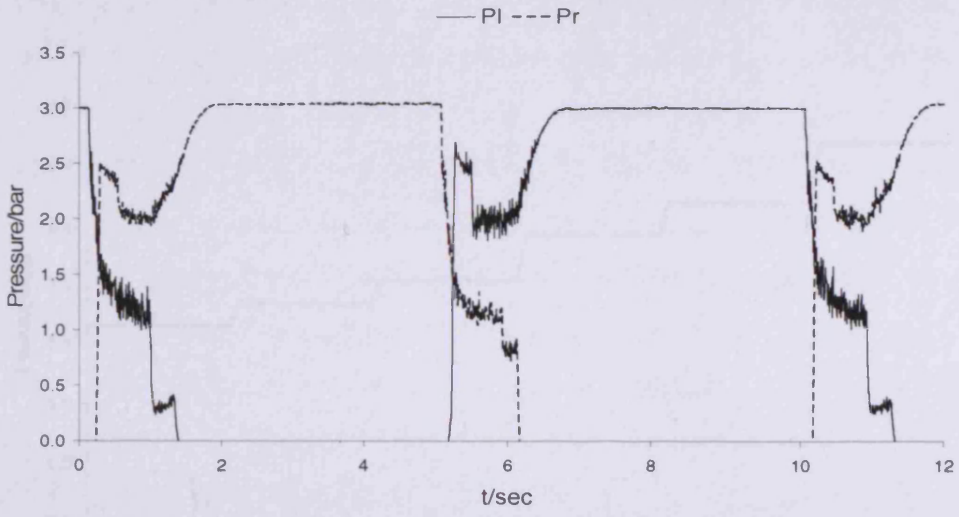

Figure 3.14: Right chamber pressure (Pr) and left chamber pressure (Pl) variations during conventional actuation cycles (Ps = 3bar)

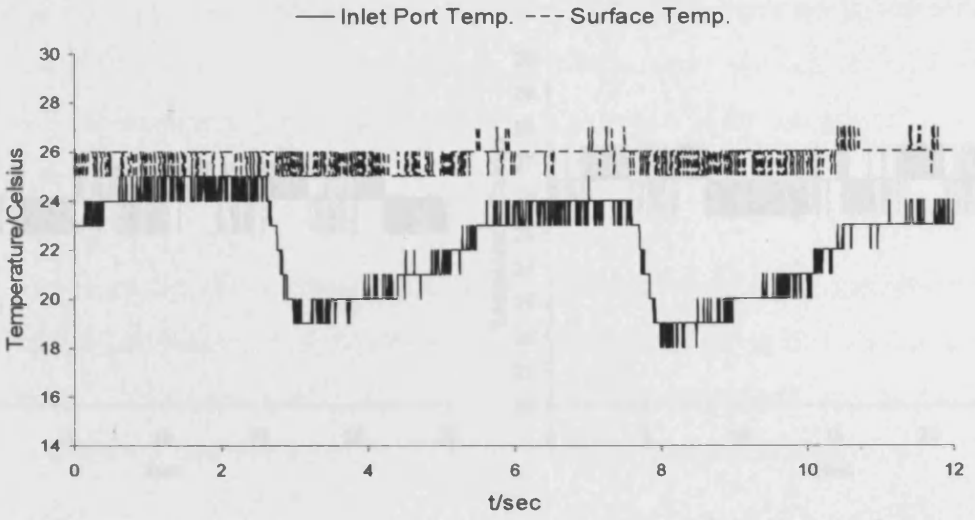

Figure 3.15: Cylinder inlet port and cylinder surface temperature variation in conventional PTP actuation

It can be seen that the maximum temperature variation is approximately 5.0^0C for air at the inlet port. The trend for inlet port temperature is that as the experiment progresses, the average temperature decreases while still retaining the same maximum temperature difference as before. The surface temperature meanwhile remains the same throughout the experiment at room temperature of 26^0C.

Another experiment conducted was varying the air pressure in a fixed volume within a uniform time-step. Below is the result of the experiment performed.

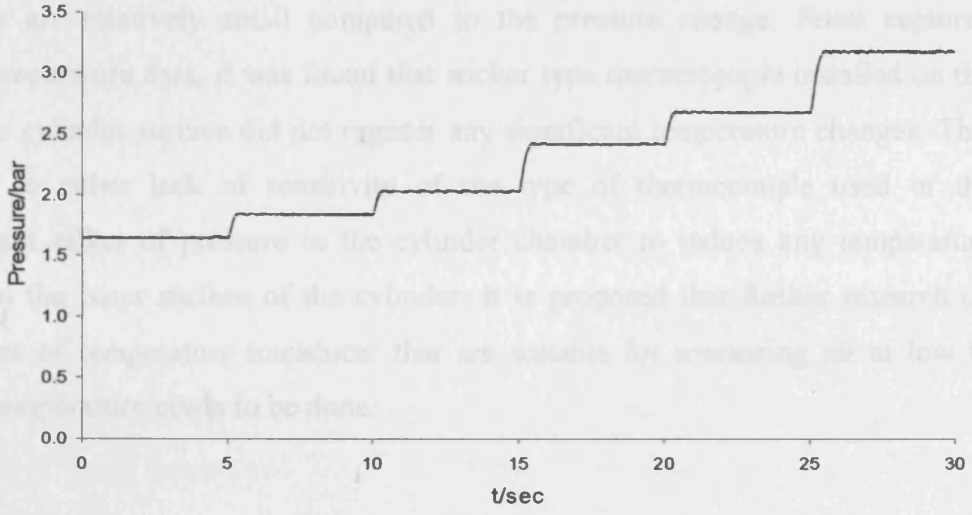

Figure 3.16: Pressure variation in a fixed volume

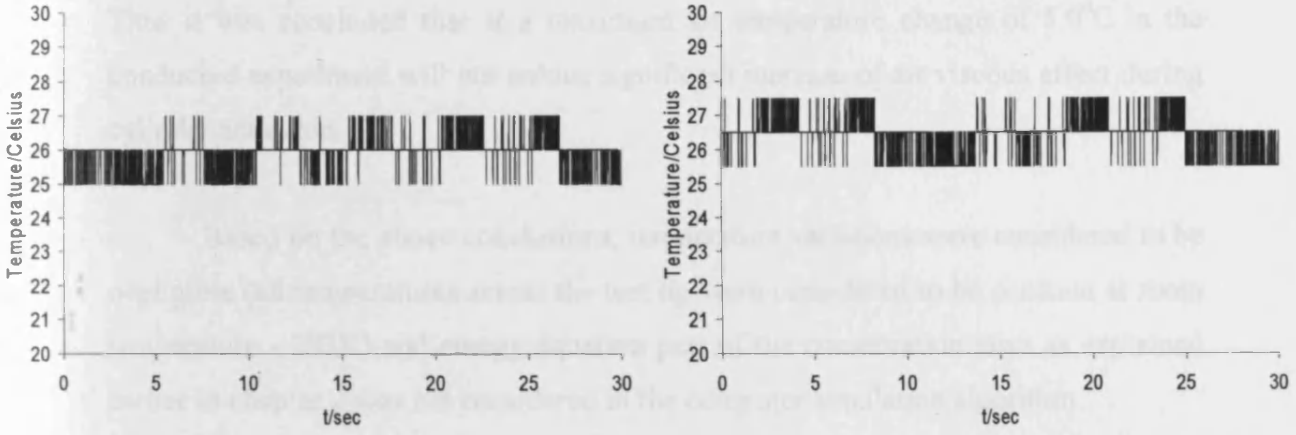

(a) Inlet port temperature (b) Cylinder surface temperature

Figure 3.17: Temperature variation in a fixed volume experiment

The temperatures at the inlet port and the pneumatic cylinder surface of the fixed volume were monitored. The pressure change applied to the fixed volume varies from a minimum of 1.65bar to a maximum of 3.18bar. It was found that the temperature change is significantly small compared with the pressure change applied. The average temperature recorded at the inlet port and the cylinder surface were 26^0C and 26.5^0C respectively.

It was concluded at the end of the experiments that the temperature variation at the cylinder inlet port during both the conventional and energy saving cylinder actuations are relatively small compared to the pressure change. From captured surface temperature data, it was found that sticker type thermocouple installed on the pneumatic cylinder surface did not register any significant temperature changes. This may due to either lack of sensitivity of the type of thermocouple used or the insignificant effect of pressure in the cylinder chamber to induce any temperature change on the outer surface of the cylinder. It is proposed that further research on other types of temperature transducer that are suitable for measuring air at low to medium temperature needs to be done.

Based on the international standard atmosphere data[23], it was found that the kinematic viscosity value of air v is small even with large increase in temperature. Thus it was concluded that at a maximum air temperature change of 5.0^0C in the conducted experiment will not induce significant increase of air viscous effect during cylinder actuation.

Based on the above conclusions, temperature variations were considered to be negligible (all temperatures across the test rig were considered to be constant at room temperature - 293K) and energy equation part of the conservation laws as explained earlier in chapter 2 was not considered in the computer simulation algorithm.

3.6.4 IFM Electronics calorimetric mass flowmeter

The working principle behind calorimetric type flowmeter is that it is based on the variation of the electrical resistivity of materials in relation to temperature[24]. Generally the resistivity increases proportionally with temperature depending on the type of material employed.

The resistivity of sensor material can be defined as shown by the equation below.

$$\sigma = \frac{R_h A_h}{l_h} \qquad (3.1)$$

A_h is the cross-sectional area of the sensor, R_h is the electrical resistance at temperature T_h and l_h is the sensor length.

IFM flowmeter uses two temperature sensors which are also called hot-wire that are in close contact with the fluid but are thermally insulated from each other. The dimensions of these sensors are very small so that the change in resistance is high enough to allow accurate measurement of its changes as well as avoiding disruption to the air flow being measured. These two sensors are positioned halfway in the transducer's pipe and are perpendicular to the direction of the fluid flow.

Diagrammatically it can be shown as:

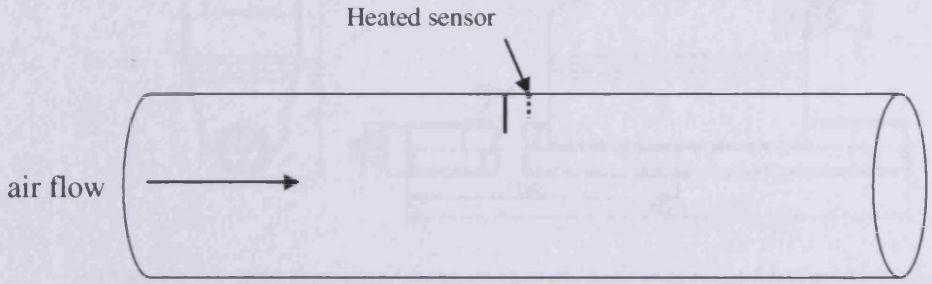

Figure 3.18: Sensor position in the IFM flowmeter pipe

One of the two sensors is constantly heated and the cooling effect of the flowing fluid is used to monitor the flowrate. In a stationary (no flow) fluid condition there is a constant temperature difference between the two temperature sensors. When the fluid flow increases, heat energy is drawn from the heated sensor and the temperature difference between the sensors are reduced. The reduction is proportional to the flow rate of the fluid. Response times will vary due the thermal conductivity of the fluid. In general lower thermal conductivity requires higher velocity for proper measurement.

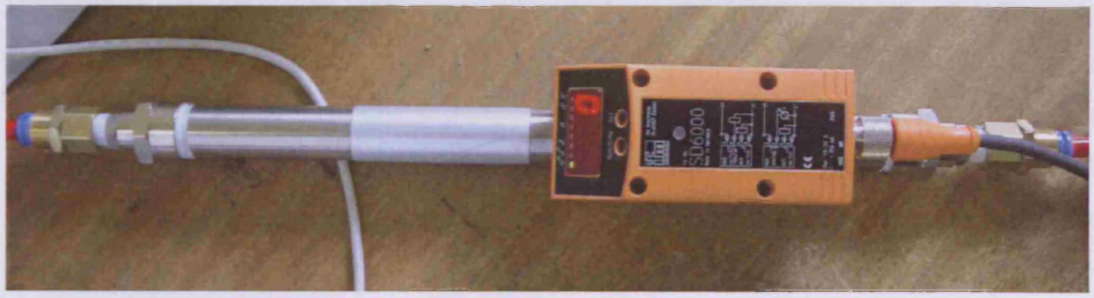

Figure 3.19: IFM mass flowmeter

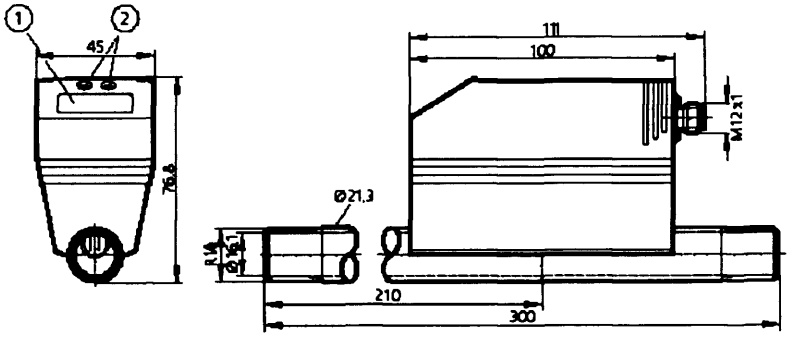

Figure 3.20: IFM flowmeter cross-section diagram excerpted from product manual

In this research, IFM flowmeter model SD6000 is used. This flowmeter has a maximum operating pressure of 16bar while the compressed air pressure from the main supply line available in the laboratory is between 6.7bar and 7.2bar. This transducer has a fast response time with a quoted figure of 0.1second and a maximum flowrate measuring range of 1250L/min thus making it suitable for capturing the dynamic state of the flowrate.

3.6.5 Microstar Laboratories DAP 4200a

Data acquisition processor is needed to sample the measured data obtained from transducers used on the test rig such as pressure transducers and flowmeters. Microstar Laboratories data acquisition processor (DAP) model 4200a is used for performing data capturing task.

This DAP occupies one expansion slot in the PC and has a high sampling time of 100ns or (100×10^{-9}) seconds. It has both input and output range of ±10Volts DC thus making it highly adaptable for controlling components such as valves and pressure regulators. However voltage relay unit and bench-top power supplies are needed to increase these output signals since all solenoid directional valves used in this research has an operating voltage of 24Volts DC. This DAP is able to sample 16 input channels and can send output signals through 6 other channels via expansion card simultaneously. This specification makes it a powerful DAP and have more than enough capabilities to manage data transfer between transducers on the test rig and the PC.

Another advantage of this DAP is that it comes with its own programming language named DAPView. DAPView enables user to perform data sampling and generate output signals from PC to the test rig. It also has the ability to download commands from other programming languages such as Microsoft Visual C++ and Borland Delphi thus making it possible for user to perform signal generation based on more complex mathematical algorithm. Below is the picture of the DAP 4200a and the BNC-type connector interface for output and input signals.

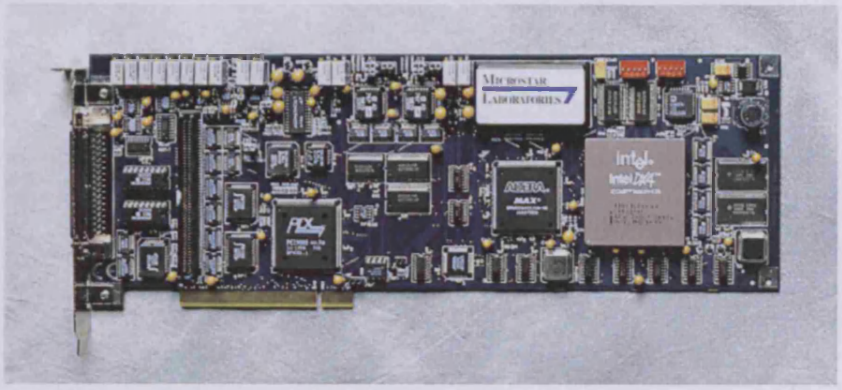

Figure 3.21: Microstar Laboratories DAP 4200a

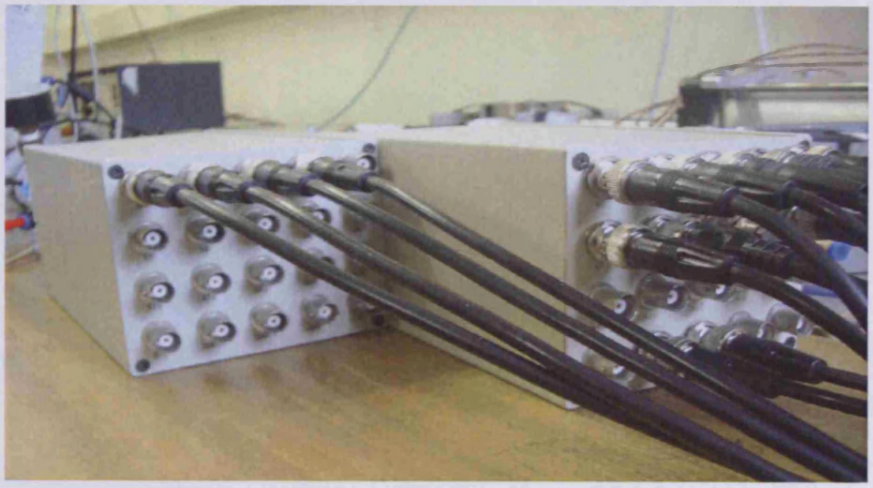

Figure 3.22: DAP I/O channel interface

3.6.6 Microstar DAPView

DAPView is a control suite that comes together with DAP 4200a package. It enables user to perform data sampling and output signal generation from PC to the

test rig. Another advantage of this control program is that it also has the ability to download commands from other programming languages such as Microsoft Visual C++ thus making it possible for user to perform signal generation based on more complex mathematical algorithm. Appendix 7 displays a sample of DAPView control program.

The 1st section declares all the variables used in the DAPView control program. This includes the number of output signal channels used, input and output channel name and variables declaration. Note that in DAPView, channels are named as pipes.

The 2nd section is related to the input specification to the DAP card. This includes the number of input channels, the physical designation of input channels at the I/O interface and finally the sampling time for each of the input channel. In the example below, the sampling time is specified as 50μs or 50×10^{-6} s.

The 3rd section details the algorithm performed on the variables declared earlier in the 1st section such as binary value to voltage value conversions. The link to an external downloaded program is defined as "CONTROL" and this performs the algorithm programmed in Microsoft Visual C++. This is the powerful feature of DAPView since it enables the communication between the DAP card, the DAPView control program and the programming language used. With this feature more complex algorithm can be defined in the usual programming language such as Borland Delphi or Microsoft Visual C++; and then downloaded into the DAPView control program in which the real-time processing is performed. "MERGE" command deals with streaming the captured data to an output file called log . This is where all the captured data are stored and can later be transferred to work spreadsheets such as Microsoft Excel for further analysis.

The last section deals with the monitoring of the generated wave signal which is generated by the DAP card. In this case the generated signal was copied as instructed in the 3rd section by the "COPY" command and then re-routed back to the DAP card as an input signal.

Chapter 3 can be summarised as follows. The test rig as outlined by the pneumatic circuit presented in Figure (3.1) is constructed and data acquisition processor (DAP) is incorporated to capture real-time data of pressure, temperature, and mass flowrate by the use of pressure transducers, thermocouples and mass flowmeters.

Working principle of system components such as pressure regulator, air operated valves, the pneumatic cylinder, voltage relay unit and bench-top power supplies were discussed. Sensors used for data capturing such as pressure transducers, Linear Variable Differential Transformer (LVDT), type-T thermocouples, mass flowmeters and data acquisition processor used including its programming language were are also discussed and vital information regarding their specifications and working principle are included where necessary.

This information is important in order to understand the role of each of the system components as well as to fully utilise the constructed test rig. Real-time data captured from experiments conducted on the test rig are then utilised in the computer simulation algorithm. These simulated data are then compared with the captured experimental data and results are then presented in chapter 4 for the transmission line modelling and chapter 6 for the energy saving system modelling.

In this chapter, the thermal-dynamics experiments conducted were also presented. These experiments investigate the relationship between pressure and temperature under conventional PTP actuation as well as temperature variations under varying pressure in a fixed volume. It was found that the surface temperature of the pneumatic cylinder remains constant at room temperature of around 26^0C in both experiments. It was also found that the maximum temperature variations registered at the inlet port of the cylinder under conventional PTP actuation is about 5^0C while this temperature remains constant in a fixed volume experiment.

The temperature variations were considered negligible and system will be assumed to be at room temperature in the simulation algorithm while energy equation part of the Navier-Stokes equations were excluded due to the fact of insignificant change in air viscous effect based on the maximum air temperature variation recorded.

Chapter 4

Mathematical Model of Fluid Transmission Line

Mathematical modelling is the most commonly used and preferred technique in fluid power component modelling. With the aid of experimental measurements, this method enables simulation and identification of fluid power components dynamic[25,26] behaviours and responses under specific conditions. The usual practice of utilising this method is:

a) To derive the mathematical equations using basic laws with reference to continuity, momentum, force, etc of the component. This usually involves combination of theoretical and empirical analysis.
b) Equations can be very complex and require simplification. This can be done by experience and detailed understanding of the mechanism in operation.
c) Finally numerical techniques are used to solve the set of derived equations.

In this chapter, several key components in pneumatic modelling techniques are discussed. These are restriction/orifice modelling, lumped modelling and finite difference modelling. Restriction/orifice modelling is used to model fluid flow control device such as valves, jets, etc. Both the lumped and finite difference can be use to model air transmission line though finite difference modelling is more complex to use compared to lumped modelling. However lumped modelling can model pneumatic systems to reasonable accuracy depending on the types of the system modelled based on a certain degree of assumptions made. Fluid container bulk modulus effect is proposed to be included in any future simulation algorithm. This enables better understanding of its effect on air dynamics and enables more accurate computer simulation of the energy saving methods proposed.

There are many types of finite difference modelling namely Upwind, MacCormack, Lax, Lax-Wendroff, Leap Frog, etc[13]. All these methods differ in the sense of applications, accuracy, and complexity not to mention computing time. Each has its own merits and disadvantages though the suitable type to be chosen depends

on the system under study. Further elaboration on finite difference will be discussed later under the segment 4.3 Finite Difference Modelling.

In pneumatic system analysis, the dynamics of air transmission lines[27,28,29] needs to be considered as transmission lines affect the system performance. Transmission lines contribute to the time-delay in a pneumatic motion control system. This time-delay may largely affect the system stability and cause limitations in the control design. This effect may also cause large oscillations and shorten the life span of pneumatic components. This chapter includes experiments and simulations of experiment results aimed at testing the dynamic response of pressure and flowrate along the air transmission line when the demand of flow is in the form of an on-off characteristic.

Computer simulations of experiment results were outlined. Experiments were conducted in order to identify the transmission line effect in the energy saving system proposed. The identification of important parameters such as density, mass, displacement, velocity and air dynamic viscosity is outlined. The experiment procedure is explained and a comparison between the lumped and finite difference approach in transmission line modelling are presented.

4.1 Restriction/Orifice modelling

The most commonly used device to control fluid flow is the variable orifice. It can be said that it is the fluid equivalent of an electrical resistor. It is popular due to the fact that it is simple, reliable and easy to manufacture.

Many pneumatically powered systems only have to be capable of full cylinder extension or retraction hence the controlling orifices need only be in the fully open or fully closed configuration. In this thesis, the flow control valves used in all experiments operate in this manner.

An important aspect in utilising the orifice equation is the working fluid itself. If the working fluid is highly incompressible for example water or hydraulic oil, then

volumetric flowrate Q can be used and is a reasonable assumption for conventional hydraulic fluids. However if the working fluid is air as in pneumatic systems, mass flowrate $\dot{m}$ should be considered since in the case of compressible flow, volume and pressure are interdependent. Note that the following texts and figures are based on McCloy[30] which provides excellent reference for restriction/orifice equations.

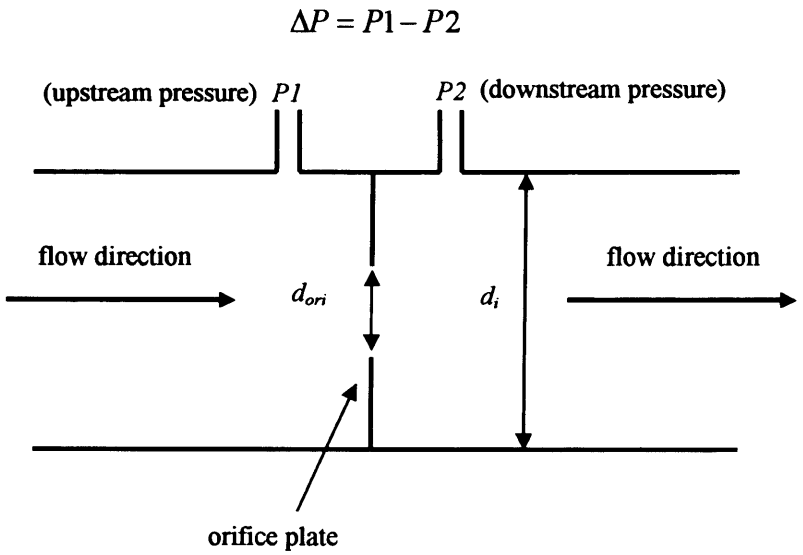

Figure 4.1: Flow through an orifice[30]

The mass rate of flow $\dot{m}$ formula can be written as follows:

$$\dot{m} = \frac{C_d \cdot C_m \cdot A_t \cdot P_u}{\sqrt{T_s}} \quad \text{..... (4.1)}$$

Mass flow parameter C_m can be written as:

$$C_m = \sqrt{\frac{2\gamma}{R(\gamma-1)}\left\{\left(\frac{P_{vc}}{P_u}\right)^{2/\gamma} - \left(\frac{P_{vc}}{P_u}\right)^{(\gamma+1/\gamma)}\right\}} \quad \text{..... (4.2)}$$

The above C_m equation only applies when $\frac{P_{vc}}{P_u} > \left(\frac{2}{\gamma+1}\right)^{\gamma/\gamma-1} = 0.528$. It is also worth to note that when $\left(\frac{P_{vc}}{P_u}\right)$ is less than this value, the flow is said to be choked and C_m becomes:

$$C_m = \left(\frac{2}{\gamma+1}\right)^{1/\gamma-1}\sqrt{\frac{2\gamma}{R(\gamma+1)}} = 0.0405 \quad \text{..... (4.3)}$$

Under choked conditions, if for example P_u is fixed, a decrease in P_{vc} will not result in an increase in $\dot{m}$ value.

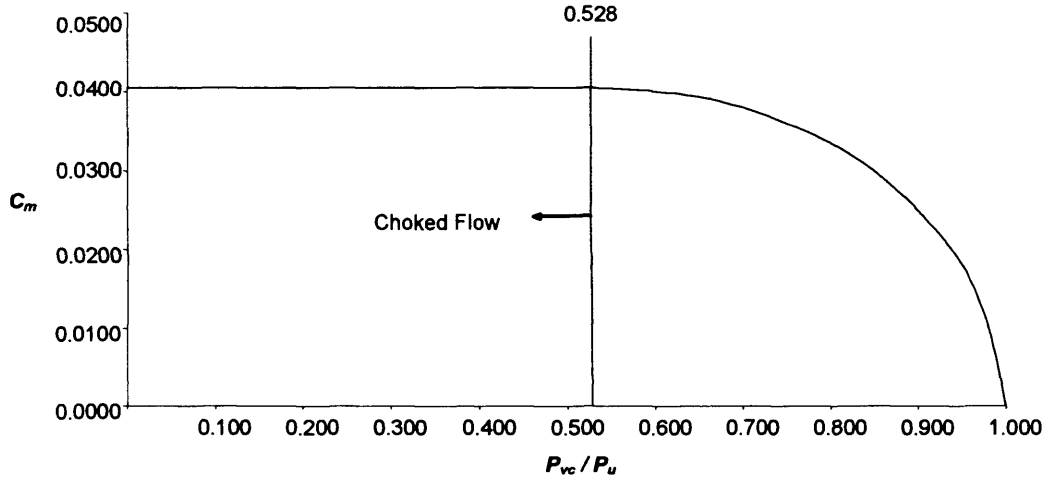

Figure 4.2: Variation of C_m value with pressure ratio[30]

Theoretically pressure at vena contracta P_{vc} is less than the pressure at the downstream of the orifice. Furthermore it is physically complex and impossible with the current test rig to measure the exact pressure at vena contracta. In the consecutive computer simulations, the P_{vc} value is assumed to be the same as the pressure downstream of the orifice.

Considering the thermal-dynamic effect, it is understood that from equation (4.1) the mass flowrate $\dot{m}$ is inversely proportional to the square-root value of the system temperature T_s. An increase in system temperature will result in a decrease in mass flowrate if other parameters are to be kept the same.

Determination of discharge coefficient C_d is an important aspect in utilising orifice equation. Theoretically it is a function of Reynolds number Re and exact orifice geometry. However it is often suffice to determine this particular coefficient analytically based on von Mises model and thus important assumptions needs to be specified. The coefficient of discharge C_d can be represented by this formula:

$$C_d = C_c C_{vel} \quad (4.4)$$

C_c is the contraction coefficient and C_{vel} is the flow velocity coefficient. It is assumed that the flow is steady and viscosity effects are negligible. The flow is also assumed to be irrotational and in two-dimensional behaviour. Gravity effects were considered to be negligible and the working fluid is considered as incompressible.

The assumption that the viscosity effects were ignored implies that there is no friction loss from upstream to vena contracta and hence the value of C_{vel} is unity. In most cases, flow in a control valve is generally far from being irrotational. However vortices occurring upstream of the orifice have a very small effect on the system as well as vortices occurring downstream of the vena contracta. Gravity effects were ignored since it presents a small impact in most conventional fluid control valves.

It is assumed that the valves used in the test rig as shall be shown later can be generally considered as a cylinder having a floor opening. As mentioned earlier C_d were determined analytically using von Mises model. The contraction coefficient C_c which is a component of C_d as presented by equation (4.4) can be obtained from correct interpretation of von Mises results.

Figure (4.3(a)) shows a configuration described by von Mises as a side lying opening in a horizontal floor.

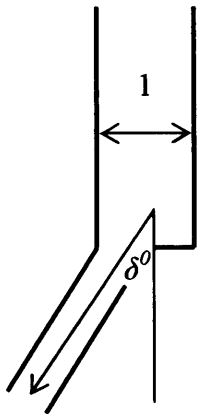

(a) von Mises model

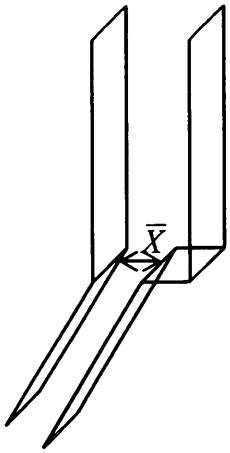

(b) Spool valve orifice

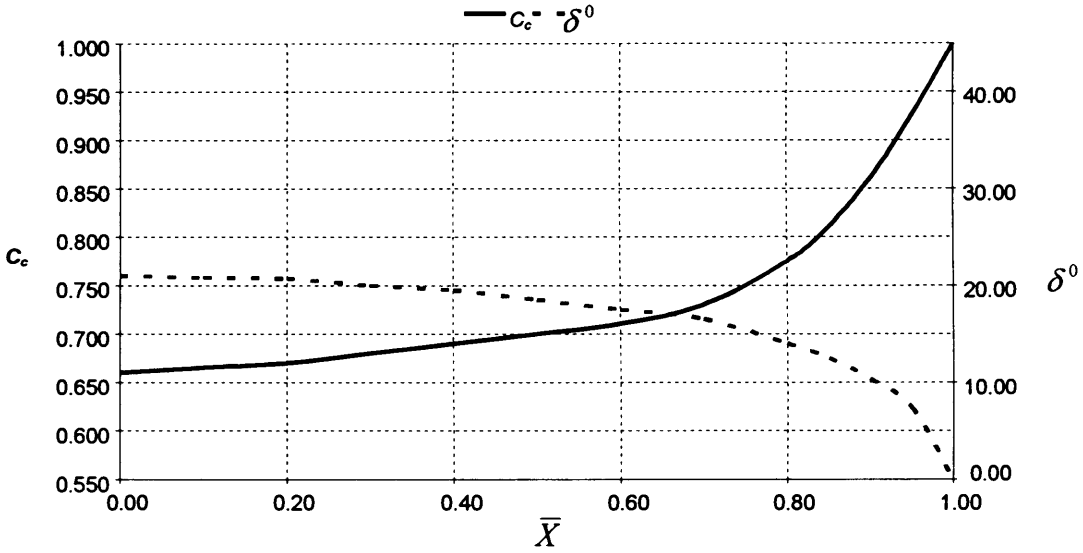

(c) Chart of von Mises contraction coefficient (C_c), discharge angle (δ^o) and floor opening ($\bar{X}$) for a two-dimensional spool valve

Figure 4.3: Contraction coefficient and discharge angle for a two-dimensional spool valve[30]

It can be immediately gathered that assumptions applied can be said as a simplification of the model. However based on results gathered from simulation of the energy saving test rig that will be presented later in chapter 6, it was found that simulation results do present preferable similarities with the experiment data and thus it was concluded that the determination of C_d value using this model and assumptions made were acceptable.

The chosen C_d value of 0.72 was used in the computer simulation for air being discharge between the main valve and the transmission line and this is done by trial. Based on Figure (4.3(c)) the corresponding jet angle was found to be 17.5^0 and having a corresponding floor opening ($\overline{X}$) factor of 0.62. Due to the confidentiality of valve design among manufacturers, analytical determination based on von Mises model is the most suitable way of modelling air flow through a valve orifice.

4.2 Lumped volume modelling

In general, the lumped component model is a way of simplifying the behaviour of spatially distributed systems into a topology consisting of discrete entities that approximate the behaviour of the distributed system under certain assumptions. This is done by modelling both the steady-state behaviour including additional dynamic behaviour and then assigning them to the respective component blocks. For example, a 10m long pipe can be treated as a large body having the same volume.

In the development stage of this research, the considered lumped system consists of a large volume ($1.0\times10^{-4}\,m^3$) at the end of a long circular cross-section transmission line having 7.0m length and a continuous supply pressure *Ps* of 6.5bar at the inlet of the transmission line. The transmission line under investigation has a cross-sectional diameter of 5.0mm and is equally divided into 4 segments as shown in Figure (4.4). The lumped analogy of the system is presented in Figure (4.5).

Initial conditions are that the valve is closed and pressures in the transmission line and in the large volume are all at atmospheric pressure. Once the valve is open, the air travels downstream through the valve from the inlet of the transmission line and into the large volume through an orifice. This simulation is done by utilising orifice equation as described earlier. Diagrammatically it can be presented below.

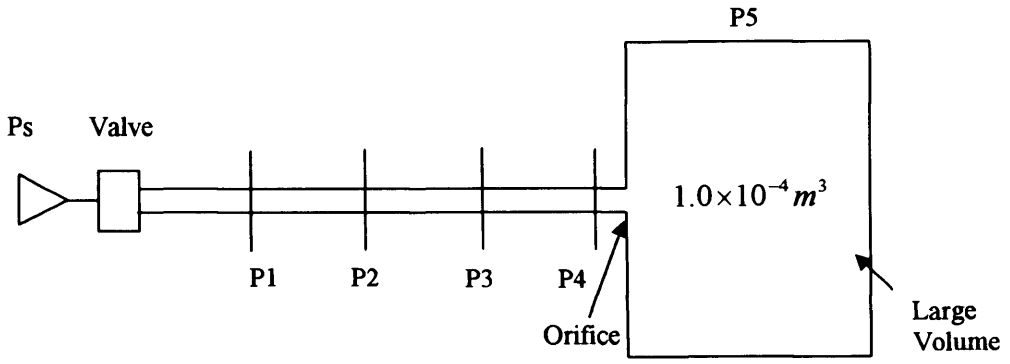

Figure 4.4: Air flow into a large volume

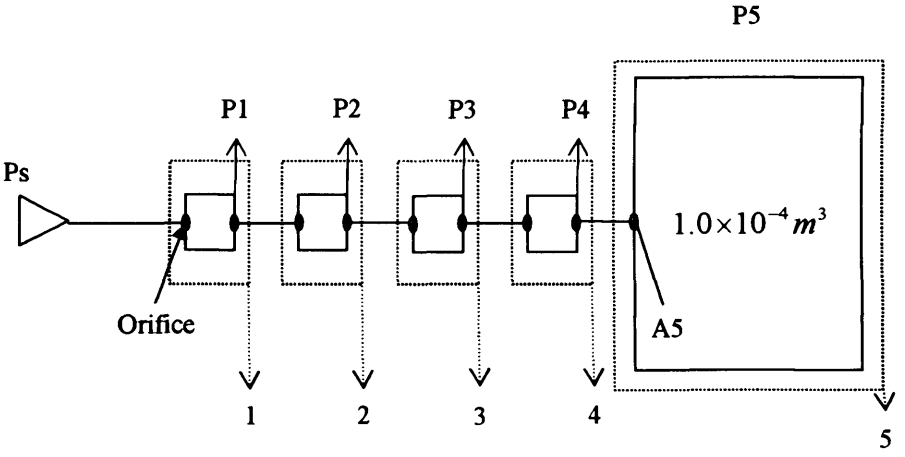

Figure 4.5: Lumped analogy of system in Figure 4.4

This type of arrangement is the preferable initial step into modelling more complex systems. This enables easier future modifications of the lumped system to incorporate an actuator at the end of the air transmission line since the actuator volume is considerably larger than the volume of the transmission line. Furthermore basic relationship between pressures, mass, volume, gas constant, and temperature can be better understood. Other parameters such as discharge coefficient C_d, mass flow parameter C_m and mass flowrate $\dot{m}$ were also utilised.

Figure (4.6) shows the result of the lumped modelling approach based on the pneumatic system set-up shown in Figure (4.4) above[31]. The corresponding Microsoft Visual C++ program is included in the appendix section named Appendix 1.

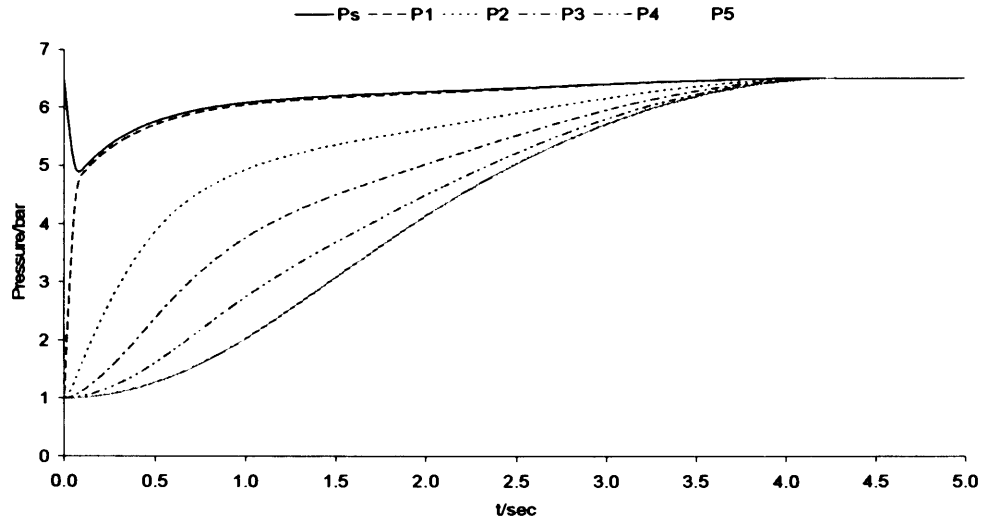

Figure 4.6: Lumped simulation of transmission line having a large volume

In the computer simulation, several differential equations were used and they are continuity equation, state equation and force equation. Once mass flowrate $\dot{m}$ was obtained from equation (4.1), it was then substituted into the continuity equation as shown below:

$$\frac{dm_j}{dt} = \dot{m}_{j-1} - \dot{m}_j \quad \text{..... (4.5)}$$

The obtained mass flowrate $\dot{m}$ flowing through the transmission line is then substituted into the state equation as follows:

$$\frac{dP_j}{dt} = \frac{RT_s}{V_j}\left(\dot{m}_{j-1} - \dot{m}_j\right) \quad \text{..... (4.6)}$$

By multiplying $\frac{dP_j}{dt}$ with sampling time T, the pressure change at position j at that instant of time can be obtained.

The assumption made is that the air flowing through the transmission line is under laminar condition. Based on D'Arcy equation[14], friction factor (4f) can be calculated and the overall friction force F_{fr} at position j can be calculated as follows:

$$F_{fr_j} = (4f)\frac{l_t u_j^2 \rho_j}{2d_i} A_t \quad \text{..... (4.7)}$$

For laminar flow, friction factor ($4f$) can be written as:

$$(4f) = \frac{64}{\mathrm{Re}_j} \quad \text{..... (4.8)}$$

where Reynolds number at position j is given by:

$$\mathrm{Re}_j = \frac{\rho_j u_j d_i}{\mu_j} \quad \text{..... (4.9)}$$

Substituting equations (4.8, 4.9) into equation (4.7) yields:

$$F_{fr_j} = \left(\frac{64\mu_j}{\rho_j u_j d_i}\right)\frac{l_t u_j^2 \rho_j}{2d_i} A_t \quad \text{..... (4.10)}$$

since

$$A_t = \frac{\pi d_i^2}{4} \quad \text{..... (4.11)}$$

Equation (4.10) can be re-written as below:

$$F_{fr_j} = 8\pi\mu_j l_t u_j \quad \text{..... (4.12)}$$

The friction force against the compressed air was obtained by using equation (4.12). It was then substituted into force equation based on Newton's Second Law.

$$m_j \frac{du_j}{dt} = m_j a_j = A_t\left(P_{j-1} - P_j\right) - F_{fr_j} \quad \text{..... (4.13)}$$

By rearranging the force equation, the acceleration of the air flow was obtained.

$$\frac{du_j}{dt} = \frac{\left(A_t\left(P_{j-1} - P_j\right) - F_{fr_j}\right)}{m_j} \quad \text{..... (4.14)}$$

The distance travelled by the air flow can also be determined by using the displacement equation as follows:

$$Z_j = \frac{1}{2}\frac{du_j}{dt}T^2 \quad \text{..... (4.15)}$$

The disadvantage of using lumped modelling is that it considers orifice equation for mass flowrate at each segment sides. However, the tube has little change in cross-section on shape and area. Comparison between modelling of pneumatic system using lumped volume and finite difference are presented in 4.10.4 and 4.10.5 respectively.

4.3 Finite Difference modelling

In mathematics, finite difference is similar to differential quotient, except that it uses finite rather than infinitesimal quantities. In the finite difference approach, the continuous problem domain is converted in such a way that dependent variables are considered to exist only at discrete points. Usually this is called discretization[13]. The derivatives are approximated by differences resulting in an algebraic representation of the partial differential equation (PDE). There are several issues that are usually associated in solving PDEs using the finite difference method and they are truncation error, discretization error, consistency and stability.

Truncation error in computer simulation is when an exact analytic solution to a PDE is affected by rounding to a finite number of digits in the arithmetic operations. This is due to the existence of large number if dependent, repetitive operations that are usually involved.

Discretization error exists when the continuous problem in PDEs are replaced with a discrete one and is defined as the difference between the exact solution of PDE and the exact solution of finite difference equation. It can thus be said that these differences would equal to the sum of the discretization error and the truncation error associated with the finite difference calculation.

A finite difference representation of a PDE can be said to be consistent when the difference between the PDE and its difference representation vanishes as the mesh is refined. This will be the case when the truncation error approaches zero as the grid is refined.

Stability issues deal with marching problem. A numerical scheme is said to be stable when errors from any source (truncation, etc.) are not permitted to grow in the sequence of numerical procedures as the calculation proceeds from one marching step to the next. The solution to the stability problem is usually time consuming compared with other types of errors. In the case of fluid transmission line modelling, the mechanism of the flow must be understood well in order to apply the correct finite difference solution to the involved PDEs especially regarding the direction of the fluid flow.

Depending on the type of finite difference method chosen, this scheme often requires high computing power and memory at its disposal. The advantage of utilising this method is that conservation laws namely continuity, momentum and even energy equations can be applied. This enables the dynamic characteristics of the working fluid to be observed such as pressure ripples due to pressure wave propagation in the fluid transmission line. Effects such as temperature variation of the fluidic system can also be modelled if one considers the conservation law of energy. In other words, this feature makes it possible to model fluid systems to some excellent accuracy and at the same time satisfying the universal laws of conservation.

Often in modelling of fluid dynamics, 2^{nd} order schemes are preferable to 1^{st} order due to the fact that 1^{st} order schemes are inherently inaccurate. Obviously there are higher order schemes available (3^{rd} and 4^{th} order), however these schemes are more complex to apply since numerical stability is harder to achieve. Furthermore

such schemes create more equations that needed to be solved in each time step thus requiring higher computing power and memory. In most cases, 2nd order schemes are accurate enough and have a preferable balance between computing time and accuracy in results obtained. Note that the following texts are mainly based on Tannehill[13] which provides excellent reference for finite difference modelling.

There are basically 3 types of discretization namely backward, forward and central difference. Backward difference is typically associated with the Upwind method or sometimes called Upstream or Windward method. Forward difference meanwhile is used in Euler and MacCormack method while central difference is used in the Lax-Wendroff method. In this thesis, computer simulation is based around a combination of both 2nd order Upwind and 2nd order MacCormack finite difference method.

In order to illustrate the 3 types of discretization method explained above, a simple example will be given by using a first order, one-dimensional form of wave equation which can be written as shown below. This equation governs the propagation of sound waves travelling at a wave speed c in a uniform medium.

$$\frac{\partial u}{\partial t} + c\frac{\partial u}{\partial x} = 0 \qquad (4.16)$$

For **backward difference**, equation (4.16) can be re-written in finite difference form as:

$$\frac{u_j^{n+1} - u_j^n}{\Delta t} + c\frac{u_j^n - u_{j-1}^n}{\Delta x} = 0 \qquad \text{when } c > 0 \qquad (4.17)$$

Solution (4.17) obtained is called 1st order Upwind method. The discretization points are between segments j and $j-1$ while n denotes the time-level. For central difference example, again equation (4.16) can be written as:

$$\frac{u_j^{n+1} - \left[\frac{\left(u_{j+1}^n + u_{j-1}^n\right)}{2}\right]}{\Delta t} + c\frac{u_{j+1}^n - u_{j-1}^n}{2\Delta x} = 0 \quad \text{..... (4.18)}$$

Equation (4.18) is called 1st order Lax solution. Note that for **central difference** the discretization points are between $j+1$ and $j-1$.

For **forward difference** method,

$$\frac{u_j^{n+1} - u_j^n}{\Delta t} + c\frac{u_{j+1}^n - u_j^n}{\Delta x} = 0 \qquad \text{when } c > 0 \quad \text{..... (4.19)}$$

Equation (4.19) is called 1st order Euler solution. Note the discretization points are between $j+1$ and j.

All of the above examples are mathematically explicit. Sometimes implicit solutions can also be used to solve PDEs. However this depends on the type of problems encountered. Generally explicit methods can solve most of PDEs. In this thesis all mathematical solutions are carried out explicitly.

Due to the fact that there many techniques in applying finite difference solution to PDE problems; only a handful of these techniques are discussed in this thesis.

A simulation was conducted to exhibit different characteristics of using different types of finite difference method. Namely these methods are 1st order Lax, 2nd order Lax-Wendroff, 2nd order MacCormack and 2nd order Upwind. In this simulation, inviscid Burger's equation[13] is used in the form of:

$$\frac{\partial u}{\partial t} + \frac{\partial F}{\partial x} = 0 \quad \text{..... (4.20)}$$

where F component is defined as:

$$F = \frac{u^2}{2} \quad \text{..... (4.21)}$$

These methods are then applied to a discontinuity of 0-1. Result of this simulation is presented below.

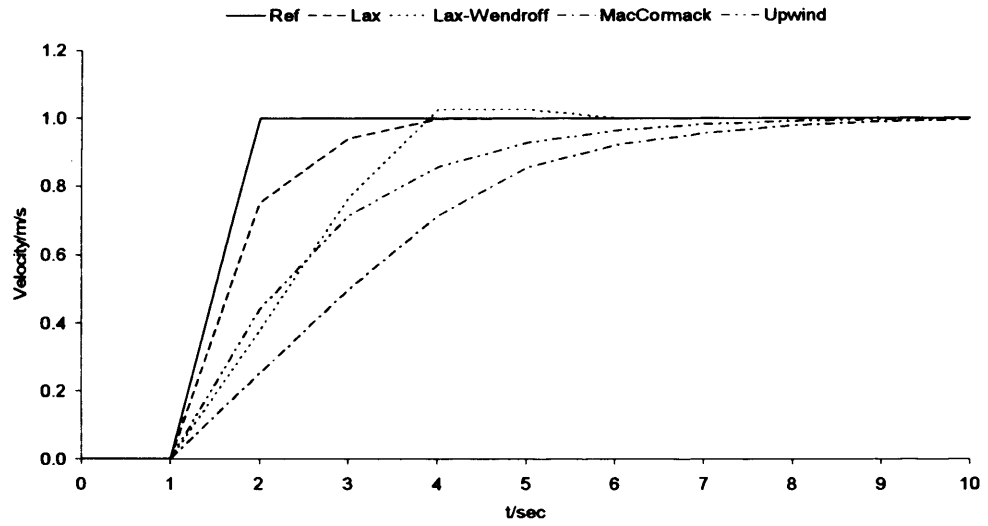

Figure 4.7: Variation of different finite difference techniques on 0-1 discontinuity

Note that all the solutions are monotone or in other words, the solutions do not oscillate. This is highly desirable when discontinuities are encountered. However the desirability of monotone behaviour must reconcile with the highly dissipative character of the results. As a point of reference, 1st order Lax method use centred difference, Lax-Wendroff method is a 2nd order version of 1st order Lax method and also uses centred difference. 2nd order MacCormack method uses predictor-corrector steps and utilises forward difference while 2nd order Upwind method is another variant of MacCormack method except that it uses backward difference. Listed below are the equations used.

1st order Lax method:

$$u_j^{n+1} = \frac{u_{j+1}^n + u_{j-1}^n}{2} - \frac{\Delta t}{\Delta x}\frac{F_{j+1}^n - F_{j-1}^n}{2} \quad \text{..... (4.22)}$$

2nd order Lax-Wendroff method:

$$u_j^{n+1} = u_j^n - \frac{\Delta t}{\Delta x}\frac{F_{j+1}^n - F_{j-1}^n}{2} + \frac{1}{2}\left(\frac{\Delta t}{\Delta x}\right)^2 \times \left[A_{j+\frac{1}{2}}^n\left(F_{j+1}^n - F_j^n\right) - A_{j-\frac{1}{2}}^n\left(F_j^n - F_{j-1}^n\right)\right]$$

$$A_{j+\frac{1}{2}} = \frac{u_j + u_{j+1}}{2} \quad \text{and} \quad A_{j-\frac{1}{2}} = \frac{u_j + u_{j-1}}{2} \qquad (4.23)$$

2nd order MacCormack method:

Predictor step: $$\overline{u_j^{n+1}} = u_j^n - \frac{\Delta t}{\Delta x}\left(F_{j+1}^n - F_j^n\right) \qquad (4.24)$$

Corrector step: $$\frac{1}{2}\left[u_j^n + \overline{u_j^{n+1}} - \frac{\Delta t}{\Delta x}\left(\overline{F_j^{n+1}} - \overline{F_{j-1}^{n+1}}\right)\right] \qquad (4.25)$$

2nd order Upwind method:

Predictor step: $$\overline{u_j^{n+1}} = u_j^n - \frac{\Delta t}{\Delta x}\left(F_j^n - F_{j-1}^n\right) \qquad (4.26)$$

Corrector step: $$\frac{1}{2}\left[u_j^n + \overline{u_j^{n+1}} - \frac{\Delta t}{\Delta x}\left(\overline{F_{j+1}^{n+1}} - \overline{F_j^{n+1}}\right)\right] \qquad (4.27)$$

The suitability of methods to be chosen depends on the type of application, ease of use and computational feasibility. Furthermore considerations such as sampling time and segment length are important in obtaining the required result and at the same time avoiding numerical instability. All the factors regarding finite difference modelling cannot possibly be discussed in this thesis due to various methods available and the fact that each differs in terms of stability issues, mathematical algorithm and applications. For further information, it is highly recommended that reader consult an excellent article review by Leer[32] and finite difference schemes by Tannehill[13].

4.4 Application of finite difference modelling to an air flow

Based on the conservation laws derived in chapter 2 and finite difference method earlier in this chapter, it is possible to apply finite difference scheme to model air flow in transmission line. As mentioned earlier, in order to apply this scheme, the

direction of the air flow must be known so that appropriate differencing method can be applied. In this subchapter, the applied finite difference scheme is explained.

The first step is to consider a unit volume of air flowing into an end blocked transmission line from left to right just before it hits the end wall. The transmission line is then divided into 3 equal segments as shown in Figure 4.8.

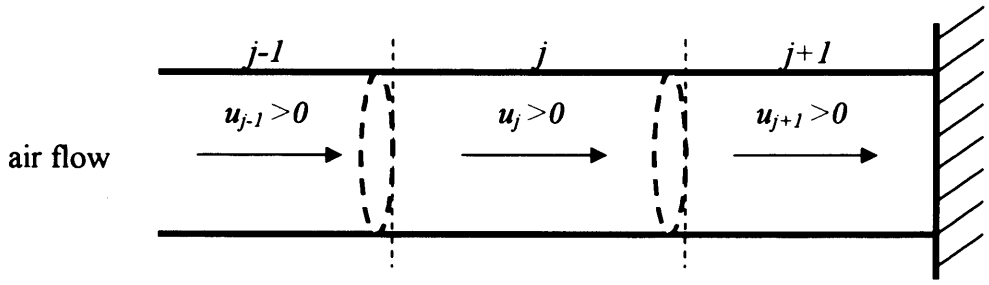

Figure 4.8: Air flow from left to right in a blocked transmission line

In this case one-dimensional flow is considered and the suitable discretization method that should be applied is backward differencing since the changes induced at say position *j* is primarily caused by the flow upstream to that position *j-1* for air flowing from left to right. Therefore based on the vector form of one-dimensional Navier-Stokes equations and omitting energy equations; equations (2.45, 2.46) as described earlier in chapter 2 can be written as:

$$D=\begin{bmatrix}\rho\\ \rho u\end{bmatrix} \qquad (4.28)$$

$$E=\begin{bmatrix}\rho u\\ \rho u^2+P-\tau_{xx}\end{bmatrix} \qquad (4.29)$$

where (τ_{xx}) is:

$$\tau_{xx}=\frac{2}{3}\mu\left(2\frac{\partial u}{\partial x}\right) \qquad (4.30)$$

Now by considering backward difference, equation that needs to be solved in each segment j is:

$$\overline{D_j^{n+1}} = D_j^n - \frac{\Delta t}{\Delta x}\left(E_j^n - E_{j-1}^n\right) \quad (4.31)$$

Again utilising the same approach, once the flow had hit the blocked end, the flow will experience compression due to momentum effect, and then starts to flow in the opposite direction. Once the flow is fully flowing in the opposite direction and using the same segments notation as before, air flow direction as shown in Figure (4.9) is obtained.

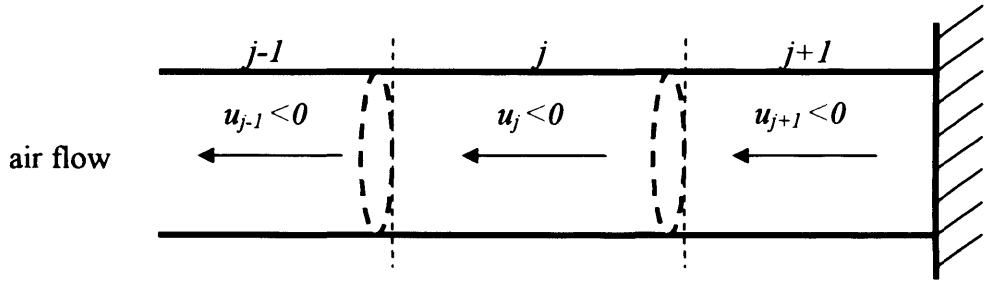

Figure 4.9: Air flow from right to left in a blocked transmission line

In this case, forward differencing discretization can be considered since the change induced at position j is primarily caused by the flow upstream from that position $j+1$. Now we have:

$$\overline{D_j^{n+1}} = D_j^n - \frac{\Delta t}{\Delta x}\left(E_{j+1}^n - E_j^n\right) \quad (4.32)$$

However, in order to utilise both equations (4.31, 4.32), the flow direction must be deduced mathematically. Solution to this problem is outlined below. Consider Figure (4.10) when the flow hits the blocked end; the flow head will undergo compression due to the momentum effect and after a certain time t, it will flow in the opposite direction and travel back up the transmission line (right to left):

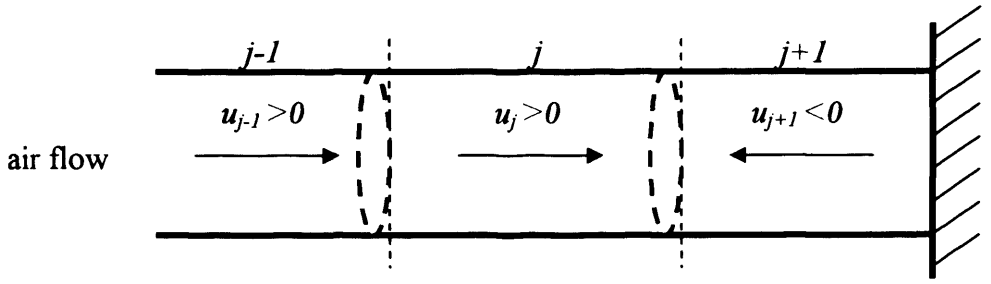

Figure 4.10: Air flow under compression in a blocked transmission line

Theoretically, velocity element in segment $j+1$ will decrease to zero and becomes negative (moving in the opposite direction) first, followed by segment j and finally segment $j-1$ due to the compression of the flow head at the blocked end. By using this information, it is possible to set up a rule on which of the mathematical algorithm (equation 4.31 or 4.32) is to be used during any iteration step.

Mathematically, when the velocity element in segment $j-1$ reaches zero or less, it can be deduced that the flow is fully flowing in the reverse direction (right to left). In a reverse scenario, when the velocity element in segment $j+1$ reaches zero or less, then the flow is fully flowing in left to right direction provided that the other end of the transmission line is blocked as well. With this analysis, the direction of the flow can be determined.

The determination of flow direction and specification of correct boundary conditions are important in obtaining the desired results and avoiding undesirable numerical oscillations. As mentioned earlier, it is possible that in poorly defined sequence of mathematical algorithm, numerical oscillations will lead to instability, misleading results and can cause the simulation to crash.

4.5 Decoding the vector equations

Another important factor of finite difference approach in air flow modelling is determining the primitive variables needed to calculate the updated pressure P, mass flowrate $\dot{m}$ and dynamic viscosity μ values before completing each iteration step. These are density ρ and velocity u from the vector form of one-dimensional Navier-

Stokes equation (4.28). After each iteration step, the variables can be found by re-writing the D vector in the form shown below.

$$D = \begin{bmatrix} \rho \\ \rho u \end{bmatrix} = \begin{bmatrix} U_1 \\ U_2 \end{bmatrix} \quad (4.33)$$

$$\rho = U_1 \quad (4.34)$$

$$u = U_2 / U_1 \quad (4.35)$$

As before mass flowrate $\dot{m}$ can then be calculated from equation (4.5) and pressure P from equation (4.6). However in finite difference approach the air density ρ can be determined directly from equation (4.34) and air velocity directly from equation (4.35). The dynamic viscosity μ can be calculated using the relationship between kinematic viscosity of air v and air density ρ as shown below.

$$\mu = \rho v \quad (4.36)$$

The viscosity is the fluid resistance to shear or flow and is a measure of the frictional fluid property[16,33]. The resistance is caused by intermolecular friction exerted when layers of fluids attempts to slide by each other. The dynamic viscosity μ is the tangential force per unit area required to move one horizontal plane with respect to the other at unit velocity when maintained at unit distance. Kinematic viscosity v is the ratio of dynamic viscosity μ to density ρ.

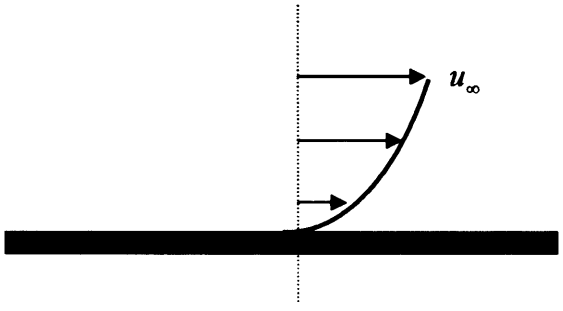

Figure 4.11: Air velocity profile over a fixed surface

When a viscous fluid flows over a fixed surface, layers of fluid next to the surface are held back by the viscous forces and stick to the surface; thus the air velocity at the fixed surface is zero and increases to its free stream value u_∞ in a velocity profile as presented in Figure (4.11).

The kinematic viscosity of air v was determined from the published standard air properties[23]. For air condition at room temperature (20°C) and under normal atmospheric pressure the value determined was found to be 1.51×10^{-5} m^2s^{-1}.

Armed with these primitive variables and utilising the equation of state (2.42) as mentioned earlier in chapter 2, the air mass m, pressure P, density ρ, velocity u and dynamic viscosity μ can be updated accordingly during each iteration step. Important air parameters can be therefore determined at any designated position across the system in the computer simulation.

4.6 Average air flow velocity

The calculation of average air flow velocity u_m as applied to vector form for compressible Navier-Stokes equations (4.28 and 4.29) is important with regards to the velocity profile of the flow considered. The air flow is assumed to have a laminar type velocity profile as shown in Figure (4.12).

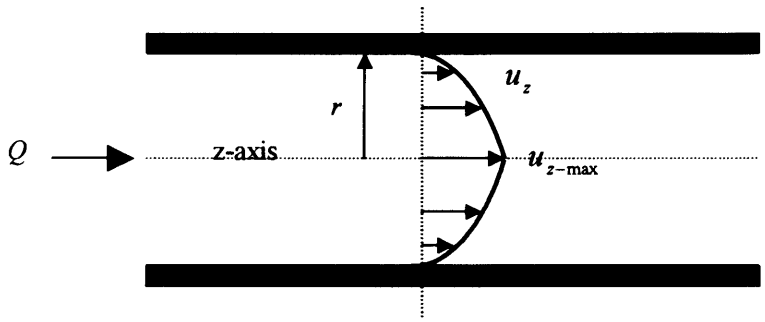

Figure 4.12: Laminar flow velocity profile

The maximum flow velocity occurs right at the centre of the pipe on the z-axis while zero flow occurs exactly at the wall of the container. Poiseuille law[15,16] state that the flow velocity u_z at any cross-section has a parabolic distribution. In order to calculate the velocity u_z in the z-axis direction, Poiseuille law as shown below can be used.

$$u_z = \frac{1}{4\mu}\left(\frac{\partial P}{\partial z}\right)\left(r^2 - R_t^2\right) = u_{z-\max}\left(1 - \frac{r^2}{R_t^2}\right) \quad \text{(4.37)}$$

where

$$u_{z-\max} = -\frac{1}{4\mu}\left(\frac{\partial P}{\partial z}\right)R_t^2 \approx \frac{\Delta P}{4\mu l_t}R_t^2 \quad \text{(4.38)}$$

ΔP is the pressure drop along the tube of length l_t. Volumetric flowrate Q can be calculated as shown below.

$$Q = \frac{\pi R_t^4 \Delta P}{8\mu l_t} \quad \text{(4.39)}$$

Based on flowrate Q above, the mean velocity u_m can be expressed as shown below:

$$u_m = Q/A_t \quad \text{(4.40)}$$

Inserting equation (4.39) into (4.40) yields the air mean velocity u_m.

$$u_m = \frac{\pi R_t^4 \Delta P}{8\mu l_t} \cdot \frac{1}{\pi R_t^2} = \frac{R_t^2 \Delta P}{8\mu l_t} \quad \text{(4.41)}$$

The position of this mean velocity u_m can also be determined as shown below based on equation (4.38).

$$\frac{u_m}{u_{z-\max}} = \frac{R_t^2 \Delta P}{8\mu l_t} \times \frac{4\mu l_t}{R_t^2 \Delta P} = \frac{1}{2} \quad \text{(4.42)}$$

Since the ratio of mean velocity u_m against the maximum velocity $u_{z\text{-}max}$ is ½, inserting this ratio into both mean and maximum velocity equations (4.38 and 4.41) provides the radial position r at which this mean velocity occurs as shown below:

$$\frac{\Delta P}{4\mu l_t} R_t^2 \left(1 - \frac{r^2}{R_t^2}\right) = \frac{1}{2} \frac{\Delta P}{4\mu l_t} R_t^2 \quad \text{(4.43)}$$

Cancelling the same variables on both sides yields:

$$r^2 = \frac{R_t^2}{2} \quad \text{(4.44)}$$

Therefore:

$$r = \frac{R_t}{\sqrt{2}} \quad \text{(4.45)}$$

4.7 Bulk modulus

The compressibility of working fluid is a major factor in determining system's resonant frequency which in turn puts limitation on the output speed of the system's response. For pneumatic systems, since air is the working medium, the effect of compressibility is an important issue.

Air volume in a fixed volume (in a unit length of transmission line) that compresses under applied force can be represented as shown below.

$$\frac{\Delta V}{V} = -\frac{\Delta P}{\beta_a} \quad (4.46)$$

where ΔV is the volume change, V is the initial volume, ΔP is the pressure increase due to force applied and β_a is the air bulk modulus. The reciprocal of bulk modulus is called compressibility.

Since

$$V_t = V_a \quad (4.47)$$

where V_t is the transmission line volume and V_a is the volume occupied by the air. The relationship between the volume change of the transmission line ΔV_t and the volume change of the air ΔV_a can be deduced as:

$$\Delta V_t = -\Delta V_a \quad (4.48)$$

Based on equation (4.46), air bulk modulus β_a and transmission line bulk modulus β_t can be re-written as:

$$\beta_a = \frac{-V_a \Delta P}{\Delta V_a} \quad (4.49)$$

$$\beta_t = \frac{-V_t \Delta P}{\Delta V_t} \quad (4.50)$$

Rearranging both of the bulk modulus equations (4.49 and 4.50) into a reciprocal effective bulk modulus equation β_e, we have:

$$\frac{1}{\beta_e} = \frac{1}{\beta_a} + \frac{1}{\beta_t} \quad \text{(4.51)}$$

Based on McCloy[30], if the process is considered adiabatic whereby the heat flowing into or out of the volume of air being compressed is restricted, the air bulk modulus β_a can be represented by:

$$\beta_a = \frac{C_p}{C_v} P \quad \text{(4.52)}$$

Specific heat capacity of air at constant pressure C_p is defined as 1005.10J/kgK and specific heat capacity of air at constant volume C_v as 717.90J/kgK.

If the heat flow is constant in which the process is done very slowly, the air bulk modulus β_a can be represented by:

$$\beta_a = P \quad \text{(4.53)}$$

Therefore assuming that the process in which the air is being compressed is adiabatic, the bulk modulus of air can be written as:

$$\beta_a = \frac{1.0051}{0.7179} P \quad \text{(4.54)}$$

If pressure is assumed to be atmospheric at $101.32 \times 10^3 \text{N/m}^2$, consequently the air bulk modulus is found to be $141.85 \times 10^3 \text{N/m}^2$.

From Watton[34] bulk modulus for a transmission line having a circular cross-section can be presented as:

$$\frac{1}{\beta_t} = \frac{2}{\varepsilon}\left[\frac{d_i^{\,2} + d_o^{\,2}}{d_o^{\,2} - d_i^{\,2}} + \alpha\right] \qquad (4.55)$$

Due to the confidentiality of Young's Modulus ε and Poisson's ratio α values for the polyurethane pneumatic tubing used in the test rig, the parameters were determined from Engineering Laboratories Inc., a precision industrial polyurethane ball manufacturer. The parameters determined were $\varepsilon = 621.00\times10^3\ \text{N/m}^2$ and $\alpha = 0.5$. Therefore based on equation (4.55), bulk modulus for the tube of inner diameter of 5mm and outer diameter of 8mm was determined as $111.60\times10^3\ \text{N/m}^2$.

$$\frac{1}{\beta_e} = \frac{1}{141.85\times10^3} + \frac{1}{111.60\times10^3} \qquad (4.56)$$

Finally the effective bulk modulus can be determined as shown above, based on equation (4.51). It was found that the effective bulk modulus β_e for air in a polyurethane pneumatic tube of a circular cross-section is $62.46\times10^3\ \text{N/m}^2$ under standard atmospheric pressure compression. The effective bulk modulus β_e found was too small compared to the bulk modulus for air β_a. Therefore the parameters of Young's modulus ε and Poisson's ratio α used in the calculation example above cannot be true for the determination of the polyurethane transmission line used in the experiment.

The determination of the effective bulk modulus of the transmission line was then based on experiment conducted using water as the working medium and applying high pressure air to compress the water inside a blocked pneumatic tube. The measurement of the change of fluid height under pressure enables one to calculate the volume change of the fluid assuming that the outer diameter and the length of the transmission line remains the same. By applying the bulk modulus equations shown previously, it is possible to determine the exact value of the bulk modulus of the transmission line provided that the Poisson's ratio is taken to be 0.5 which means that

the material is perfectly incompressible. However due to the fact that the determined transmission line bulk modulus β_t (11.61×10^6 N/m^2) is significantly larger than the bulk modulus of air β_a (141.85×10^3 N/m^2), the effect of transmission line bulk modulus was omitted from the computer simulation algorithm.

4.8 Volumetric flowrate conversion

In pneumatic system, mass flowrate $\dot{m}$ is considered rather than volumetric flowrate Q since in the case of compressible flow, volume V and pressure P are interdependent.

According to the flowmeter manufacturer IFM Electronics Ltd., the conversion can be performed by utilising air density ρ property which has a value of 1.225kgm^{-3}. This air density ρ value is true for air at zero sea-level, under atmospheric pressure of 1.0132bar and at a temperature of 293K.

The conversion from volumetric flowrate Q to mass flowrate $\dot{m}$ can be done by utilising the equation shown below. Note that the density ρ value considered is constant under any working pressure P since the volumetric flowrate Q reading given off by the IFM flowmeter had already taken into account the variation of pressure P with density ρ.

$$\dot{m} = \rho \cdot Q \quad \text{..... (4.57)}$$

4.9 Pressure and flowrate response in an air transmission line

In this experiment, polyurethane air transmission line with internal diameter of 5.0mm and a wall thickness of 1.5mm is used. Two IFM flowmeter were utilised. Each unit is placed at upstream and downstream of the transmission line. The air pressure along the line is measured by 5 pressure transducers. A large volume of $1.0\times10^{-4} m^3$ is connected to the transmission line via an on/off valve.

The flow discharge rate can be adjusted by utilising a restrictor at the downstream of the system and a silencer is incorporated at the end of the transmission line. The dynamic pressure response effect caused by a lumped volume was also considered.

The air was supplied by a central station far away from the test rig and the system pressure of the air supplied to the test rig under no-flow state is 7.2bar. The ambient temperature was taken to be 20^0C and is considered to be constant throughout the experiment. Below is the circuit diagram for the experiment conducted.

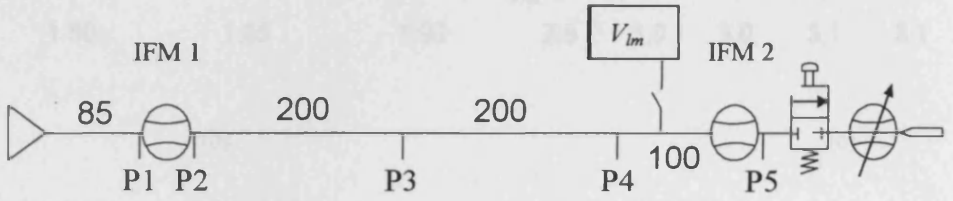

Figure 4.13: Circuit diagram (all dimensions are in cm)

The test rig is operated manually by opening the directional valve to discharge the air from the system and closing it when the system reaches steady state. In this chapter two results are shown and they are results of the system with and without lumped volume V_{lm} which has a value of 2.19×10^{-3} m^3.

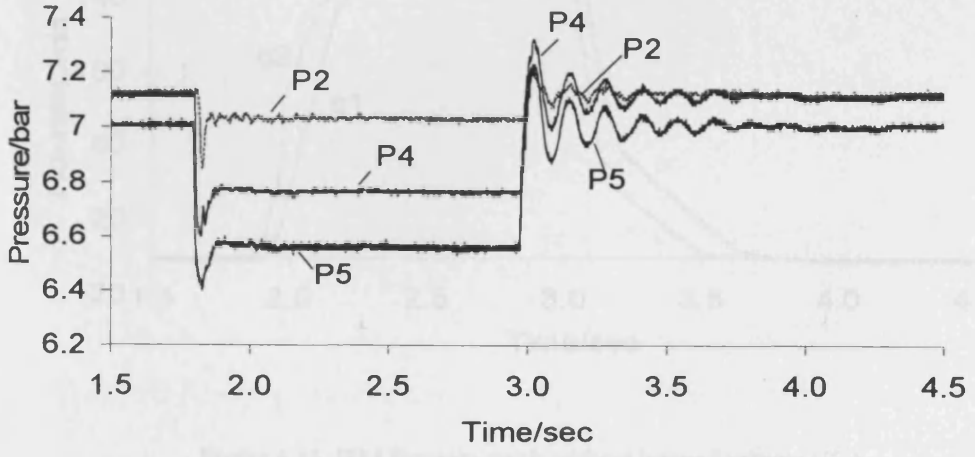

(a)

[continued]

Figure 4.14: Pressure response without lump volume (V_{lm})

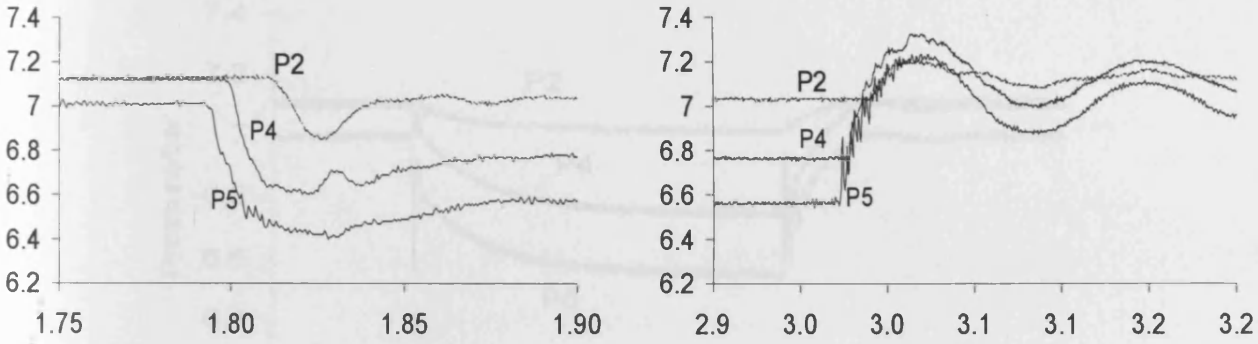

(b) (c)

[end]

Figure 4.14: Pressure response without lump volume (V_{lm})

The following is the volumetric flowrate result:

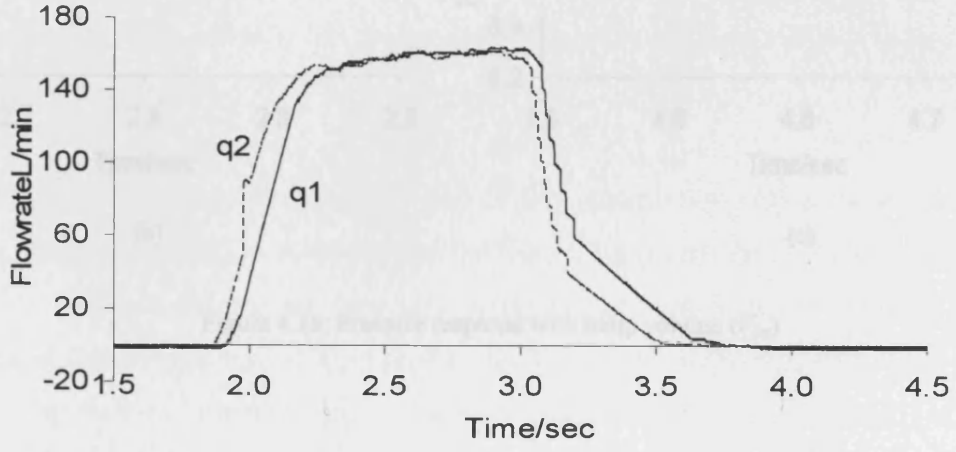

Figure 4.15: IFM flowrate result without lumped volume (V_{lm})

Results with lumped volume (V_{lm}) included in the transmission line are as shown below:

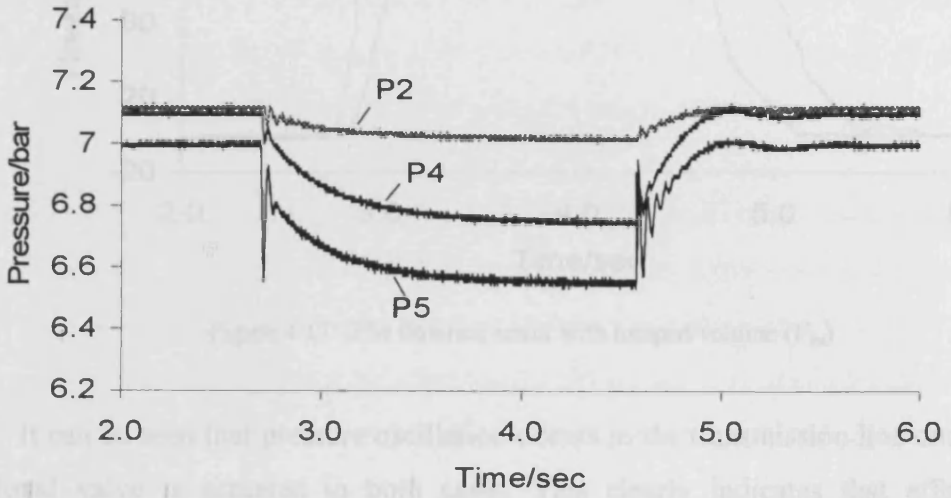

(a)

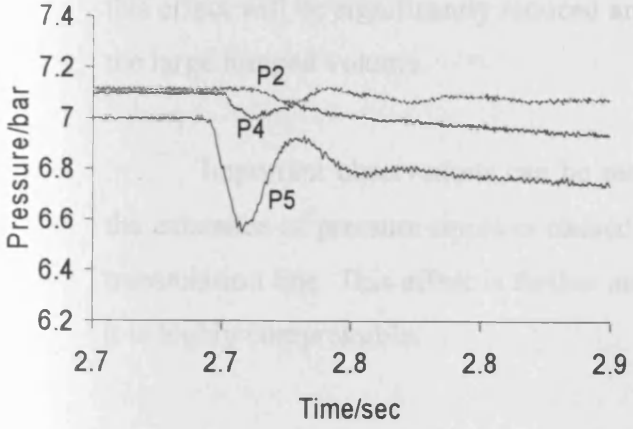

(b)

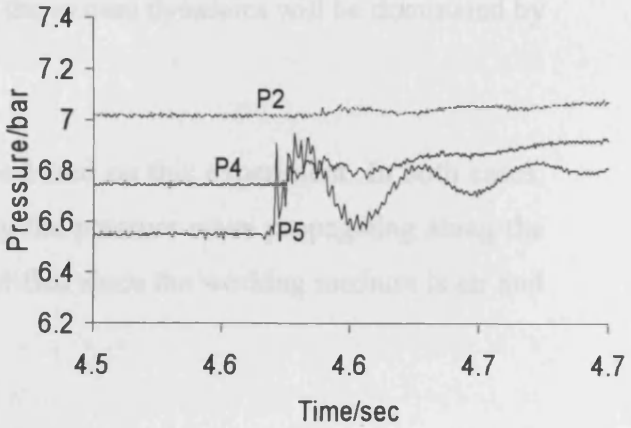

(c)

Figure 4.16: Pressure response with lump volume (V_{lm})

Volumetric flowrate result is shown in Figure (4.17).

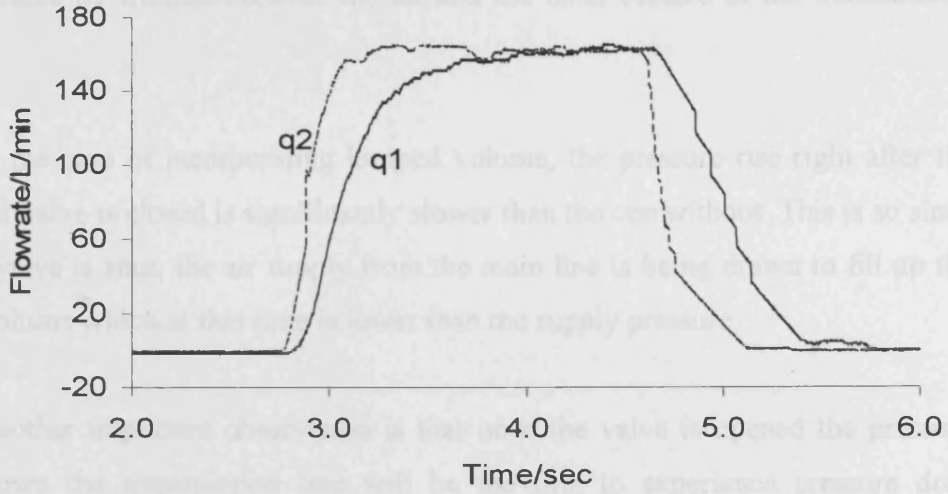

Figure 4.17: IFM flowrate result with lumped volume (V_{lm})

It can be seen that pressure oscillation occurs in the transmission line once the directional valve is actuated in both cases. This clearly indicates that effect of transmission line which is of great importance in a pneumatic system. However if the lumped volume is significantly larger than the overall volume of the transmission line, this effect will be significantly reduced and the system dynamics will be dominated by the large lumped volume.

Important observations can be made based on this experiment. In both cases, the existence of pressure ripple is caused by the pressure wave propagating along the transmission line. This effect is further amplified since the working medium is air and it is highly compressible.

Once the directional valve at the end of the transmission line is closed, there will be a sudden deceleration at the head of the flow. This causes the air at the blocked end to be compressed since air flow still exists at the preceding segments of the transmission line in that time *t*. Due to the effect of momentum, this will force the head flow against the blocked end and causes compression of the medium. After certain time *t*, this wave will travel back up the transmission line due to the fact that the pressure at the preceding segments is lower than the compressed air at the blocked end. This cycle of wave propagating in the transmission line will repeat itself until the pressure wave diminishes due to energy loss caused by viscous effect of the fluid and

heat generated by friction between the air and the inner surface of the transmission line.

In the case of incorporating lumped volume, the pressure rise right after the directional valve is closed is significantly slower than the one without. This is so since once the valve is shut, the air supply from the main line is being drawn to fill up the lumped volume which at that time is lower than the supply pressure.

Another important observation is that once the valve is opened the pressure further down the transmission line will be the first to experience pressure drop followed by the pressure in the preceding segments. Once this valve is closed, again the pressure at the end of the line will increase to the supply pressure first followed by the preceding segments. This observation can be confirmed with the data captured from the IFM flowmeter. The flowmeter situated at the end of the transmission line responds first in cases of valve opened and valve closed. This is also true in both results (with and without lumped volume).

From these discussions, the mechanism of fluid flow in transmission line can be better understood and the importance of transmission line effects can be studied.

4.10 Transmission line dynamics experiment

The objective of this experiment is to investigate the air dynamics in a pneumatic transmission line when the air is stimulated using a critical test method. In order to obtain good simulation results, it is important to identify the initial and boundary conditions of the system under investigation. Based on the experimental setup, the necessary parameters such as pneumatic tube dimensions (diameter and length), system pressure and initial pressure in various positions across the system including mass flowrates were acknowledged. Below are the circuit diagram and the corresponding computer model of the air transmission line experiment.

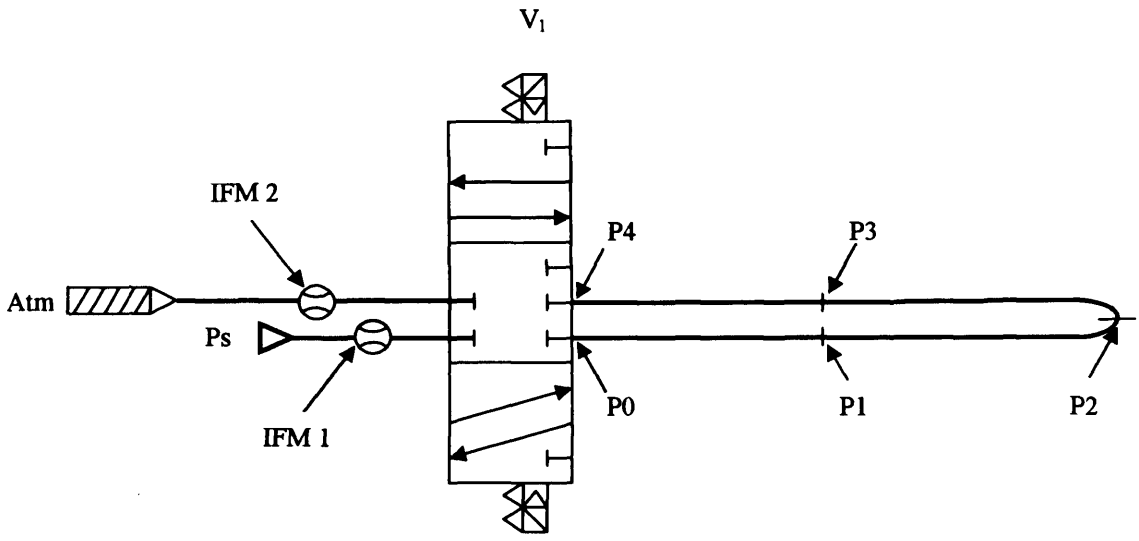

Figure 4.18: Air transmission line experiment circuit

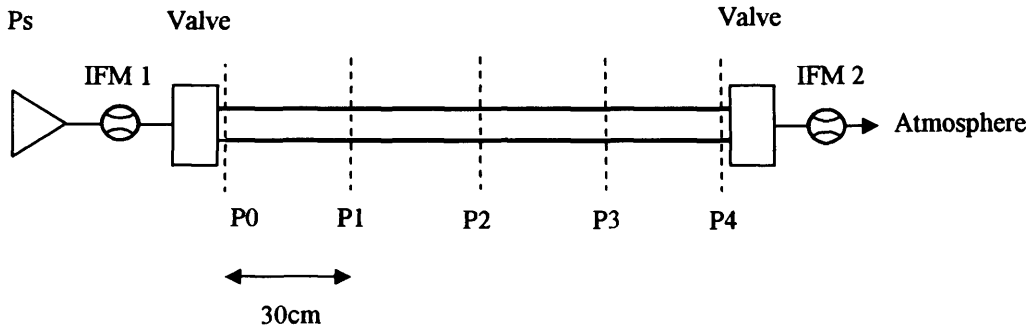

Figure 4.19: Simulation model of the air transmission line experiment

4.10.1 Experiment apparatus

In this experiment, the air is passed through a pneumatic tube having a 5mm diameter with a total length of 1.2m and exhausted to the atmosphere at the end. The transmission line is equally divided into 4 and a pressure transducer is placed in each segment. An SMC 3-position-closed-centre solenoid directional valve (SY7340-5DZ-Q) is used to regulate the air flow. This valve has an operating voltage of 24Volts DC and has a maximum operating pressure of 7.0bar. Picture of the unit is shown in Figure (4.20).

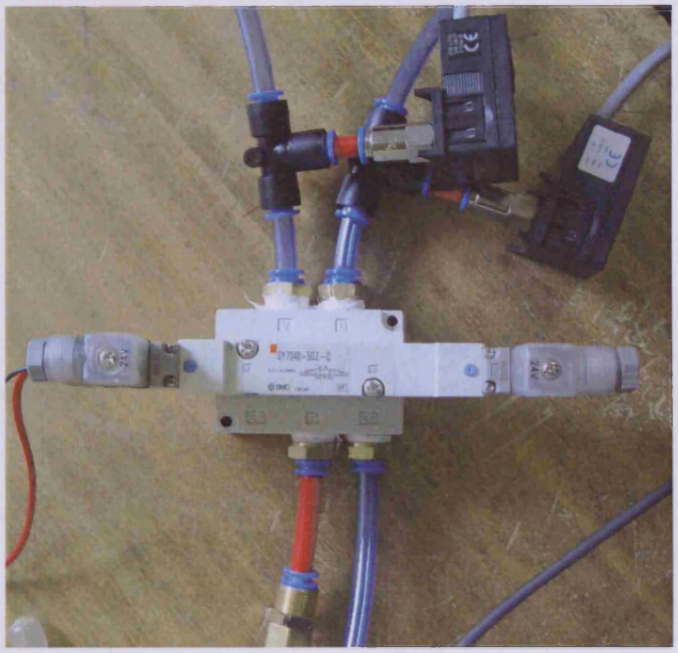

Figure 4.20: SMC solenoid directional valve

Two IFM (SD6000) flowmeters are used in this experiment to obtain the mass flowrate flowing into and out of the system. The first unit is placed before the solenoid directional valve and the other at the end of the transmission line to confirm the reading of the first unit.

4.10.2 Experiment procedure

At the beginning of the experiment, the air is allowed to flow through the transmission line via the directional valve by charging V1 side of the directional valve. When the flow reaches steady-state (no variation in pressure reading along the transmission line), the valve is discharged and thus places the spool in the closed-centre position. At this stage the air in the transmission line becomes trapped since both the inlet and outlet ports of the solenoid directional valve were closed simultaneously. Pressure readings along the transmission line were taken until the air reaches the new steady-state condition. Data were captured using Microstar DAP 4200a.

4.10.3 Experiment data

Figure (4.21) shows the pressure reading taken from the experiment just after the valve was discharged at approximately 7.8s into the experiment.

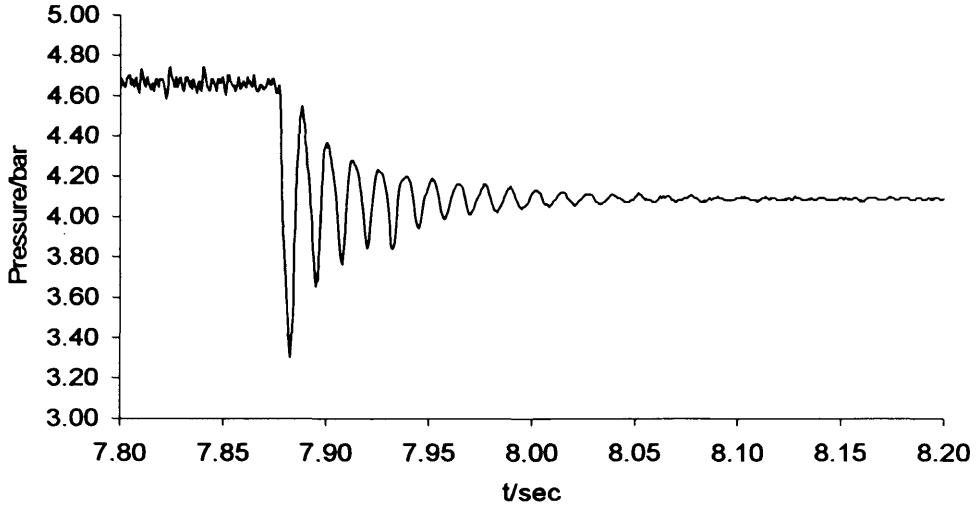

(a) P0

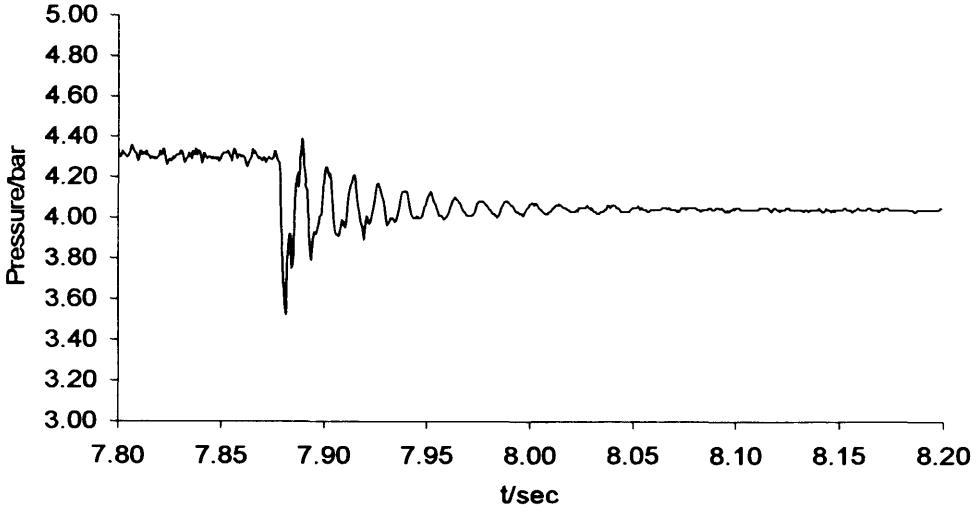

(b) P1

[continued]

Figure 4.21: Experimental data of transmission line experiment at 5 positions (P0,P1,P2,P3,P4)

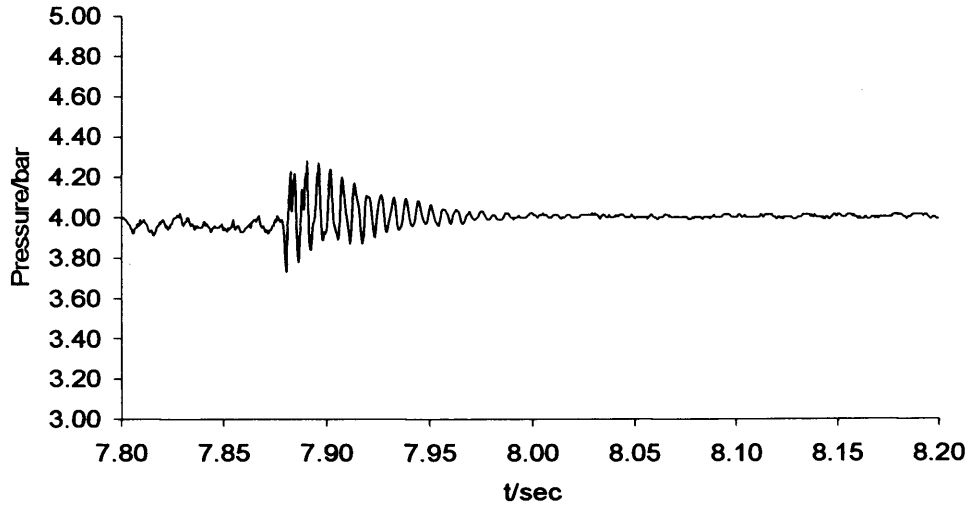

(c) P2

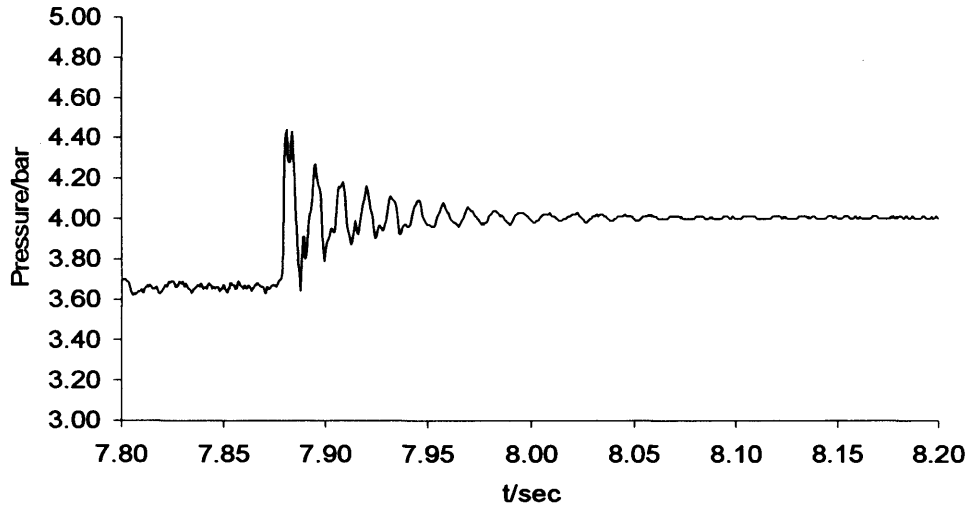

(d) P3

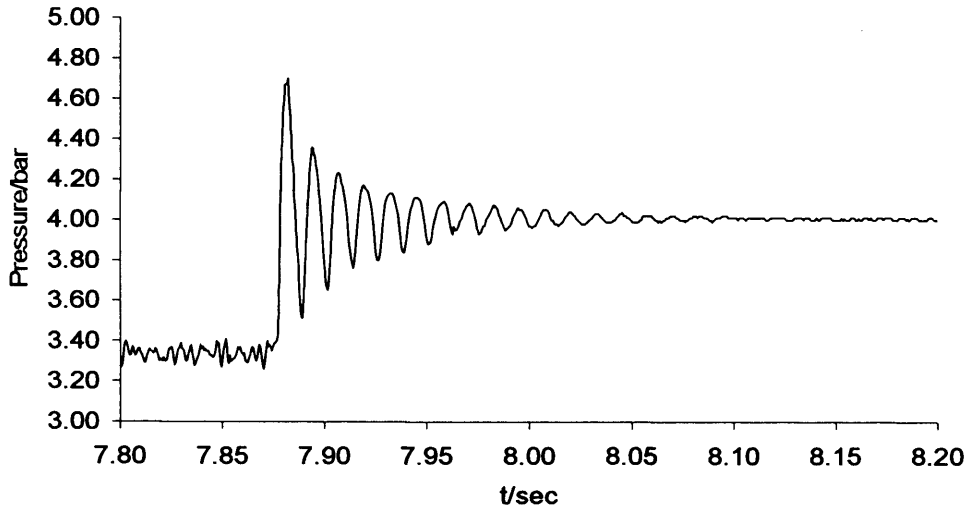

(e) P4 **[end]**

Figure 4.21: Experimental data of transmission line experiment at 5 positions (P0,P1,P2,P3,P4)

It is obvious from the captured data that pressure ripple due to wave propagating between the closed ends of the transmission line exists. It is possible to model the experimental data based on both the lumped and finite difference approach described earlier in this chapter.

Lumped modelling will provide the most direct simulation solution compared to the finite difference approach. Computational time is significantly reduced in lumped modelling due to the fact that equations involved in the solution algorithm are significantly less complex compared to the finite difference approach. Furthermore the sampling time and spatial distribution is less sensitive to cause numerical instability in the solution. However this will be done at the expense of simulation accuracy.

Finite difference approach takes much more computing power due to the complexity of the equations involved. However, it proves to be the more accurate of the two since it enables the dynamics of the air flow to be modelled. However as mentioned before, the sampling time and spatial distribution can cause numerical instability if they were not specified properly. For comparison purpose, both lumped and finite difference simulation results for transmission line modelling are presented in this chapter.

4.10.4 Lumped simulation

In this approach, important parameters that were specified were segment length l_j which is 0.3m, tube diameter d_i of 5mm and discharge coefficient C_d of 0.72. Initial pressure values in each of the 5 positions along the transmission line including initial mass flowrate of 24.79×10^{-3} kg/s were taken directly from the measured data. Crucial equations that need to be solved are mass flowrate $\dot{m}$ and mass flow parameter C_m as presented by equations (4.1 and 4.2). Below is the lumped simulation result. The corresponding computer simulation program is included in the Appendix section named Appendix 2.

Table 4.1: Initial pressure values along the transmission line

Pressure position	Pressure/bar
P0	4.66
P1	4.30
P2	3.95
P3	3.66
P4	3.33

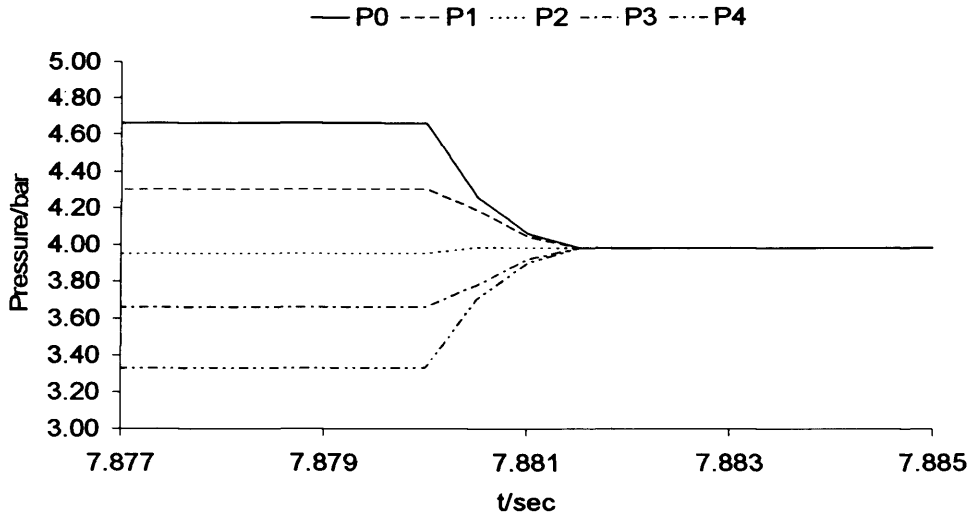

Figure 4.22: Lumped Modelling of the transmission line experiment

The identification of air mass m_j, pressure P_j, density ρ_j, velocity u_j and air displacement Z_j for each segment are performed based on the equations (4.5 to 4.15). The sampling time of the simulation T was 1μs while the number of iterations performed was 1.00×10^7. Note that in using lumped approach, pressure ripples due to wave propagation in transmission line are absent. However the final pressure after the system reaches steady-state condition converges close to the captured data value which is approximately at 3.98bar.

It is apparent that in air flow modelling, lumped approach is unable to provide accurate insight of the air dynamic response in a transmission line. Therefore to properly simulate the air dynamics, finite difference approach is proposed.

4.10.5 Finite Difference simulation

One-dimensional compressible Navier-Stokes equations (4.28 and 4.29) are used in finite difference approach. By applying the same initial conditions as presented in Table (4.1) for lumped modelling, simulation result as shown below was obtained. The simulation program is provided in the Appendix section named Appendix 3.

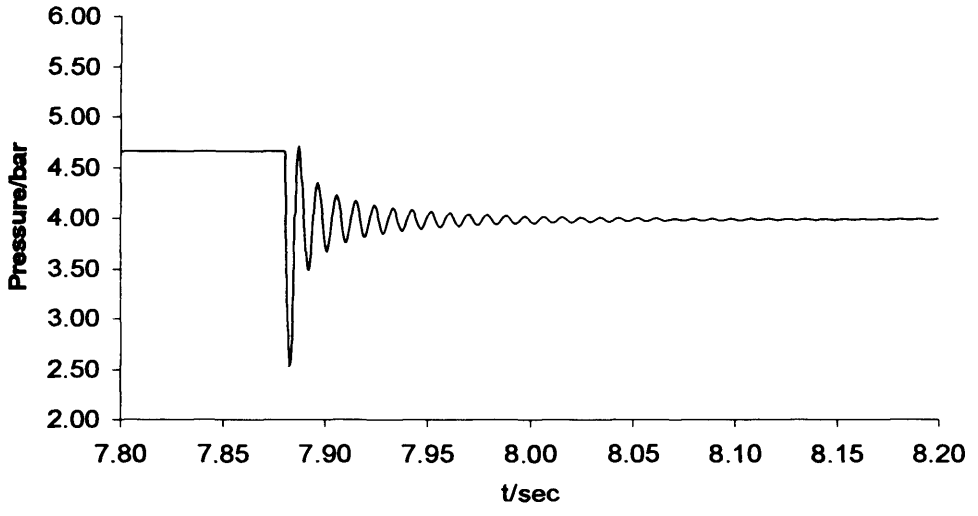

(a) P0

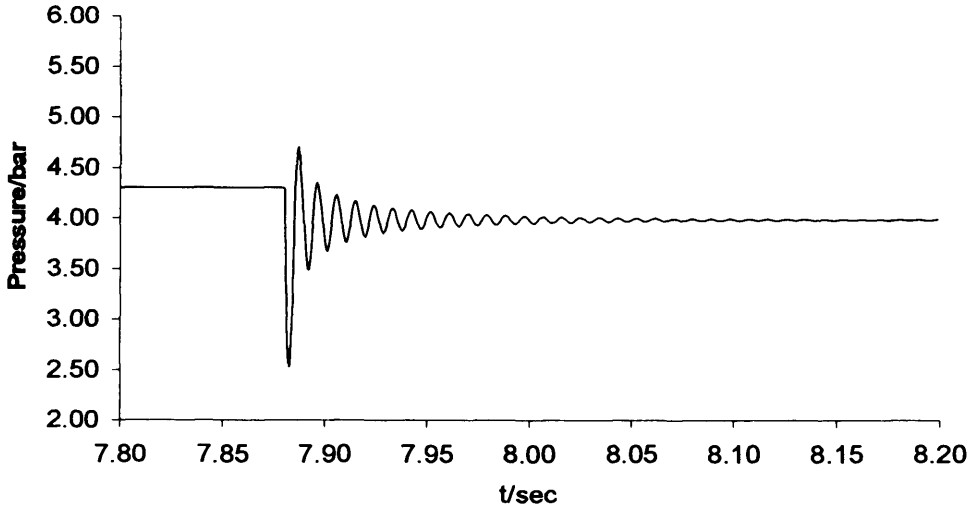

(b) P1

[continued]

Figure 4.23: Finite Difference modelling of the transmission line experiment

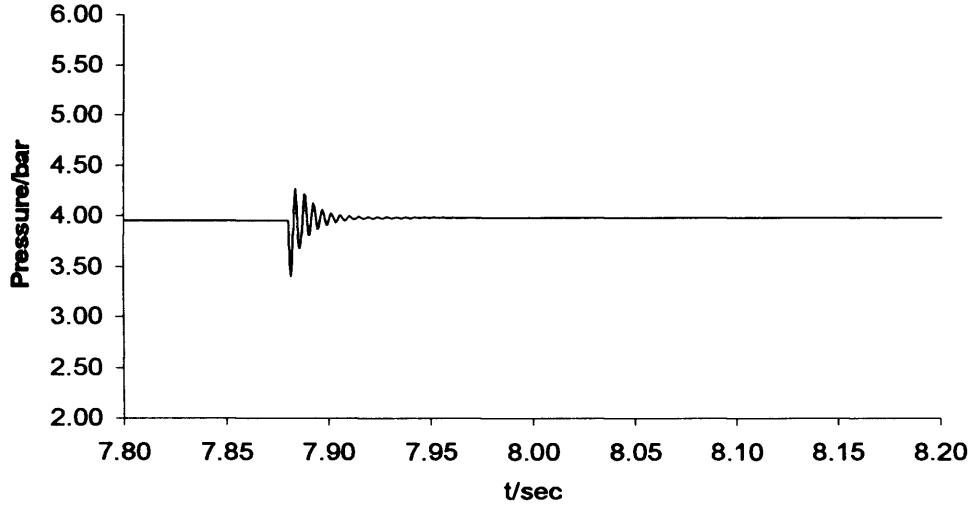

(c) P2

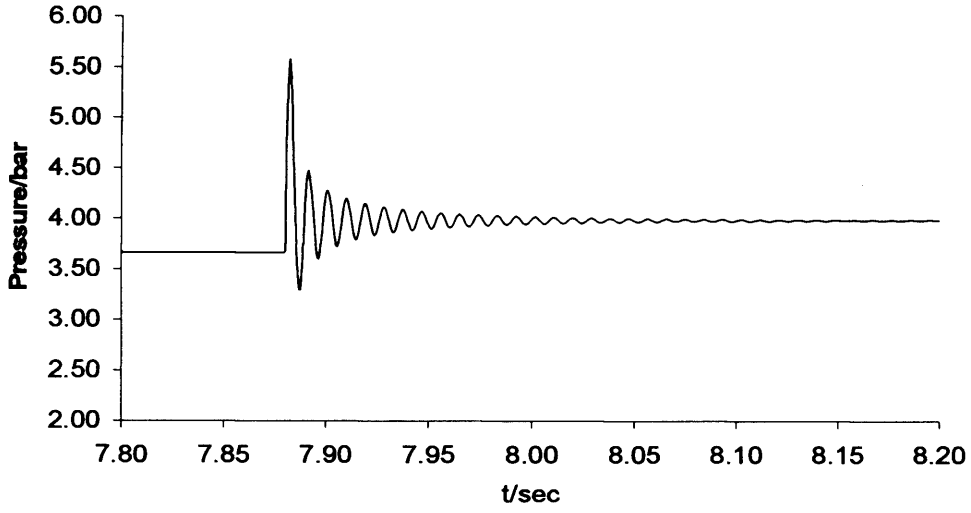

(d) P3

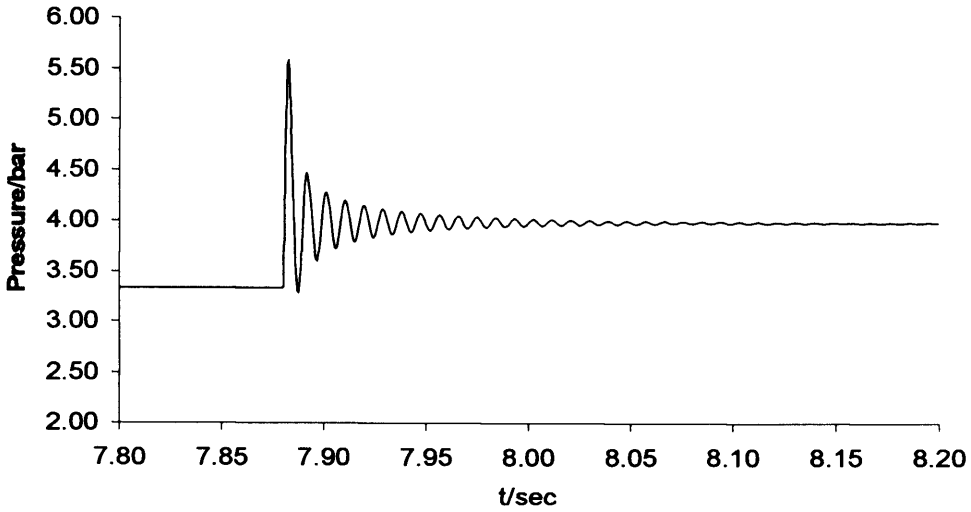

(e) P4 **[end]**

Figure 4.23: Finite Difference modelling of the transmission line experiment

The identification of air mass m_j, pressure P_j, density ρ_j, velocity u_j and dynamic viscosity μ_j in each segment is performed by decoding the vector equations as shown earlier. The sampling time of the simulation T was 1μs while the number of iterations performed was 1.00×10^7 . Note that the pressure ripples are correctly present in the computer simulation result although the peak values are higher than the experiment data by approximately 0.8bar. This may due to the fact that the shear-stress tensors used in this simulation gives lower friction values than the experiment. As mentioned earlier in equation (4.30), shear-stress tensors are dependent on dynamic viscosity μ value which is then related to the specified kinematic viscosity ν of 1.51×10^{-5} m^2/s. However the pressure ripples diminishes at approximately the same time as the captured data which is around 8.1s into the experiment.

It was found that the characteristic of the measured pressure wave propagation in Figure (4.23) diminishes with time due to energy loss. This occurs due to heat generated by viscous friction between fluid surface and the transmission line inner surface during flow.

It took approximately about 11.5ms for one complete cycle of pressure wave propagation in a 1.2m length of transmission line to be completed. This translates into a pressure wave frequency value of approximately 86.96Hz.

These pressure ripples and other parameters can be captured in spatial time domain by constructing a graph of pressure P against transmission line length l_t , in a time frame t. Based on measured data, Figure (4.24) shows the pressure wave formation process during the initial 11.5ms along the transmission line. The time difference between each pressure wave "snap-shot" is 0.5ms and the range of the wave propagation monitored is between 7.8770s and 7.8885s.

The pressure wave value is at its maximum at the blocked ends and decreases towards the centre position of the transmission line. The pressure wave form is of the opposite characteristic from one end to another. When the pressure wave is at its highest at position P4, the pressure wave at position P0 is at its lowest since the

pressure wave was travelling towards position P4. This process repeats itself until all the pressure wave energy had been consumed.

Note that the pressure transducer's volumes and the existence of small volumes of the transmission line at which the pressure transducers are mounted will affect the computer simulation results. However based on the results obtained as shown in three-dimensional format in Figure (4.24) and Figure (4.25) as well as two-dimensional format in Figure (4.26), this factor poses little effect to the system as the simulated results displays close similarity to the experimental results.

Zero reference time (t=0s) for the pressure wave propagation charts is taken right after both ends of the transmission line are blocked (t=7.8770s) and the pressure wave propagation in the transmission line starts to occur until all the pressure wave energy had been consumed and the system reaches steady state condition at (t=7.8885s) to ease the observation of this phenomenon.

4.10.6 Three-Dimensional format of pressure wave propagation charts

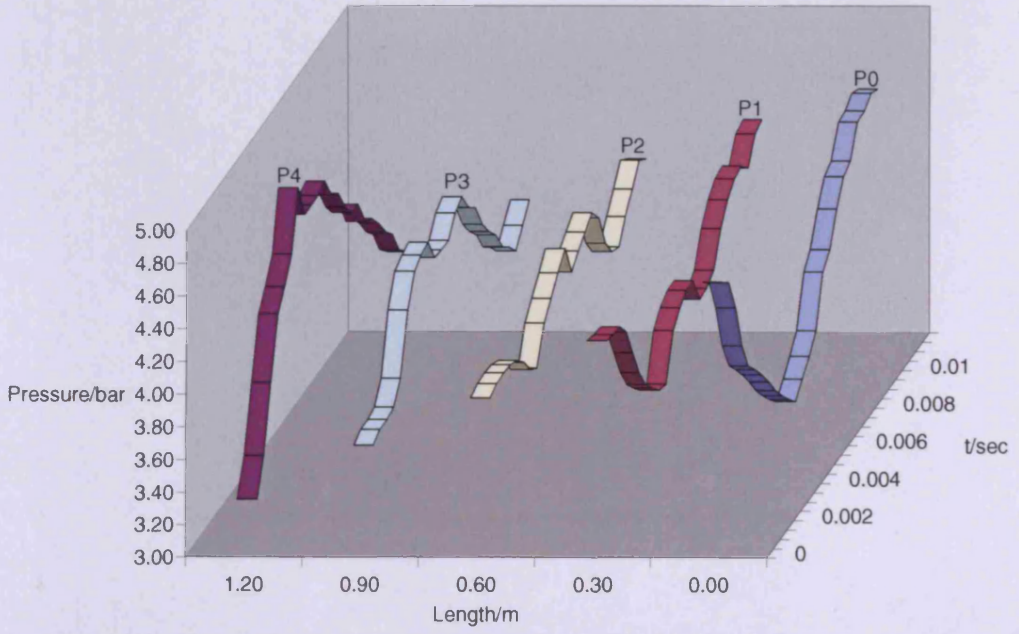

Figure 4.24: Pressure wave propagation in the transmission line based on measured data [View 1]

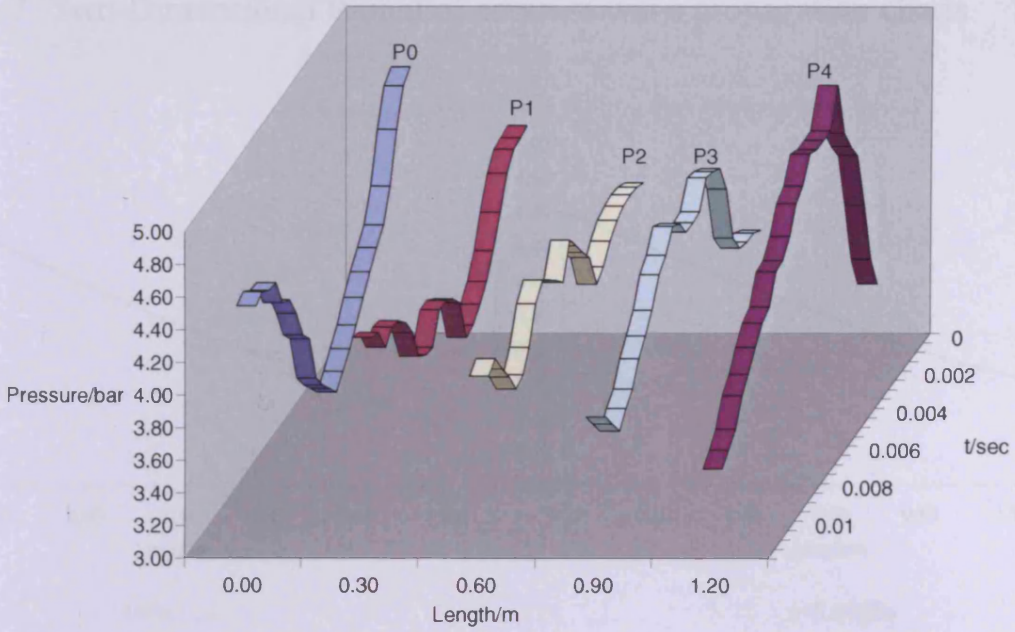

Figure 4.25: Pressure wave propagation in the transmission line based on measured data [View 2]

4.10.7 Two-Dimensional format of pressure wave propagation charts

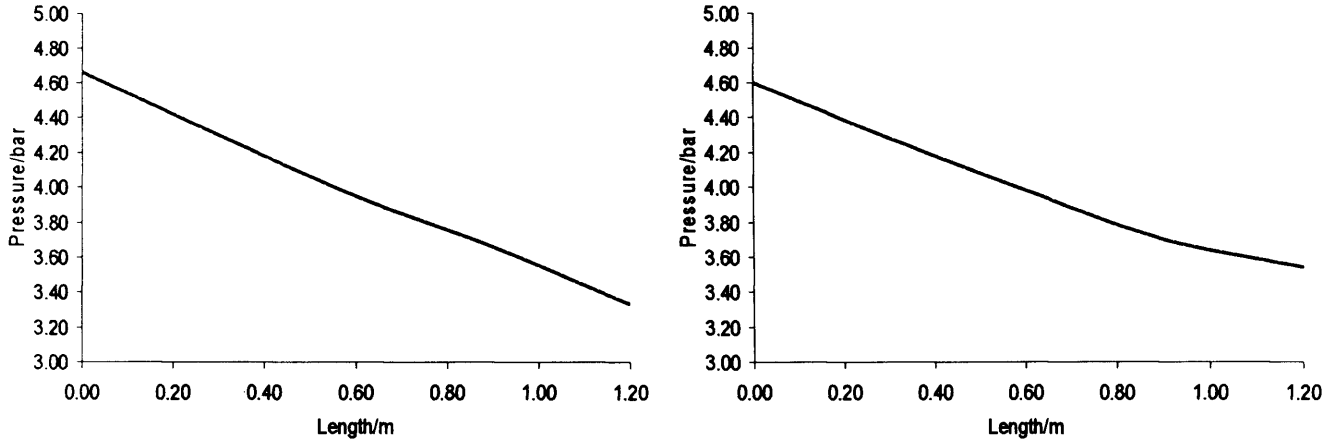

t=0s

t=0.0005s

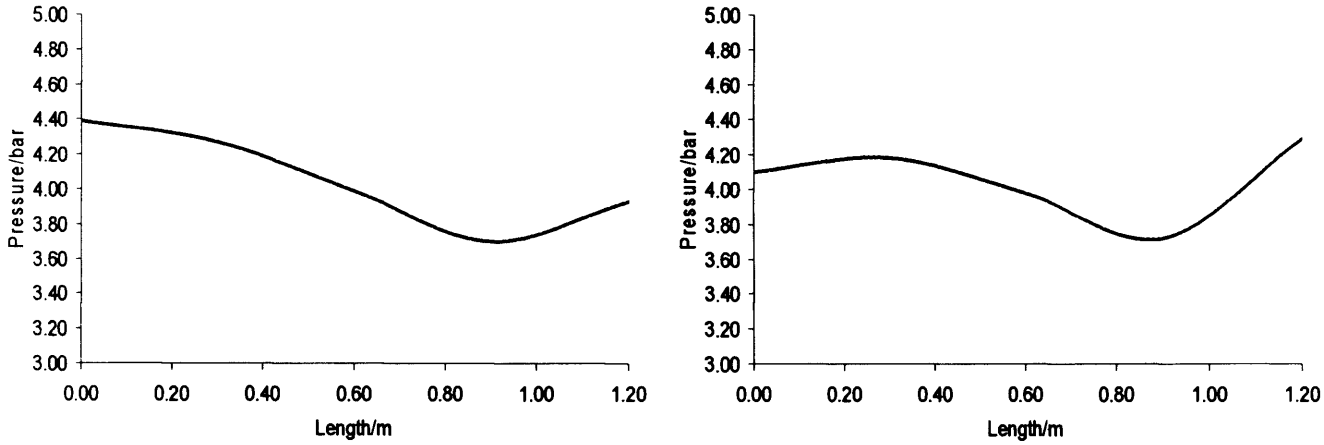

t=0.0010s

t=0.0015s

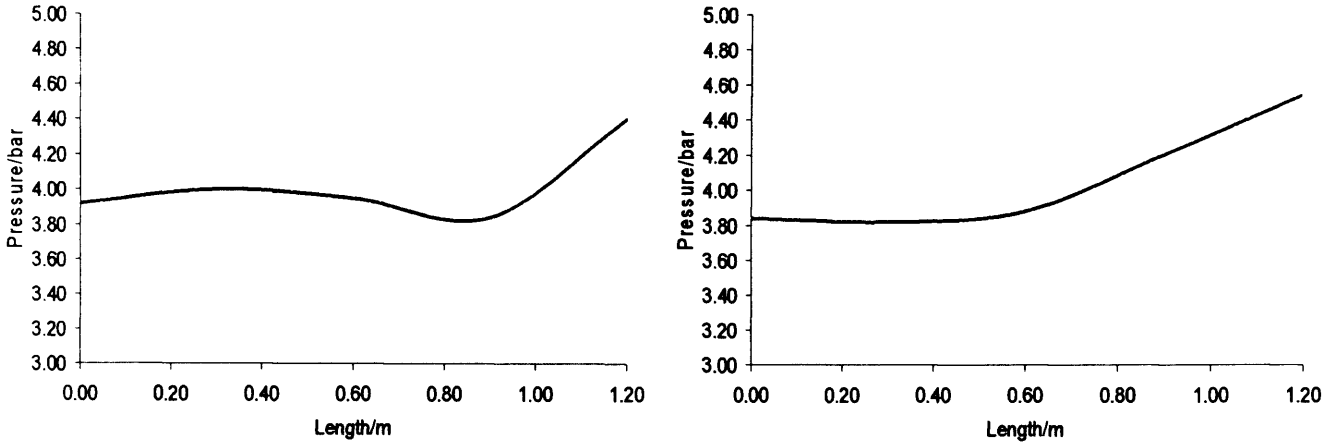

t=0.0020s

t=0.0025s

[continued]

Figure 4.26: Pressure wave propagation in the transmission line based on measured data

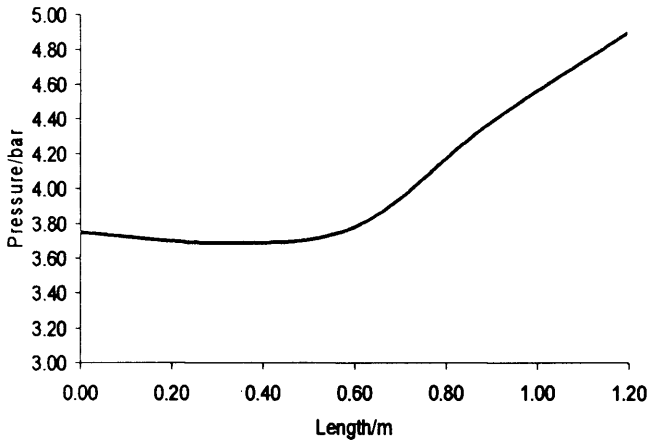

t=0.0030s

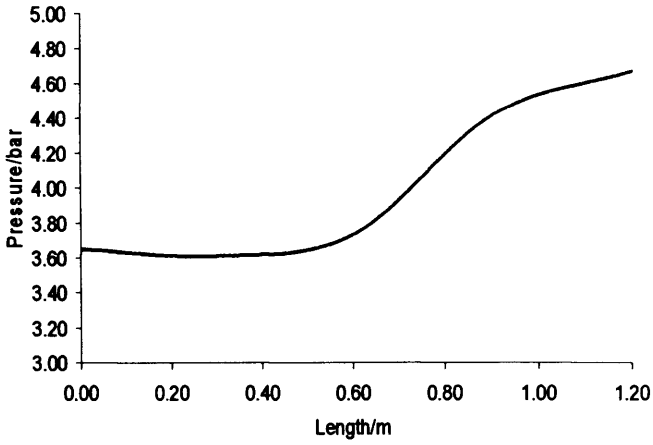

t=0.0035s

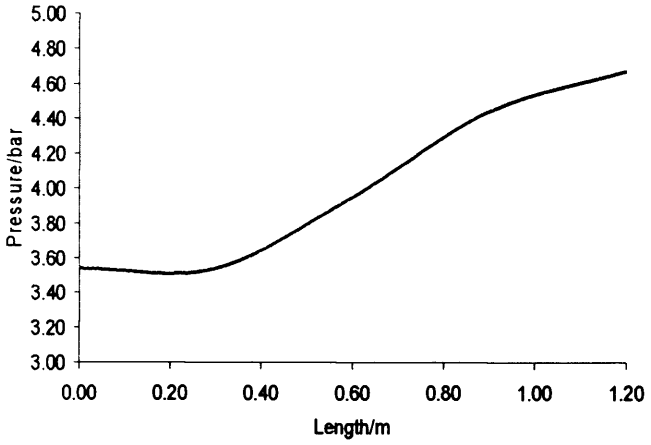

t=0.0040s

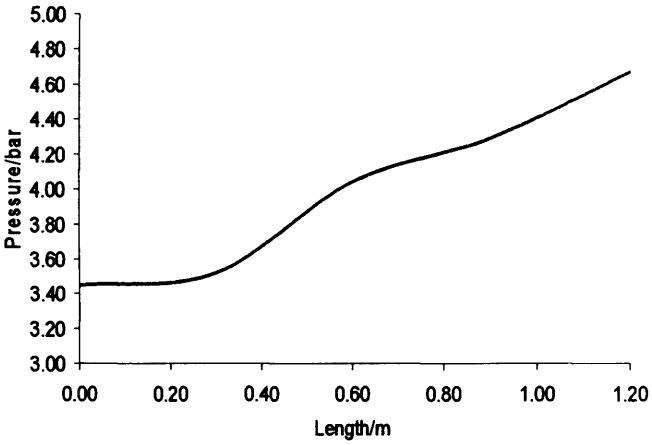

t=0.0045s

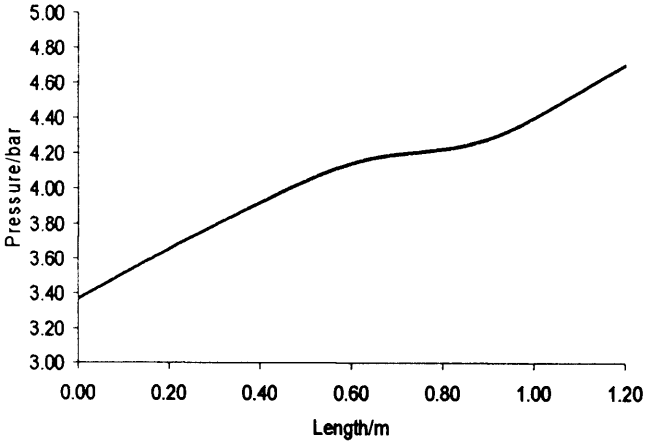

t=0.0050s

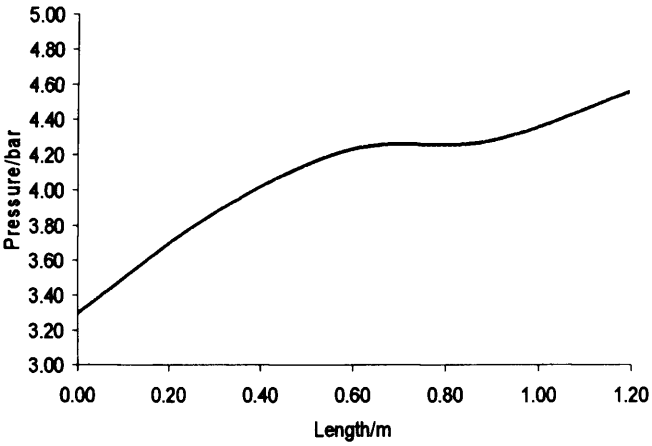

t=0.0055s

[continued]

Figure 4.26: Pressure wave propagation in the transmission line based on measured data

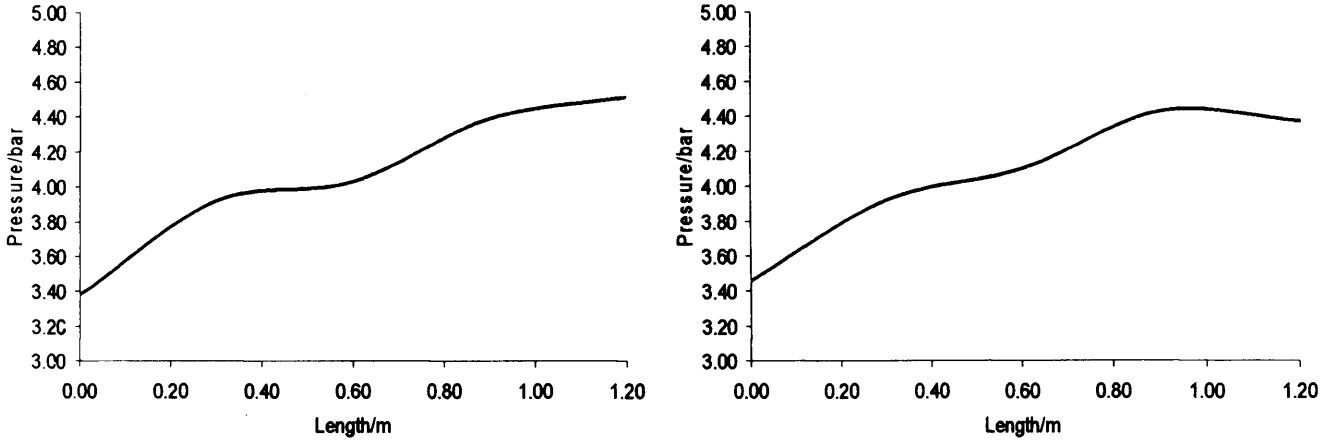

t=0.0060s

t=0.0065s

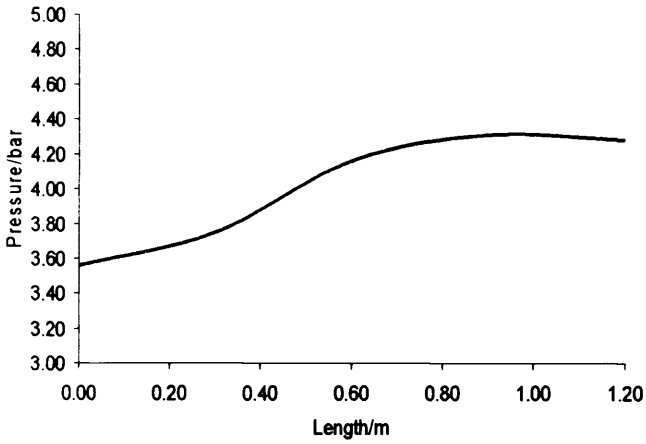

t=0.0070s

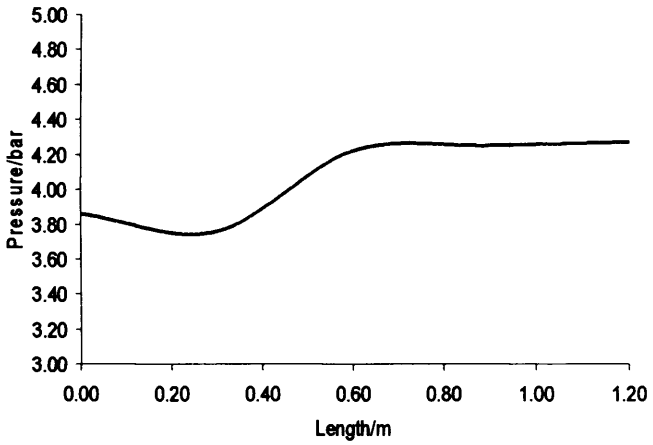

t=0.0075s

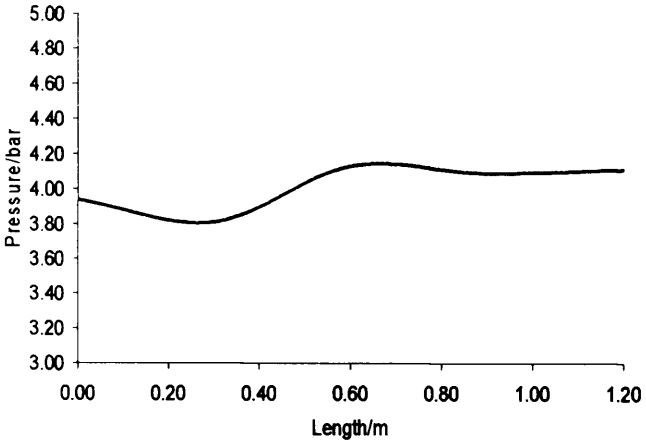

t=0.0080s

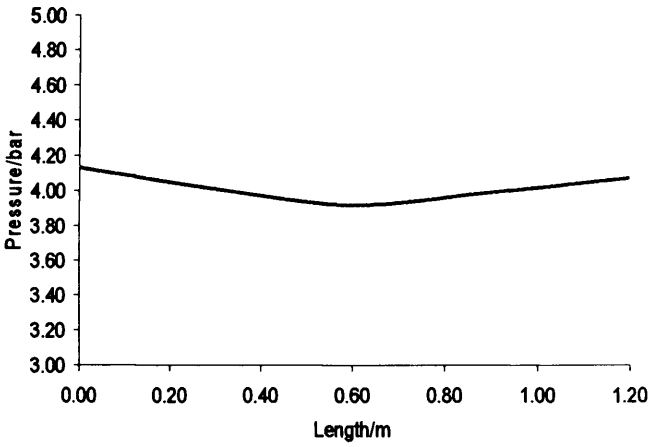

t=0.0085s

[continued]

Figure 4.26: Pressure wave propagation in the transmission line based on measured data

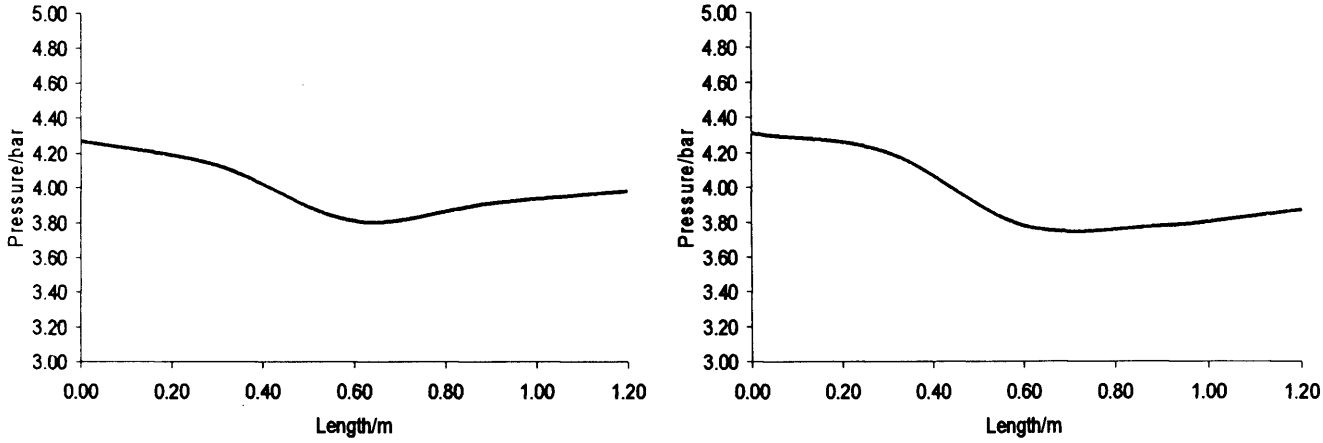

t=0.0090s

t=0.0095s

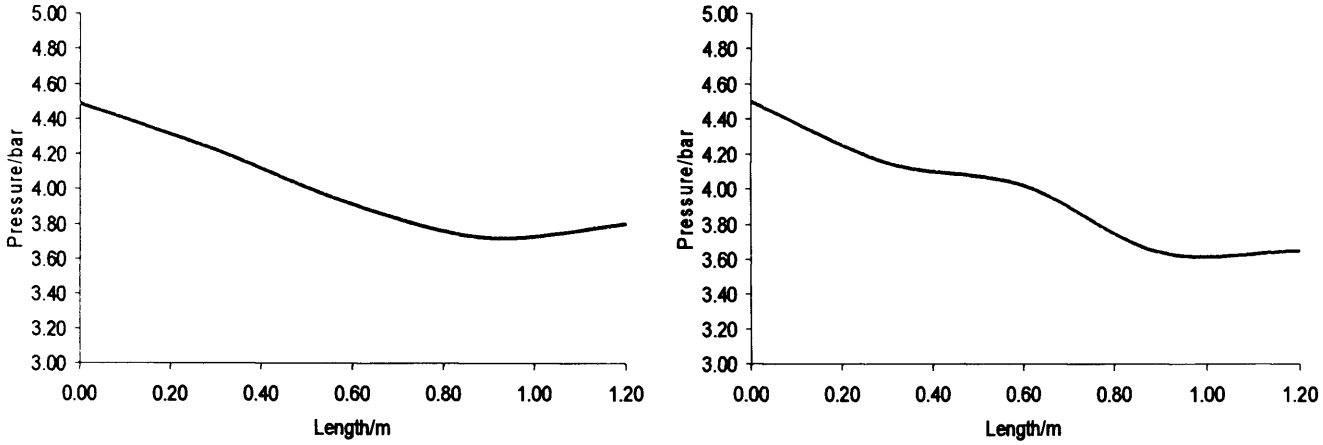

t=0.0100s

t=0.0105s

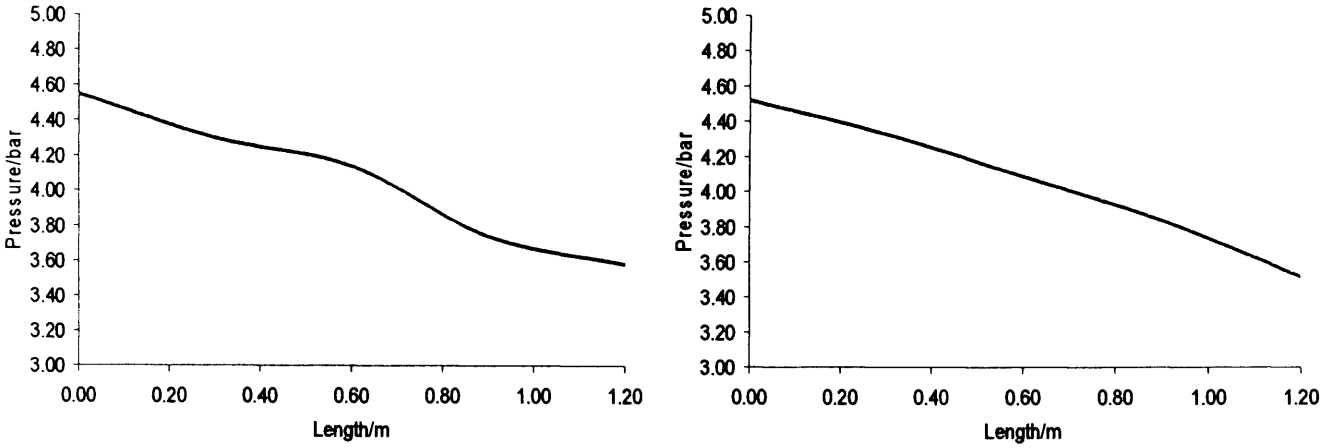

t=0.0110s

t=0.0115s

[end]

Figure 4.26: Pressure wave propagation in the transmission line based on measured data

To summarise, chapter 4 presented the mathematical model of the pneumatic transmission line. Results obtained form the basis for the modelling of energy saving system as presented later in chapter 6.

Restriction/Orifice modelling including lumped volume and finite difference approaches was presented as a possible means to model the air dynamics in the pneumatic transmission line. Author also presented that different types of finite difference techniques applied to a 1-0 discontinuity exhibits different characteristics depending on the type of differencing used namely backward, forward or central.

Several experiments were performed to observe the air dynamics in a pneumatic transmission line. First experiment investigates the pressure and volumetric flowrate response in an air transmission line with and without the presence of a large volume. The second experiment meanwhile studies the occurrence of pressure ripples or waves propagation in a blocked pneumatic transmission line. These experiments were presented and discussed in this chapter.

Based on conservation laws derived in chapter 2, 2^{nd} order finite difference schemes using backward and forward differencing can be applied to model air flow and pressure wave propagation a pneumatic transmission line. It was found that lumped volume modelling cannot be use to model pressure wave propagation although it is useful for modelling large volumes such as a pneumatic cylinder where pressure ripples do not occur. Finite difference approach however can model these pressure ripples although it proves to be much more complex to apply compared to lumped approach.

It is suggested that it is possible to use both lumped modelling and finite difference method to model the energy saving system. The pneumatic cylinder can be modelled using lumped volume approach while the pneumatic transmission line can then be modelled using the finite difference approach. This approach to modelling of a pneumatic system proves to be successful in achieving the balance between accuracy, ease of application and computing power. This simulation technique can be said to be successful as reflected by the energy saving system simulation results presented in chapter 6.

Chapter 5

Energy Saving Realization and Results

In this chapter, the mathematical algorithm for predicted cut-off actuation is discussed including the mechanism process of utilising this approach. Comparison of energy saving achieved is compared with both the conventional and end-stroke cut-off processes. Important parameters such as the air expansion index γ modifying factor K and cylinder's friction F_{frp} are also included. Results obtained are compared and discussed at the end of this chapter.

5.1 Conventional Actuation

In a conventional operation, the cylinder is actuated without cut-off of the supply pressure at the main directional valve during the whole process. This is the method most commonly used for pneumatic PTP actuation in industrial applications. Note that as the piston reaches the end-stroke, compressed air is still being delivered to the driving chamber. The pressure *Pr* in the driving chamber increases until it reaches the supply pressure *Ps*. The pressure *Pl* in the exhaust chamber decreases to the atmospheric pressure. The states of signal V1 and V2 remains unchanged until retraction is required. The two solenoid valves for exhausting purposes are not used during this actuation.

5.2 End-stroke cut-off actuation

In this form of actuation, V1 is charged to 24 Volts and V2 is discharged for delivering air to the driving chamber Pr and exhausting air from the left chamber Pl. The supply pressure is then cut-off by discharging V1 when the piston reaches the end stroke. V1 and V2 are then discharged and hence the main valve will be in its neutral position and no further air is delivered to the cylinder. The pressure Pr in the driving chamber remains constant rather than increasing to the supply pressure as in the conventional actuation.

5.3 Predicted cut-off actuation

At the beginning of the cylinder extension, the system mechanism in the early stage of the actuation is the same as in using either the method of end-stroke cut-off or conventional processes. However the supply pressure is cut-off by discharging (V1) before the piston reaches the end-stroke. As the kinetic energy at the moving piston and time-delay caused by friction at the solenoid pilot valves as well as air compressibility which are present, the cut-off criteria predicted by mathematical equation (1.3) in chapter 1 (shown below for easy reference) is affected. Therefore a modified algorithm is given in equation (5.1) below.

$$P > P_{st}\left(V_o/V\right)^{\gamma} \quad \text{..... (1.3)}$$

$$P > K \cdot P_{st}\left(V_o/V\right)^{\gamma} \quad \text{..... (5.1)}$$

K is the modifying factor determined from successful experimental runs of predicted cut-off actuation. The K value varies from 0.1 at system pressure Ps of 1.5bar and 0.2 at system pressure of Ps 2.5bar. Note that the modifying factor value is determined under the condition of satisfied performance on maximum energy saving without stick-slip occurrence. Further discussion on modifying factor K is presented at the end of this chapter.

The state of compressed air in the driving chamber and the actuator displacement are evaluated online and once the criterion set by equation (5.1) above has been met, the cut-off to air supply was performed and the air potential energy contained in the driving chamber is enough to overcome the friction thus driving the piston satisfactorily right to the maximum stroke.

The expansion of the air in the driving chamber follows the model identified in equation (1.1) in chapter 1 which is re-iterated below.

$$PV^{\gamma} = P_c V_c^{\gamma} \quad \text{..... (1.1)}$$

Pressure in the driving chamber decreases during the air expansion process to a much lower value compared to the pressure value in both the conventional and end-stroke cut-off methods. Throughout the whole cylinder actuation process, the air operated valve connected to the left side of the cylinder is also actuated by charging (V3) for maximising air exhaustion in the exhausting chamber. Below is the pneumatic circuit used for this research.

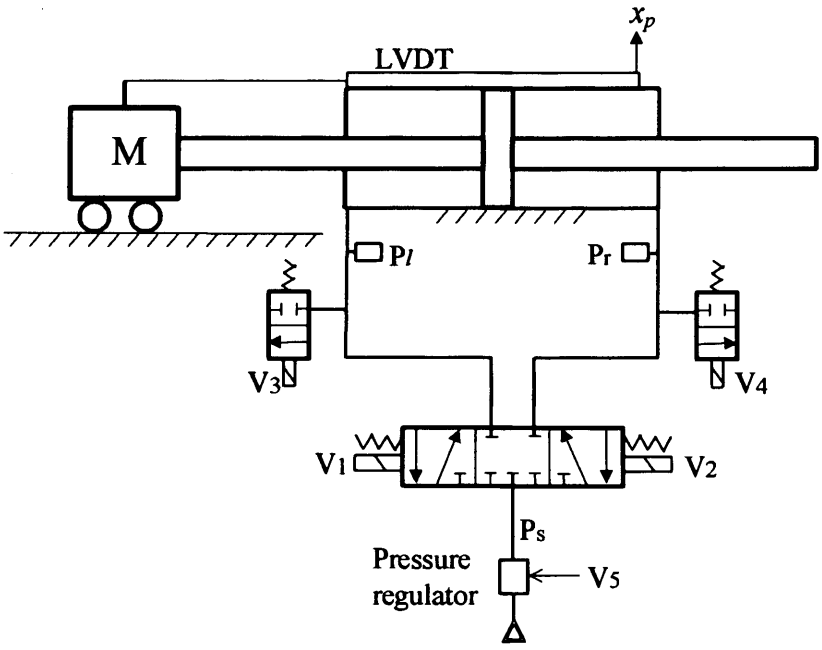

Figure 5.1: Experiment pneumatic circuit

5.4 Air expansion index

The state change of the fixed mass of air in the cylinder has received attention with respect to determining the air expansion index. Experiment was undertaken by cutting-off the air supply and investigating the changes of pressure versus volume in the cylinder driving chamber. In this instance the air in the chamber is expanding without any change in mass. By using the state change of air data and applying it to the gas law of equation (1.1), the air expansion index can be identified using the following logarithmic equation.

$$\gamma = \frac{\log P_2 - \log P_1}{\log V_1 - \log V_2} \quad \text{..... (5.2)}$$

Subscripts '$_1$' and '$_2$' denote the two states of the fixed mass of air in the driving chamber. Experiments were undertaken under system pressure Ps of 1.5bar and 2.5bar respectively.

The value of the air expansion index γ was identified as 2.7, which is far from the well known ideal values which ranges from 1.0 under isothermal condition and 1.4 at adiabatic condition. These values had already been verified by previous research[35].

The difference between the air expansion index γ found and ideal values as described above may be subjected to three realities in the experiment which are very different from the ideal test conditions. The first is that there could be leakages that exist in the pneumatic cylinder at any seals which will cause a larger value of γ identified. Secondly the air was not under steady-state condition when the data were captured. Finally the actuation process was conducted under neither isothermal nor adiabatic conditions. Validation of the air expansion index is identified by predicting the chamber pressure as shown in Figure (5.2).

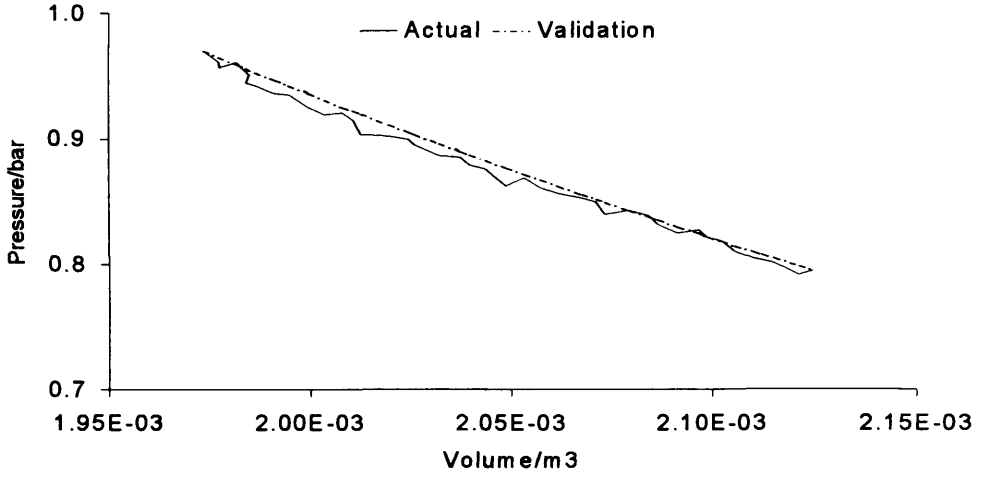

(a) System pressure (Ps) 1.5bar

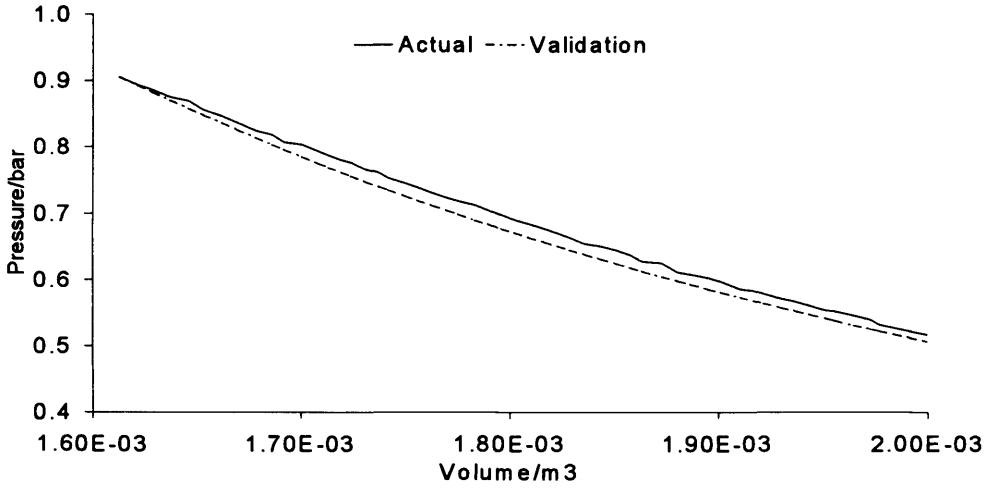

(b) System pressure (Ps) 2.5bar

Figure 5.2: Validation of air expansion index identified, $\gamma = 2.7$

The root mean squares[36] (RMS) of error between prediction and measured data are 0.001bar at system pressure (Ps) of 1.5bar and 0.002bar at 2.5bar test and the relevant formula is as shown below.

$$RMS_{error} = \sqrt{\frac{1}{N_s}\Sigma(P_r - P_l)^2} \quad \text{..... (5.3)}$$

where N_s is the total number of sampled data.

5.5 Energy consumption

Compressed air energy production and consumption under ideal conditions was studied by Kagawa[3] and explicit expression of work done was described under conditions that there are no friction at the actuator and exhausting chamber pressure is assumed to be atmospheric. In a pneumatic cylinder extension process, the total air energy consumption can be expressed as follows:

$$E_c = W_d + E_a + E_L \quad \text{(5.4)}$$

where E_c is the total air energy consumed at air supply, W_d is the work done by the air, E_a is the potential energy in the air and E_L as energy losses. The work done W_d term can be expressed as follow:

$$W_d = \int_0^{V_o} (P_r - P_l) dV \quad \text{(5.5)}$$

where P_l and P_r are pressures in the left and right chamber of the cylinder respectively and V is the volume in the driving chamber. These parameters are varying with time. V_o is the full volume of the cylinder. Part of the energy used in the work done is consumed to overcome the friction force and becomes heat while others are converted into kinetic energy as can be shown by the following form:

$$E_k = \frac{1}{2} M_p \cdot v_p^{\,2} \quad \text{(5.6)}$$

where M_p is the total mass of piston-rod including the mass at the end-rod on a trolley while v_p is the relative velocity of piston to the cylinder. Kinetic energy is finally converted to heat energy at the end stroke during the compression of air as the piston hat moves into the cushioning sleeve at the cylinder end. If the driving chamber pressure is higher than atmospheric value at the end-stroke, potential energy of the compressed air exists. The work value of the compressed air is the work that it can do

in a virtual and ideal process in that the enclosed air expands up to the state that the pressure becomes atmospheric.

$$E_a = \int_{V_c}^{V_a} (P - P_a) dV \quad \text{..... (5.7)}$$

where V_a is the volume expanded to atmospheric value P_a from the initial pressure at the cut-off instance P_c while at the volume V_c. If an isothermal expansion process is considered; that is to say.

$$P_a V_a = P_c V_c \quad \text{..... (5.8)}$$

The potential energy integral result can be written as:

$$E_a = P_c V_c \left(\ln \frac{P_c}{P_a} + \frac{P_a}{P_c} - 1 \right) \quad \text{..... (5.9)}$$

The energy losses E_L can be caused by internal/external air leakage and heat radiation which is unavoidable in practice.

In a point-to-point (PTP) process, the work done W_d depends on the value of load applied to the system, the required actuation velocity and the actuator friction characteristics. Once actuators and valves were selected and the actuation specification at the given load were determined, the value of W_d can be identified.

The air potential energy E_a is wasted once the actuation is completed. The value of E_a can vary under different operation methods. In this study, attention is given to minimise the energy losses E_L. The criterion of an energy saving ratio is as follow.

$$\eta = \frac{E_{an} - E_{ac}}{E_{an}} \times 100\% \quad \text{..... (5.10)}$$

where E_{an} and E_{ac} are the potential energies of pneumatic cylinder actuation under both conventional and cut-off processes respectively.

5.6 Characteristics of friction

Friction[37,38,39] exists inherently in pneumatic cylinders due to the required sealing between the piston and the cylinder wall[40,] and it is non-linear to the piston velocity. The overall friction can be modelled in terms of static friction, Coulomb force and viscous effect as shown in Figure (5.3)[41]. At the very instant just before the piston starts to move from rest, the static friction F_s dominates the overall friction F_{frp}. Once the piston starts to move, the friction force F_{frp} drops considerably to F_c which is the Coulomb force. As the piston velocity increases, viscous friction which is proportional to the piston velocity will be more significant in addition to the friction constant c_{fr} which can be written as follows.

$$F_{frp} = c_{fr} + (K_v \cdot v_p) \quad \text{..... (5.11)}$$

where K_v is the viscous coefficient and v_p is the piston velocity.

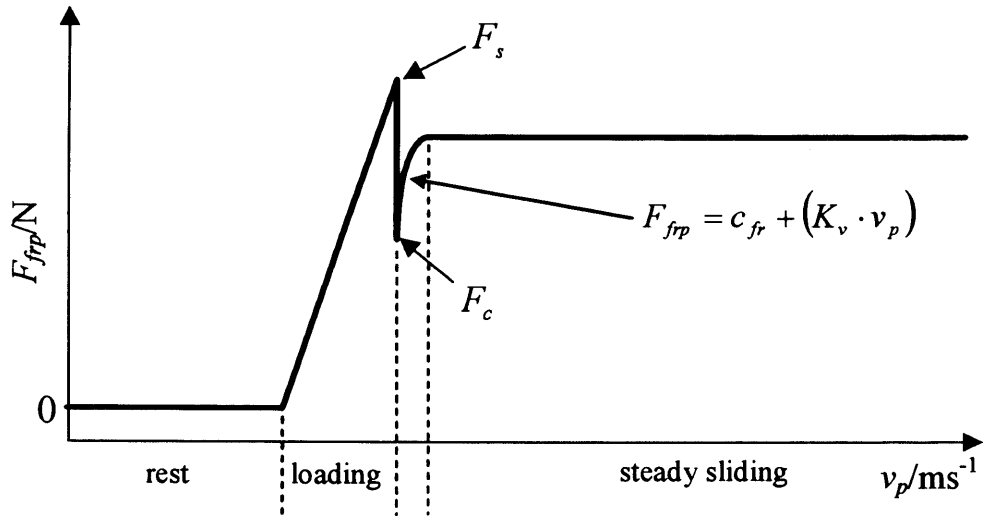

Figure 5.3: Characteristics of friction in pneumatic cylinders[41]

Friction will cause time-delay and can reduce system stability. Techniques are hence required to eliminate/attenuate the time-delay effect in control design[42,43]. Friction understanding is crucial when considering application of friction characteristics in PTP control of a pneumatic cylinder. The non-linear characteristics of friction may lead to a stick-slip phenomenon if the cylinder is moving within a very low velocity region as was presented by previous researches[8,44].

Haessig[44] had investigated the physical phenomenon of stick-slip friction under which the author presented two new models called the bristle and the reset integrator due to the fact that the standard slip-stick friction model poorly describes the friction force at zero velocity. The bristle model is based on the principle of contact/bonding between a sliding body and a stationary body by means of massless, pliable bristles. The friction between the two surfaces is then assumed to be caused by the number of bristles each contributing a small load to the total friction load. Therefore as more bristles exist between the two bodies, more friction load is created that opposes the sliding motion. The theory is that when the strain of any particular bristle reaches a certain pre-defined value, the bond is broken and a new bond having a smaller strain is then created. The relationship of friction load is then made a function of velocity by varying the number of bristles existed. This model achieves high accuracy although it is complicated and computationally inefficient.

Reset integrator model meanwhile is still based on the bristle model and the key to this method is the use of a single position variable generated internally rather than numerous randomly positioned bristles. This single position variable is then either toggled on or off in the friction load algorithm depending on the pre-defined relative velocity between the contacting surfaces. The author concluded that reset integrator model is much simpler and more efficient to apply while still retaining the virtues of the complex bristle model.

Wang[45] meanwhile had identified friction parameters of pneumatic cylinders by means of genetic algorithms (GA) in which the author proposes the use of sum of absolute errors that gives a better convergence rate and robustness to the evaluation function of the genetic algorithms compared to the traditional method of mean-squared errors (MSE).

In this thesis, the characteristic of friction is identified by applying measured experimental data to equation (5.11). The static friction force is calculated by using the pressure difference between the driving and the exhausting chamber just before the piston starts to move. The friction constant and viscous coefficient is identified using captured data from experiments conducted for different piston velocities. Different ranges of piston velocities were obtained from varying system pressures. With higher system pressure, faster piston velocity is achieved. Note that Table (5.1) displays the averaged data values of two sets of experimental runs and the calculated piston velocity values are true to three decimal places. Below are the results of experiments conducted in determining the friction characteristic of the pneumatic cylinder used in the test rig.

Table 5.1: Tabulated forces in driving and exhausting chambers

Piston velocity v_p (m/s)	Driving chamber force F_r (N)	Exhausting chamber force F_l (N)	Piston friction force $[F_r-F_l]$ F_{frp} (N)
0.000	**359**	**359**	**359**
0.010	1249	1133	115
0.014	1224	1087	137
0.019	1235	1087	148
0.048	1408	1145	263
0.072	1146	844	302
0.101	902	682	220
0.130	879	636	243
0.134	1249	879	370
0.154	903	474	428
0.173	868	497	370
0.202	1064	636	428
0.226	1041	613	428
0.235	1422	995	428
0.240	1411	844	567
0.250	1758	1191	567

Table (5.1) is the calculated force in the driving chamber F_r and the force in the exhaust chamber F_l based on the measured data. The forces were calculated by using the relationship between pressure P, force F and area on which the force is acting A as shown below.

$$F = \frac{P}{A} \quad \text{..... (5.12)}$$

The net driving force is the difference between forces of the driving and the exhausting chambers since this are the forces experienced by the piston in the pneumatic cylinder when the main supply valve is opened; be it still at rest or in motion. These calculated data were then plotted in a force versus velocity graph.

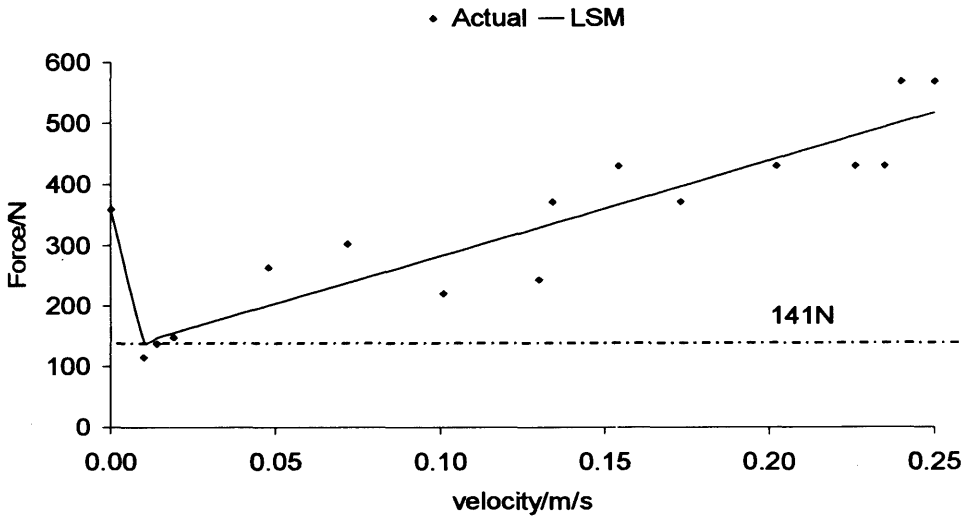

Figure 5.4: Plotted calculated forces in a force-velocity graph

Best fit line is drawn through the force distribution plot and by treating the measured data using least squares method (LSM)[46], the viscous coefficient value K_v was determined as shown by the equation below.

$$K_v = \frac{\Sigma(v_p \cdot F_{frp}) - \left[\frac{1}{N} \cdot \Sigma(v_p) \cdot \Sigma(F_{frp})\right]}{\Sigma(v_p{}^2) - \left[\frac{1}{N} \cdot (\Sigma v_p)^2\right]} \quad \text{..... (5.13)}$$

where N_s is the total number of the treated samples. The calculation for friction constant c_{fr} was done by utilising the mean values of both the friction force F_{frp} and velocity v_p including the obtained viscous coefficient value K_v. The best fit line can then be drawn by utilising the determined variables based on equation (5.11). Table (5.2) outlines the calculations performed in a tabulated format.

Table 5.2: Variables K_v, c_{fr} and best fit line determination

Piston velocity v_p (m/s)	v_p^2 (m^2/s^2)	Piston friction force $[F_r-F_i]$ F_{frp} (N)	$v_p F_{frp}$ (Nm/s)	LMS best fit line plot F_{frp} (N)
0.000	0.000E+00	359	359	359
0.010	1.000E-04	115	1	141
0.014	1.960E-04	137	2	148
0.019	3.610E-04	148	3	155
0.048	2.304E-03	263	13	201
0.072	5.184E-03	302	22	238
0.101	1.020E-02	220	22	283
0.130	1.690E-02	243	32	328
0.134	1.796E-02	370	50	334
0.154	2.372E-02	428	66	366
0.173	2.993E-02	370	64	395
0.202	4.080E-02	428	86	440
0.226	5.108E-02	428	97	478
0.235	5.523E-02	428	101	492
0.240	5.760E-02	567	136	499
0.250	6.250E-02	567	142	515
Total sum (Σ)				
2.008	3.741E-01	5014	835	
Piston mean velocity v_p (m/s)		**Mean piston friction force F_{frp} (N)**		
0.134		**334**		

K_v (LSM)	**1557**	**Ns/m**
c_{fr} (LSM)	**126**	**N**

The static friction F_s is identified to be 359N, Coulomb force F_c of 141N, friction constant c_{fr} of 126N and viscous coefficient K_v value as 1557Ns/m which were then incorporated into the algorithm proposed to determine the cut-off time for energy saving.

Investigation of friction force characteristic enables the determination of cut-off time in the system control algorithm and provides the necessary parameters for the force equation in the computer simulation. The force equation enables the piston acceleration identification and thus leads to the determination of the piston displacement. This will be dealt later in chapter 6.

5.7 Energy saving achieved

Figure (5.5) shows the air potential energy losses E_a which is wasted in the actuation of the pneumatic cylinder under conventional, end-stroke cut-off and predicted cut-off processes respectively. Each approach was done under different system pressure Ps of 1.5bar and 2.5bar respectively.

Using the energy saving ratio given in equation (5.10), the energy saved in operation of cut-off at end-stroke is 43.5% at 1.5bar system pressure and 40.1% at 2.5bar while in predicted cut-off method, 59.5% at 1.5bar system pressure and 80.2% at 2.5bar. Note that the air energy is being significantly saved compared to conventional approach when using both of the energy saving methods proposed[11].

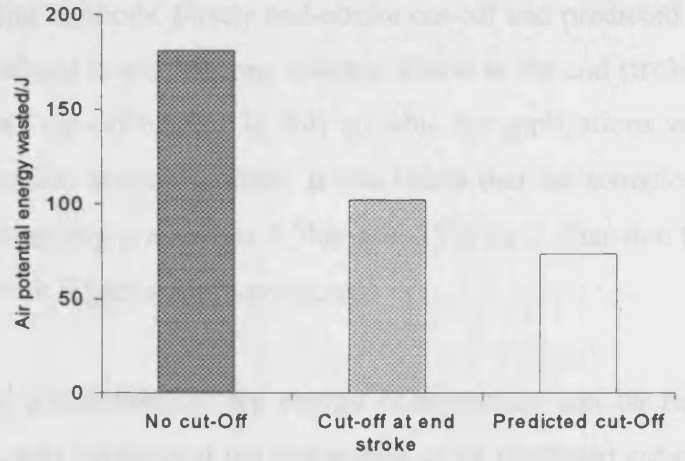

(a) System pressure 1.5bar

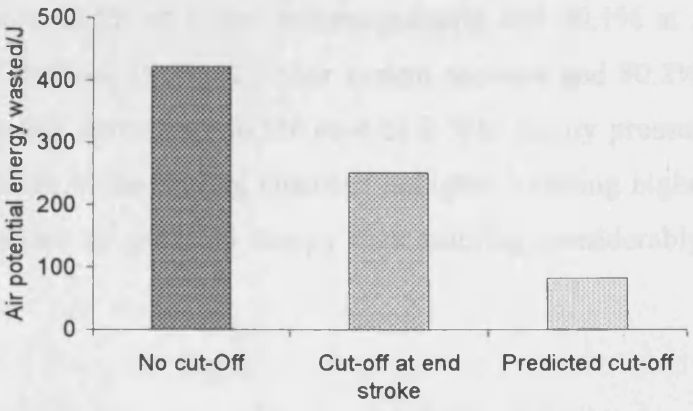

(b) System pressure 2.5bar

Figure 5.5: Air potential energy wasted in actuation

5.8 Discussion

This section is divided into 4 segments each bringing into context important aspects of implementing proposed energy saving methods such as cut-off effects on actuation, time-delay and pneumatic cylinder cushioning.

5.8.1 General conclusions

Investigation on conventional process including end-stroke cut-off and predicted cut-off energy saving methods were implemented. In each approach, experiment was conducted with supply pressure of 1.5bar and 2.5bar.

There are two important factors that need to be considered in implementing these energy saving methods. Firstly end-stroke cut-off and predicted cut-off methods can only be considered in applications where stiffness at the end stroke is not essential. Secondly predicted cut-off method is only suitable for applications where the time to complete the actuation is not important. It was found that the actuation time increases by 20% when the supply pressure is 1.5bar and 25% for 2.5bar due to earlier cut-off implementation with higher system pressure.

There are possibilities where energy consumption can be reduced either by cutting-off the supply pressure at the end-stroke or by predicted cut-off using the gas law equation. In this research, it was found that the energy saved in operation of cut-off at end-stroke is 43.5% at 1.5bar system pressure and 40.1% at 2.5bar while in predicted cut-off method, 59.5% at 1.5bar system pressure and 80.2% at 2.5bar. The greater energy saving percentage in the case of 2.5bar supply pressure is due to the fact that the pressure in the driving chamber is higher, creating higher driving force and generating higher air potential energy thus enabling considerably earlier cut-off time.

5.8.2 Effect of cut-off to actuation process

Figure (5.6) and (5.7) shows the predicted cut-off undertaken at (t=1.14s) at system pressure Ps of 1.5bar, 80.3% of the total actuation time to reach end-stroke; and at (t=0.62s) at Ps of 2.5bar, 36.9% of the total actuation time. Obviously cut-off time varies according to different system pressure Ps.

Little effect to the actuation is shown in experiment conducted at system pressure Ps of 1.5bar as the cut-off is implemented close to the end-stroke. However earlier cut-off implementation was undertaken at Ps of 2.5bar and the piston reaches the end-stroke 0.38s later compared to both the end-stroke cut-off and conventional processes. On the other hand, though predicted cut-off proves to be slower, it achieves maximum energy saving percentage as well as without the occurrence of stick-slip phenomena. Furthermore this time lag can be reduced by enlarging the modifying factor K.

5.8.3 Effect of time-delay of directional valve

Time-delay[43,47] is present in pneumatic system responses due to friction and air compressibility. This effect can be observed based on Figures (5.6) and (5.7) at the response of pressures and displacement to the control signal given (V1). The time-delay shown is contributed mainly by the air pilot solenoid valve in addition to the transmission line effect. System pressure also affects the time-delay of the valves, and respectively they are 0.215s at system pressure Ps of 1.5bar and 0.185s at Ps of 2.5bar as explained earlier in chapter 3.

5.8.4 Effect of cylinder cushioning

As mentioned in chapter 3, cylinder cushioning is needed to reduce the impact of the piston when it reaches maximum stroke. As the piston cap enters the cushion sleeve at the end of the cylinder, air in the exhausting chamber escapes to the atmosphere though a smaller orifice rather than the larger one thus causing the actuation velocity to be significantly reduced.

In both conventional and end-stroke cut-off processes, before cut-off is implemented the pressure in the driving chamber will increase as air is still flowing into the cylinder from the main directional valve and the pressure decreases in the exhausting chamber as the cylinder actuation decreases to a halt. In the case of predicted cut-off method, both pressures in the driving and the exhausting chambers continue to decrease since air-supply is cut-off earlier into the process while the driving chamber volume keeps increasing as the piston moves to the end of the cylinder. In this stage of the process, the piston velocity also decreases as it looses force in the driving chamber.

Internal cylinder cushioning depends on the sudden pressure rise in the exhausting chamber. Due to the fact that both chamber pressures decreases earlier in the predicted cut-off process, the cushioning effect is significantly reduced. This may damage the cylinder due to high velocity impact between the piston and the cylinder cushion sleeve. If the impact force is higher, the piston can even "bounce-off" when it reaches the end-stroke. Important consideration must be given in determining the modifying factor K in order to avoid cylinder damage and unwanted cylinder behaviour while at the same time performing the actuation task satisfactorily and minimising air consumption.

Finally, the modifying factor K was found to be highly sensitive to the working environment of the system such as system temperature, loaded mass and pneumatic cylinder's friction. It may also be affected by losses such as air leakages at valves and transmission line connections. Thus from this research it is concluded that the modifying factor K found is only applicable for this type of pneumatic cylinder. Further research is needed to accurately determine as well as to understand factors that contribute to its value. The determination of a global modifying factor K that can be used for other pneumatic cylinders employed under different working conditions will be valuable in order to apply predicted cut-off energy saving scheme under a broader scope.

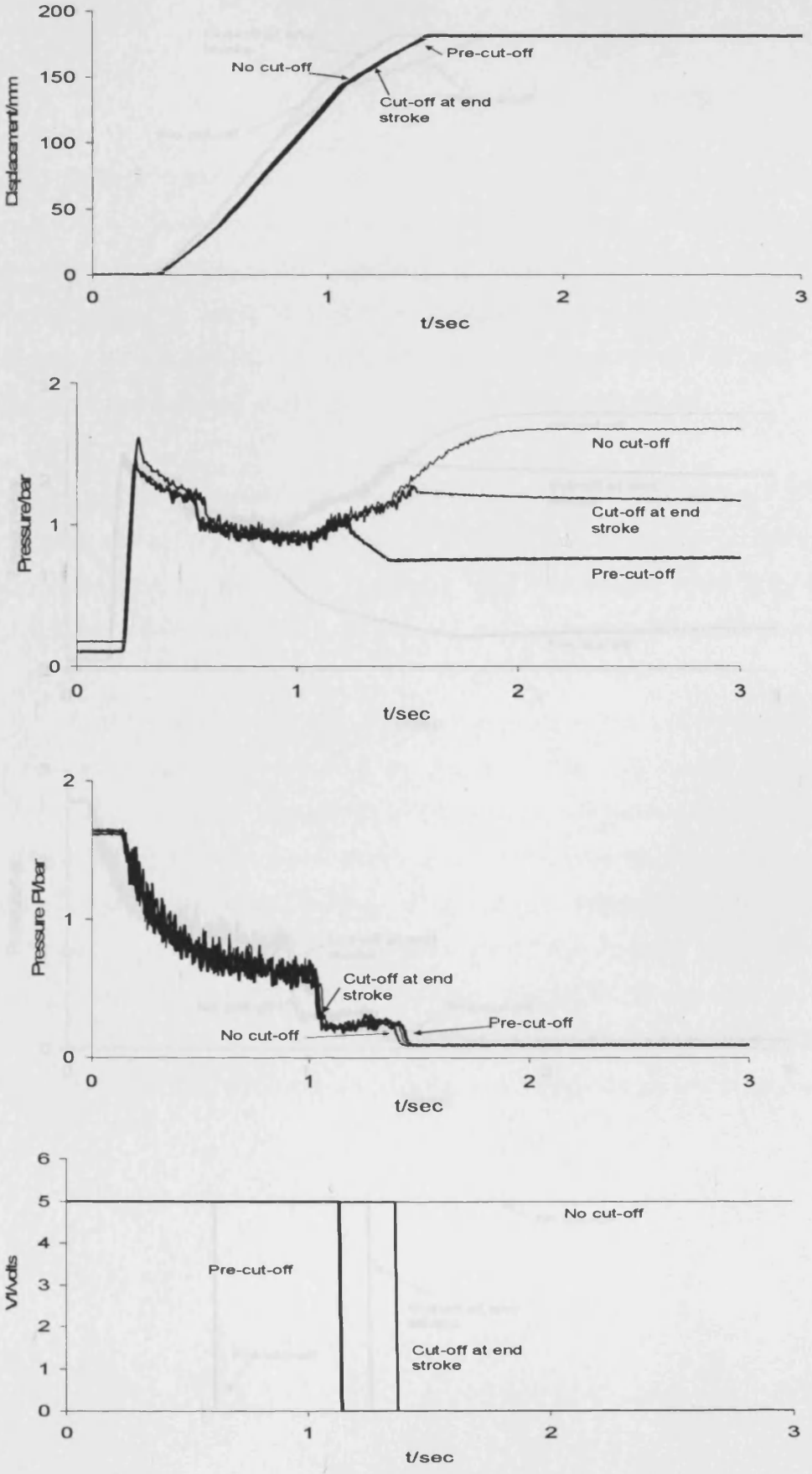

Figure 5.6: Cylinder actuation, system pressure 1.5bar

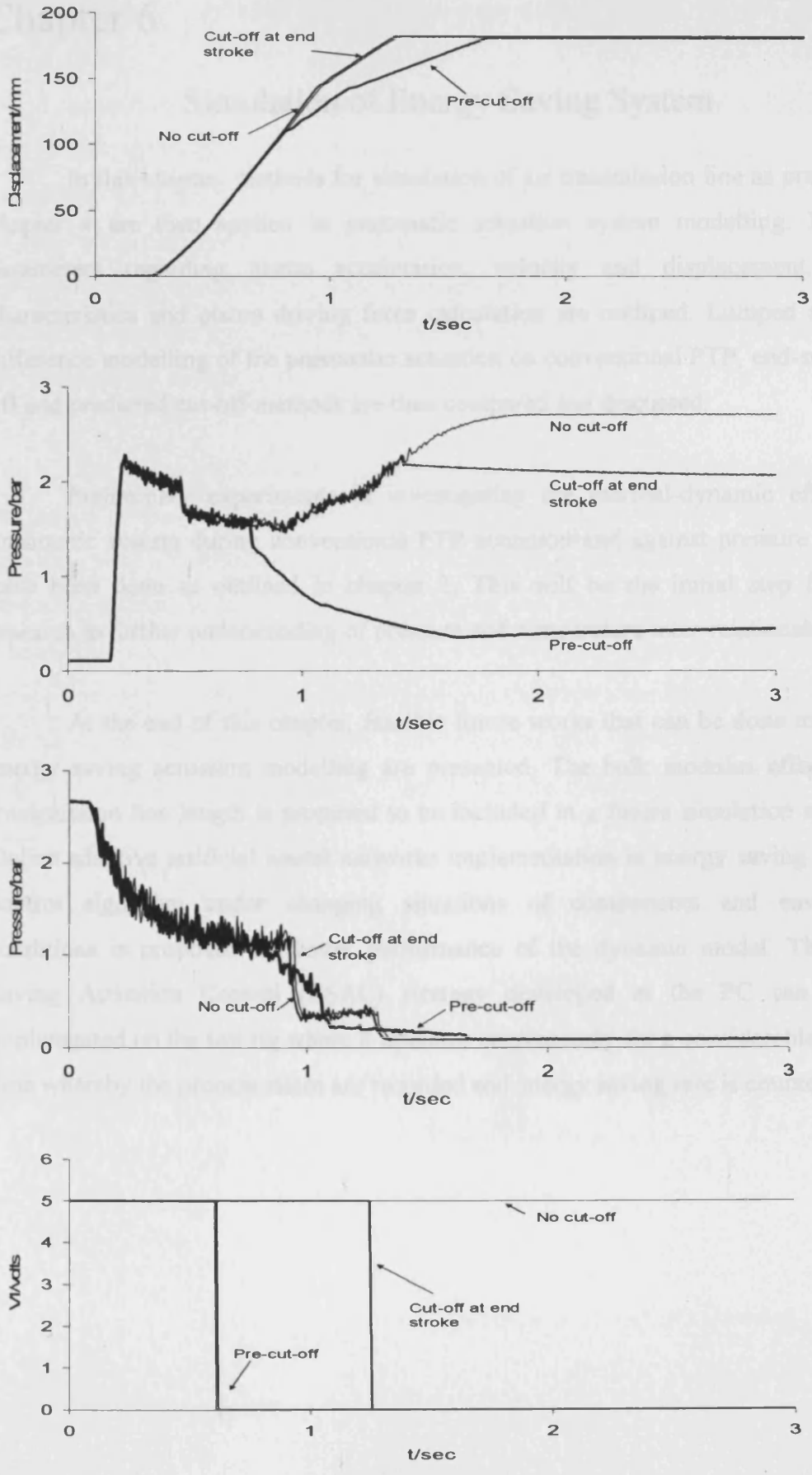

Figure 5.7: Cylinder actuation, system pressure 2.5 bar

Chapter 6

Simulation of Energy Saving System

In this chapter, methods for simulation of air transmission line as presented in chapter 4 are then applied to pneumatic actuation system modelling. Important parameters regarding piston acceleration, velocity and displacement, friction characteristics and piston driving force calculation are outlined. Lumped and finite difference modelling of the pneumatic actuation on conventional PTP, end-stroke cut-off and predicted cut-off methods are then compared and discussed.

Preliminary experiments in investigating the thermal-dynamic effect in a pneumatic system during conventional PTP actuation and against pressure variation have been done as outlined in chapter 3. This will be the initial step for future research to further understanding of pressure and temperature inter-relationship.

At the end of this chapter, feasible future works that can be done to improve energy saving actuation modelling are presented. The bulk modulus effect on the transmission line length is proposed to be included in a future simulation algorithm. Online adaptive artificial neural networks implementation in energy saving actuation control algorithm under changing situations of components and environment conditions is proposed for better performance of the dynamic model. The energy Saving Actuation Control (ESAC) strategy developed at the PC can then be implemented on the test rig where it operates continuously for a considerable working time whereby the process states are recorded and energy saving rate is counted.

6.1 Pneumatic cylinder actuation modelling

In the simulation of pneumatic cylinder actuation of both the conventional and energy saving methods (end-stroke and predicted cut-off), the transmission line modelling for both the lumped and finite difference approach were modified to include the pneumatic cylinder at the end of the transmission line. The pneumatic cylinder is modelled as having a large volume that changes constantly as the piston is actuated due to the force created by the pressure difference between the driving and the exhausting chamber.

The initial and boundary conditions of the system simulated are based upon the test rig set-up in the performed experiment as presented earlier in chapter 5. In the conventional PTP actuation, no cut-off was applied to the supply pressure during the actuation course. In the end-stroke cut-off, as the name suggests, when the piston reaches the end-stroke, cut-off were applied to the supply pressure while in predicted cut-off the supply pressure was cut-off prior to the piston reaching the end-stroke. In chapter 1, detailed explanations of each actuation type were presented. The model used in the computer simulations of the pneumatic cylinder actuations is shown in Figure (6.1).

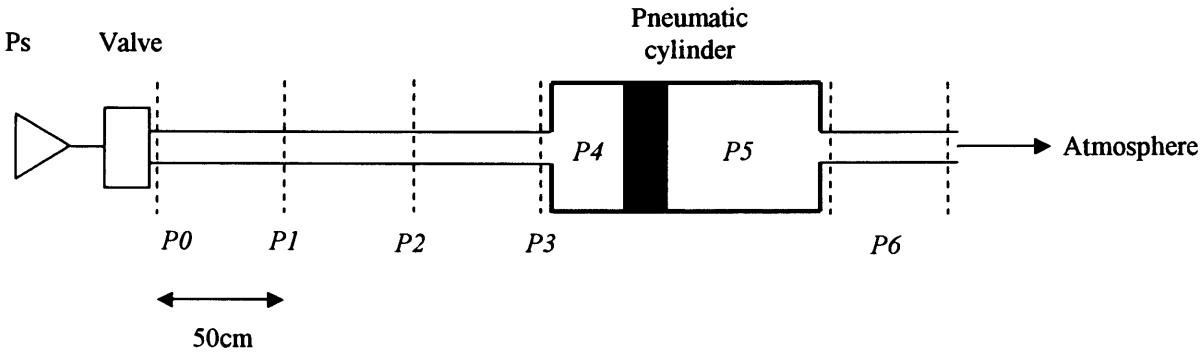

Figure 6.1: Simulation model for the pneumatic cylinder actuations

Pressure *P3* is designated to be the pressure at the inlet port of the pneumatic cylinder while *P4* is the pressure in the driving chamber of the cylinder. Similarly *P5* and *P6* are pressures in the exhausting chamber and at the outlet port of the pneumatic cylinder respectively.

Based on pneumatic cylinder friction characteristic as identified in chapter 5, the friction force presented by the pneumatic cylinder is then incorporated in the computer simulation algorithm. This enables the determination of cut-off time in predicted cut-off actuation method and provides the net piston force calculation.

The dynamics of the piston can be represented using Newton's Second Law as:

$$(M+Mo)\frac{dv_p}{dt} = (P_4 - P_5)A_p - F_{frp} \quad \text{..... (6.1)}$$

where M is the mass attached at the end of the cylinder's rod and Mo is other masses associated with the loading of the pneumatic cylinder besides the mass placed on the trolley. It is considered that these "other masses" amounted to 1kg on top of the 10kg weight of the loaded trolley. A_p is the piston cross-sectional area while F_{frp} is the piston friction force opposing the driving actuation. Pneumatic cylinder friction characteristic as determined by experiments in chapter 5 is then incorporated into equation (6.1).

$$F_{frp} = c_{fr} + (K_v \cdot v_p) \quad \text{..... (6.2)}$$

where the required parameters are as follows. F_s 359N, F_c 141N, c_{fr} 126N and K_v 1557Ns/m.

From equation (6.1) it is possible to determine the piston's acceleration a_p, velocity v_p and its displacement x_p as will be shown consecutively.

In discrete time-domain, the velocity v_p and displacement of the piston x_p can be updated by:

$$\Delta v_p = \frac{dv_p}{dt} \cdot T \quad \text{..... (6.3)}$$

$$\Delta x_p = v_p T \quad \text{..... (6.4)}$$

Simulation results are presented in this chapter starting with lumped modelling and then followed by finite difference modelling. Displacement of the pneumatic cylinder is also included for each actuation method operating at two different supply pressures specified (1.5bar and 2.5bar).

Note that it has not been possible to measure directly the pressure in the driving and exhausting chambers. The closest positions at which pressure transducers can be installed at the pneumatic cylinder are at both the inlet and outlet ports. However in the computer simulation, pressures at both the inlet *P3* and outlet *P4* ports including the driving *P5* and exhausting *P6* chambers can be simulated.

The actuator dynamics is integrated with the transmission line dynamics and Gas Law in the simulation of conventional, end-stroke cut-off and predicted cut-off actuations. Orifice and transmission line equations as studied in chapter 4 including the equation to determine cut-off time in predicted cut-off actuation are repeated as follows. For predicted cut-off actuation, once pressure in the driving chamber Pr meets the criteria as shown in equation (6.5), cut-off is actuated at the main directional valve.

$$P > K \cdot P_{st}\left(V_o / V\right)^n \quad \text{..... (6.5)}$$

K is the modifying factor which is found by trial. The K value varies from 0.1 at system pressure Ps of 1.5bar and 0.2 at system pressure of Ps 2.5bar. However in the computer simulation, the K value had to be changed for the simulation results to match the captured data. This may due to factors such as air leakages at valves and connections, losses of air flow and thermal-dynamics which are not included in the

computer simulation. The K value used in the computer simulations is 2.2 for 1.5bar and 1.2 for 2.5bar system pressure.

For lumped modelling, the corresponding equation to determine the mass flowrate flowing through an orifice is given by:

$$\dot{m} = \frac{C_d \cdot C_m \cdot A_t \cdot P_u}{\sqrt{T_s}} \quad \text{(6.6)}$$

This was then substituted into:

$$\frac{dm_j}{dt} = \dot{m}_{j-1} - \dot{m}_j \quad \text{(6.7)}$$

The obtained mass flowrate $\dot{m}$ flowing through the orifice is then substituted into state equation as follows:

$$\frac{dP_j}{dt} = \frac{RT_s}{V_j}\left(\dot{m}_{j-1} - \dot{m}_j\right) \quad \text{(6.8)}$$

By multiplying $\frac{dP_j}{dt}$ with sampling time T, the pressure change at position j at that instant of time can be obtained.

Based on D'Arcy equation[14], the overall viscous friction force F_{fr} against air flow at position j can be obtained as follows. The derivation of equation (6.9) had been presented earlier in chapter 4.

$$F_{fr_j} = 8\pi\mu_j l_t u_j \quad \text{(6.9)}$$

This is then substituted into force equation based on Newton's Second Law.

$$m_j \frac{du_j}{dt} = m_j a_j = A_t\left(P_{j-1} - P_j\right) - F_{fr_j} \quad \text{(6.10)}$$

Thus by rearranging the force equation, the acceleration of the air flow is obtained.

$$\frac{du_j}{dt} = \frac{\left(A_t\left(P_{j-1} - P_j\right) - F_{fr_j}\right)}{m_j} \quad \text{(6.11)}$$

Finally the air flow displacement Z can be determined using equation (6.12) shown below.

$$Z_j = \frac{1}{2}\frac{du_j}{dt}T^2 \quad \text{(6.12)}$$

For finite difference modelling approach, the required equations are shown as follows.

$$D = \begin{bmatrix} \rho \\ \rho u \end{bmatrix} \quad \text{(6.13)}$$

$$E = \begin{bmatrix} \rho u \\ \rho u^2 + P - \tau_{xx} \end{bmatrix} \quad \text{(6.14)}$$

where (τ_{xx}) is:

$$\tau_{xx} = \frac{2}{3}\mu\left(2\frac{\partial u}{\partial x}\right) \quad \text{(6.15)}$$

Equations (6.13) through to equation (6.15) are based on vector form of one-dimensional compressible Navier-Stokes equations as presented in detail earlier in

chapter 4. By utilising the air flow direction determination algorithm , both backward and forward type differencing can be utilised for simulating the pressure wave propagation in the system. The following are backward and forward differencing equations used.

Backward differencing:

$$D_j^{\overline{n+1}} = D_j^n - \frac{\Delta t}{\Delta x}\left(E_j^n - E_{j-1}^n\right) \quad (6.15)$$

Forward differencing:

$$D_j^{\overline{n+1}} = D_j^n - \frac{\Delta t}{\Delta x}\left(E_{j+1}^n - E_j^n\right) \quad (6.16)$$

The pneumatic actuator volumes (driving and exhausting chambers) are modelled using lumped approach since these volumes are significantly larger when compared to the volume in each segment of the modelled transmission line.

The initial conditions used during the modelling of the system using both lumped and finite difference methods are tabulated as follows.

For simulation of pneumatic cylinder actuations conducted under supply pressure of 1.5bar, the following initial conditions of pressure at each designated positions as represented by Figure (6.1) is shown in Table (6.1).

Table 6.1: Initial pressures at Ps 1.5bar

Pressure position	Pressure/bar
P0	1.00
P1	1.00
P2	1.00
P3	1.00
P4	1.00
P5	1.54
P6	1.54

Similarly for simulation of pneumatic cylinder actuations conducted under supply pressure of 2.5bar, the following initial conditions of pressure at each designated positions are as follows.

Table 6.2: Initial pressures at Ps 2.5bar

Pressure position	Pressure/bar
P0	1.00
P1	1.00
P2	1.00
P3	1.00
P4	1.00
P5	2.56
P6	2.56

System parameters of the computer simulations conducted for the energy saving system using both lumped and finite difference methods can be referred to the Microsoft Visual C++ programs included in Appendix 1 through to Appendix 5. This includes parameters such as pneumatic transmission line section lengths and diameters, system temperature T_s, loaded mass M, the pneumatic cylinder piston's cross-sectional area A_p and its maximum stroke x_{pmax}, cushion regions and initial volumes of both the left chamber P_l and right chamber P_r including the pneumatic cylinder static friction value F_s.

Note that the pressures at the exhausting chamber and the consecutive outlet port are at supply pressure value since the simulations are based on experimental data in which the cylinder had just completed a conventional retraction motion. Cylinder actuation simulations under conventional, end-stroke cut-off and predicted cut-off processes using lumped and finite difference methods are conducted at a sampling time T of 1.0×10^{-6} s and calculation iterations are performed 5.0×10^{6} times. The predicted cut-off computer simulation programs for both lumped and finite difference methods are attached as Appendix 4 and Appendix 5 respectively. The conventional and end-stroke cut-off computer simulation programs for both lumped and finite difference approach are not included due to the fact that the predicted cut-off simulations are constructed based on the former simulations.

6.2 Conventional PTP actuation modelling

6.2.1 Supply pressure at 1.5bar

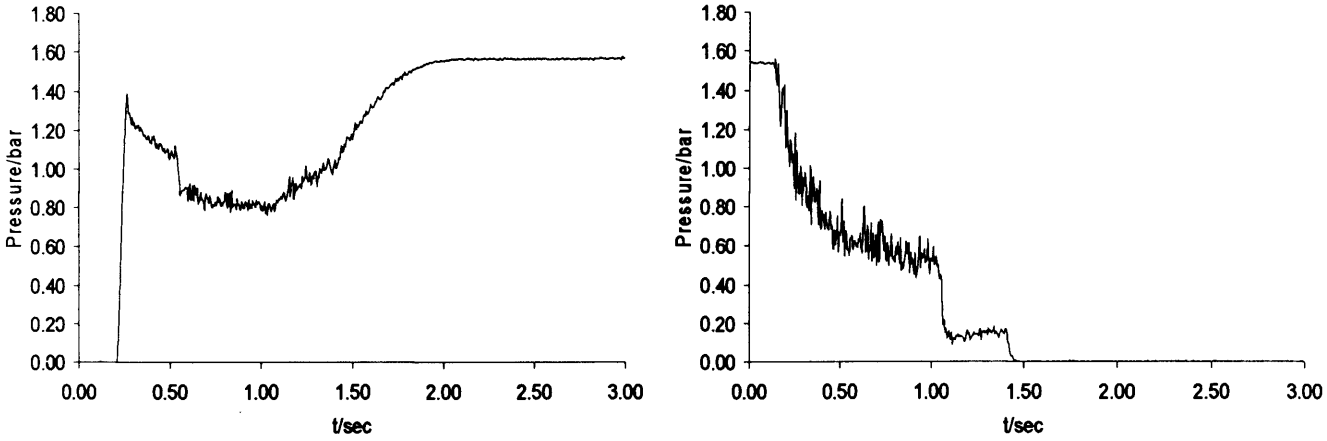

(a) Measured results

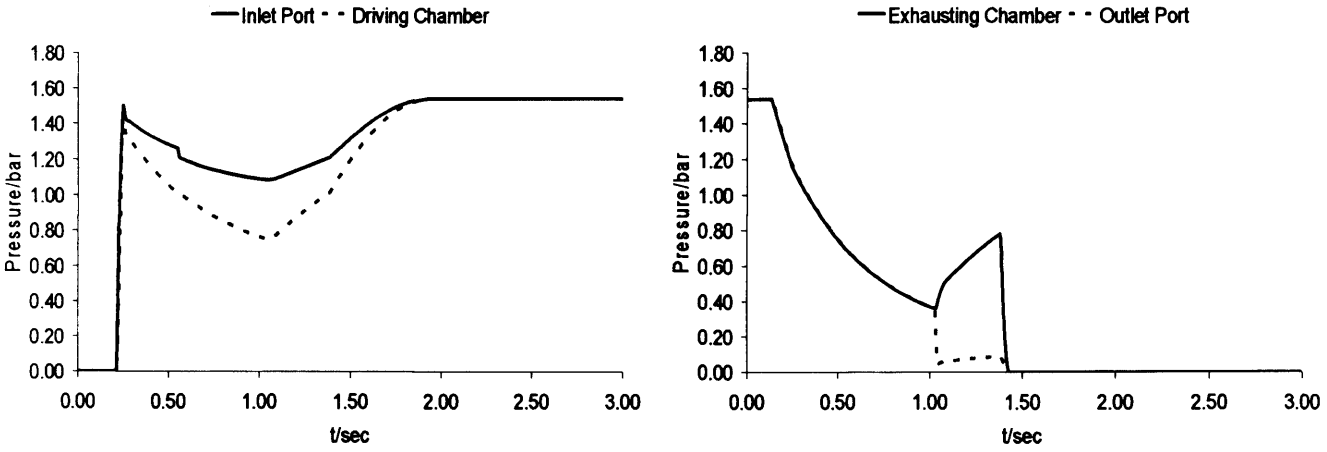

(b) Lumped simulation results

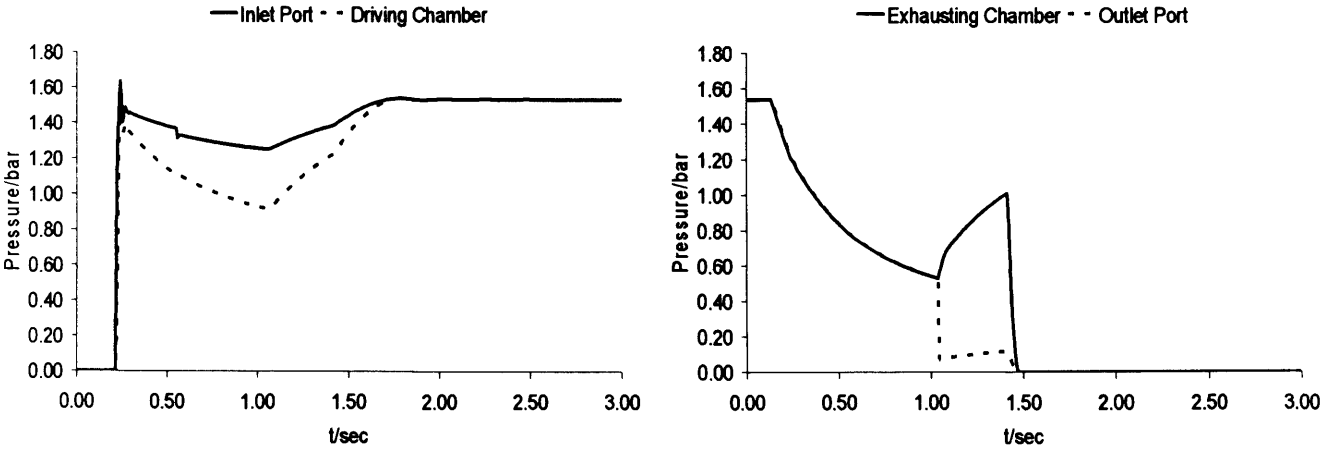

(c) Finite difference simulation results

Figure 6.2: Conventional actuation simulation (Ps: 1.5bar)

6.2.2 Supply pressure at 2.5bar

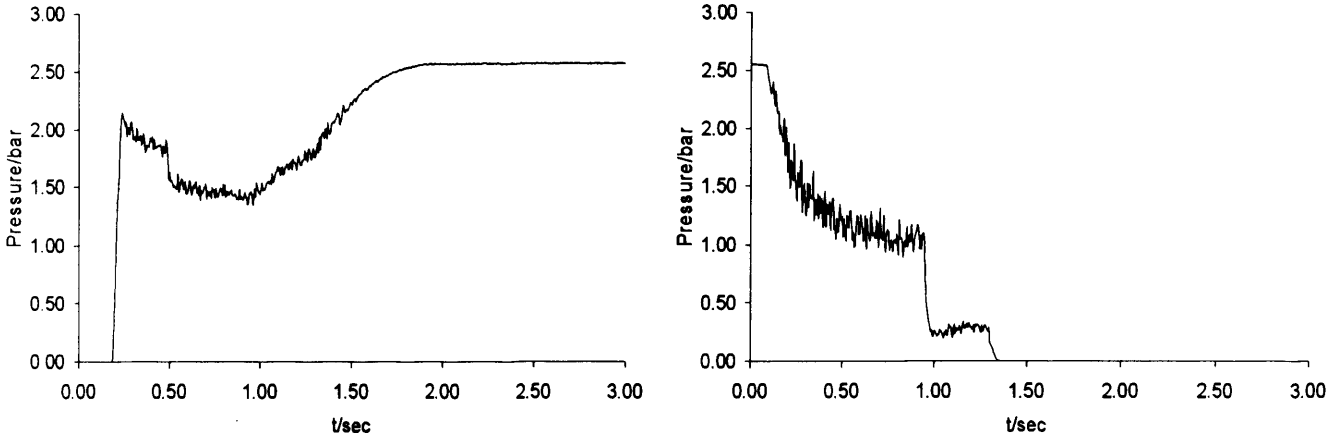

Inlet Port Outlet Port

(a) Measured results

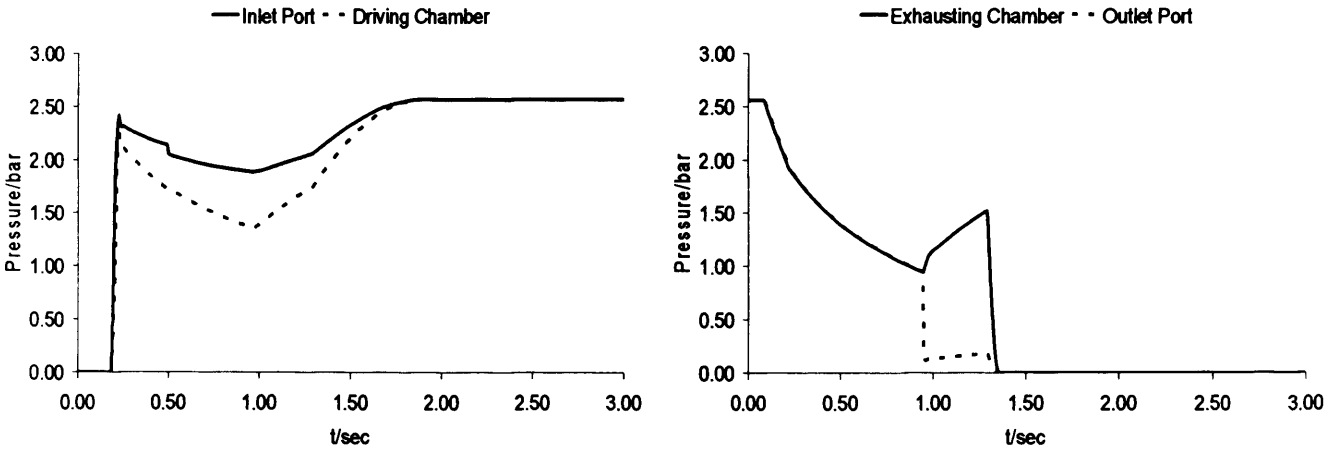

(b) Lumped simulation results

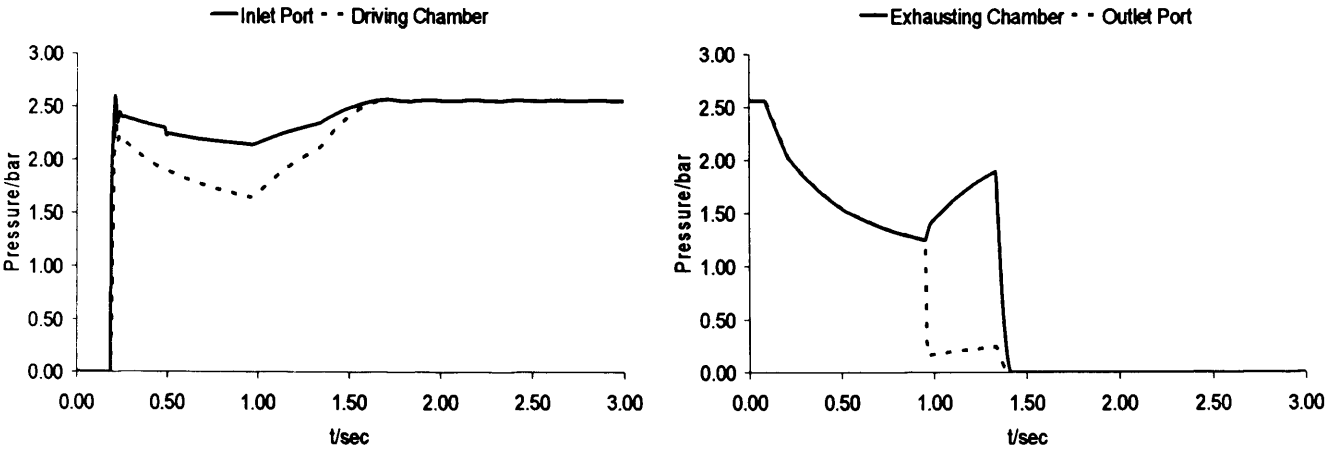

(c) Finite difference simulation results

Figure 6.3: Conventional actuation simulation (Ps: 2.5bar)

6.3 End-stroke cut-off actuation modelling

6.3.1 Supply pressure at 1.5bar

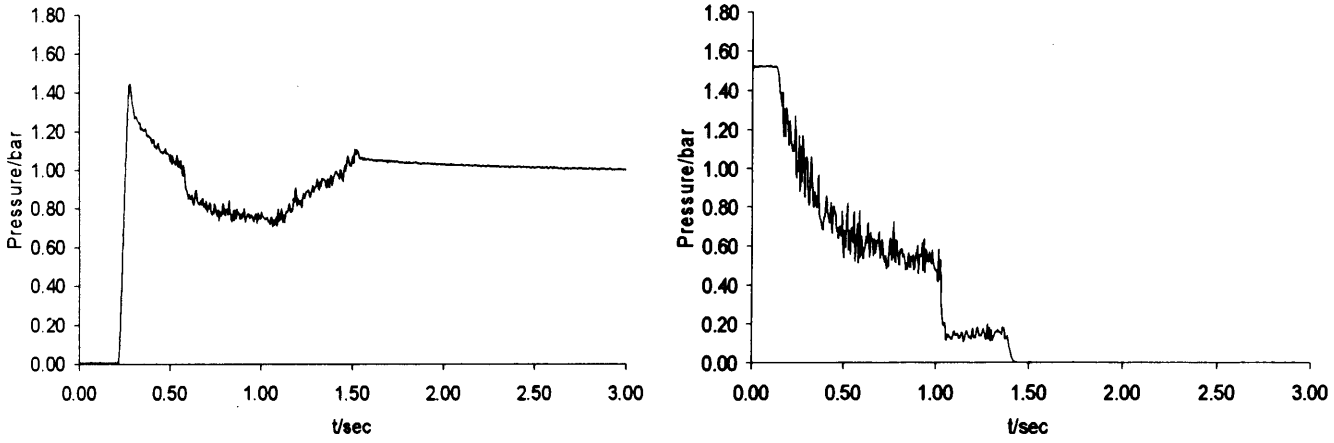

(a) Measured results

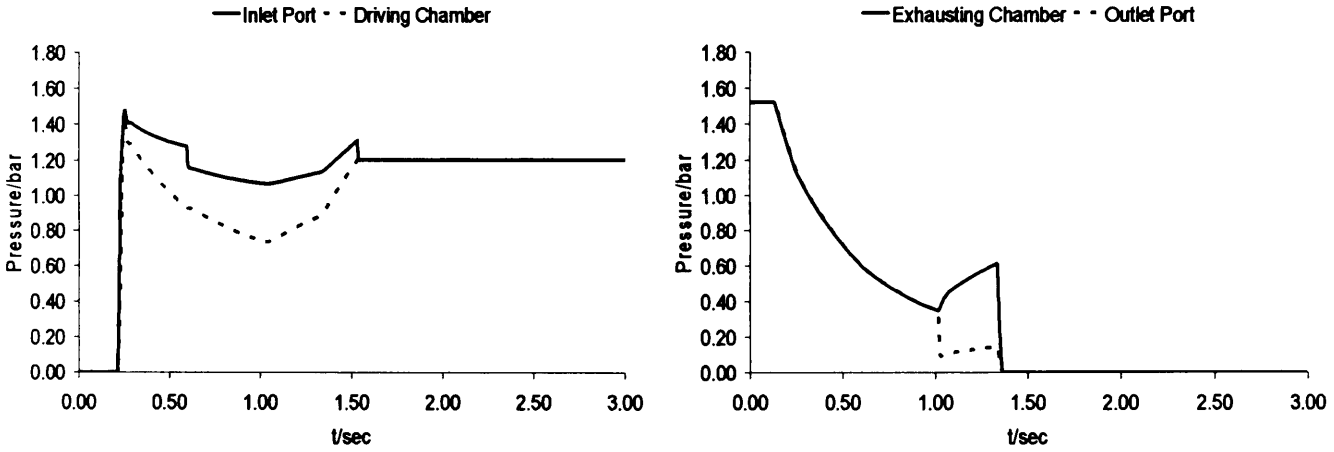

(b) Lumped simulation results

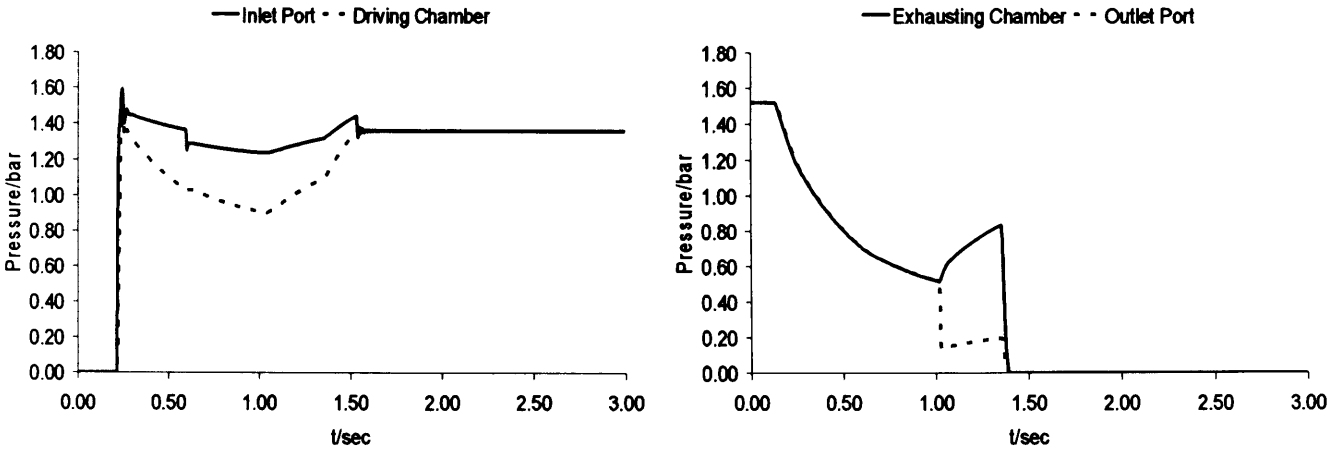

(c) Finite difference simulation results

Figure 6.4: End-stroke cut-off actuation simulation (Ps: 1.5bar)

6.3.2 Supply pressure at 2.5bar

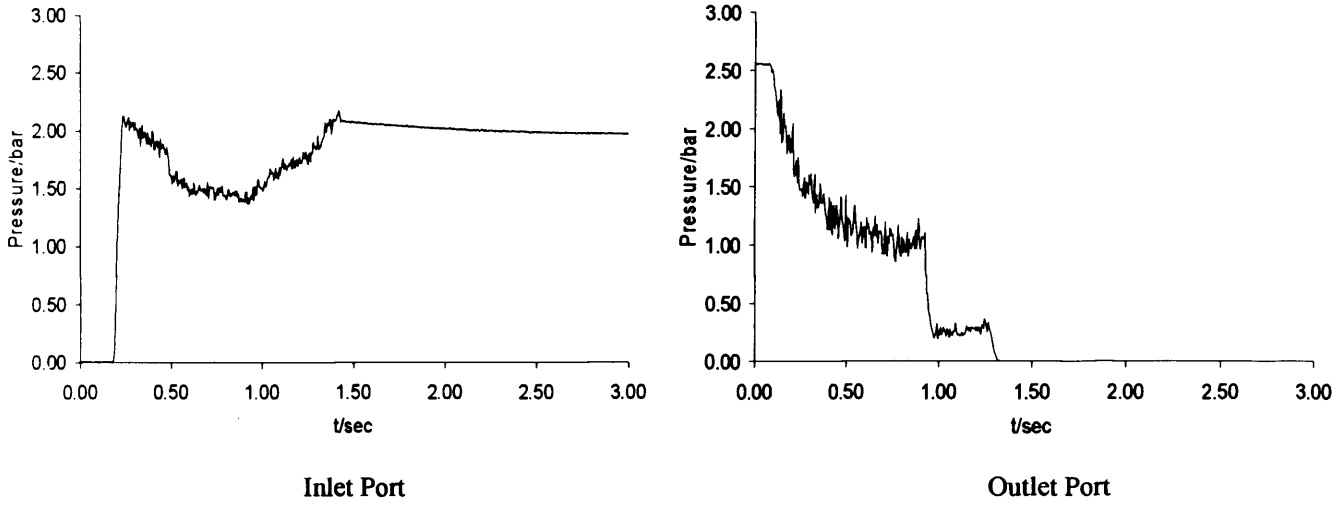

Inlet Port Outlet Port

(a) Measured results

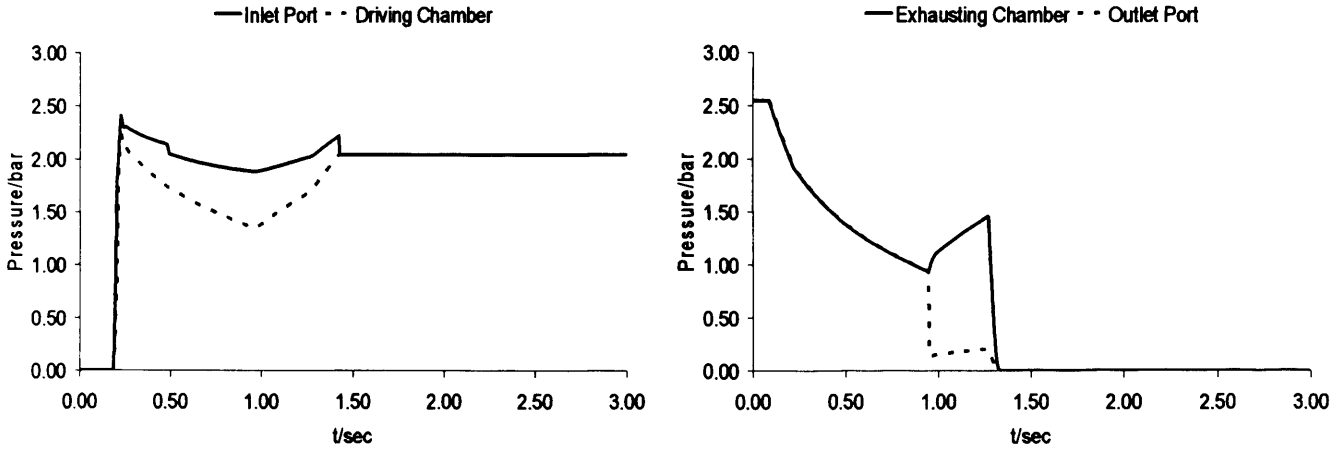

(b) Lumped simulation results

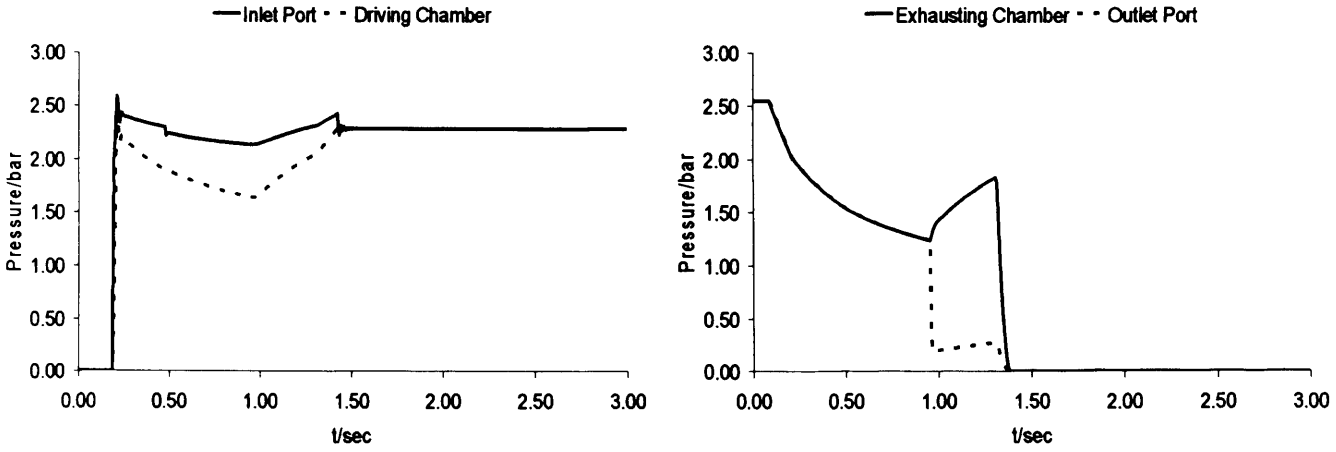

(c) Finite difference results

Figure 6.5: End-stroke cut-off actuation simulation (Ps: 2.5bar)

6.4 Predicted cut-off actuation modelling

6.4.1 Supply pressure at 1.5bar

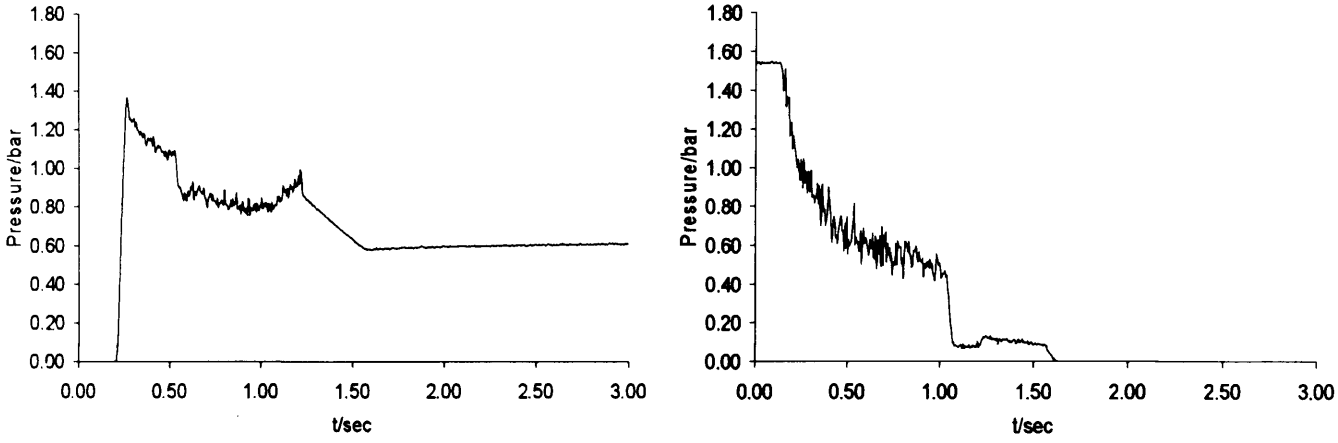

Inlet Port Outlet Port

(a) Measured results

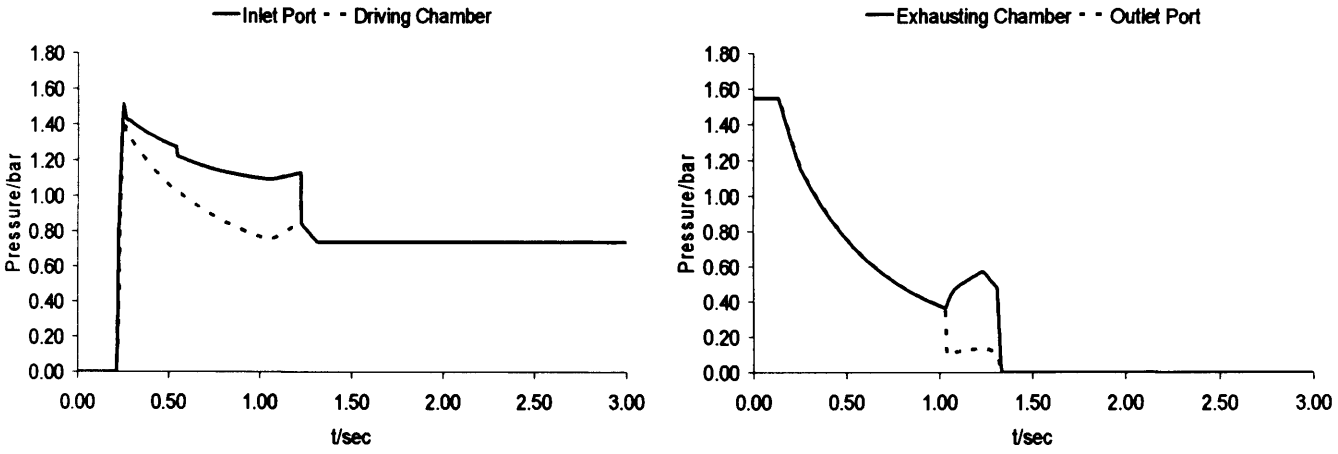

(b) Lumped simulation results

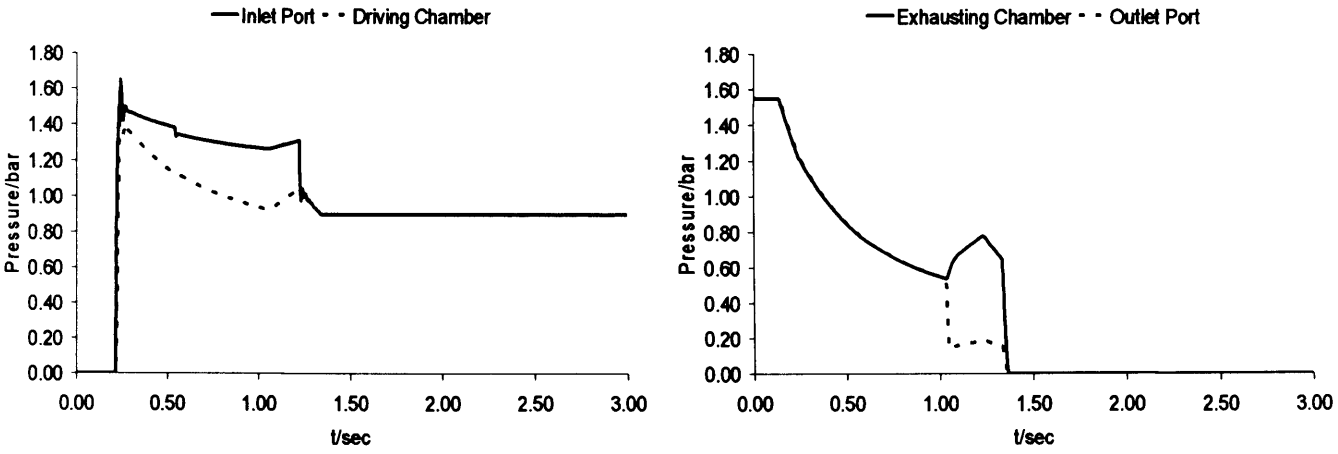

(c) Finite difference approach

Figure 6.6: Predicted cut-off actuation simulation (Ps: 1.5bar)

6.4.2 Supply pressure at 2.5bar

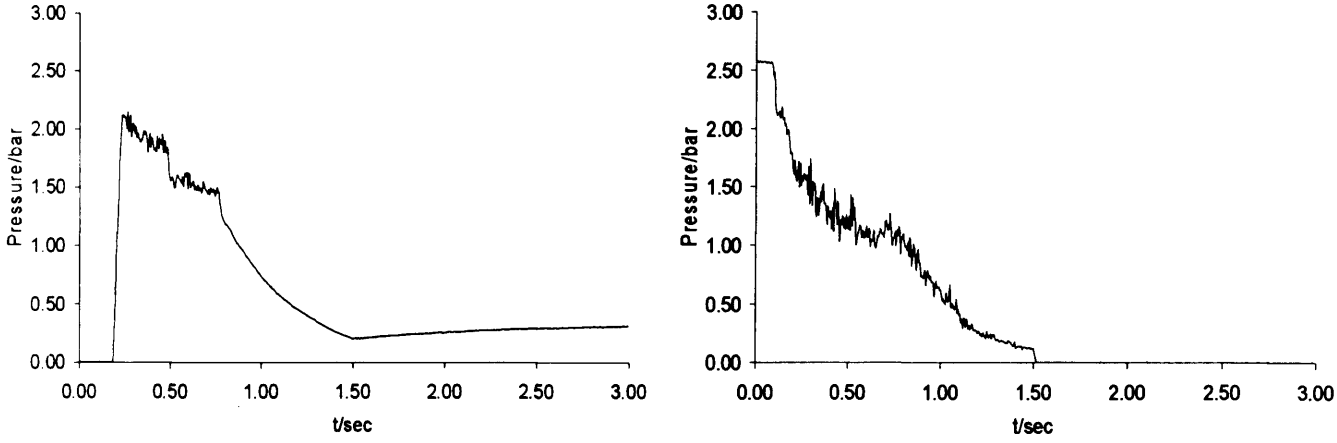

Inlet Port Outlet Port

(a) Measured results

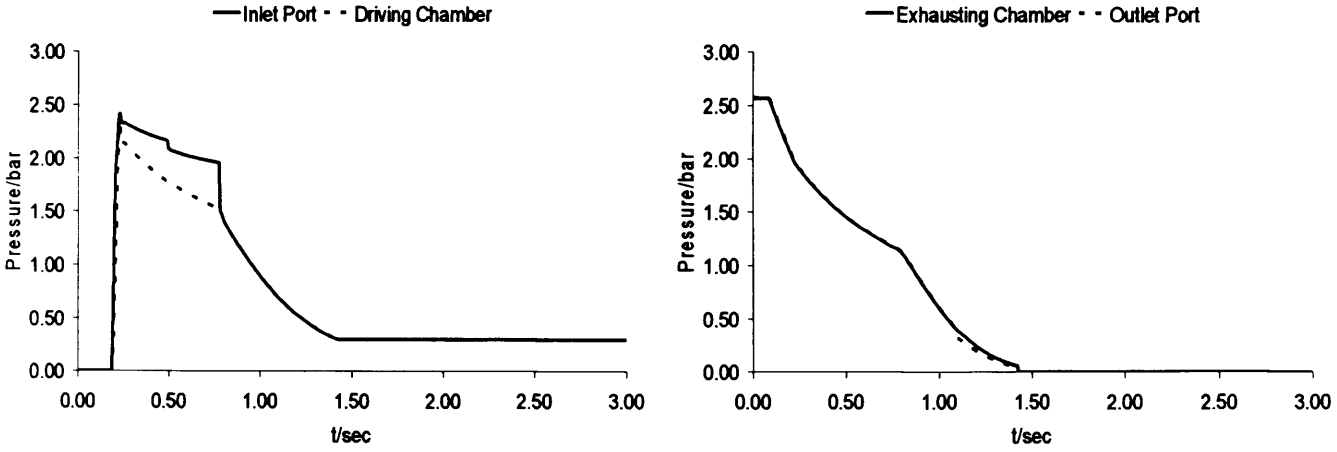

(b) Lumped simulation results

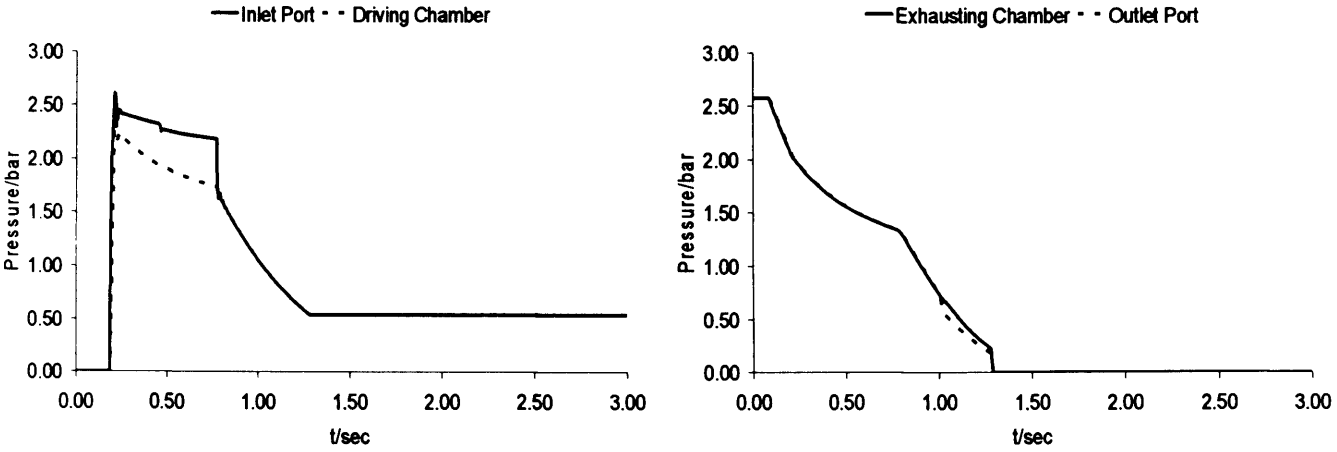

(c) Finite difference simulation results

Figure 6.7: Predicted cut-off actuation simulation (Ps: 2.5bar)

6.5 Pneumatic actuator displacements

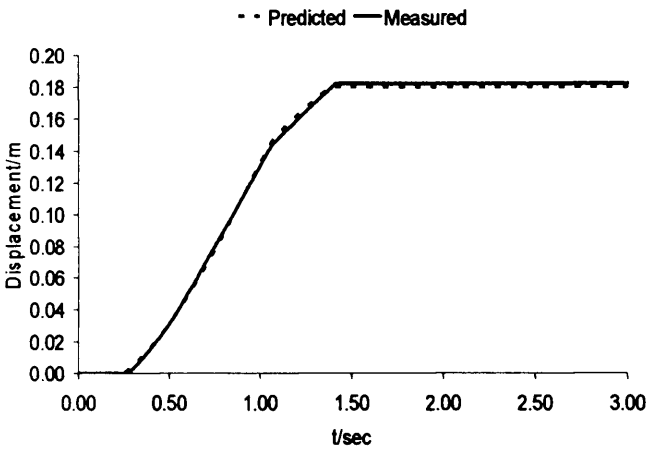

Ps = 1.5bar

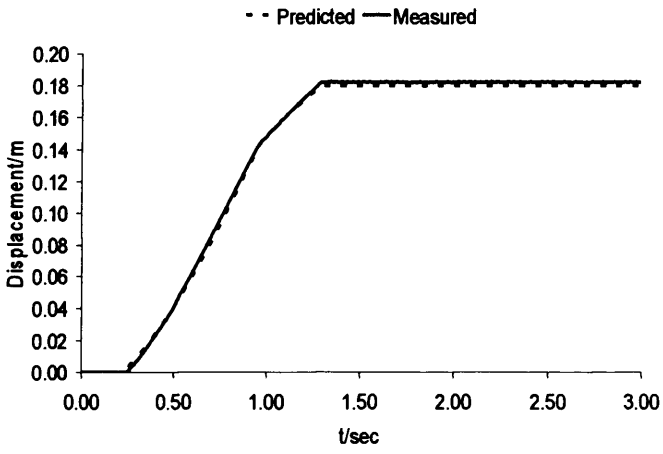

Ps = 2.5bar

(a) Conventional cylinder actuation

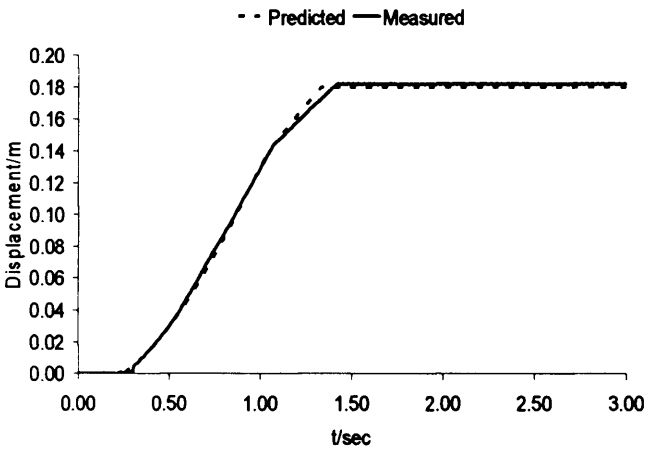

Ps = 1.5bar

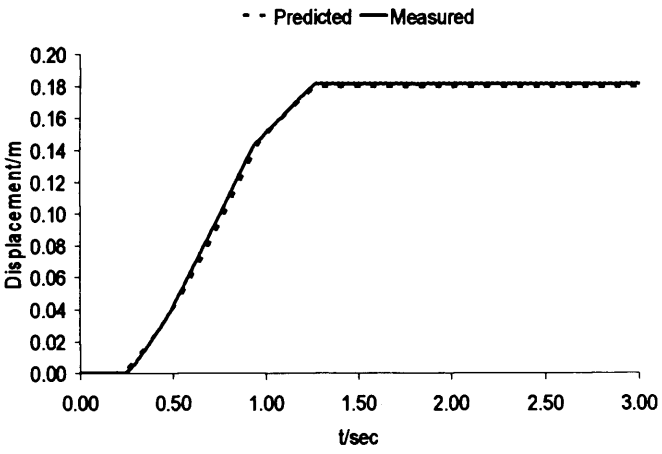

Ps = 2.5bar

(b) End-stroke cut-off cylinder actuation

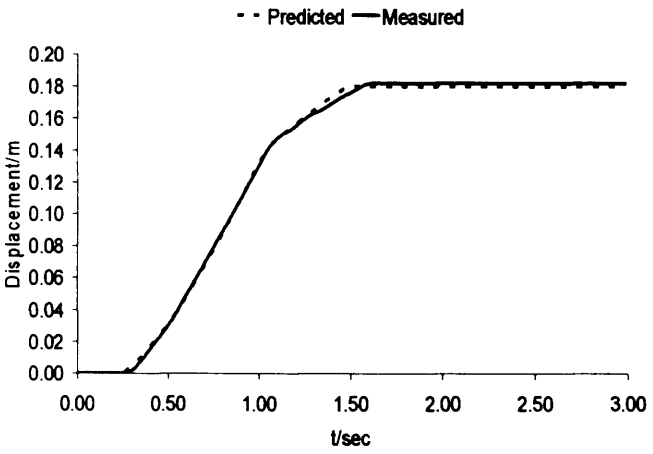

Ps = 1.5bar

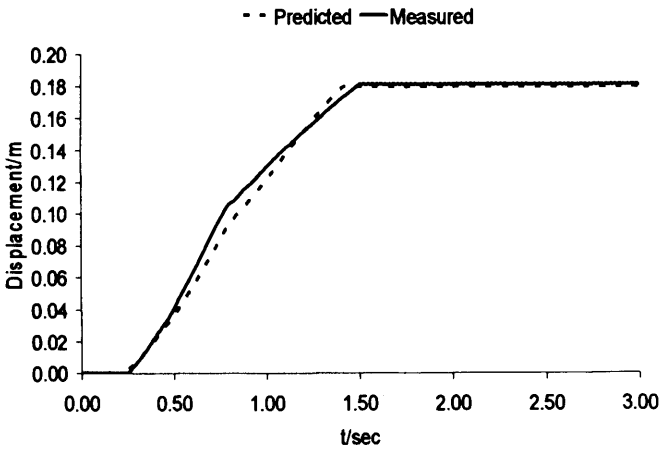

Ps = 2.5bar

(c) Predicted cut-off cylinder actuation

Figure 6.8: Pneumatic cylinder piston displacements under different actuation conditions

6.6 Discussion

As mentioned in previous chapters of this thesis, pressure ripples due to pressure wave propagation in transmission line exist. Based on the transmission line experiments presented earlier in this chapter, it is evident that this phenomenon occurs when there is a sudden deceleration of fluid flowing in a transmission line. This occurs when there is a sudden closure or blockage at either one or both ends of a transmission line.

The mechanism of air dynamics in transmission line experiment presented earlier in chapter 4 is similar to a certain degree to the air dynamics of pneumatic cylinder actuations outlined in this chapter. In transmission line experiment conducted, the air is trapped between blocked ends of the transmission line while in pneumatic cylinder actuation, once cut-off is implemented, the air is trapped between the driving chamber and the discharged main directional valve.

Based on measured results of conventional, end-stroke cut-off and predicted cut-off of the pneumatic cylinder actuations, it was found that pressure ripples in the system are absent. This is due to the fact that the presence of a large volume at the end of the transmission line in the form of the actuator's driving chamber. This chamber absorbs the pressure wave propagation that occurs in the transmission line once the cut-off to the supply pressure is implemented. This is true since the volume of the driving chamber once cut-off is actuated at the main directional valve is significantly larger compared to the volume of the transmission line.

For conventional cylinder actuation, the pressure in the driving chamber increase to the supply pressure once the piston reaches its end-stroke position. Note that the initial pressure in the driving chamber increases to 1.4bar for Ps of 1.5bar and approximately 2.2bar for Ps of 2.5bar to overcome the piston's static friction F_s as mentioned earlier in chapter 5. During this period, all the forces in the driving chamber is consumed to move the piston from rest and there are no movement of the piston within this very small time-frame. This phenomenon is true for all cylinder actuation conditions.

Note that the initial pressure decrease in the driving chamber occurs due to the initial cushion region of the pneumatic cylinder. In this case, the air is flowing into the driving chamber through the smaller orifice of the cushion mechanism first, followed by both the small and the larger orifice after the cylinder cushion region had been passed by the piston. The pressure drops considerably after this when there is a sudden increase of air flowrate being pushed into the driving chamber. The same mechanism is experienced by the pneumatic cylinder under end-stroke cut-off and predicted cut-off actuations during the movement of the piston within the initial cylinder cushion region.

The described mechanism can be confirmed by the measured and simulated displacement of the cylinder that shows the slow initial displacement followed by a sudden acceleration at the beginning of the stroke. The displacement of the cylinder undergo a steady velocity once the cushion region is passed and then experience a sudden deceleration due to piston entering the cylinder's end cushion region. Finally the actuation ends once the maximum stroke has been reached.

When the piston is moving within the cylinder's end cushion region, the simulated pressure in the exhausting chamber experience a sudden increase due to the air being pushed out through a smaller orifice of the outlet port. As mentioned earlier in chapter 3, this phenomenon is required to reduce the impacting force between the piston and the end caps. The outlet port meanwhile experience a sudden decrease in pressure due to the sudden loss of air flowrate (air exhausted through the smaller orifice of the exhausting chamber) during this process. Finally both the pressures in exhausting chamber and the outlet port of the pneumatic actuator becomes atmospheric once all the air in the exhausting chamber had been exhausted. This mechanism is true for conventional, end-stroke cut-off and predicted cut-off cylinder actuations.

In end-stroke cut-off actuation, once the maximum cylinder stroke is reached, the main directional valve was discharged and supply pressure was cut-off from the system. Instead of a pressure rise to the supply pressure as in conventional process, the simulated pressure in the driving chamber remains constant at the last pressure value just before cut-off is implemented. The measured pressure value however

exhibits a continuous slow decrease of pressure in the driving chamber once cut-off is initiated. This phenomenon may be caused by two reasons. First is that there might be leakages in the system. Second is that this is due to the decrease of air temperature during the previous expansion process. This occurs under both supplied pressures Ps of 1.5bar and 2.5bar. The simulated inlet port pressure experience a sudden pressure drop at the end-stroke due to loss of supply pressure once the main directional valve is discharged.

In the predicted cut-off actuations, once the criteria as presented in equation (6.5) had been met, cut-off is implemented by discharging the main directional valve during which no air supply is being delivered to the driving chamber before the maximum cylinder stroke is reached. The working stroke then is powered by the expansion of the compressed air in the driving chamber until the maximum cylinder stroke is achieved. This type of pneumatic actuation maximises the amount of air potential energy that can be saved if large cylinder stiffness at the end-stroke is not required. After cut-off implementation, simulated pressure at the inlet port and both the measured and simulated pressures in the driving chamber decreases as the high pressure air of constant mass is expanded in the driving chamber. These pressures continuously decreases as the driving chamber volume increases until the maximum stroke is achieved and the pressures becomes stagnant. However compared with the measured pressure at the inlet port, it was found that there is a slight pressure increase over time. This is due to the thermal-dynamic effect mainly in the form of heat flow generated by the sliding friction between the piston's sealing and the cylinder's inner wall.

Observations of the measured data also indicates the time-delay effect of the air operated valves used in the experiment. This can be seen in the end-stroke cut-off actuations. Once signal V1 from the PC is disconnected for air supply pressure cut-off, the pressure is still rising in the driving chamber. This can be seen clearly in the end-stroke cut-off actuation with the supply pressure Ps of 2.5bar by monitoring the corresponding pressure and piston's displacement at which the piston reaches the end-stroke. The time-delay of the air operated valves depends on the system's supply pressure Ps and this had been found decreasing with increasing supply pressure. The

corresponding time-delay of the air operated valves used under different system pressures had been presented in chapter 3 previously.

Pressure ripples can be observed in the simulated pressure at the inlet port of the cylinder during conventional processes and when cut off is initiated for both end-stroke cut-off and predicted cut-off actuations under all supply pressure condition. As mentioned before in chapter 4, this is due to the pressure wave propagations that occurs in the transmission line between the inlet port and main directional valve. However due to its high frequency nature and the absence of pressure ripples in the measured data might suggest that improvements are needed in the computer simulation model.

These simulated pressure ripples are found by magnifying the simulated pressure results at the moment the piston reaches maximum stroke for conventional actuation and when cut-off to the supply pressure is initiated for both end-stroke cut-off and predicted cut-off actuations.

These results are shown in Figures (6.9, 6.10, and 6.11) and are presented in the following order; conventional PTP actuation, followed by end-stroke cut-off actuation and finally predicted cut-off actuation. All these simulated actuations are based on working pressures of 1.5bar and 2.5bar respectively as mentioned earlier in this chapter.

It can be said that the approach to computer simulation of the pneumatic system operating under conventional no cut-off, end-stroke cut-off and predicted cut-off has been successful since the measured system overall pressure response can be approximated to the pressure changes in the simulated results at both the inlet and outlet of the actuator.

6.7 Pressure ripples in simulated results

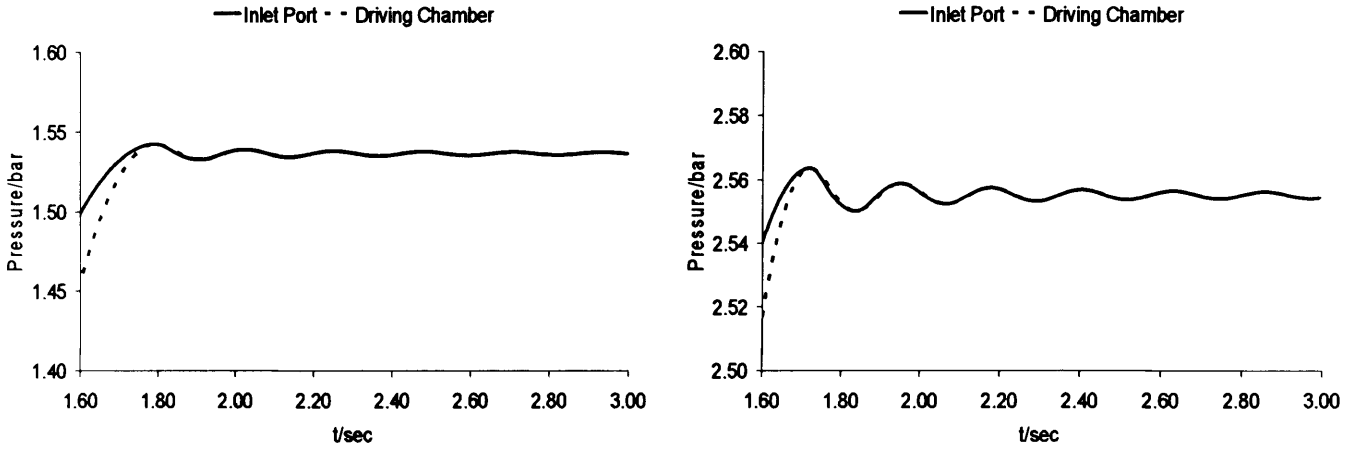

Ps: 1.5bar Ps: 2.5bar

Figure 6.9: Pressure ripples in conventional actuation simulation

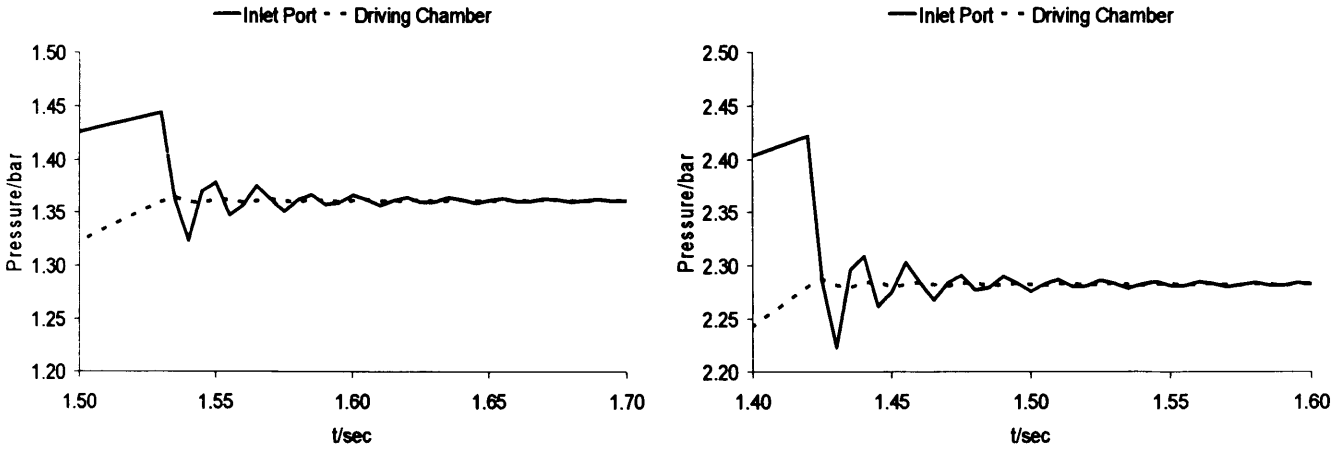

Ps: 1.5bar Ps: 2.5bar

Figure 6.10: Pressure ripples in end-stroke cut-off actuation simulation

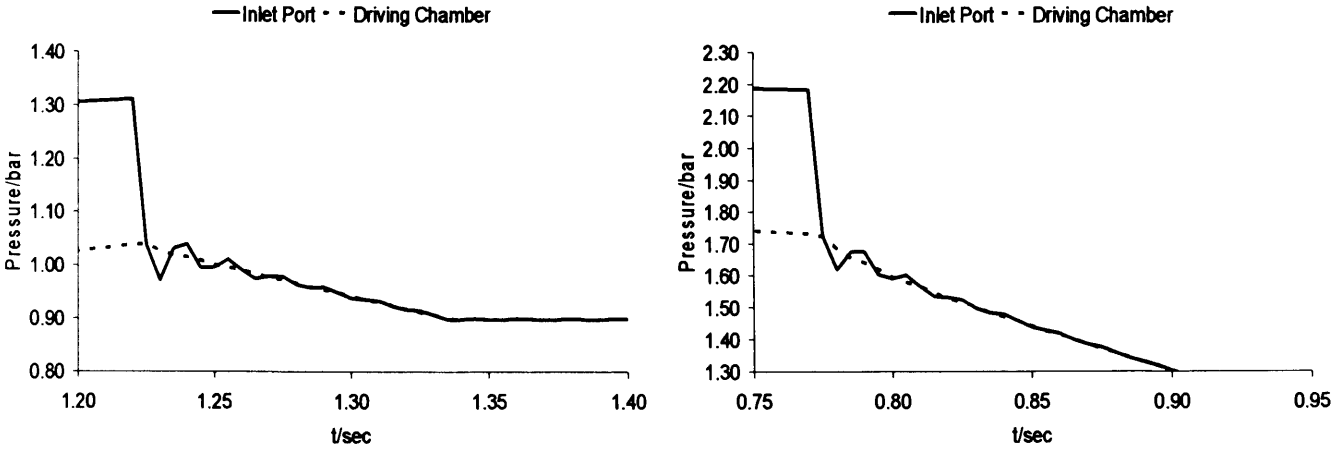

Ps: 1.5bar Ps: 2.5bar

Figure 6.11: Pressure ripples in predicted cut-off actuation simulation

The pressure behaviour in the exhausting chamber under predicted cut-off process is similar to both the conventional and end-stroke cut-off actuations. Due to the fact that the pressure in the driving chamber is cut-off before the end-stroke is achieved, the piston undergoes early deceleration due to the loss of driving force during the extension motion of the piston. This in turn reduces the amount of pressure build-up in the exhausting chamber and hence resulting in a reduced cushioning. However this proves to be acceptable since early deceleration of the piston prior to reaching the end-stroke means that the impact force between the piston cap and the end cap is reduced, hence the reduced cushioning is sufficient to prevent damage to the cylinder.

Based on this observation, the modifying factor K that needs to be specified depends on a number of considerations that need to be made in order to satisfy the demanded actuation while maximising the amount of air potential that can be saved. This is important in order to avoid damage to the cylinder due to possible increase in impact damage due to loss of cylinder air cushioning once predicted cut-off is implemented. Main considerations involves the mass of load to the cylinder's end-rod, the system's supply pressure Ps, the temperature under which the system is operating T_s and the total actuation time. For higher supply pressure, cut-off can be applied earlier during the power stroke of the cylinder due to the availability of higher air potential energy in the driving chamber. However, this will result in a longer working stroke time (extension process) and further reduced cylinder cushioning at the end-stroke.

This can be confirmed by both the measured and the simulated cylinder displacements of predicted cut-off actuations took longer working stroke times compared to their respective conventional and end-stroke cut-off actuation processes.

The comparison between the amount of air potential energy wasted and the energy saving ratio between measured and simulated pneumatic actuations are presented in Figure (6.12) and Figure (6.13). Close match between measured and simulated figures concludes that the simulation of the pneumatic cylinder actuations operating under conventional no cut-off, end-stroke cut-off and predicted cut-off to be successful.

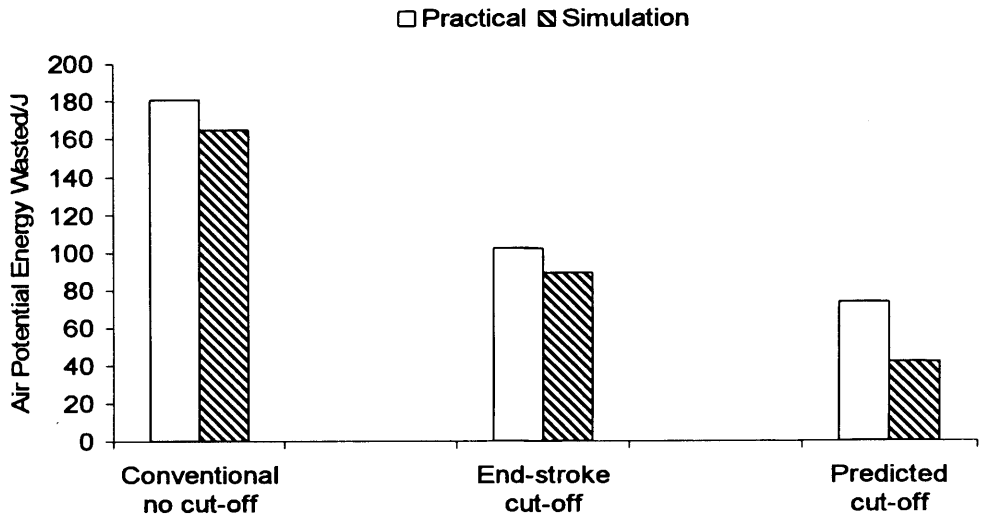

(a) System pressure Ps = 1.5bar

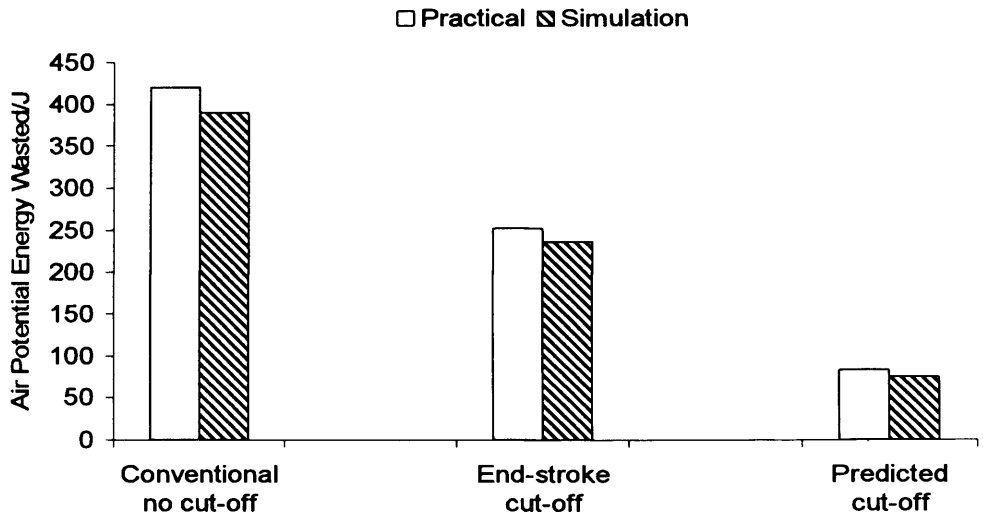

(a) System pressure Ps = 2.5bar

Figure 6.12: Air potential energy wasted in actuation

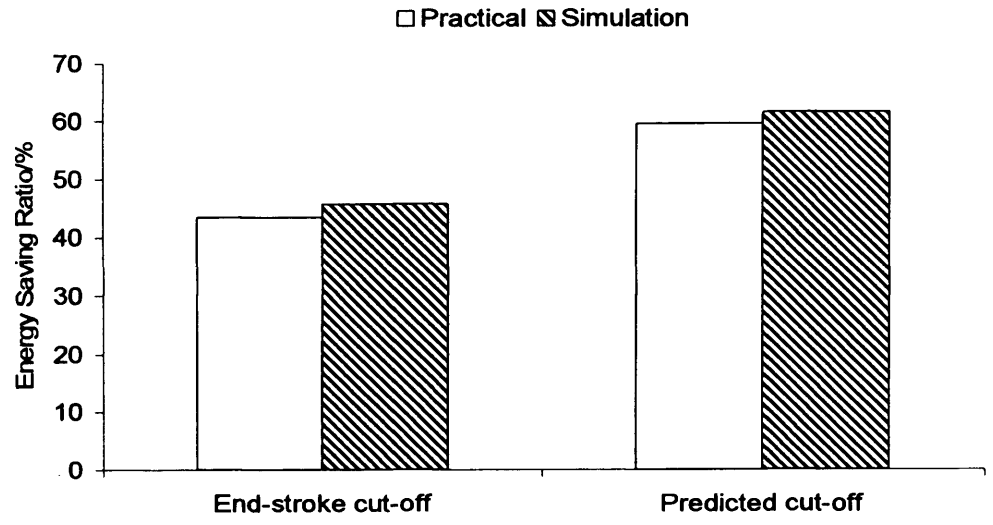

(a) System pressure Ps = 1.5bar

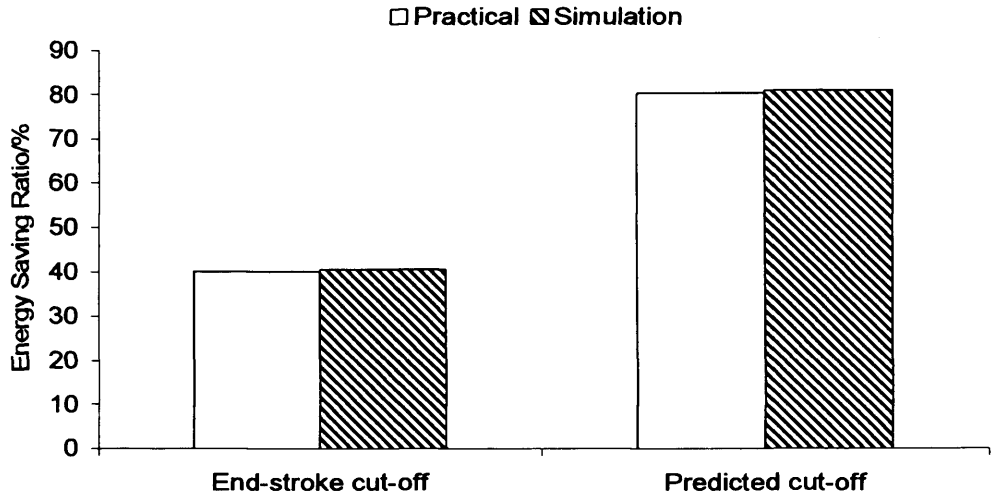

(b) System pressure Ps = 2.5bar

Figure 6.13: Air potential energy wasted in actuation

6.8 Future research

In this segment, further considerations that can be incorporated to improve the simulated results are presented. In terms of conservation laws, energy equation can also be incorporated together with the continuity and momentum equations. This will enable the determination of variation in temperature across the system during the pneumatic cylinder actuation under various actuation conditions.

The bulk modulus of the pneumatic transmission line was determined by experiment which measures the tube volume change when pressure is increased. However the length of the tube is also varied. This variation of the tube length under different working pressures needs to be considered in future computer simulations.

In a pneumatic system, the working fluid is highly compressible. Another step proposed to improve the air dynamics simulation is to include the effect of bulk modulus which is a mean to measure the fluid compressibility. Data regarding the Young's modulus ε and Poisson's ratio α can be determined experimentally by conducting relevant experiments on the pneumatic transmission line material. This can be done by consulting the manufacturer or referring to previous research conducted in determining these properties for a polymer type material.

Thermocouples were installed at a later stage of this research. These type-T thermocouples enable the measurement of temperature at the inlet port and on the surface of the pneumatic cylinder. Results of temperature variation against pressure in both conventional PTP actuation and pressure step experiment had been presented in chapter 3. Installing more temperature transducers at various positions across the test rig will enable the determination of initial temperature values that can be used for the utilisation of energy equation in future computer simulations.

Regarding the control system algorithm, the energy saving method can be based on the concept of logical decision making at the control valve used for actuation. A model based Energy Saving Actuation Control (ESAC) strategy is to be investigated in future research. The theme of the ESAC strategy is that an accurate model of the dynamic process can be obtained now using advanced techniques such as artificial neural networks[25,48]. This should allow the future actuating response to be predictable and control action can be taken in advance to minimise cost function, which in this research is the energy wasted while simultaneously satisfying the given actuation demand.

Points that need to be considered will be the determination of cut-off time for various situations based on the dynamic modelling of the actuation process, maintenance of the actuation demand, evaluation of the energy saving control algorithm and robustness of the method against disturbances. Dynamic modelling can be undertaken based on neural network models considering the non-linearity and complexity of pneumatic systems[25,49,50].

Neural network models can be trained from learning experimental data and techniques developed in previous researches[25,48]. Future responses of the actuation process will be predicted based on the models obtained, allowing the optimum cut-off time to be determined by a control algorithm regarding energy saving and maintaining the actuation demand. Disturbances from changes on the load, supply pressure, actuating speed control and component behaviour can also be considered at the modelling stage and energy saving control stage. Evaluation of the strategy at the research level can be undertaken using an energy saving rate counted from the recorded data in a database. Figure (6.14) is the proposed model-based energy saving actuation control strategy.

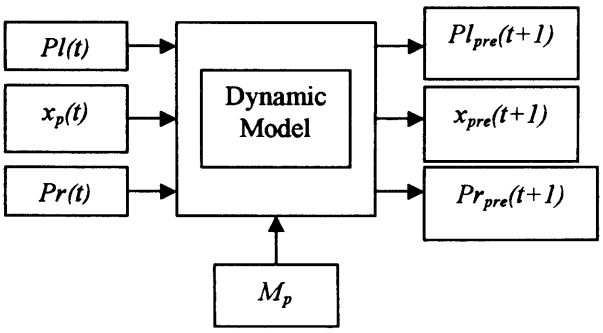

(a) Data based modelling

[continued]

Figure 6.14: Proposed neural network based pneumatic energy saving control system

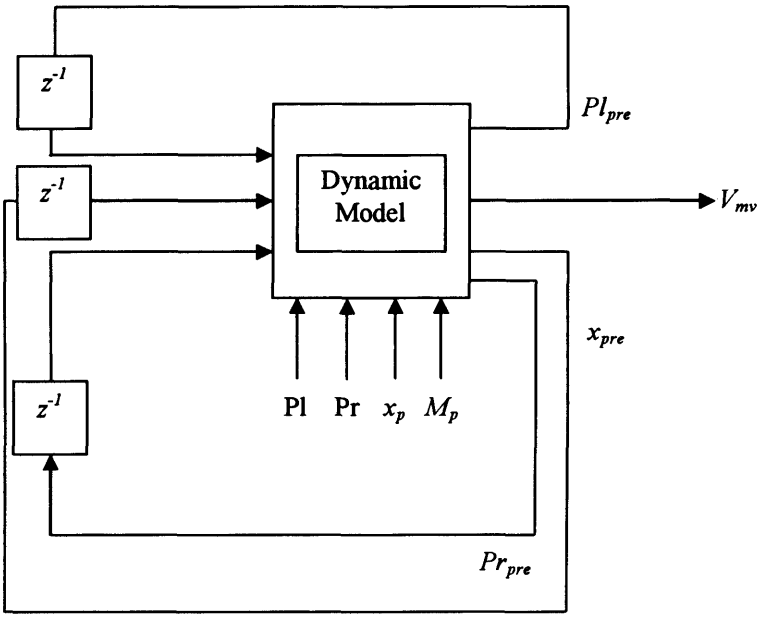

(b) Model based prediction and control

[end]

Figure 6.14: Proposed neural network based pneumatic energy saving control system

The trained multi-variable neural models can be utilised in the strategy for energy saving actuation control without disrupting the actuation demand. At every instance when the piston is approaching the end-stroke, based on the present states Pl, Pr, x_p and their history states measured, the model will make actuation prediction regarding the maximum distance x_{pmax} it can achieve if the supply pressure is cut-off at that time. If the predicted x_{pmax} is less than the stroke demand, there is no control changes applied at the main directional valve. If the x_{pmax} is larger than the stroke demand but the time required for the stroke is longer than demanded, again there is no control change applied. Otherwise, control changes at the main directional valve V_{mv} are implemented to cut-off the supply pressure for the present cylinder actuation.

Chapter 7

Conclusions

A novel energy saving method for pneumatic actuation is proposed which is predicted cut-off of the air supply. In conventional PTP pneumatic cylinder actuation, the air in the driving chamber is wasted. In this research, no cut-off, end-stroke cut-off and cut-off using model prediction energy saving schemes are investigated. Significant amount of air potential energy saving is achieved compared with the conventional PTP pneumatic actuation for the proposed energy saving system.

Table 7.1: Air potential energy saved using proposed energy saving actuations compared with conventional PTP pneumatic actuation

Supply pressure (bar)	**Air supply cut-off at end stroke**	**Air supply cut-off using model prediction**
1.5	43.5%	59.5%
2.5	40.1%	80.2%

A new experiment method, trapping moving air in a transmission line to stimulate air dynamics is used to cause pressure oscillation. The evolution of this pressure wave propagation along the transmission line had been investigated.

Transmission line modelling using finite difference algorithm on equations of fluid continuity and momentum successfully matches the measured pressure wave though errors can be seen. Interactive use of backward and forward differencing schemes in finite difference algorithm according to fluid flow direction is found largely affecting the simulation results.

The characteristics of the pneumatic actuator which is needed in the proposed energy saving method has been identified by using experiments. It is found that the static friction is much larger than the Coulomb friction.

Models of transmission line, actuator and control valves are integrated for the system actuation simulation under conventional, end-stroke cut-off and predicted cut-off cylinder actuations. The system simulation is shown to be effective compared with the measured experiment data though errors exist between them.

Predicted cut-off can be applied in maximising energy saving. However for the cut-off implementation to be successful, the correct friction characteristics of the pneumatic cylinder need to be determined. Furthermore in order to avoid stick-slip phenomenon due to premature cut-off and late cut-off implementation where the amount of energy saved would be insignificant, the correct modifying factor must be specified. This is complex since this depends on the working conditions of the system such as the loaded mass, system temperature and the supply pressure. It was found that in maximising energy saving, the cylinder's actuation time is compromised.

Table 7.2: Percentage actuation time increase using predicted air supply cut-off for energy saving compared with conventional pneumatic PTP actuation

Supply pressure (bar)	Actuation time increment (%)
1.5	20
2.5	25

Cylinder cushioning is affected when implementing predicted energy saving actuation due to the reduced pressure in the driving chamber after cut-off implementation. Once cut-off is initiated, the piston decelerates causing reduced pressure rise in the exhausting chamber and hence reducing the air cushioning of the cylinder. Correct adjustment of the cylinder cushion setting under different working conditions is vital in order to avoid cylinder damage.

End-stroke cut-off can also reduce the consumption of air in a conventional PTP actuation. Several benefits identified are that this approach is much simpler to apply since cut-off to the supply pressure is implemented at the end-stroke and the actuation time is not compromised since the system behaves as conventional PTP actuation during the extension process. However compared to predicted cut-off approach, the amount of energy saved is reduced and depending on the system's

working conditions, the total actuation time difference between these two energy saving methods can be small.

Using air as the working medium presents several key problems. It is widely known that air is highly compressible and thus affects the overall system response. The investigation regarding air dynamics especially in transmission line is needed to understand the air flow mechanism and thus provides the necessary consideration that can be included in the future system control algorithm.

The bulk modulus of the pneumatic transmission line is found to be much larger than the air bulk modulus thus the changes in the diameter of the transmission line can be ignored. However the change in length of the transmission line due to variations of pressure in the transmission line needs to be considered.

Another important aspect in pneumatic system investigation is the determination of working fluid viscosity since this affects the pressure wave propagation characteristics in transmission lines. This pressure wave propagation diminishes over time due to energy loss. The energy loss is mainly in the form of viscous friction between the fluid and the inner wall of the transmission line. From this understanding, the determination of the air viscosity value is vital in order to model the air dynamics in the transmission line to an acceptable degree of accuracy. Another important observation regarding this aspect is that the air viscosity value is sensitive to the change in system temperature. However even for large temperature changes, it was found that the air viscosity value remains small compared to other forms of fluid.

Air expansion ratio can be determined during the expansion of air under condition which there is no air mass change. The air expansion ratio was found to be different from the well known value of 1.4. This difference in value is possibly subjected to three main reasons. The first is that there might be leakages in the pneumatic cylinder, secondly the conditions under which the system is subjected to is neither isothermal nor adiabatic and finally the air was not in steady state condition when the data was captured.

The need to stimulate the air in a transmission line is important in the investigation of air dynamics. In pneumatic systems, transmission lines present several problems in system control. The need for fast response transducers is essential to capture the measured parameters of the stimulated air. In this research, the air dynamics was stimulated by trapping the free flowing air via closing the ends of the transmission line simultaneously. The advantage of this approach is that the air dynamics can be stimulated and then captured while the boundary conditions of the system that needs to be specified in the computer simulation can then be simplified.

Three-dimensional format of the Navier-Stokes equations were derived from conservation laws which are continuity, momentum and energy equations. However Navier-Stokes equations in three-dimensional format are complex to solve especially in specifying the correct boundary conditions. Assumptions are then needed to simplify modelling while still obtaining the required results. Poiseuille law can be used to determine the average velocity of one-dimensional flow and the respective position at which it occurs. In this research the pneumatic system modelling were done in one-dimensional format by utilising both lumped and finite difference methods.

Vector form of equations offers a more convenient way of applying the algorithm into the computer programming language and enables the decoding of the specified algorithm to obtain the primitive variables needed to compute the changes of the respective air parameters such as mass, pressure, density, velocity and viscosity before completing each time step.

Lumped modelling can be used to model pneumatic system to some accuracy depending on the system modelled and assumptions applied. It is easier to implement compared to finite difference approach and consumes less computing power due to the simplicity of the equations involved. However this method cannot be used to predict the propagation of pressure wave in transmission line though the general pressure characteristics in the pneumatic system can be modelled.

It was found that the finite difference approach to model the air transmission lines proves to be capable of predicting the pressure ripples that occurs due to the propagation of pressure wave in the transmission line compared to the lumped approach. However, this method is more complex to apply and consumes much more computing power compared to lumped modelling. Furthermore numerical stability issues regarding this approach such as truncation and discretization errors are highly sensitive to the specified sampling time and spatial distribution especially at discontinuities. The requirement for correct declarations of both initial and boundary conditions as well as the system's mesh size are vital to avoid solution instabilities such as numerical oscillations.

The combination of lumped and finite difference is possible whereby the transmission line can be modelled using finite difference approach while the large volume attached to the transmission line is modelled using lumped modelling method. This proves to be successful as presented by the simulated results of the pneumatic cylinder actuations presented in chapter 6. In this approach the essential air dynamics of the transmission line can be predicted while still retaining the characteristics of the system modelled. Furthermore the computing power consumption can be significantly reduced since finite difference approach is only used for the transmission line part.

Time-delay of air operated valves used in this research varies with the system supply pressure. It is proposed that electrical solenoid valves are to be used instead to minimise time-delay. The delayed actuation of directional valves in the proposed energy saving system affects the implementation time of supply pressure cut-off and this will reduce the maximum amount of air potential energy that can be saved.

Installation of thermocouples at positions across the system will enable the correct determination of system's initial temperatures. Energy equation can then be included in future computer simulation algorithm to predict temperature variation of air at any position in the system. This also enables more accurate prediction of pressure and density since these parameters are inter-related. Two type-T thermocouples are currently used to monitor temperature changes at the inlet of the pneumatic cylinder and on the surface of the cylinder itself. However further research is needed to determine accurate ways of obtaining temperature changes in a

pneumatic system. This includes the investigation of other types of temperature transducers that is suitable for measuring low to medium air temperature changes.

It is proposed that neural network approach is to be used to predict the cylinder's future displacement. This is due to the fact that the proposed energy saving methods investigated during this research requires means of measuring the displacement of the pneumatic cylinder such as an LVDT. This is not cost-effective for implementation where multiple actuators are involved especially in production lines. With online adaptive neural network approach as presented in chapter 6, it is possible to maximise energy saving and performing the demanded actuation satisfactorily while dismissing the need for displacement transducers. Furthermore neural network based control system can be trained to be adaptable to changes of operating conditions and system components.

References

1. Esposito, A. *Fluid Power with Applications.* Prentice-Hall, 2000, pp. 451-453.

2. CADDET Newsletter. *Compressed Air Costs Reduced by Automatic Control System.* Issue 01, January 1995.

3. Kagawa, T. et al. *Energy Assessment in Pneumatic System and Air Power Meter.* Proceedings of Workshop on Power Transmission and Motion Control, Bath University, UK. Professional Engineering Publishing Ltd, 11th-13th September 2002, pp. 377-387.

4. Pu, J. et al. *A New Strategy for Closed-loop Control of Servo-Pneumatic Systems with Improved Energy Efficiency and System Response.* Proceedings of the 5th Scandinavian International Conference on Fluid Power, Linköping, Sweden, 28th-30th May 1997, pp. 1-14.

5. Wang, J. et al. *Energy Efficiency Analysis and Optimal Control of Servo Pneumatic Cylinders.* Proceedings of the 2005 IEEE International Conference on Control Application, Toronto, Canada, 28th-31st August 2005.

6. Al-Dakkan, K.A. et al. *Energy Saving Control for Pneumatic Servo Systems.* Proceedings of the 2003 IEEE/ASME International Conference on Advanced Intelligent Mechatronics (AIM 2003), Kobe, Japan, 20th-24th July 2003, pp. 284-289.

7. Reade, L. *Air on the Side of Caution.* Eureka Magazine, 1st July 1999.

8. Arinaga, T. et al. *Approach for Energy Saving in Pneumatic Systems.* Proceedings of 1st FPNI – PhD Symposium, Hamburg, Germany, 20th-22nd September 2000, pp. 49-56.

9. Dijen, F. S. G. van. *Pneumatic Mechanisation.* Culemborg: Kemperman, 1975, pp. 16-38.

10. Trade and Technical Press Ltd. *Pneumatic Handbook.* Morden, Surrey, 1966, pp. 162-171.

11. Xue, Y., Yusop, M. Y. M., Ji, X. *Energy Saving in Pneumatic Actuation using the Gas Law Prediction.* Proceedings of Workshop on Power Transmission and Motion Control, Bath University, UK. Professional Engineering Publishing Ltd, 2003, pp. 319-331. ISBN 1 86058414-4

12. Shelley, T. *Cushion Return Speeds Automation Efficiency.* Eureka Magazine, 1st September 1999.

13. Tannehill, J. C. et al. *Computational Fluid Mechanics and Heat Transfer.* 2nd Edition, Taylor & Francis, London, 1997, pp. 176-188, pp. 249-271.

14. Rotty, R. M. *Introduction to Gas Dynamics.* Wiley, New York, 1962, pp. 19, pp. 24-35.

15. Granger, R. A. *Fluid Mechanics.* Dover Publications, New York, 1995, pp. 160-190, pp. 461.

16. John, J. E. A. *Gas Dynamics.* Allyn and Bacon, Boston, 1969, pp. 6-21, pp. 157, pp. 323-324.

17. Winder, R. *Developing C++ Software.* Chichester, New York, 1993, pp. 43-68.

18. Brunell, R. *Hydraulic and Pneumatic Cylinders.* Morden, Surrey: Trade and Technical Press, pp. 12-14.

19. Yeaple, F. D. *Hydraulic and Pneumatic Power and Control: design, performance, application.* McGraw-Hill, London, 1966, pp. 223-237.

20. Bolton, W. *Pneumatic and Hydraulic Systems.* Butterworth-Heinemann, Oxford, 1997, pp. 61-68.

21. Lenk, J. D. *ABC's of Thermocouples.* Foulsham-Sams, Slough, 1968, pp. 7, pp. 25.

22. *Manual on the use of thermocouples in temperature measurement.* Sponsored by ASTM Committee E-20 on Temperature Measurement and Sub-Committee E-20.04 on Thermocouples, ASTM, Philadelphia, 1981, pp. 3, pp. 20-22.

23. Douglas, J. F. et al. *Fluid Mechanics.* 3rd Edition, Harlow-Longman, 1995, pp. 808-810.

24. Sandborn, V. A. *Resistance Temperature Transducers.* Metrology Press, Colorado, 1972, pp.2

25. Xue, Y. and Watton, J. *Dynamics Modelling of Fluid Power Systems Applying a Global Error Descent Algorithm to a Self-Organising Radial Basis Function Network.* Mechatronics, Volume 8, 1998, pp. 727-745.

26. Close, C. M. *Modelling and Analysis of Dynamic Systems.* Houghton-Mifflin, London, 1978, pp. 2.

27. Tokashiki, L. R. et al. *Dynamic Characteristics of Pneumatic Cylinders Including Pipes.* Proceedings of Workshop on Power Transmission and Motion Control, Bath University, UK. Professional Engineering Publishing Ltd, 1996, pp. 382-395.

28. Senoo, M. et al. *Simulation of Network of Pipelines.* The 4th JHPS International Symposium of Fluid Power, Tokyo, Japan, 1999, pp. 213-218.

29. Krus, P. *Distributed Modelling for Simulation of Pneumatic Systems.* The 5th JHPS International Symposium of Fluid Power, Tokyo, Japan, 1999, pp. 443-452.

30. McCloy, D. *Control of Fluid Power: analysis and design.* 2nd Edition, Ellis Horwood, Chichester, 1980, pp. 80-88.

31. Xue, Y. and Yusop, M. Y. M. *Time Domain Simulation of Air Transmission Lines.* The 8th International Symposium on Fluid Control, Measurement and Visualization, Chengdu, China, 2005, paper 277.

32. Leer, B. van. *Upwind and High Resolution Methods for Compressible Flow: From Donor Cell to Residual Distribution Schemes.* Communications in Computational Physics, Volume 1, No.2, April 2006, pp. 195-206.

33. White, F. M. *Viscous Fluid Flow.* McGraw-Hill, New York, 1974, pp. 22.

34. Watton, J. *Fluid Power Systems.* Prentice Hall, 1989, pp. 31.

35. Watton, J. and Xue, Y. *Identification of Fluid Power Component and Circuit Behaviour using Dynamic Flow Rate Measurement.* Proceedings of Institution of Mechanical Engineers, Part C, 1995, pp. 179-191.

36. Griffiths, D. *Understanding Data: principles and practice of statistics.* Wiley, 1998, pp. 137.

37. Hutchings, I. M. *Friction and Wear of Engineering Materials.* Edward Arnold, 1992, pp. 1.

38. Rabinowicz, E. *Friction and Wear of Materials.* Wiley, New York, 1995, pp. 65.

39. Kragel'skii, I. V. *Friction and Wear: calculation methods.* Pergamon, 1982, pp. 1.

40. Kazama, T. and Fujiwara, M. *Experiment on Frictional Characteristics of Pneumatic Cylinders.* The 4th JHPS International Symposium on Fluid Power, Tokyo, Japan, 15th-17th November 1999, pp. 453-458.

41. Tosatti, E. and Persson, B.N.J. *Physics of Sliding Friction.* Kluwer Academic Publishers, Boston, 1996, pp. 3.

42. Horowitz, I. *Some Properties of Delayed Controls.* International Journal of Control, Volume 38, No. 5, 1983, pp. 977-990.

43. Xue, Y. and Watton, J. *Position Control of a Pneumatic Servo Actuator with Time-Delay using Neural Network Predictor.* The 5th JHPS International Symposium of Fluid Power, Nara, Japan, 12th-15th November 2002, Paper 3A1-2.

44. Haessig Jr, D.A. and Friedland, B. *On the Modelling and Simulation of Friction.* Journal of Dynamic Systems, Measurement and Control, Volume 113, September 1991, pp. 354-362.

45. Wang, J. et al. *Identification of Pneumatic Cylinder Friction Parameters Using Genetic Algorithms.* IEEE/ASME Transactions on Mechatronics, Volume 9, No.1, March 2004, pp. 100-107.

46. Green, J. R. *Statistical Treatment of Experimental Data.* Elsevier Scientific, Amsterdam, 1977, pp. 282.

47. Smith, O. J. M. *Closer Control of Loops with Dead-Time.* Chemical Engineering Progress Translation, Volume 53, No. 5, 1957, pp. 217-219.

48. Xue, Y. and Watton, J. *A Self-Organising Neural Network Approach to Data-Based Modelling of Fluid Power Systems Dynamics using the GMDH Algorithm.* Proceedings of Institution of Mechanical Engineers, Part 1, 1995, pp. 229-240.

49. Nishiumi, T. and Watton, J. *Model Reference Adaptive Control of an Electrohydraulic Motor Drive using an Artificial Neural Network Compensator.* Proceedings of Institution of Mechanical Engineers, Journal of Systems and Control Engineering, Volume 211, 1997, pp. 111-122.

50. Le, T. T. et al. *Fault Diagnosis and Classification of Fluid Power Systems using a Dynamics Feature Extraction Technique and a Neural Network.* Proceedings of Institution of Mechanical Engineers, Journal of Systems and Control Engineering, Volume 212, 1998, pp. 87-97.

Appendix 1

```
////////////////////////////////////////////////////////////////////////
// Lumped Approach
// Transmission Line Including Large Volume Modelling
////////////////////////////////////////////////////////////////////////

#include<stdio.h>
#include<stdlib.h>
#include<math.h>

#define N               10000                   //Test Steps
#define Ns              5                       //Number of Sections of the tube
#define T               0.001                   //Sampling Intervals
#define Ku              1000

#define Cdt             0.02                    //Gas Discharge Coefficient at tube
#define CdO             0.20                    //Gas  Discharge  Coefficient  at  the
orifice of valve to tube
#define Cdc             0.20                    //Gas Discharge Coefficient at the main
pipe and valve chamber
#define Cdv             0.02                    //Gas Discharge Coefficient at the tube
end

#define CR              0.528                   //Choke Ratio: PVc/Pu
#define Cm              0.0405                  //Mass Flow Parameter
#define gamma           1.40                    //Specific Heat Ratio (for air 1.4)
#define VU              1.50e-05                //Kinematic Viscosity/m2/s
#define Ra              1.225                   //Air density/kg/m3
#define R               287.00                  //Gas Constant,J(kg/K)
#define Ps              6.5e+05                 //System Pressure/Pa
#define Pa              1.0e+05                 //Atmos. Pressure/Pa
#define Ts              (273+20)                //System Temperature/K

#define dp              0.02                    //Pipe Diameter/m
#define av2             (pi*pow(dp,2)/4)        //Pipe Cross Section Area/m2
#define Lp              0.20                    //Main   pipe   length   beyond   which
pressure being PS/m
#define Vp              (av2*Lp)                //Main   pipe   volume   beyond   which
pressure being PS/m3
#define ac              (0.01*av2)
#define L               7.0                     //Tube Length/m
#define dt              5.0e-03                 //Tube Internal Diameter/m
#define Ll              (L/(Ns-1))              //Section Length/m
#define pi              3.141592                //pi Constant
#define A               (pi*pow(dt,2)/4)        //Cross-Section Area/m2
#define Vl              (A*L/(Ns-1))            //Section Volume/m3

#define V               0.0001                  //Volume/m3
#define MO              (V*Ra)                  //Initial air mass/kg
#define a               (0.5*A)                 //Cross-Section Area/m2
#define Cp              1.0e+05                 //Convert Pressure into Bar

#define DF              "TLineMod.txt"

double pv,Cmb,mv,p[Ns],pd[Ns],u[Ns],dut[Ns],md[Ns];
double m[Ns],z[Ns],fr[Ns],Ro[Ns],g[Ns],pc,gc,mcd,pcd,zc;
float t;
int i,k,j;

////////////////////////////////////////////////////////////////////////////////////

void G0()
{
        if((p[0]/pc)<=CR)
                Cmb=Cm;
        else
        {
```

```
                zc=(2*gamma/(R*(gamma-1)))*(pow(p[0]/pc,2/gamma)-
pow(p[0]/pc,(gamma+1)/gamma));
                if (zc<0)
                        zc=0;
                Cmb=sqrt(zc);
        }

        if(zc<0)
                g[0]=g[0];
        else
                g[0]=CdO*Cmb*a*pc/sqrt(Ts);
}

void Gc()
{
        if((pc/Ps)<=CR)
                Cmb=Cm;
        else
        {
                zc=(2*gamma/(R*(gamma-1)))*(pow(pc/Ps,2/gamma)-pow(pc/Ps,(gamma+1)/gamma));
                if (zc<0)
                        zc=0;
                Cmb=sqrt(zc);
        }

        gc=Cdc*Cmb*ac*Ps/sqrt(Ts);
}

////////////////////////////////////////////////////////////////////////////////////////////

void G0();
void Gc();

void main()
{
        FILE *fp;
        fp=fopen(DF,"w");

        for (i=0;i<Ns;i++)
        {
                g[i]=0.0;
                p[i]=Pa;
                Ro[i]=p[i]/(R*Ts);
                u[i]=0.0;
                pd[i]=0.0;
                dut[i]=0.0;
                md[i]=0.0;
                z[i]=0.0;
                fr[i]=0.0;
                m[i]=Ro[i]*V1;
                pc=Ps;
        }

        int scp=0;

        for (k=0;k<N;k++)
        {
                t=float (k*T);
                fprintf(fp,"%f\t",t);

                G0();
                Gc();

                mcd=gc-g[0];
                pcd=(R*Ts/Vp)*mcd;

                for (i=0;i<(Ns-1);i++)
                {
                        md[i]=g[i]-g[i+1];
                        pd[i]=(R*Ts/V1)*md[i];
```

```
                dut[i]=Ku*(A*(p[i]-p[i+1])-fr[i])/m[i];

                if (i==scp)
                {
                        z[i]+=dut[i]*T*T/2;

                        if (z[i]>L1)
                        {
                                if((p[i+1]/p[i])<=CR)
                                {
                                        Cmb=Cm;
                                }

                                else
                                {
                                        zc=(2*gamma/(R*(gamma-
1)))*(pow(p[i+1]/p[i],2/gamma)-pow(p[i+1]/p[i],(gamma+1)/gamma));

                                        if (zc<0)
                                        {
                                                zc=0;
                                        }

                                        Cmb=sqrt(zc);
                                }

                                g[i+1]=Cdt*Cmb*A*p[i]/sqrt(Ts);
                                scp++;
                        }
                }

                p[i]+=pd[i]*T;
                Ro[i]=p[i]/(R*Ts);
                m[i]=Ro[i]*V1;

                if (i>0)
                {
                        if(i<(scp+1))
                        {
                                if ((p[i]/p[i-1])<=CR)
                                {
                                        Cmb=Cm;
                                }

                                else
                                {
                                        zc=(2*gamma/(R*(gamma-1)))*(pow(p[i]/p[i-
1],2/gamma)-pow(p[i]/p[i-1],(gamma+1)/gamma));

                                        if (zc<0)
                                        {
                                                zc=0;
                                        }

                                        Cmb=sqrt(zc);
                                }

                                g[i]=Cdt*Cmb*A*p[i-1]/sqrt(Ts);
                        }

                        u[i]=g[i]/(A*Ro[i]);
                        fr[i]=8*pi*VU*Ro[i]*L1*u[i];
                }
        }

        md[Ns-1]=g[Ns-1];
        pd[Ns-1]=(R*Ts/V)*md[Ns-1];
        p[Ns-1]+=pd[Ns-1]*T;

        if (scp==(Ns-1))
```

```
		{
			if((p[Ns-1]/p[Ns-2])<=CR)
			{
				Cmb=Cm;
			}

			else
			{
				zc=(2*gamma/(R*(gamma-1)))*(pow(p[Ns-1]/p[Ns-2],2/gamma)-
pow(p[Ns-1]/p[Ns-2],(gamma+1)/gamma));

				if (zc<0)
				{
					zc=0;
				}

				Cmb=sqrt(zc);
			}

			g[Ns-1]=Cdv*Cmb*A*p[Ns-2]/sqrt(Ts);
		}

		pc+=pcd*T;

		if((k%1)==0)
		{
			fprintf(fp,"%lf\t%lf\t",pc/Cp,gc);
			for (j=0;j<Ns;j++)
				fprintf(fp,"%lf\t",p[j]/Cp);
			for (j=0;j<Ns;j++)
				fprintf(fp,"%lf\t",g[j]);
			fprintf(fp,"\n");
		}
	}

	fclose(fp);
}
```

Appendix 2

```
//////////////////////////////////////////////////////////////////////////
// Lumped Approach
// Transmission Line Modelling
//////////////////////////////////////////////////////////////////////////

#include<stdio.h>
#include<stdlib.h>
#include<math.h>
#include<time.h>

#define N               1.00e+07                //Test steps
#define T               1.00e-06                //Sampling interval,seconds
#define Pa              (1.00e+05)              //Atmos. pressure/Pa
#define R               287                     //Gas constant,J/(kg.K)
#define Ts              (273+20)                //System temperature/K
#define Ra              (Pa/(R*Ts))             //Air density/kg/m3
#define pi              3.141592                //pi constant

#define d0              5.00e-03                //Tube Diameter/m
#define L0              0.30                    //Tube Length/m
#define A0              (pi*d0*d0/4)            //Tube Cross Section area/m2
#define V0              (L0*A0)                 //Tube Volume/m3

#define L1              0.30                    //Tube Length/m
#define A1              (pi*d0*d0/4)            //Tube Cross Section Area/m2
#define V1              (L1*A1)                 //Tube Volume/m3

#define L2              0.30                    //Tube Length/m
#define A2              (pi*d0*d0/4)            //Tube Cross Section Area/m2
#define V2              (A2*L2)                 //Tube Volume/m3

#define L3              0.30                    //Tube Length/m
#define A3              (pi*d0*d0/4)            //Tube Cross Section Area/m2
#define V3              (A3*L3)                 //Tube Volume/m3

#define L4              0.30                    //Tube Length/m
#define A4              (pi*d0*d0/4)            //Tube Cross Section Area/m2
#define V4              (L4*A4)                 //Tube Volume/m3

#define Cp              1.00e+05                //Convert pressure Pa - Bar
#define CdV             0.72                    //Gas discharge coefficient at Main
Valve
#define CdC             0.72                    //Gas discharge coefficient at Cylinder
Inlet
#define Cdt             0.72                    //Gas discharge coefficient at Tube
#define Cd              0.72                    //Gas discharge coefficient at Cylinder
Outlet
#define Cm              0.0405                  //Mass flow parameter for choked
#define gamma           1.40                    //Specific heat ratio 1.4

#define DP              "Pressure.txt"
#define DM              "Mass.txt"
#define DR              "Density.txt"

double m0,m0d,m1,m1d,m2,m2d,m3,m3d,m4,m4d;
double p0,p1,p2,p3,p4,Cma,Cmb,Cmc,Cmd;
double rho0,rho1,rho2,rho3,rho4;
double ct1,ct2,ct3,ct4;
float t;
int i;

void main()
{
        void Static();
        void Process1();
        void Process2();
```

```
        void Process3();
        void Process4();
        void Exit();

        FILE *fPressure;
        FILE *fMass;
        FILE *fDensity;

        fPressure=fopen(DP,"w");
        fMass=fopen(DM,"w");
        fDensity=fopen(DR,"w");

        Static();

        for(i=0;i<N;i++)
        {
                t=float(i*T);

                if(t>7.88)
                {
                        Process1();
                        Process2();
                        Process3();
                        Process4();

                        m0+=(-m1d)*T;
                        m1+=(m1d-m2d)*T;
                        m2+=(m2d-m3d)*T;
                        m3+=(m3d-m4d)*T;
                        m4+=(m4d)*T;

                        rho0=m0/V0;
                        rho1=m1/V1;
                        rho2=m2/V2;
                        rho3=m3/V3;
                        rho4=m4/V4;

                        p0=rho0*R*Ts;
                        p1=rho1*R*Ts;
                        p2=rho2*R*Ts;
                        p3=rho3*R*Ts;
                        p4=rho4*R*Ts;
                }

                Exit();

                if(i%500==0)
                {

        fprintf(fPressure,"%f\t%lf\t%lf\t%lf\t%lf\t%lf\n",t,p0/Cp,p1/Cp,p2/Cp,p3/Cp,p4/Cp);
        fprintf(fMass,"%f\t%lf\t%lf\t%lf\t%lf\t%lf\n",t,m0,m1,m2,m3,m4);
        fprintf(fDensity,"%f\t%lf\t%lf\t%lf\t%lf\t%lf\n",t,rho0,rho1,rho2,rho3,rho4);
                }
        }

        fclose(fDensity);
}

void Process1()
{
        if((p1/p0)<=0.528)
        {
                Cma=Cm;
        }

        else
        {
                ct1=(2*gamma/(R*(gamma-1)))*(pow(p1/p0,2/gamma)-pow(p1/p0,(gamma+1)/gamma));

                if(ct1<0)
```

```
                {
                        ct1=0.0;
                }

                Cma=sqrt(ct1);
        }

        m1d=Cdt*Cma*A1*p0/sqrt(Ts);
}

void Process2()
{
        if((p2/p1)<=0.528)
        {
                Cmb=Cm;
        }

        else
        {
                ct2=(2*gamma/(R*(gamma-1)))*(pow(p2/p1,2/gamma)-pow(p2/p1,(gamma+1)/gamma));

                if(ct2<0)
                {
                        ct2=0.0;
                }

                Cmb=sqrt(ct2);
        }

        m2d=CdV*Cmb*A2*p1/sqrt(Ts);
}

void Process3()
{
        if((p3/p2)<=0.528)
        {
                Cmc=Cm;
        }

        else
        {
                ct3=(2*gamma/(R*(gamma-1)))*(pow(p3/p2,2/gamma)-pow(p3/p2,(gamma+1)/gamma));

                if(ct3<0)
                {
                        ct3=0.0;
                }

                Cmc=sqrt(ct3);
        }

        m3d=CdC*Cmc*A3*p2/sqrt(Ts);
}

void Process4()
{
        if((p4/p3)<=0.528)
        {
                Cmd=Cm;
        }

        else
        {
                ct4=(2*gamma/(R*(gamma-1)))*(pow(p4/p3,2/gamma)-pow(p4/p3,(gamma+1)/gamma));

                if(ct4<0)
                {
                        ct4=0.0;
                }
```

```
                Cmd=sqrt(ct4);
        }

        m4d=Cd*Cmd*A4*p3/sqrt(Ts);
}

void Static()
{
        p0=3.66e+05+Pa;
        p1=3.30e+05+Pa;
        p2=2.95e+05+Pa;
        p3=2.66e+05+Pa;
        p4=2.33e+05+Pa;

        m0=(p0*V0)/(R*Ts);
        m1=(p1*V1)/(R*Ts);
        m2=(p2*V2)/(R*Ts);
        m3=(p3*V3)/(R*Ts);
        m4=(p4*V4)/(R*Ts);

        rho0=m0/V0;
        rho1=m1/V1;
        rho2=m2/V2;
        rho3=m3/V3;
        rho4=m4/V4;
}

void Exit()
{
        if(t>=10.00)
        exit(0);
}
```

Appendix 3

```
////////////////////////////////////////////////////////////////////////
// Finite Difference Approach (2nd Order)
// Transmission Line Modelling
////////////////////////////////////////////////////////////////////////

#include <stdio.h>
#include <stdlib.h>
#include <math.h>

#define N               1.00e+07                    //Iteration steps
#define Ns              5                           //Segments number
#define Nf              2                           //Double Iteration
#define T               1.00e-06                    //Sampling interval (s)

#define dt              5.00e-03                    //Tube Diameter (m)
#define LT              1.50                        //Total Tube Length (m)
#define Lt              (LT/Ns)                     //Tube Length (m)

#define Ts              (273+20)                    //System temperature (K)
#define PAtm            1.00e+05                    //Atmos. pressure (Pa)
#define ConP            1.00e+05                    //Convert pressure Pa - Bar
#define pi              3.141592                    //pi constant

#define R               287                         //Gas constant (m2/(s2K))
#define niu             (1.51e-05*3.00e+05)         //Kinematic Viscosity (m2/s) (1.51e-05)
#define cp              1005.1                      //Specific Heat Capacity of air
#define cv              717.9                       //Specific Heat Capacity of air
#define gamma           (cp/cv)                     //Specific heat ratio (for air 1.4)

#define Cm              0.0405                      //Mass flow parameter for choked
#define Cdt             0.72                        //Gas discharge coefficient at Tube

#define DPT             "Pressure.txt"
#define DPM             "MassFlowrate.txt"
#define DPV             "Velocity.txt"

float   t;
int     i,j;
int     flagBF=0;
int     flag1,flag2,flag3;

double  Cma,Cmd,ct1,ct4;

double  L[Ns+1],A[Ns+1],V[Ns+1];
double  M[Ns+1],m[Ns+1],md[Ns+1];
double  Pm[Ns+1];
double  rho[Ns+1];
double  ux[Ns+1];
double  miu[Ns+1];
double  PrV[Ns+1][Nf+1];
double  CrV[Ns+1][Nf+1];
double  Hux[Ns+1];

void main()
{
        void SegmentsStatic();
        void ProcessExit();

        FILE *fPressure;
        FILE *fMassFlowRate;
        FILE *fVelocity;

        fPressure=fopen(DPT,"w");
        fMassFlowRate=fopen(DPM,"w");
        fVelocity=fopen(DPV,"w");
```

```
        for(j=0;j<5;j++)
        {
                L[j]=Lt;
                A[j]=pi*pow(dt,2)/4;
                V[j]=L[j]*A[j];
        }

        SegmentsStatic();

        for(i=0;i<N;i++)
        {
                t=float(i*T);

                if(t>7.88)
                {
                        if(flagBF==0)
                        {
                                if((Pm[1]/Pm[0])<=0.528)
                                {
                                        Cma=Cm;
                                }

                                else
                                {
                                        ct1=(2*gamma/(R*(gamma-1)))*(pow(Pm[1]/Pm[0],2/gamma)-
pow(Pm[1]/Pm[0],(gamma+1)/gamma));

                                        if(ct1<0)
                                        {
                                                ct1=0.0;
                                        }

                                        Cma=sqrt(ct1);
                                }

                                md[1]=Cdt*Cma*A[1]*Pm[0]/sqrt(Ts);

////////////////////////////////////////////////////////////////////////

                                //Uv1   (calculates new rho[j])
                                PrV[2][1]=rho[2]-(T/L[2])*(rho[2]*ux[2]-rho[2-1]*ux[2-1]);

                                //Uv2   (calculates new rho[2]*u[2])
                                PrV[2][2]=(rho[2]*ux[2])-(T/L[2])
                                *((rho[2]*pow(ux[2],2)+(Pm[2])-(4/3)*(miu[2])*(ux[2+1]-
ux[2])/L[2])
                                -(rho[2-1]*pow(ux[2-1],2)+(Pm[2-1])-(4/3)*(miu[2-1])*(ux[2]-
ux[2-1])/L[2]));

                                //Uv1   (calculates new rho[2])
                                CrV[2][1]=0.5*(rho[2]+PrV[2][1]);

                                //Uv2   (calculates new rho[2]*u[2])
                                CrV[2][2]=0.5*((rho[2]*ux[2])+PrV[2][2]);

                                md[2]=PrV[2][2]*A[2];

////////////////////////////////////////////////////////////////////////

                                //Uv1   (calculates new rho[3])
                                PrV[3][1]=rho[3]-(T/L[3])*(rho[3]*ux[3]-rho[3-1]*ux[3-1]);

                                //Uv2   (calculates new rho[3]*u[3])
                                PrV[3][2]=(rho[3]*ux[3])-(T/L[3])
                                *((rho[3]*pow(ux[3],2)+(Pm[3])-(4/3)*(miu[3])*(ux[3+1]-
ux[3])/L[3])
                                -(rho[3-1]*pow(ux[3-1],2)+(Pm[3-1])-(4/3)*(miu[3-1])*(ux[3]-
ux[3-1])/L[3]));

                                //Uv1   (calculates new rho[3])
```

```
                        CrV[3][1]=0.5*(rho[3]+PrV[3][1]);

                        //Uv2   (calculates new rho[3]*u[3])
                        CrV[3][2]=0.5*((rho[3]*ux[3])+PrV[3][2]);

                        md[3]=PrV[3][2]*A[3];

////////////////////////////////////////////////////////////////////////

                        if((Pm[4]/Pm[3])<=0.528)
                        {
                                Cmd=Cm;
                        }

                        else
                        {

                                ct4=(2*gamma/(R*(gamma-1)))*(pow(Pm[4]/Pm[3],2/gamma)-
pow(Pm[4]/Pm[3],(gamma+1)/gamma));

                                if(ct4<0)
                                {
                                        ct4=0.0;
                                }

                                Cmd=sqrt(ct4);
                        }

                        md[4]=Cdt*Cmd*A[4]*Pm[3]/sqrt(Ts);

                }

////////////////////////////////////////////////////////////////////////
////////////////////////////////////////////////////////////////////////

                if(flagBF==1)
                {
                        if((Pm[0]/Pm[1])<=0.528)
                        {
                                Cma=Cm;
                        }

                        else
                        {

                                ct1=(2*gamma/(R*(gamma-1)))*(pow(Pm[0]/Pm[1],2/gamma)-
pow(Pm[0]/Pm[1],(gamma+1)/gamma));

                                if(ct1<0)
                                {
                                        ct1=0.0;
                                }

                                Cma=sqrt(ct1);
                        }

                        md[0]=-Cdt*Cma*A[0]*Pm[1]/sqrt(Ts);

////////////////////////////////////////////////////////////////////////

                        //Uv1   (calculates new rho[j])
                        PrV[1][1]=rho[1]-(T/L[1])*(rho[1+1]*ux[1+1]-rho[1]*ux[1]);

                        //Uv2   (calculates new rho[1]*u[1])
                        PrV[1][2]=(rho[1]*ux[1])-(T/L[1])
                        *((rho[1+1]*pow(ux[1+1],2)+(Pm[1+1])-
(4/3)*(miu[1+1])*(ux[1+1]-ux[1])/L[1])
                        -(rho[1]*pow(ux[1],2)+(Pm[1])-(4/3)*(miu[1])*(ux[1]-ux[1-
1])/L[1]));
```

```
                        //Uv1   (calculates new rho[1])
                        CrV[1][1]=0.5*(rho[1]+PrV[1][1]);

                        //Uv2   (calculates new rho[1]*u[1])
                        CrV[1][2]=0.5*((rho[1]*ux[1])+PrV[1][2]);

                        md[1]=PrV[1][2]*A[1];

////////////////////////////////////////////////////////////////////////

                        //Uv1   (calculates new rho[j])
                        PrV[2][1]=rho[2]-(T/L[2])*(rho[2+1]*ux[2+1]-rho[2]*ux[2]);

                        //Uv2   (calculates new rho[2]*u[2])
                        PrV[2][2]=(rho[2]*ux[2])-(T/L[2])
                        *((rho[2+1]*pow(ux[2+1],2)+(Pm[2+1])-
(4/3)*(miu[2+1])*(ux[2+1]-ux[2])/L[2])
                        -(rho[2]*pow(ux[2],2)+(Pm[2])-(4/3)*(miu[2])*(ux[2]-ux[2-
1])/L[2]));

                        //Uv1   (calculates new rho[2])
                        CrV[2][1]=0.5*(rho[2]+PrV[2][1]);

                        //Uv2   (calculates new rho[2]*u[2])
                        CrV[2][2]=0.5*((rho[2]*ux[2])+PrV[2][2]);

                        md[2]=PrV[2][2]*A[2];

////////////////////////////////////////////////////////////////////////

                        if((Pm[3]/Pm[4])<=0.528)
                        {
                                Cmd=Cm;
                        }

                        else
                        {

                                ct4=(2*gamma/(R*(gamma-1)))*(pow(Pm[3]/Pm[4],2/gamma)-
pow(Pm[3]/Pm[4],(gamma+1)/gamma));

                                if(ct4<0)
                                {
                                        ct4=0.0;
                                }

                                Cmd=sqrt(ct4);
                        }

                        md[3]=-Cdt*Cmd*A[3]*Pm[4]/sqrt(Ts);
                }

////////////////////////////////////////////////////////////////////////
////////////////////////////////////////////////////////////////////////

                if(flagBF==0)
                {
                        for(j=0;j<5;j++)
                        {
                                Hux[j]=ux[j];
                        }

                        for(j=0;j<1;j++)
                        {
                                m[j]+=(-md[j+1])*T;
                                Pm[j]=m[j]*R*Ts/V[j];
                                rho[j]=Pm[j]/(R*Ts);
                                ux[j]=md[j]/(rho[j]*A[j]);
                                miu[j]=niu*rho[j];
                        }
```

```
                for(j=1;j<2;j++)
                {
                        m[j]+=(md[j]-md[j+1])*T;
                        Pm[j]=m[j]*R*Ts/V[j];
                        rho[j]=Pm[j]/(R*Ts);
                        ux[j]=md[j]/(rho[j]*A[j]);
                        miu[j]=niu*rho[j];
                }

                for(j=2;j<3;j++)
                {
                        m[j]+=(md[j]-md[j+1])*T;
                        Pm[j]=m[j]*R*Ts/V[j];
                        rho[j]=PrV[j][1];
                        ux[j]=PrV[j][2]/PrV[j][1];
                        miu[j]=niu*rho[j];
                }

                for(j=3;j<4;j++)
                {
                        m[j]+=(md[j]-md[j+1])*T;
                        Pm[j]=m[j]*R*Ts/V[j];
                        rho[j]=PrV[j][1];
                        ux[j]=PrV[j][2]/PrV[j][1];
                        miu[j]=niu*rho[j];
                }

                for(j=4;j<5;j++)
                {
                        m[j]+=(md[j])*T;
                        Pm[j]=m[j]*R*Ts/V[j];
                        rho[j]=Pm[j]/(R*Ts);
                        ux[j]=md[j]/(rho[j]*A[j]);
                        miu[j]=niu*rho[j];
                }
        }

////////////////////////////////////////////////////////////////////////
////////////////////////////////////////////////////////////////////////

        if(flagBF==1)
        {
                for(j=0;j<5;j++)
                {
                        Hux[j]=ux[j];
                }

                for(j=4;j<5;j++)
                {
                        m[j]+=(md[j-1])*T;
                        Pm[j]=m[j]*R*Ts/V[j];
                        rho[j]=Pm[j]/(R*Ts);
                }

                for(j=3;j<4;j++)
                {
                        m[j]+=(-md[j]+md[j-1])*T;
                        Pm[j]=m[j]*R*Ts/V[j];
                        rho[j]=Pm[j]/(R*Ts);
                        ux[j]=md[j]/(rho[j]*A[j]);
                        miu[j]=niu*rho[j];
                }

                for(j=2;j<3;j++)
                {
                        m[j]+=(-md[j]+md[j-1])*T;
                        Pm[j]=m[j]*R*Ts/V[j];
                        rho[j]=PrV[j][1];
                        ux[j]=PrV[j][2]/PrV[j][1];
```

```
                miu[j]=niu*rho[j];
        }

        for(j=1;j<2;j++)
        {
                m[j]+=(-md[j]+md[j-1])*T;
                Pm[j]=m[j]*R*Ts/V[j];
                rho[j]=PrV[j][1];
                ux[j]=PrV[j][2]/PrV[j][1];
                miu[j]=niu*rho[j];
        }

        for(j=0;j<1;j++)
        {
                m[j]+=(-md[j])*T;
                Pm[j]=m[j]*R*Ts/V[j];
                rho[j]=Pm[j]/(R*Ts);
                ux[j]=md[j]/(rho[j]*A[j]);
                miu[j]=niu*rho[j];
        }
}

////////////////////////////////////////////////////////////////////////

if(Hux[1]>0)
{
        if(ux[1]<=0)
        {
                flag1=1;
        }
}

if(Hux[2]>0)
{
        if(ux[2]<0)
        {
                flag2=1;
        }
}

if(Hux[3]>0)
{
        if(ux[3]<0)
        {
                flag3=1;
        }
}

////////////////////////////////////////////////////////////////////////

if(Hux[1]<0)
{
        if(ux[1]>0)
        {
                flag1=2;
        }
}

if(Hux[2]<0)
{
        if(ux[2]>0)
        {
                flag2=2;
        }
}

if(Hux[3]<0)
{
        if(ux[3]>=0)
        {
```

```
                        flag3=2;
                }
        }

////////////////////////////////////////////////////////////////////////

        if(flag1==1)
        {
                if(flag2==1)
                {
                        if(flag3==1)
                        {
                                flagBF=1;
                                flag1=0;
                                flag2=0;
                                flag3=0;

                                ux[1]=ux[2];
                                ux[2]=ux[3];
                                ux[3]=0.0;

                                for(j=0;j<5;j++)
                                {
                                        rho[j]=m[j]/V[j];
                                        miu[j]=niu*rho[j];
                                }
                        }
                }
        }

////////////////////////////////////////////////////////////////////////

        if(flag1==2)
        {
                if(flag2==2)
                {
                        if(flag3==2)
                        {
                                flagBF=0;
                                flag1=0;
                                flag2=0;
                                flag3=0;

                                ux[3]=ux[2];
                                ux[2]=ux[1];
                                ux[1]=0.0;

                                for(j=0;j<5;j++)
                                {
                                        rho[j]=m[j]/V[j];
                                        miu[j]=niu*rho[j];
                                }
                        }
                }
        }
}

////////////////////////////////////////////////////////////////////////
////////////////////////////////////////////////////////////////////////

ProcessExit();

if(i%500==0)
{
        fprintf(fPressure,"%f\t",t);
        for(j=0;j<5;j++)
        {
                fprintf(fPressure,"%lf\t",Pm[j]/ConP);
        }
        fprintf(fPressure,"\n");
```

```
                        fprintf(fMassFlowRate,"%f\t",t);
                        for(j=0;j<5;j++)
                        {
                                fprintf(fMassFlowRate,"%lf\t",m[j]);
                        }
                        fprintf(fMassFlowRate,"\n");

                        fprintf(fVelocity,"%f\t",t);
                        for(j=0;j<5;j++)
                        {
                                fprintf(fVelocity,"%lf\t",ux[j]);
                        }
                        fprintf(fVelocity,"\n");
                }
        }

        fclose(fVelocity);
}

////////////////////////////////////////////////////////////////////////////
////////////////////////////////////////////////////////////////////////////

void SegmentsStatic()
{
        Pm[0]=(3.66e+05+PAtm);
        Pm[1]=(3.30e+05+PAtm);
        Pm[2]=(2.95e+05+PAtm);
        Pm[3]=(2.66e+05+PAtm);
        Pm[4]=(2.33e+05+PAtm);

        for(j=0;j<5;j++)                                //Initial Conditions for All Segments
        {
                md[j]=0.0247967;
                rho[j]=Pm[j]/(R*Ts);
                m[j]=V[j]*rho[j];
                ux[j]=md[j]/(rho[j]*A[j]);
                miu[j]=niu*rho[j];
        }
}

////////////////////////////////////////////////////////////////////////////

void ProcessExit()
{
        if(t>=10.00)
                exit(0);
}

////////////////////////////////////////////////////////////////////////////
////////////////////////////////////////////////////////////////////////////
```

Appendix 4

```
////////////////////////////////////////////////////////////////////////////
// Actuator pressure response - Lumped Approach - Predicted Cut-Off
////////////////////////////////////////////////////////////////////////////

#include<stdio.h>
#include<stdlib.h>
#include<math.h>
#include<time.h>

#define N               24000                   //Test steps
#define T               1.25e-04                //Sampling interval,seconds
#define M               10.0                    //Mass of Load/kg
#define MO              1.0                     //Other Masses/kg
#define Pa              (1.00e+05)              //Atmos. pressure/Pa
#define R               287                     //Gas constant,J/(kg.K)
#define Ts              (273+20)                //System temperature/K
#define Ra              (Pa/(R*Ts))             //Air density/kg/m3
#define pi              3.141592                //pi constant

#define d1              (5.00e-03)              //Tube Diameter/m
#define A1              (pi*d1*d1/4)            //Tube Cross Section Area/m2
#define L1              0.40                    //Tube Length Before Main Valve/m
#define V1              (L1*A1)                 //Tube Volume Before Main Valve/m3
#define M1              (V1*Ra)                 //Initial Air Mass at V1/kg/m3
#define Km1             1.00                    //Main Valve Orifice Factor (Normal)
#define Km2             0.00                    //Main Valve Orifice Factor (Cut-Off)

#define L2              1.00                    //Tube Diameter+Main Pipe Length/m
#define A2              (pi*d1*d1/4)            //Tube Diameter+Main Pipe Cross Section
Area/m2
#define V2              (A2*L2)                 //Tube Diameter+Main Pipe/m3
#define M2              (V2*Ra)                 //Initial Air Mass at V2/kg/m3

#define L5              0.50                    //Tube Diameter+Main Pipe Length/m
#define A5              (pi*d1*d1/4)            //Tube Diameter+Main Pipe Cross Section
Area/m2
#define V5              (A5*L5)                 //Tube Diameter+Main Pipe/m3
#define M5              (V5*Ra)                 //Initial Air Mass at V5/kg/m3

#define d6              5.00e-03                //Tube Diameter/m
#define A6              (pi*d6*d6/4)            //Tube Cross Section Area/m2
#define L6              0.40                    //Tube Length After Main Valve/m
#define V6              (L6*A6)                 //Tube Volume After Main Valve/m3
#define M6              (V6*Ra)                 //Initial Air Mass at V1/kg/m3

#define D               0.125                   //Overall Piston Diameter/m
#define d               0.030                   //Rod Diameter/m
#define Ac              (pi*(D*D-d*d)/4)        //Piston Cross Section Area/m2
#define Xc              0.180                   //Max Cylinder Stroke/m
#define K1              0.85                    //Orifice Size Factor/K(Driving Chamber)
#define K2              0.50                    //Orifice Size Factor/K(Exhaust Chamber)
#define l1              0.038                   //Initial Cushion Region/m
#define l2              0.140                   //End Cushion Region/m
#define L3              0.005                   //Smallest Cylinder Stroke/m
#define Vwr             (Ac*L3)                 //Initial Driving Chamber Volume/m3
#define Vw              ((Ac*Xc)+Vwr+Vwr)       //Whole Volume/m3
#define Vwl             ((Ac*Xc)+Vwr)           //Initial Exhaust Chamber Volume/m3
#define A4              A1                      //Cylinder Outlet Cross-section area/m2

#define M3              (Vwr*Ra)                //Initial air mass/kg(ChamberVolume)
#define d3              (3/8)*(25.4/1000)       //Cylinder Inlet diameter/m
#define A3              A1                      //Cylinder Inlet Cross-section area/m2

#define Ps              (1.55e+05+Pa)           //System pressure/Pa

#define Cp              1.00e+05                //Convert pressure Pa - Bar
```

```
#define CdV             0.72                            //Gas discharge coefficient at Main
Valve
#define CdC             0.72                            //Gas discharge coefficient at Cylinder
Inlet
#define Cdt             0.72                            //Gas discharge coefficient at Tube
#define Cd              0.72                            //Gas discharge coefficient at Cylinder
Outlet
#define Cm              0.0405                          //Mass flow parameter for choked
#define gamma           1.40                            //Specific heat ratio (for air 1.4)

#define Fs              358.90                          //Static Friction/N
#define Arb             2.20                            //Arbitrary Constant for Cut-Off
Implementation
#define n               2.70                            //Real Law Exponent Value

#define DL              "VLine.txt"
#define DC              "VCylinder.txt"

static double
Am1,m1,m1d=0.0,m2,m2d=0.0,m3,m3d=0.0,m4,m4d=0.0,m5,m5d=0.0,m6,m6d=0.0,p1,p2,p3,p3c,p4,p5,p6
,Cma,Cmb,Cmc,Cmx,Cmy,Cmz;
static double ct1,ct2,ct3,ct4,ct5,ct6,Fr,a=0.0,v=0.0,x=0.0,Frp,F,Av1,Av2,V3,V4,C,Kv,A,B;
float t; int i,
setproc1=0,setproc2=0,setproc3=0,setproc4=0,setproc5=0,setproc6=0,sign=0,flag=0,signal=0;

void main()
{
        void Process1();
        void Process2();
        void Process3();
        void Process4();
        void Process5();
        void Process6();
        void Dynamics();
        void Orifice();
        void End();
        void Exit();

        FILE *fl;
        FILE *fc;

        fl=fopen(DL,"w");
        fc=fopen(DC,"w");

        for(i=0;i<N;i++)
        {
                t=float(i*T);

                A=pow(x,n);
                B=pow(Xc,n);

                Orifice();

                Process1();
                Process2();
                Process3();
                Process4();
                Process5();
                Process6();

                m1+=(m1d-m2d)*T;
                m2+=(m2d-m3d)*T;

                p1=m1*R*Ts/V1;
                p2=m2*R*Ts/V2;

                m3+=(m3d)*T;
                m4-=(m4d)*T;

                m5+=(m4d-m5d)*T;
```

```
                m6+=(m5d-m6d)*T;

                p5=m5*R*Ts/V5;
                p6=m6*R*Ts/V6;

                Dynamics();

                v=v+a*T;
                x=x+v*T;

                if(x>=Xc)
                {
                        V3=Vwl;
                        V4=Vwr;
                }

                else
                {
                        V3=Vwr+(Ac*x);
                        V4=Vwl-(Ac*x);
                }

                p3c=Fs/Ac;

                p3=m3*R*Ts/V3;
                p4=m4*R*Ts/V4;

                End();
                Exit();

                if(i%40==0)
                {

        fprintf(fl,"%f\t%lf\t%lf\t%lf\t%lf\t%lf\t%lf\t%lf\t%lf\t%lf\t%lf\t%lf\t%lf\t%lf\n",t,m1,m
2,m3,m4,m5,m6,p1/Cp,p2/Cp,p3/Cp,p4/Cp,p5/Cp,p6/Cp);

        fprintf(fc,"%f\t%lf\t%lf\t%lf\t%lf\t%lf\t%lf\t%lf\t%lf\t%lf\t%lf\t%lf\t%lf\t%lf\n",t,m2,m
5,p2/Cp,p5/Cp,F,Fr,x,v,a,Av1,Av2,Am1);
                }
        }

        fclose(fc);
}

void Process1()
{
        if(setproc1==0)
        {
                if(t<=0.215)
                {
                        m1=M1;  p1=Pa;
                }

                else
                {
                        m1=M1;  p1=Pa;  setproc1=1;
                }
        }

        if((p1/Ps)<=0.528)

                Cma=Cm;

        else
        {

                ct1=(2*gamma/(R*(gamma-1)))*(pow(p1/Ps,2/gamma)-pow(p1/Ps,(gamma+1)/gamma));

                if(ct1<0)
                        ct1=0.0;
```

```
                Cma=sqrt(ct1);
        }

        if((p3*A)>=Arb*(p3c*B))
        {
                if(t>=1.22)
                {
                        Am1=A1*Km2;
                }

                else
                {
                        Am1=A1*Km1;
                }
        }

        else
        {
                Am1=A1*Km1;
        }

        m1d=Cdt*Cma*Am1*p1/sqrt(Ts);
}

void Process2()
{
        if(setproc2==0)
        {
                m2=M2;  p2=Pa;  setproc2=1;
        }

        if((p2/p1)<=0.528)

                Cmb=Cm;

        else
        {
                ct2=(2*gamma/(R*(gamma-1)))*(pow(p2/p1,2/gamma)-pow(p2/p1,(gamma+1)/gamma));

                if(ct2<0)
                        ct2=0.0;

                Cmb=sqrt(ct2);
        }

        m2d=CdV*Cmb*A2*p2/sqrt(Ts);
}

void Process3()
{
        if(setproc3==0)
        {
                m3=M3;  p3=Pa;  setproc3=1;
        }

        if((p3/p2)<=0.528)

                Cmc=Cm;

        else
        {
                ct3=(2*gamma/(R*(gamma-1)))*(pow(p3/p2,2/gamma)-pow(p3/p2,(gamma+1)/gamma));

                if(ct3<0)
                        ct3=0.0;

                Cmc=sqrt(ct3);
        }
```

```
        m3d=CdC*Cmc*Av1*p3/sqrt(Ts);
}

void Process4()
{
        if(setproc4 == 0)
        {

                if(t<=0.135)
                {
                        p4=Ps;  m4=(Vwl*p4)/(R*Ts);
                }

                else
                {
                        p4=Ps;  m4=(Vwl*p4)/(R*Ts);    setproc4=1;
                }
        }

        if((Pa/p4)<=0.528)

                Cmx=Cm;

        else
        {
                ct4=(2*gamma/(R*(gamma-1)))*(pow(Pa/p4,2/gamma)-pow(Pa/p4,(gamma+1)/gamma));

                if(ct4<0)
                        ct4=0.0;
                Cmx=sqrt(ct4);
        }

        m4d=Cd*Cmx*Av2*p4/sqrt(Ts);
}

void Process5()
{
        if(setproc5 == 0)
                {
                        p5=Ps;  m5=(V5*p5)/(R*Ts);     setproc5=1;
                }

        if((Pa/p5)<=0.528)

                Cmy=Cm;

        else
        {
                ct5=(2*gamma/(R*(gamma-1)))*(pow(Pa/p5,2/gamma)-pow(Pa/p5,(gamma+1)/gamma));

                if(ct5<0)
                        ct5=0.0;
                Cmy=sqrt(ct5);
        }

        m5d=Cd*Cmy*A5*p5/sqrt(Ts);
}

void Process6()
{
        if(setproc6 == 0)
        {
                p6=Ps;  m6=(V6*p6)/(R*Ts);     setproc6=1;
        }

        if((Pa/p6)<=0.528)

                Cmz=Cm;

        else
```

```
        {
                ct6=(2*gamma/(R*(gamma-1)))*(pow(Pa/p6,2/gamma)-pow(Pa/p6,(gamma+1)/gamma));

                if(ct6<0)
                        ct6=0.0;
                Cmz=sqrt(ct6);
        }

        m6d=Cd*Cmz*A6*p6/sqrt(Ts);
}

void Dynamics()
{
        if(sign==0)
        {
                if ((p3-p4)*Ac<=Fs)
                        flag=0;
                else
                {
                        flag=1; sign=1;
                }
        }

        if(flag==0)
        {
                Fr=(p3-p4)*Ac;
                a=0;
        }
        else
        {
                C=123.77;
                Kv=1443.68;
                Fr=C+(Kv*v);

                F=((p3-p4)*Ac)-Fr;
                a=F/(M+MO);
        }
}

void Orifice()
{
        if(x<l1)
        {
                Av1=A3*K1;
                Av2=A4;
        }
        else
                if(x>=l2)
                {
                        Av1=A3;
                        Av2=A4*K2;
                }
                else
                {
                        Av1=A3;
                        Av2=A4;
                }
}

void End()
{
        if(x>=Xc)
        {
                a=0;
                v=0;
                x=Xc;
        }
}

void Exit()
```

```
{
        if(t>=3.000)
                exit(0);
}
```

Appendix 5

```
////////////////////////////////////////////////////////////////////////
// Finite Difference Approach (2nd Order)
// Predicted Cut-Off Cylinder Actuation Modelling
////////////////////////////////////////////////////////////////////////

#include<stdio.h>
#include<stdlib.h>
#include<math.h>

#define N               5.00e+06                    //Iteration steps
#define Ns              7                           //Segments number
#define Nf              2                           //Double Iteration
#define T               1.00e-06                    //Sampling interval (s)
#define PAtm            1.00e+05                    //Atmos. pressure (Pa)
#define PSys            (1.55e+05+PAtm)             //System pressure (Pa)
#define R               287                         //Gas constant (J/(kg.K))
#define Ts              (273+20)                    //System temperature (K)
#define niu             1.51e-05                    //Kinematic Viscosity (m2/s)
#define pi              3.141592                    //pi constant

#define MLoad           10.0                        //Mass of Load/kg
#define MOther          1.0                         //Other Masses/kg
#define D               0.125                       //Overall Piston Diameter/m
#define d               0.030                       //Rod Diameter/m
#define Xc              0.180                       //Max Cylinder Stroke/m
#define Ac              (pi*(pow(D,2)-pow(d,2))/4)  //Piston Cross Section Area/m2
#define Km1             1.00                        //Main Valve Orifice Factor (Normal)
#define Km2             0.00                        //Main Valve Orifice Factor (Cut-Off)
#define K1              0.85                        //Orifice Size Factor/K(Driving Chamber)
#define K2              0.50                        //Orifice Size Factor/K(Exhaust Chamber)
#define l1              0.038                       //Initial Cushion Region/m
#define l2              0.140                       //End Cushion Region/m
#define L3              0.005                       //Smallest Cylinder Stroke/m
#define Vwr             (Ac*L3)                     //Initial Driving Chamber Volume/m3
#define Vw              ((Ac*Xc)+Vwr+Vwr)           //Whole Volume/m3
#define Vwl             ((Ac*Xc)+Vwr)               //Initial Exhaust Chamber Volume/m3
#define Fs              353.39                      //Static Friction/N
#define Arb             2.20                        //Arbitrary Constant for Cut-Off
Implementation
#define n               2.70                        //Real Law Exponent Value

#define dt              5.00e-03                    //Tube Diameter (m)
#define LT              3.50                        //Total Tube Length (m)
#define Lt              (LT/Ns)                     //Tube Length (m)

#define ConP            1.00e+05                    //Convert pressure Pa - Bar
#define cp              1005.1                      //Specific Heat Capacity of air @
constant pressure (J/kgK)
#define cv              717.90                      //Specific Heat Capacity of air @
constant volume (J/kgK)
#define gamma  (cp/cv)                              //Specific heat ratio (for air 1.4)

#define Cm              0.0405                      //Mass flow parameter for choked
#define Cdt             0.72                        //Gas discharge coefficient at Tube

#define DPT             "Pressure.txt"
#define DPM             "MassFlowrate.txt"
#define DPV             "Velocity.txt"
#define DPD             "Density.txt"
#define DPX             "Displacement.txt"

float   t;
int     i,j;
int     setproc1=0,setproc2=0;
int     setproc3=0,setproc4=0;
int     setproc5=0,setproc6=0;
```

```
int     sign,flag,flagBF=0;
int     flag1,flag2,flag3;

double  Cma,Cmd,Cme,Cmf,ct1,ct4,ct5,ct6;
double  M[Ns+1],m[Ns+1],md[Ns+1];
double  Pm[Ns+1];
double  rho[Ns+1];
double  Hux[Ns+1];
double  ux[Ns+1];
double  miu[Ns+1];
double  L[Ns+1],A[Ns+1],V[Ns+1];
double  PrV[Ns+1][Nf+1];

double  F,Fr,a=0.0,v=0.0,x=0.0,C,Kv;
double  Av4,Av5;
double  Am0,Am1;
double  AReal,BReal;
double  Pm4c;

void main()
{
        void Orifice();
        void Segment1LumpedB();
        void Segment2FDB();
        void Segment3FDB();
        void Segment4LumpedB();
        void Segment0LumpedF();
        void Segment1FDF();
        void Segment2FDF();
        void Segment3LumpedF();
        void Segment5Lumped();
        void Segment6Lumped();
        void Dynamics();
        void End();
        void ProcessExit();

        FILE *fPressure;
        FILE *fMassFlowRate;
        FILE *fVelocity;
        FILE *fDensity;
        FILE *fDisplacement;

        fPressure=fopen(DPT,"w");
        fMassFlowRate=fopen(DPM,"w");
        fVelocity=fopen(DPV,"w");
        fDensity=fopen(DPD,"w");
        fDisplacement=fopen(DPX,"w");

////////////////////////////////////////////////////////////////////////////

        for(j=1;j<4;j++)
        {
                L[j]=Lt;
                A[j]=pi*pow(dt,2)/4;
                V[j]=L[j]*A[j];
        }

        for(j=4;j<6;j++)
        {
                A[j]=pi*pow(dt,2)/4;
        }

        for(j=6;j<7;j++)
        {
                L[j]=Lt;
                A[j]=pi*pow(dt,2)/4;
                V[j]=L[j]*A[j];
        }

        for(j=0;j<1;j++)
```

```
	{
		L[j]=1.00e+05;
		A[j]=pi*pow(dt,2)/4;
		V[j]=L[j]*A[j];

		Pm[j]=PSys;
		rho[j]=Pm[j]/(R*Ts);
		m[j]=V[j]*rho[j];
		md[j]=0.0;
		ux[j]=md[j]/(rho[j]*A[j]);
		miu[j]=niu*rho[j];
	}

////////////////////////////////////////////////////////////////////////////

	for(i=0;i<N;i++)
	{
		t=float(i*T);

		Orifice();

		AReal=pow(x,n);
		BReal=pow(Xc,n);

////////////////////////////////////////////////////////////////////////////

		if(flagBF==0)
		{
			Segment1LumpedB();

			for(j=2;j<3;j++)
			{
				Segment2FDB();
			}

			for(j=3;j<4;j++)
			{
				Segment3FDB();
			}

			Segment4LumpedB();

			Segment5Lumped();

			Segment6Lumped();

			for(j=0;j<7;j++)
			{
				Hux[j]=ux[j];
			}

			for(j=0;j<1;j++)
			{
				m[j]+=(-md[j+1])*T;
				Pm[j]=m[j]*R*Ts/V[j];
				rho[j]=Pm[j]/(R*Ts);
				ux[j]=md[j]/(rho[j]*A[j]);
				miu[j]=niu*rho[j];
			}

			for(j=1;j<2;j++)
			{
				m[j]+=(md[j]-md[j+1])*T;
				Pm[j]=m[j]*R*Ts/V[j];
				rho[j]=Pm[j]/(R*Ts);
				ux[j]=md[j]/(rho[j]*A[j]);
				miu[j]=niu*rho[j];
			}

			for(j=2;j<3;j++)
```

```
{
        m[j]+=(md[j]-md[j+1])*T;
        Pm[j]=m[j]*R*Ts/V[j];
        rho[j]=PrV[j][1];
        ux[j]=PrV[j][2]/PrV[j][1];
        miu[j]=niu*rho[j];
}

for(j=3;j<4;j++)
{
        m[j]+=(md[j]-md[j+1])*T;
        Pm[j]=m[j]*R*Ts/V[j];
        rho[j]=PrV[j][1];
        ux[j]=PrV[j][2]/PrV[j][1];
        miu[j]=niu*rho[j];
}

Dynamics();

v=v+a*T;
x=x+v*T;

if(x>=Xc)
{
        V[4]=Vwl;
        V[5]=Vwr;
}

else
{
        V[4]=Vwr+(Ac*x);
        V[5]=Vwl-(Ac*x);
}

Pm4c=Fs/Ac;

for(j=4;j<5;j++)
{
        m[j]+=(md[j])*T;
        Pm[j]=m[j]*R*Ts/V[j];
        rho[j]=Pm[j]/(R*Ts);
        ux[j]=md[j]/(rho[j]*A[j]);
        miu[j]=niu*rho[j];
}

for(j=5;j<6;j++)
{
        m[j]-=(md[j])*T;
        Pm[j]=m[j]*R*Ts/V[j];
        rho[j]=Pm[j]/(R*Ts);
        ux[j]=md[j]/(rho[j]*A[j]);
        miu[j]=niu*rho[j];
}

for(j=6;j<7;j++)
{
        m[j]+=(md[j-1]-md[j])*T;
        Pm[j]=m[j]*R*Ts/V[j];
        rho[j]=Pm[j]/(R*Ts);
        ux[j]=md[j]/(rho[j]*A[j]);
        miu[j]=niu*rho[j];
}

End();

if(Hux[2]>0)
{
        if(ux[2]<=0)
        {
                flag2=1;
```

```
                }
        }

        if(Hux[3]>0)
        {
                if(ux[3]<0)
                {
                        flag3=1;
                }
        }

        if(flag2==1)
        {
                if(flag3==1)
                {
                        flagBF=1;
                        flag2=0;
                        flag3=0;

                        ux[1]=ux[2];
                        ux[2]=ux[3];
                        ux[3]=0.0;

                        for(j=0;j<7;j++)
                        {
                                rho[j]=m[j]/V[j];
                                miu[j]=niu*rho[j];
                        }
                }
        }
}

//////////////////////////////////////////////////////////////////////////

        if(flagBF==1)
        {
                Segment3LumpedF();

                for(j=2;j<3;j++)
                {
                        Segment2FDF();
                }

                for(j=1;j<2;j++)
                {
                        Segment1FDF();
                }

                Segment0LumpedF();

                Segment5Lumped();

                Segment6Lumped();

                for(j=0;j<7;j++)
                {
                        Hux[j]=ux[j];
                }

                for(j=0;j<1;j++)
                {
                        m[j]+=(-md[j])*T;
                        Pm[j]=m[j]*R*Ts/V[j];
                        rho[j]=Pm[j]/(R*Ts);
                        ux[j]=md[j]/(rho[j]*A[j]);
                        miu[j]=niu*rho[j];
                }

                for(j=1;j<2;j++)
                {
```

```
        m[j]+=(-md[j]+md[j-1])*T;
        Pm[j]=m[j]*R*Ts/V[j];
        rho[j]=PrV[j][1];
        ux[j]=PrV[j][2]/PrV[j][1];
        miu[j]=niu*rho[j];
}

for(j=2;j<3;j++)
{
        m[j]+=(-md[j]+md[j-1])*T;
        Pm[j]=m[j]*R*Ts/V[j];
        rho[j]=PrV[j][1];
        ux[j]=PrV[j][2]/PrV[j][1];
        miu[j]=niu*rho[j];
}

for(j=3;j<4;j++)
{
        m[j]+=(-md[j]+md[j-1])*T;
        Pm[j]=m[j]*R*Ts/V[j];
        rho[j]=Pm[j]/(R*Ts);
        ux[j]=md[j]/(rho[j]*A[j]);
        miu[j]=niu*rho[j];
}

Dynamics();

v=v+a*T;
x=x+v*T;

if(x>=Xc)
{
        V[4]=Vwl;
        V[5]=Vwr;
}

else
{
        V[4]=Vwr+(Ac*x);
        V[5]=Vwl-(Ac*x);
}

for(j=4;j<5;j++)
{
        m[j]+=(md[j-1])*T;
        Pm[j]=m[j]*R*Ts/V[j];
        rho[j]=Pm[j]/(R*Ts);
        ux[j]=md[j]/(rho[j]*A[j]);
        miu[j]=niu*rho[j];
}

for(j=5;j<6;j++)
{
        m[j]-=(md[j])*T;
        Pm[j]=m[j]*R*Ts/V[j];
        rho[j]=Pm[j]/(R*Ts);
        ux[j]=md[j]/(rho[j]*A[j]);
        miu[j]=niu*rho[j];
}

for(j=6;j<7;j++)
{
        m[j]+=(md[j-1]-md[j])*T;
        Pm[j]=m[j]*R*Ts/V[j];
        rho[j]=Pm[j]/(R*Ts);
        ux[j]=md[j]/(rho[j]*A[j]);
        miu[j]=niu*rho[j];
}

End();
```

```
        if(Hux[1]<0)
        {
                if(ux[1]>0)
                {
                        flag1=2;
                }
        }

        if(Hux[2]<0)
        {
                if(ux[2]>0)
                {
                        flag2=2;
                }
        }

        if(Hux[3]<0)
        {
                if(ux[3]>=0)
                {
                        flag3=2;
                }
        }

        if(flag1==2)
        {
                if(flag2==2)
                {
                        if(flag3==2)
                        {
                                flagBF=0;
                                flag1=0;
                                flag2=0;
                                flag3=0;

                                ux[1]=0.0;
                                ux[2]=ux[1];
                                ux[3]=ux[2];

                                for(j=0;j<7;j++)
                                {
                                        rho[j]=m[j]/V[j];
                                        miu[j]=niu*rho[j];
                                }
                        }
                }
        }
}

ProcessExit();

if(i%5000==0)
{
        fprintf(fPressure,"%f\t",t);
        for(j=1;j<7;j++)
        {
                fprintf(fPressure,"%lf\t",Pm[j]/ConP);
        }
        fprintf(fPressure,"\n");

        fprintf(fMassFlowRate,"%f\t",t);
        for(j=1;j<7;j++)
        {
                fprintf(fMassFlowRate,"%lf\t",md[j]);
        }
        fprintf(fMassFlowRate,"\n");

        fprintf(fVelocity,"%f\t",t);
        for(j=1;j<7;j++)
```

```
                        {
                                fprintf(fVelocity,"%lf\t",ux[j]);
                        }
                        fprintf(fVelocity,"\n");

                        fprintf(fDensity,"%f\t",t);
                        for(j=1;j<7;j++)
                        {
                                fprintf(fDensity,"%lf\t",rho[j]);
                        }
                        fprintf(fDensity,"\n");

                        fprintf(fDisplacement,"%f\t%lf\n",t,x);
                }
        }

        fclose(fDisplacement);
}

void Orifice()
{
        if(x<l1)
        {
                Av4=A[4]*K1;
                Av5=A[5];
        }
        else
        {
                if(x>=l2)
                {
                        Av4=A[4];
                        Av5=A[5]*K2;
                }
                else
                {
                        Av4=A[4];
                        Av5=A[5];
                }
        }
}

void Segment0LumpedF()                          //Forward Differencing
{
        if((PSys/Pm[1])<=0.528)
        {
                Cma=Cm;
        }

        else
        {
                ct1=(2*gamma/(R*(gamma-1)))*(pow(PSys/Pm[1],2/gamma)-
pow(PSys/Pm[1],(gamma+1)/gamma));

                if(ct1<0)
                {
                        ct1=0.0;
                }

                Cma=sqrt(ct1);
        }

        if((Pm[4]*AReal)>=Arb*(Pm4c*BReal))
        {
                if(t>=1.22)
                {
                        Am0=A[0]*Km2;
                }

                else
                {
```

```
                        Am0=A[0]*Km1;
                }
        }

        else
        {
                Am0=A[0]*Km1;
        }

        md[0]=-Cdt*Cma*Am0*Pm[1]/sqrt(Ts);
}

void Segment1LumpedB()                          //Backward Differencing
{
        if(setproc1==0)
        {
                if(t<=0.215)
                {
                        Pm[1]=PAtm;
                        rho[1]=Pm[1]/(R*Ts);
                        m[1]=V[1]*rho[1];
                        md[1]=0.0;
                        ux[1]=md[1]/(rho[1]*A[1]);
                        miu[1]=niu*rho[1];
                }

                else
                {
                        Pm[1]=PAtm;
                        rho[1]=Pm[1]/(R*Ts);
                        m[1]=V[1]*rho[1];
                        md[1]=0.0;
                        ux[1]=md[1]/(rho[1]*A[1]);
                        miu[1]=niu*rho[1];
                        setproc1=1;
                }
        }

        if((Pm[1]/PSys)<=0.528)
        {
                Cma=Cm;
        }

        else
        {
                ct1=(2*gamma/(R*(gamma-1)))*(pow(Pm[1]/PSys,2/gamma)-
pow(Pm[1]/PSys,(gamma+1)/gamma));

                if(ct1<0)
                {
                        ct1=0.0;
                }

                Cma=sqrt(ct1);
        }

        if((Pm[4]*AReal)>=Arb*(Pm4c*BReal))
        {
                if(t>=1.22)
                {
                        Am1=A[1]*Km2;
                }

                else
                {
                        Am1=A[1]*Km1;
                }
        }

        else
```

```
        {
                Am1=A[1]*Km1;
        }

        md[1]=Cdt*Cma*Am1*PSys/sqrt(Ts);
}

void Segment1FDF()                                      //Forward Differencing
{
        //Uv1   (calculates new rho[j])
    PrV[j][1]=rho[j]-(T/L[j])*(rho[j+1]*ux[j+1]-rho[j]*ux[j]);

        //Uv2   (calculates new rho[j]*u[j])
    PrV[j][2]=(rho[j]*ux[j])-(T/L[j])
                        *((rho[j+1]*pow(ux[j+1],2)+(Pm[j+1])-(4/3)*(miu[j+1])*(ux[j+1]-
ux[j])/L[j])
                        -(rho[j]*pow(ux[j],2)+(Pm[j])-(4/3)*(miu[j])*(ux[j]-ux[j-1])/L[j]));

        md[j]=PrV[j][2]*A[j];
}

void Segment2FDB()                                      //Backward Differencing
{
        if(setproc2==0)
        {
                        Pm[j]=PAtm;
                        rho[j]=Pm[j]/(R*Ts);
                        m[j]=V[j]*rho[j];
                        md[j]=0.0;
                        ux[j]=md[j]/(rho[j]*A[j]);
                        miu[j]=niu*rho[j];
                        setproc2=1;
        }

        //Uv1   (calculates new rho[j])
    PrV[j][1]=rho[j]-(T/L[j])*(rho[j]*ux[j]-rho[j-1]*ux[j-1]);

        //Uv2   (calculates new rho[j]*u[j])
    PrV[j][2]=(rho[j]*ux[j])-(T/L[j])
                        *((rho[j]*pow(ux[j],2)+(Pm[j])-(4/3)*(miu[j])*(ux[j+1]-ux[j])/L[j])
                        -(rho[j-1]*pow(ux[j-1],2)+(Pm[j-1])-(4/3)*(miu[j-1])*(ux[j]-ux[j-
1])/L[j]));

        md[j]=PrV[j][2]*A[j];
}

void Segment2FDF()                                      //Forward Differencing
{
        //Uv1   (calculates new rho[j])
    PrV[j][1]=rho[j]-(T/L[j])*(rho[j+1]*ux[j+1]-rho[j]*ux[j]);

        //Uv2   (calculates new rho[j]*u[j])
    PrV[j][2]=(rho[j]*ux[j])-(T/L[j])
                        *((rho[j+1]*pow(ux[j+1],2)+(Pm[j+1])-(4/3)*(miu[j+1])*(ux[j+1]-
ux[j])/L[j])
                        -(rho[j]*pow(ux[j],2)+(Pm[j])-(4/3)*(miu[j])*(ux[j]-ux[j-1])/L[j]));

        md[j]=PrV[j][2]*A[j];
}

void Segment3FDB()                                      //Backward Differencing
{
        if(setproc3==0)
        {
                        Pm[j]=PAtm;
                        rho[j]=Pm[j]/(R*Ts);
                        m[j]=V[j]*rho[j];
                        md[j]=0.0;
                        ux[j]=md[j]/(rho[j]*A[j]);
                        miu[j]=niu*rho[j];
```

```
                    setproc3=1;
        }

        //Uv1   (calculates new rho[j])
    PrV[j][1]=rho[j]-(T/L[j])*(rho[j]*ux[j]-rho[j-1]*ux[j-1]);

        //Uv2   (calculates new rho[j]*u[j])
    PrV[j][2]=(rho[j]*ux[j])-(T/L[j])
                    *((rho[j]*pow(ux[j],2)+(Pm[j])-(4/3)*(miu[j])*(ux[j+1]-ux[j])/L[j])
                    -(rho[j-1]*pow(ux[j-1],2)+(Pm[j-1])-(4/3)*(miu[j-1])*(ux[j]-ux[j-
1])/L[j]));

        md[j]=PrV[j][2]*A[j];
}

void Segment3LumpedF()                          //Forward Differencing
{
        if((Pm[3]/Pm[4])<=0.528)
        {
                Cmd=Cm;
        }

        else
        {
                ct4=(2*gamma/(R*(gamma-1)))*(pow(Pm[3]/Pm[4],2/gamma)-
pow(Pm[3]/Pm[4],(gamma+1)/gamma));

                if(ct4<0)
                {
                        ct4=0.0;
                }

                Cmd=sqrt(ct4);
        }

        md[3]=-Cdt*Cmd*A[3]*Pm[4]/sqrt(Ts);
}

void Segment4LumpedB()                          //Backward Differencing
{
        if(setproc4==0)
        {
                    Pm[4]=PAtm;
                    rho[4]=Pm[4]/(R*Ts);
                    m[4]=(Vwr+(Ac*x))*rho[4];
                    md[4]=0.0;
                    ux[4]=md[4]/(rho[4]*A[4]);
                    miu[4]=niu*rho[4];
                    setproc4=1;
        }

        if((Pm[4]/Pm[3])<=0.528)
        {
                Cmd=Cm;
        }

        else
        {
                ct4=(2*gamma/(R*(gamma-1)))*(pow(Pm[4]/Pm[3],2/gamma)-
pow(Pm[4]/Pm[3],(gamma+1)/gamma));

                if(ct4<0)
                {
                        ct4=0.0;
                }

                Cmd=sqrt(ct4);
        }

        md[4]=Cdt*Cmd*Av4*Pm[3]/sqrt(Ts);
```

```
}

void Segment5Lumped()
{
        if(setproc5==0)
        {
                if(t<=0.135)
                {
                        Pm[5]=PSys;
                        rho[5]=Pm[5]/(R*Ts);
                        m[5]=(Vwl-(Ac*x))*rho[5];
                        md[5]=0.0;
                        ux[5]=md[5]/(rho[5]*A[5]);
                        miu[5]=niu*rho[5];
                }

                else
                {
                        Pm[5]=PSys;
                        rho[5]=Pm[5]/(R*Ts);
                        m[5]=(Vwl-(Ac*x))*rho[5];
                        ux[5]=md[5]/(rho[5]*A[5]);
                        miu[5]=niu*rho[5];
                        setproc5=1;
                }
        }

        if((PAtm/Pm[5])<=0.528)
        {
                Cme=Cm;
        }

        else
        {
                ct5=(2*gamma/(R*(gamma-1)))*(pow(PAtm/Pm[5],2/gamma)-
pow(PAtm/Pm[5],(gamma+1)/gamma));

                if(ct5<0)
                {
                        ct5=0.0;
                }

                Cme=sqrt(ct5);
        }

        md[5]=Cdt*Cme*Av5*Pm[5]/sqrt(Ts);
}

void Segment6Lumped()
{
        if(setproc6==0)
        {
                        Pm[6]=PSys;
                        rho[6]=Pm[6]/(R*Ts);
                        m[6]=V[6]*rho[6];
                        md[6]=0.0;
                        ux[6]=md[6]/(rho[6]*A[6]);
                        miu[6]=niu*rho[6];
                        setproc6=1;
        }

        if((PAtm/Pm[6])<=0.528)
        {
                Cmf=Cm;
        }

        else
        {
                ct6=(2*gamma/(R*(gamma-1)))*(pow(PAtm/Pm[6],2/gamma)-
pow(PAtm/Pm[6],(gamma+1)/gamma));
```

```
                if(ct6<0)
                {
                        ct6=0.0;
                }

                Cmf=sqrt(ct6);
        }

        md[6]=Cdt*Cmf*A[6]*Pm[6]/sqrt(Ts);
}

void Dynamics()
{
        if(sign==0)
        {
                if ((Pm[4]-Pm[5])*Ac<=Fs)
                {
                        flag=0;
                }

                else
                {
                        flag=1; sign=1;
                }
        }

        if(flag==0)
        {
                Fr=(Pm[4]-Pm[5])*Ac;
                a=0.00;
        }
        else
        {
                C=123.77;
                Kv=1443.68;
                Fr=C+(Kv*v);

                F=((Pm[4]-Pm[5])*Ac)-Fr;
                a=F/(MLoad+MOther);
        }
}

void End()
{
        if(x>=Xc)
        {
                a=0;
                v=0;
                x=Xc;
        }
}

void ProcessExit()
{
        if(t>=3.00)
                exit(0);
}
```

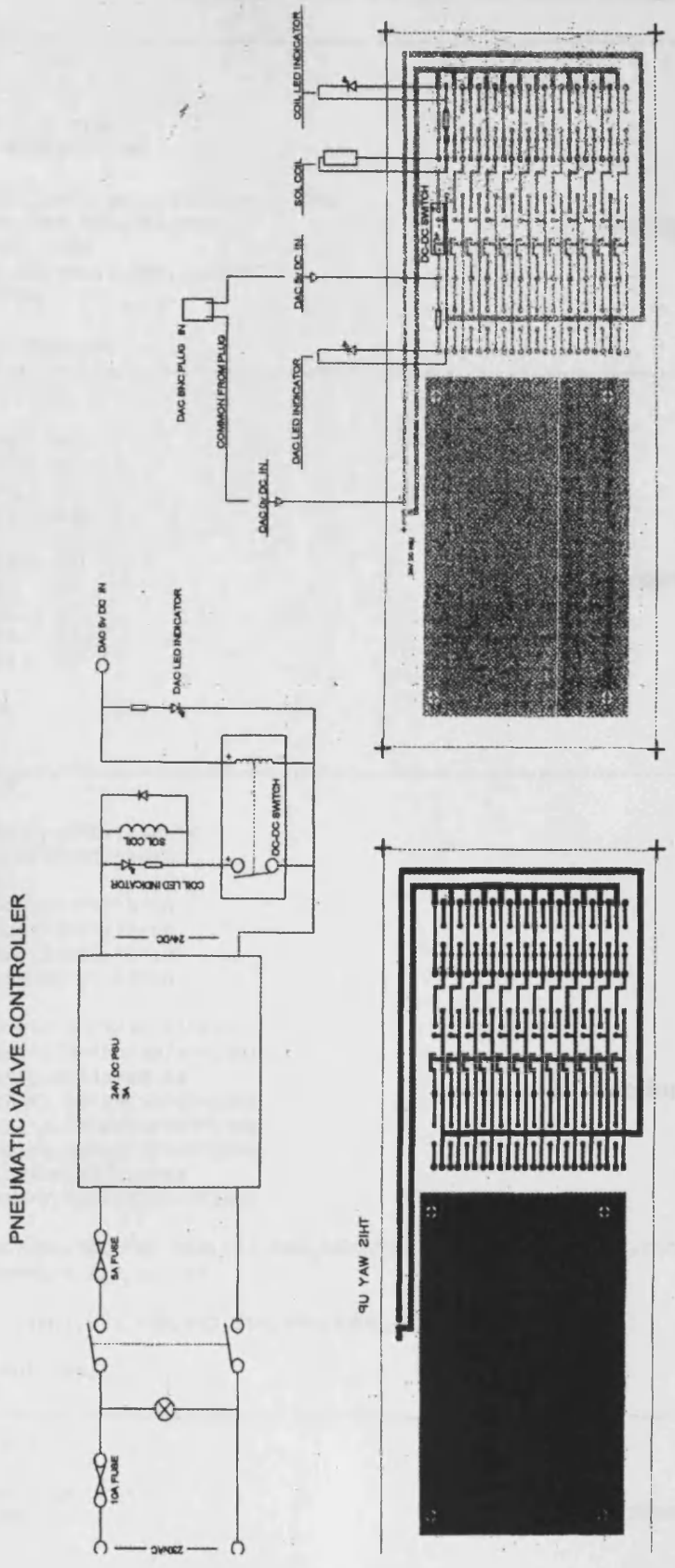

Appendix 6: Circuit diagram including PCB blueprint of the voltage relay unit

Appendix 7: Sample of DAPView control program

```
RESET

OUTPORT 0..5 TYPE=1
OPTIONS BPOUTPUT=ON

PIPES DAC0,DAC1,DAC2,DAC3,DAC4,DAC5
PIPES PT1,PT2,PT3,PT4,PT5
PIPES IFM1,IFM2
PIPES V1,V2,V3,V4,PRI,PRO,PV
PIPES PWAVE

VARIABLE GRND,REF
```

1st Section

```
IDEFINE  A 10

  SET IP0   S0
  SET IP1   S1
  SET IP2   S2
  SET IP3   S3
  SET IP4   S4
  SET IP5   S5
  SET IP6   S6
  SET IP7   S7
  SET IP8   S8
  SET IP9   S9

  TIME 50
  END
```

2nd Section

```
PDEFINE B

  PRO=(DAC0/32767)*10*10
  PV=(DAC1/32767)*10*10

  V1=(DAC2/32767)*5*10
  V2=(DAC3/32767)*5*10
  V3=(DAC4/32767)*5*10
  V4=(DAC5/32767)*5*10

  PRI=(IP0*1.00*9/32767*100)
  PT1=(IP1*1.00*10/32767*100)
  IFM2=(IP2-6124)/19.84
  PT2=(IP3*1.00*10/32767*100)
  PT3=(IP4*1.00*10/32767*100)
  PT4=(IP5*1.00*10/32767*100)
  IFM1=(IP6-6173)/19.84
  PT5=(IP7*1.00*10/32767*100)

  CONTROL(IP0,IP1,IP2,IP3,IP4,IP5,IP6,IP7,IP8,IP9,DAC0,DAC1,DAC2,DAC3,DAC4,
  DAC5,PWAVE,0,1,2,3,4,5)

  MERGE  (IFM1,PT3,PT2,PT1,PT4,PT5,IFM2,$BINOUT)

  COPY(DAC0,OP0)
  END
```

3rd Section

```
ODEFINE C 1

  SET OP0   A0
  TIME 500
  END

START A,B,C
```

4th Section